Charles University in Prague
Third Faculty of Medicine

# NEW ASPECTS OF THE CELL SUBMEMBRANE SIGNALING

**Petr HENEBERG**

Ph.D. Dissertation in Immunology

Supervised by RNDr. Petr Dráber, DrSc.
Institute of Molecular Genetics AS CR, v.v.i.

Prague, October 2007

Připomeneme pouze, že snaženo se vystihnouti i biochemickou stránku protoplasmy a že zkoumána v tom směru rozličná pletiva rostlinná i živočišná...

*Ottův slovník naučný, IV.díl,*
*J.Otto, Praha, 1891, str. 936*

Cell signaling is the key mechanism used for regulation of most of the processes influencing our bodies. Here I focused mostly on the submembrane signaling in mast cells and basophils related to their activation via the high affinity IgE receptor and some other surface receptors. This dissertation summarizes results obtained during my Ph.D. studies at the Department of Signal Transduction, Institute of Molecular Genetics AS CR, v.v.i. in Prague. Most of the results have been already published in scientific journals, only the most recent results included in this thesis are under submission or in press. The list of the papers (posessing the results obtained during my Ph.D. studies) included in this thesis follows in a chronological order:

1. Tolarová, H.; Dráberová, L.; Heneberg, P. & Dráber, P. 2004:
   **Involvement of filamentous actin in setting the threshold for degranulation in mast cells.**
   *European Journal of Immunology* 34(6): 1627-1636.

2. Volná, P.; Lebduška, P.; Dráberová, L.; Šímová, Š., Heneberg, P.; Boubelík, M.; Bugajev, V.; Malissen, B.; Wilson, B.S.; Hořejší, V.; Malissen, M. & Dráber, P. 2004:
   **Negative regulation of mast cell signaling and function by the adaptor LAB/NTAL.**
   *Journal of Experimental Medicine* 200(8): 1001-1013.

3. Heneberg, P. & Dráber, P. 2005:
   **Regulation of Cys-based protein tyrosine phosphatases *via* reactive oxygen and nitrogen species in mast cells and basophils.**
   *Current Medicinal Chemistry* 12(16): 1859-1871.

4. Heneberg, P.; Lebduška, P.; Dráberová, L.; Korb, J. & Dráber, P. 2006:
   **Topography of plasma membrane microdomains and its consequences for mast cell signaling.**
   *European Journal of Immunology* 36(10): 2795-2806.

5. Dráber, P.; Dráberová, L.; Heneberg, P.; Šmíd, F.; Farghali, H. & Dráber, P. 2007:
   **Preformed STAT3 transducer complexes in human HepG2 cells and rat hepatocytes.**
   *Cellular Signalling* 19(11): 2400-2412.

6. Lebduška, P.; Korb, J.; Tůmová, M.; Heneberg, P. & Dráber, P. 2007:
   **Topography of signaling molecules as detected by electron microscopy on plasma membrane sheets isolated from nonadherent mast cells.**
   *Journal of Immunological Methods* 328(1-2): 139-151.

7. Dráberová, L.; Shaik, G.M.; Volná, P.; Heneberg, P.; Tůmová, M.; Lebduška, P.; Korb, J. & Dráber, P. 2007:
   **Regulation of $Ca^{2+}$ signaling in mast cells by tyrosine-phosphorylated and unphosphorylated non-T cell activation linker, NTAL.**
   *Journal of Immunology* 179(8): 5169-5180.

8. Heneberg, P.; Dráberová, L. & Dráber, P. 2007:
   **Spatiotemporal distribution of PTP20 in signaling of mast cells and basophils.**
   *subm. to Eur. J. Immunol.*

I would like to use this opportunity to thank to many people, who were supportive during my Ph.D. studies, above all to my supervisor Petr Dráber, under whose guidance this work has been accomplished, and to Jiří Horák and Michal Anděl, coordinators of the research goals under support of which this thesis was done. My thanks go to each of the coauthors of the papers published, namely to (in alphabetical order) Michael Boubelík, Viktor Bugajev, Peter Dráber, Petr Dráber, Ľubica Dráberová, Hassan Farghali, Václav Hořejší, Jan Korb, Pavel Lebduška, Bernard Malissen, Marie Malissen, Gouse Mohiddin Shaik, Šárka Šímová, František Šmíd, Helena Tolarová, Magda Tůmová, Petra Volná, and Bridget S. Wilson. My personal thanks also direct to all the other colleagues at the Department of Signal Transduction not mentioned above for friendly atmosphere, to our technical staff (Romana Budovičová, Lukáš Kocanda, Dana Lorenčíková, Hana Mrázová, and Šárka Šilhánková) for the excellent technical assistance, and last but not least to my family for the patience they had with me.

I declare that I didn`t submitted this thesis nor its substantial part to achieve any other or the same academic degree. My share in results of each respective paper is specified by the statement of Petr Dráber, both supervisor and coauthor of all the papers presented.

Petr Heneberg
Prague, 30. 10. 2007

# CONTENT

# 1 ABSTRACT

This dissertation contributes to elucidation of some mechanisms of the mammalian cell submembrane signaling. Major part of the research was conducted on mast cells and basophils activated *via* the high affinity IgE receptor, FcεRI, or *via* the cell surface glycoprotein Thy-1. New roles of actin cytoskeleton in mast cell signaling via FcεRI and Thy-1 are described. Discovery of new transmembrane adaptor protein non-T cell activation linker, NTAL, short time before the initiation of work on the thesis led to the increased attention paid to this protein. Dramatic changes of signaling in mast cells deficient in NTAL, or with up- or down-regulated expression of this protein are described. NTAL was also found to be one of proteins phosphorylated following the Thy-1 aggregation. Spatiotemporal distribution of surface glycoprotein Thy-1 at different levels of resolution and some biochemical properties of cells activated *via* Thy-1 are depicted. Screen for nonreceptor hitherto unknown protein tyrosine phosphatases in mast cells and basophils was conducted and initial analysis of spatiotemporal distribution and function of phosphatase PTP20 in mast cell signaling was performed. Next, the role of reactive oxygen and nitrogen species in the regulation of mast cell protein tyrosine phosphatases was summarized. New method for isolation of plasma membrane sheets from nonadherent immune cells was established and verified. Topography of STAT3 in signaling of freshly isolated hepatocytes and HepG2 cells was detected. Potential applications of the achieved outcomes in understanding and treatment of asthma, Noonan syndrome, Williams syndrome, East Coast fever, and diabetes mellitus are discussed.

# 2 ABSTRAKT

Tato disertace je příspěvkem k objasnění některých mechanismů submembránové signalizace savčích buněk. Hlavní část výzkumů byla provedena na žírných buňkách a bazofilech aktivovaných prostřednictvím vysokoafinitního receptoru pro IgE typu I, FcεRI, anebo membránovým glykoproteinem Thy-1. Jsou popsány nové role aktinového cytoskeletu v signalizaci žírných buněk přes FcεRI a Thy-1. Objev nového transmembránového adaptorového proteinu NTAL – z anglického „non-T cell activation linker“ - krátce před započetím zpracovávání teze vedl ke zvýšené pozornosti věnované tomuto proteinu. Byly zjištěny a popsány významné změny v signalizaci žírných buněk s deficiencí v genu kódujícím protein NTAL, podobně též docházelo k výrazným změnám i v žírných buňkách, u kterých byla exprese proteinu NTAL jen snížena či zvýšena. Bylo dokumentováno, že NTAL je rovněž jedním z proteinů fosforylovaným po agregaci glykoproteinu Thy-1 na povrchu žírných buněk. Velká pozornost byla věnována časoprostorové distribuci glykoproteinu Thy-1 na různých úrovních rozlišení, přičemž byly zkoumány i některé biochemické charakteristiky buněk aktivovaných právě přes Thy-1 glykoprotein. V žírných buňkách a bazofilech byla zjišťována přítomnost dosud neznámých nereceptorových proteinových tyrosinových fosfatáz a následně byla provedena úvodní analýza časoprostorové distribuce a funkce jedné z nich, PTP20, v signalizaci žírných buněk. Dále byla formou review shrnuta role reaktivních forem kyslíku a dusíku v regulaci proteinových tyrosinových fosfatáz v žírných buňkách. Zavedena a ověřena byla metoda pro izolaci plasmatických membrán z neadherentních buněk imunitního systému. V neposlední řádě byla rovněž popsána topografie přenašeče signálů a aktivátoru transkripce 3, STAT3, v signalizaci čerstvě izolovaných hepatocytů a v buněčné linii HepG2. Diskutována je potenciální aplikace získaných poznatků v porozumění mechanismů a léčbě astmatu, syndromu Noonanové, Williamsovu syndromu, theileriózy a cukrovky.

# 3 INTRODUCTION

## 3.1 MEMBRANE MICRODOMAINS AS AN INITIATION POINT OF SUBMEMBRANE SIGNALING

Recent development in cell biology amended the original notion, inferred from the fluid-mosaic model (Singer and Nicolson, 1972), presenting plasma membrane just as a fluid lipid bilayer with membrane proteins restricted in their free diffusion by association with cytoskeletal components and other proteins. On the basis of the observations by high-speed single-particle tracking at a frame rate of 40,000 frames/second, the partitioning of the fluid plasma membrane into submicron compartments throughout the cell membrane and the hop diffusion of virtually all the molecules have been proposed (Kusumi *et al.*, 2005). This could explain why the diffusion coefficients in the plasma membrane are considerably smaller than those in artificial membranes, and why the diffusion coefficient is reduced upon molecular complex formation (oligomerization-induced trapping). The critical role is played by the actin-based submembrane cytoskeleton "fences" and anchored-transmembrane protein "pickets" in the formation of compartment boundaries (Kusumi *et al.*, 2005).

Detergent resistant membrane association of the T- and B-cell receptors and of FcεRI increases during signaling (Montixi *et al.*, 1998;Field *et al.*, 1999;Cheng *et al.*, 2001). Signaling in mast cells (Surviladze *et al.*, 2001), T-cells (Xavier *et al.*, 1998), and B-cells (Gupta and DeFranco, 2007) is sensitive to cholesterol depletion. In addition, order-preferring proteins and lipids can be observed by microscopic techniques to cluster together upon receptor ligation in mast cells (papers 2 & 4), and also FRET analysis implicates raft-dependent interactions of the Src-family kinase Lyn with the B-cell receptor (Sohn *et al.*, 2006).

Ironically, some of the strongest evidence for raft function comes from the behavior of human pathogens. A number of pathogenic bacteria (Lencer and Saslowsky, 2005;Lafont and van der Goot, 2005) and viruses (Chazal and Gerlier, 2003;Pelkmans, 2005) bind order-preferring proteins and lipids on the surface of mammalian cells and coopt host cell rafts during infection. For example cholera toxin, which binds the detergent resistant membranes-enriched ganglioside GM1, intoxicates the cells much more efficiently than the related *Escherichia coli* heat-labile type II enterotoxin LTIIb, which does not associate with detergent resistant membranes (Wolf *et al.*, 1998). Most putative raft-targeting pathogenic agents seem to use rafts for internalization into mammalian cells, suggesting a role for rafts in normal endocytic pathways (Brown, 2006).

Some questions remains regarding the targeting of peripheral proteins to lipid rafts. Best understood is the raft targeting of proteins lacking transmembrane spans. GPI anchors and tandem or closely-spaced acyl chains on these proteins are well known raft-targeting signals. Unexpectedly,

fluorescence quenching analysis showed that a tandem $NH_2$-terminal myristate/palmitate motif targeted a peripheral peptide to rafts in model membranes more strongly than tandem palmitoylation on two internal sites (Wang *et al.*, 2001b). The myristate/palmitate motif, present in Src-family kinases and in some G proteins, appears to be an especially efficient raft-targeting signal. Microscopical analysis in cells supports this idea. A tandem myristoyl/palmitoyl motif can target GFP to clusters on the inner leaflet of the plasma membrane that colocalize with rafts in the extracellular leaflet (Zacharias *et al.*, 2002). It is notable α subunits of G proteins are modified with unusual dual-palmitate motifs, in which the first palmitate is linked to an $NH_2$-terminal Gly instead of the usual internal Cys (Kleuss and Krause, 2003). By analogy with the myristate/palmitate motif, the dual-palmitate motif of G proteins might also confer high raftophilicity.

Some proteins are modified by both tandem palmitoylation (expected to increase raft affinity) and prenylation (expected to reduce raft affinity), raising the possibility that overall raft affinity may be regulated. For heterotrimeric G proteins, this could occur by dissociation of acylated Gα subunits from prenylated Gβ subunits during signaling. As expected, monomeric Gαi associates better than the Gαiβγ trimeric complex with detergent resistant membranes isolated from model membranes containing the purified proteins (Moffett *et al.*, 2000;Brown, 2006). H-Ras, modified by closely spaced dual palmitoylation and farnesylation, is also targeted to rafts, although it can be solubilized by standard Triton X-100 extraction (Plowman *et al.*, 2005). The prenyl group may bind reversibly to other proteins to regulate raft-disfavoring insertion of the moiety into the bilayer. Alternatively, other raft-favoring interactions may overcome raft-disfavoring tendency of the prenyl group.

Not all palmitoylated transmembrane proteins associate with detergent resistant membranes, and it is not known what distinguishes the two groups. Increasing the number of acyl chains may enhance detergent resistant membrane association, although protein structure is also clearly important since different numbers of acyl chains are required for detergent resistant membrane association of different proteins. For example LAT requires two chains (Zhang *et al.*, 1998b), whereas influenza hemaglutinin needs three (Melkonian *et al.*, 1999) for detergent resistant membrane association. Many singly palmitoylated proteins are excluded from detergent resistant membranes, e.g. transferrin receptor, a widely used non-raft marker protein, was originally reported to be either singly or doubly palmitoylated, depending on cell type (Jing and Trowbridge, 1990;Brown, 2006), and this issue has not been investigated further.

## 3.2 KEY MAST CELL ACTIVATION RECEPTORS

Mast cells have been recognized as cells that not only regulate allergy, but also many tissue functions, such as blood flow and coagulation, smooth-muscle contraction and peristaltics of the

intestine, mucosal secretion, wound healing, regulation of innate and adaptive immune responses and, most recently, peripheral tolerance (Galli *et al.*, 2005;Gilfillan and Tkaczyk, 2006;Lu *et al.*, 2006). Thus, in addition to allergic disorders, mast cells are involved in inflammatory diseases, neurological diseases and functional diseases such as irritable bowel syndrome, functional dyspepsia and fibromyalgia, and moreover they have a central role in host defence against bacteria and parasites through the release of cytokines that recruit neutrophils, eosinophils and TH2 cells to the site of infection (Marshall, 2004).

The mast cell plasma membrane receptors are structures receiving extracellular signals, thus beeing the key molecules responsible for the effective and specific cell signaling and response. Their engangement is triggered by an interaction of the receptors with its putative ligand leading to the receptor aggregation and/or its conformational changes. The receptors belong to very diverse structural families such as cytokine receptors, integrin receptors, G protein coupled receptors, multichain immune recognition receptors, and GPI-anchored proteins. Here I will focus on the key mast cell activation receptors, FcεRI, c-kit, and GPI-anchored proteins.

### 3.2.1 FcεRI

The key mast cell activation receptor is FcεRI – the high affinity IgE receptor. The mechanism of FcεRI crosslinking is a crucial event in the type I hypersensitivity, but seems to be of only little importance in healthy individuals. It is a multichain immune recognition receptor present in high quantities at the surface of mast cells and basophils, on some other haematopoietic cells such as eosinophils, platelets, neutrophils, and antigen-presenting cells, but also on smooth muscle cells. It was described first as a tetrameric complex (αβγγ). The α chain, a member of the immunoglobulin superfamily, contains the binding site for IgE. The β subunit, with its four transmembrane domains separating $NH_2$- and COOH-terminal cytoplasmic tails, functions to amplify signaling responses. The two disulfide-linked γ subunits are members of the γ/ζ/η family of antigen receptor subunits, consist essentially of a transmembrane region and cytoplasmic tail, and are critical for receptor signaling. Both β and γ subunits are responsible for the downstream propagation of the signal through the phosphorylation of their immunoreceptor tyrosine-based activation motif.

The structure of FcεRI varies according to species. In mice, FcεRI β chain is required for cell surface expression of FcεRI so that FcεRI is expressed as αβγγ tetramers, whereas in humans FcεRI can be expressed as an αβγγ or αγγ complex depending on cell type. For instance, in human antigen-presenting cells, FcεRI is expressed as a trimeric (αγγ) complex but as a tetramer (αβγγ) in mast cells. However, in the case of human eosinophils, platelets, and neutrophils, although both mRNA

and protein for the β chain have been detected, the existence of a functional αγγ complex could not be ruled out (Gounni, 2006).

Extensive advances have been made in the study of FcεRI signaling pathways in mast cells. Crosslinking of FcεRI via IgE-bound multivalent antigens leads to the activation of various protein tyrosine kinases starting with Lyn that revert from an inactive to an active state. Once activated, Lyn phosphorylates the immunoreceptor tyrosine-based activation motifs of FcεRI. This event leads to the propagation of signals through subsequent activation of additional cytoplasmic signaling molecules with SH2 domains such as the protein kinase Syk. Activated tyrosine kinases mediates phosphorylation of a number of proteins including LAT, Vav or PLCγ1 and PLCγ2 (Kraft and Kinet, 2007). Relatively recently, the Fyn kinase was shown to be activated directly by FcεRI-crosslinking (Parravicini *et al.*, 2002) leading to the phosphorylation of Gab2. Gab2 binds the p85 subunit of the PI3K leading to the PIP3 production and recruitment of pleckstrin homology domains of i.e. Btk, PLCγ1 or PLCγ2 to the membrane, subsequently resulting in release of calcium from internal stores. FcεRI-crosslinking also leads to the ERK phosphorylation and activation of ERK-associated MAPKs Vav, Raf1, MEK and to the activation of small GTPases such as Rac, Ras and Rho, leading to the exocytosis of granules, and generation of leukotrienes and cytokines (Gu *et al.*, 2001;Kawakami and Galli, 2002;Gounni, 2006;Kraft and Kinet, 2007).

Even binding of IgE itself can somewhat regulate mast cell functions. Thus IgE is not just a mediator of the mast cell activation when crosslinked by allergen. Exposure of mast cells to high levels of IgE results in increased surface expression of FcεRI and subsequently in increased degranulation after crosslinking of mast cell-bound IgE by allergen (Kawakami and Galli, 2002). Monomeric IgE was also reported to induce cytokine production, resistance to apoptosis, but not to induce degranulation nor leukotriene release (Kalesnikoff *et al.*, 2001). But these studies undertaken on rodent mast cells were somewhat undermined by another recent study involving human mast cells derived from human lung, which presented induction of degranulation, leukotriene production and IL-8 synthesis by monomeric IgE (Cruse *et al.*, 2005).

### 3.2.2 C-KIT

Some growth factors and cytokines promote human mast-cell development from progenitor states and/or function as regulators of mediator release. The most relevant and still unique mast-cell growth factor is SCF, the ligand of c-kit (CD117), a receptor with tyrosine-kinase activity that is expressed on the surface of all human and murine mast cells. c-kit was originally identified as a retroviral oncogene isolated from the Hardy-Zuckerman 4 feline sarcoma (Besmer *et al.*, 1986). SCF, either membrane

bound or in its soluble form, promotes mast-cell growth, differentiation, survival and homing. In addition, SCF can regulate mediator release by human mast cells by either enhancing IgE-dependent mediator release or directly inducing mediator release by mast cells kept in an SCF-deprived milieu (Bischoff, 2007).

Studies carried out using both mouse and human mast cells have shown that SCF markedly increases degranulation in response to antigen. Although some authors have concluded that SCF alone does not induce degranulation (Ishizuka *et al.*, 1998;Ishizuka *et al.*, 1999;Baumruker and Prieschl, 2000;Tkaczyk *et al.*, 2004), our unpublished data (Dráberová, Heneberg, Bugajev, Dráber unpubl.) and data of some others document degranulation at higher doses of SCF (Columbo *et al.*, 1992;Coleman *et al.*, 1993;Taylor *et al.*, 1995). Simultaneous addition of SCF and antigen also markedly increases the mRNA and/or protein concentrations of multiple cytokines. When added separately, however, these agents only increase basal cytokine production to a small extent. For this to occur, the signalling pathways that are initiated by both receptors (that is, SCF and FcεRI) must somehow be integrated to induce the synergistic responses, and the specific signals that are required by FcεRI for inducing mast-cell-mediator release must be missing from the signalling pathway initiated by c-kit (Gilfillan and Tkaczyk, 2006).

Unlike FcεRI, c-kit is a single-chain receptor having its own PTK activity. Many of the signals that are induced in mast cells by IgE-bound antigen — for example, PI3K activation, PLCγ activation, calcium mobilization and MAPK-cascade activation — are also initiated by SCF (Hundley *et al.*, 2004). But some of the signals, like those of PLCγ1 or calcium mobilization are slower and of a lower magnitude. Some authors claim that SCF treatment doesn`t lead to the phosphorylation of transmembrane adaptor protein LAT (Hundley *et al.*, 2004;Gilfillan and Tkaczyk, 2006), but these data are still questionable as some LAT phosphorylation can be detected at high doses of SCF at least in mouse BMMC (Tůmová *et al.*, unpubl.). In contrast NTAL phosphorylation following SCF treatment was commonly reported (Tkaczyk *et al.*, 2004;Hundley *et al.*, 2004;Gilfillan and Tkaczyk, 2006). In the opposite way, siRNA directed against LAT or NTAL adaptors abrogated the increase in antigen-inguced SCF-increased degranulation (Tkaczyk *et al.*, 2004;Ali *et al.*, 2004) indicating that these two adaptors are required for the synergistic effect of FcεRI and c-kit.

### 3.2.3 GPI-ANCHORED PROTEINS

Unlike the other membrane receptors, which contain transmembrane domains, the GPI-anchored proteinss are unique since they penetrate only the outer leaflet of plasma membrane *via* the bound phospholipid. The GPI-anchored proteins are composed of a phospholipid, modified polysacharide and a polypeptide. The phospholipid is bound to the polysacharide via inositol and the polysacharide is covalently linked to carboxy-terminal of the polypeptide via amide bond. The polypeptide is usually

highly glycosylated and the glycosylation significantly participates in formation of plasma membrane glycocalyx. GPI-anchored proteins are cleaved out from cell surface by phospholipases such as phosphatidylinositol-specific phospholipase C. Due to the glycosylation, GPI-anchored proteins are extremely variable and become to be targeted by a wide spectrum of extracellular ligands, including less specific interactions with lectins, selectins, and many toxins. Although GPI-anchored proteins cannot mediate direct interactions with signaling molecules in cytoplasm, they are endowed with a capability to induce cell signaling and response. Since GPI-anchored proteins are ubiquitously expressed in all eukaryotic cells (not so in prokaryotic cells (Nosjean, 1998)), their signaling capacity is involved in a broad spectrum of cell activations, including cells of immune system. Here I will focus on two GPI-anchored proteins, with which I deal here in the results section of this thesis.

Thy-1 (CD90) is a GPI-anchored cell surface protein expressed in a number of cell types including mast cells and other haematopoietic cells, endothelial cells, fibroblasts, ovarian cancer cells, or mature neurons (Saalbach *et al.*, 1999). Thy-1 has diverse cellular functions and activates multiple signaling pathways, affecting cell interactions with the extracellular environment or with other cells, and influencing cell proliferation, differentiation, and survival. It is expected to play a role in nerve regeneration, glomerulonephritis, tumorigenesis, wound healing and fibrosis in humans. Thy-1 interacts with both integrins and cytoplasmic tyrosine kinases to promote cell adhesion. Thy-1 appears to inhibit cellular migration at baseline, but it may facilitate regulated migration in response to injury, via both tyrosine kinase- and lipid raft-dependent mechanisms. The interaction with cytoplasmic tyrosine kinases may also be required for Thy-1-induced apoptosis, and potentially for the development of glomerulonephritis. Thy-1 also affects proliferation of tumor cells and fibroblasts, suggesting a role for Thy-1 in tumorigenesis and fibrogenesis. It is important to reiterate that the effects of Thy-1 are tissue- and cell type-specific (Rege and Hagood, 2006b). In mast cells, Thy-1 is known to induce activation events independent of the expression of FcεRI forming complexes with kinase Lyn, which could be dissociated by octylglukoside, but not the nonionic detergents NP40 or Brij 96 (Dráberová and Dráber, 1993). Antibody-mediated crosslinking of Thy-1 on the mast cell surface leads to the movement of Thy-1 to detergent resistant membrane complexes and results further in a series of biochemical events leading to the mast cell degranulation (Surviladze *et al.*, 1998). Some more detailed aspects of signaling through Thy-1 are described in the Results chapter of this thesis.

The second GPI-anchored protein we used to activate mast cells was TEC-21/TEX101. This glycoprotein was identified in the plasma membrane of rat basophilic leukemia cell line (Hálová *et al.*, 2002), and in testis, especially spermatocytes and spermatids but not in Sertoli cells or interstitial cells, including Leydig cells (Kurita *et al.*, 2001). TEC-21 belongs to the uPAR/Ly-6/snake neurotoxin family. The protein is constitutively included in lipid rafts of the RBL cells. Its antibody-mediated

triggering results in the enhanced phosphorylation of the tyrosine kinase Syk, LAT adaptor, elevated $Ca^{2+}$ level, and release of secretory components such as β-glucuronidase. The cellular activation through TEC-21 is independent of the FcεRI, nor accompanied by tyrosine phosphorylation of FcεRI β and γ subunits, nor by the phosphorylation of or colocalization with the Lyn kinase (Hálová *et al.*, 2002).

## 3.3 TRANSMEMBRANE ADAPTOR PROTEINS

Transmembrane adaptor proteins form a large group of previously underestimated proteins (fig. 1) important for the proper immunoreceptor signaling. Those of our interest consist of a very short extracellular peptide, single transmembrane helix and intracellular domain containing multiple tyrosine-based motifs. Formally, ζ chain of the TCR complex is such a protein, as well as the other ζ chain family proteins (η, DAP-12, DAP-10) closely associated with TCR, some Fc receptors and with some activating NK cell and myeloid cell receptors (Hořejší, 2004). LAT/LAT1, NTAL/LAB/LAT2, and PAG/Cbp are adaptors thought to be functionally associated with immunoreceptors in mast cells and some other haematopoietic cells – I will deal with them later in this chapter. Three other transmembrane adaptors associated with membrane receptors either weakly or not at all are TRIM (Bruyns *et al.*, 1998), SIT (Marie-Cardine *et al.*, 1999) and LAX (Zhu *et al.*, 2002). These proteins are not associated with membrane rafts, do not possess the palmitoylation motif and all of them appear to be involved in some aspects of regulation of immunoreceptor signaling. V.Hořejší (Hořejší, 2004) reported potential existence of several other transmembrane adaptor molecules, some of them possessing a palmitoylation motif and therefore probably associated with membrane rafts. One of them, expressed mainly in T cells and named LIME, binds Lck and Csk when phosphorylated and may be involved in some aspects of immunoreceptor signaling (Brdičková *et al.*, 2003;Hořejší, 2004).

### 3.3.1 NTAL / LAB / LAT2

NTAL/LAB/LAT2 (thereinafter NTAL only) was originally cloned as one of genes deleted in the Williams syndrome, an autosomal dominant disorder appearing with the frequency 1:10,000 of life births (Grimm and Wesselhoeft, 1980). The disorder in its full-blown form includes supravalvular aortic stenosis, multiple peripheral pulmonary arterial stenoses, elfin face, mental and statural deficiency, characteristic dental malformation, infantile hypercalcemia, and impaired visuospatial constructive cognition. NTAL is a 25-30kDa transmembrane adaptor protein associated with detergent resistant membranes in specific cell types of haematopoietic lineage. Similar to LAT, NTAL contains a putative transmembrane domain, a CxxC motif for potential palmitoylation, and a cytoplasmic domain with nine tyrosines conserved between mice and humans. The key distinction is in the absence of a putative PLCγ binding motif, analogous to that surrounding the Y132 site of human LAT. Tyrosine phosphorylation of NTAL is induced by FcεRI aggregation and c-Kit

dimerization in mast cells, FcγRI aggregation in monocytes, and BCR aggregation in B cells. NTAL is also expressed in resting NK cells but, unlike the related transmembrane adaptor protein LAT, not in resting T cells. As demonstrated in monocytes and B cells, phosphorylated NTAL recruits signaling molecules such as Grb2, Gab1 and c-Cbl into receptor-signaling complexes (Iwaki *et al.*, 2007).

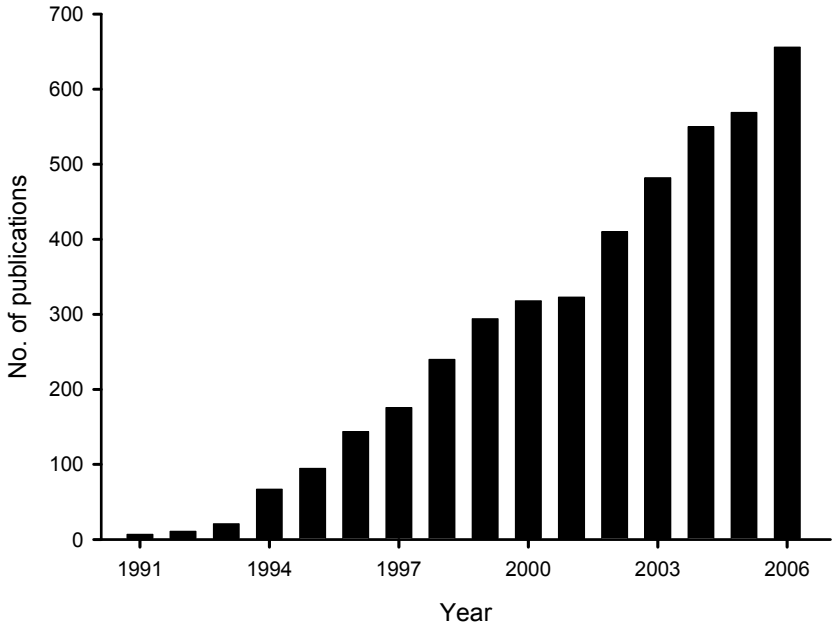


Figure 1. Number of publications about adaptor proteins is rapidly increasing. Data from the database Web of Science, Σ = 4731 publications from years 1945-2006.

Here in the Results chapter is presented one of the two existing gene knock-out studies and one of several knock-down studies of NTAL. Generally, they indicated that NTAL may function as both a positive and negative regulator of mast cell activation (paper 2; Zhu *et al.*, 2004;Mutch *et al.*, 2007), but its precise role in the activation of these and other haematopoietic cells remains still enigmatic. The current view is that NTAL does not function as a gatekeeper of mast cell degranulation. Rather, once cells are activated, it controls the extent of the degranulation response. But in contrast it seems that NTAL might be a gatekeeper of the mast cell cytokine production (Zhu *et al.*, 2004). Overexpression of NTAL in a background of LAT deficiency reconstitutes T cell development and provides partial compensation for defects in TCR signaling (Janssen *et al.*, 2004). Currently Saito`s group published that both NTAL and LAT contribute to the maintenance of Erk activation and survival through the membrane retention of the Ras-activation complex Grb2-Sos, describing differences between the LAT/Gads/SLP-76/PLCγ and LAT/NTAL/Grb2/Sos pathways (Yamasaki *et al.*, 2007).

### 3.3.2 LAT / LAT1

LAT/LAT1 (thereinafter LAT only) is another 36-38 kDa transmembrane adaptor protein similar to NTAL (see Chapter 3.3.1). It has a short extracellular domain and a long intracytoplasmic domain, which contains ten tyrosine residues in humans and nine in mice. Following TCR engagement, LAT is tyrosyl-phosphorylated by ZAP70 that is recruited to phosphorylated ITAMs and activated. Tyrosyl-phosphorylated LAT thus provides multiple docking sites for a variety of SH2 domain-containing cytosolic enzymes and adapters. These include PLCγ, PTKs of the Tec family, the p85 subunit of PI3K, the exchange factor Vav and the adapters Gads, Grap, and Grb2 (Weber *et al.*, 1998;Zhang *et*

*al.*, 1998a;Zhang *et al.*, 2000;Malbec *et al.*, 2004). Previous works based on mutational analysis of LAT identified critical tyrosine residues involved in the recruitment of these molecules in T cells - the four distal tyrosines (Y132, Y171, Y191, and Y226 in humans, and their homologues in mice Y136, Y175, Y195, and Y235). Specifically, Y132/136 was demonstrated as being the major binding site for PLCγ, and the three distal tyrosines (Y171/175, Y191/195, and Y226/235) binding sites for Gads, Grap, and Grb2 (Zhang *et al.*, 2000). The four distal tyrosines are critical for both TCR and FcεRI signaling. Unexpectedly, knock-in mice expressing LAT with a point mutation of the first or of the last three of these tyrosines exhibited an abnormal T cell development characterized by a massive expansion of TH2-like αβ or γδ T cells, respectively. This phenotype suggests that, besides positive signals, LAT might support negative signals that normally regulate terminal T cell differentiation and proliferation (Sommers *et al.*, 2002;Aguado *et al.*, 2002). As a consequence, serum IgG1 concentrations were 100-fold higher than in wild-type mice, serum IgE concentrations were in the range of milligrams per milliliter and peripheral tissues were massively infiltrated with eosinophils.

The mechanisms by which LAT controls FcεRI signaling are thought to be similar to the LAT-dependent mechanisms that control TCR signaling. FcεRI aggregation in bone marrow-derived mast cells (BMMCs) from $LAT^{-/-}$ mice triggered a reduced phosphorylation of SLP-76 and of PLCγ, resulting in decreased $Ca^{2+}$ mobilization and MAPK activation and, ultimately, in a decreased release of preformed mediators and secretion of cytokines (Saitoh *et al.*, 2000;Malbec *et al.*, 2004). Daëron`s lab (Malbec *et al.*, 2004) focused on the IgE- and IgG-induced responses in BMMCs considered as a model of mucosal-type mast cells, and PCMCs, a novel type of cultured mast cells. They found that LAT differentially regulates the biological responses of mucosal- and serosal-type mast cells, and that LAT tyrosines differentially contribute to exocytosis, cytokine secretion, and intracellular signals. LAT was found to be dispensable in BMMCs, but indispensable in PCMCs. Y132/136 of LAT was found to be necessary and apparently sufficient for LAT to support FcR signaling in PCMCs whereas BMMCs require all four distal tyrosines. The three distal tyrosines could have a negative role in the two types of mast cells, whereas Y136 could have a negative role in BMMCs, but not in PCMCs (Malbec *et al.*, 2004).

### 3.3.3 PAG / CBP

By immunoprecipitation of detergent resistant membranes, 2-dimensional gel electrophoresis, micropeptide sequence analysis, EST database searching and 5-prime and 3-prime RACE, the laboratory of V.Hořejší obtained a complementary DNA encoding PAG/Cbp (thereinafter PAG only) (Brdička *et al.*, 2000). It is a 70 kDa phosphoprotein, which shifts to approximately 85 kDa on immunoblot following cell stimulation. I contains a short 16-amino acid extracellular domain, short transmembrane domain and a cytoplasmic tail with nine putative tyrosine phosphorylation sites,

multiple putative casein kinase II and PKC phosphorylation sites and two proline-rich sequences. Of the nine putative tyrosine phosphorylation sites in the PAG molecule, six are associated with ITAM-like motifs. The highest expression is in the immune system, in lung, heart, and placenta. In haematopoietic cells the highest expression is in peripheral blood lymphocytes, monocytes, mast cells and basophils, weakly in neutrophils. Although *in vitro* analyses suggested binding to nearly all SH2-domain-containing proteins, only Fyn, Csk, and EBP50 were shown to be associated with PAG *in vivo* (Brdička *et al.*, 2000;Brdičková *et al.*, 2001;Maksumova *et al.*, 2005;Davidson *et al.*, 2007). PAG recruits Csk to the plasma membrane through Y317 independent of Fyn. It is thought that the PAG-Csk complex increases the signaling treshold required for initiation of the immune response (Brdička *et al.*, 2000).

In RBL cells, PAG is constitutively tyrosine phosphorylated; aggregation of the FcεRI leads to the increase of this phosphorylation. PAG is constitutively associated with Csk in RBL cells; this association is enhanced following FcεRI aggregation indicating that more Csk is recruited to lipid rafts upon FcεRI aggregation, which in turn might lead to the downregulation of the FcεRI-mediated signaling (Ohtake *et al.*, 2002c). Interestingly, we did not find any PAG to be associated with Csk in BMMCs, even though we confirmed the previous results from closely related RBL cells (see Results chapter). PAG overexpressing cells show reduced degranulation FcεRI-, but not PMA- or Ca-ionophore-mediated response. $Ca^{2+}$ mobilization induced by FcεRI aggregation was also impaired by PAG overexpression (Ohtake *et al.*, 2002b). Later SHP-2 was found to regulate the phosphorylation of PAG, thereby controlling Csk access to Src family kinases and promoting activation of Src family kinases (Zhang *et al.*, 2004). Interestigly, PAG was found to be overexpressed after cell infection with the intracellular protozoan parasite *Theileria parva* (Baumgartner *et al.*, 2003).

### 3.4 NONRECEPTOR PROTEIN PHOSPHATASES

Large part of my Ph.D. studies was devoted to the understanding of the function of nonreceptor protein tyrosine phosphatases in cells of the immune system, especially mast cells. Substantial progress has been made in defining the functions of haematopoietic protein tyrosine phosphatases during last years; genome sequencing effort have revealed a large and diverse superfamily of enzymes functioning in a coordinated manner with protein tyrosine kinases to control signaling pathways underlying a broad spectrum of fundamental physiological processes. Individual phosphatases can enhance or diminish cell signaling levels. At least four lines of evidence suggest that phosphatases are involved in mast cell activation induced by FcεRI. First, the pretreatment of mast cells or their tumor derivatives with pervanadate, a phosphatase inhibitor, results in a rapid tyrosine phosphorylation of numerous substrates, including FcεRI (see paper 3, fig. 3). Second, the

disruption of receptor aggregates by monovalent hapten leads to a rapid dephosphorylation of FcεRI subunits and downstream targets of Lyn and Syk (Paolini *et al.*, 1991). Third, in permeabilized

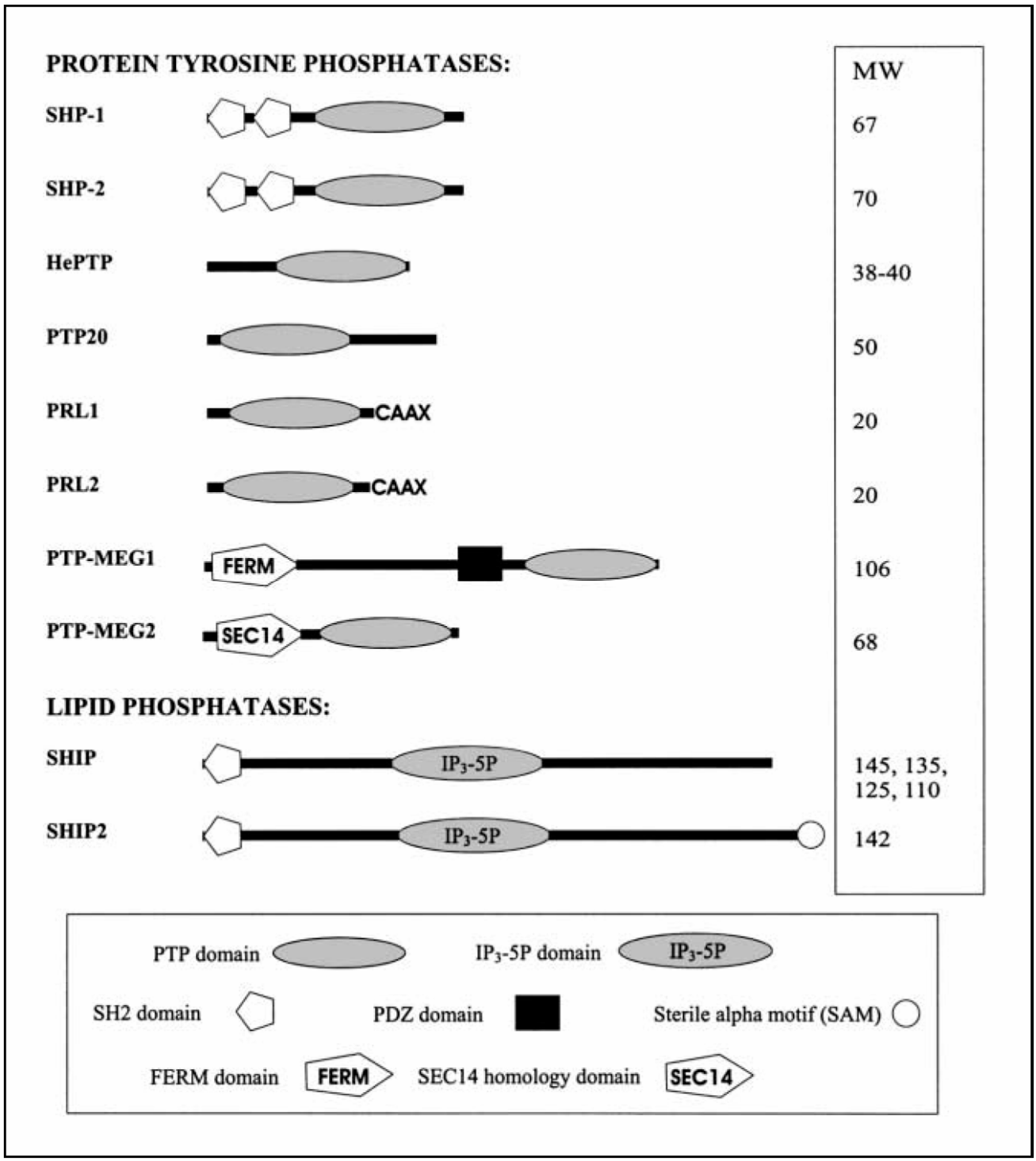


Figure 1. Domain structure of the nonreceptor PTPs and lipid phosphatases known to be expressed in mast cells and basophils. Numbers on the right indicate molecular weight of the PTPs in kilodaltons. Reprinted from the review of Heneberg & Dráber (2002d).

cells, the antigen-induced receptor phosphorylation is rapidly reversed if receptor-associated kinase activity is blocked with EDTA (Mao and Metzger, 1997). Fourth, several phosphatases exhibit changes in tyrosine phosphorylation and enzymatic activity after FcεRI aggregation (see e.g. paper 2,

fig. 5). Thus phosphatases obviously play an important role not only in resetting the cell activation system to baseline levels following removal of aggregated FcεRI but also in the regulation of numerous signal transduction molecules (Heneberg and Dráber, 2002c).

Protein tyrosine phosphatases are characterized by the presence of a conserved catalytic domain of 240–250 amino acid residues containing a unique sequence motif [I/V]HCxAGxxR[S/T]G (Denu *et al.*, 1996). Currently, they are represented by 107 genes in the human genome that encode members of four protein tyrosine phosphatase families (compared to 90 genes coding for protein tyrosine kinases) (Alonso *et al.*, 2004). Based on composition of their catalytic domains, the protein tyrosine phosphatases can be grouped into four separate families, each having a range of substrate specifities. Class I Cys-based phosphatases contain 38 well-known classical strictly tyrosine-specific phosphatases, and 61 VH1-like dual-specific phosphatases. Class II Cys-based phosphatases are represented by just one member in humans, but their orthologues are present in all major phyla including plants, numerous prokaryotes and archea. Class III. Cys-based phosphatases are Tyr/Thr specific phosphatases evolved probably from the bacterial rhodanese-like enzyme, represented by three Cdc25 cell cycle regulators. The fourth family of protein tyrosine phosphatases is characterized by using aspartic acid insted of cysteine and their dependence on cations (Rayapureddi *et al.*, 2003;Tootle *et al.*, 2003;Li *et al.*, 2003). In humans, Eya proteins with Tyr or Ser/Tyr phosphatase activity belong to this fourth family (Alonso *et al.*, 2004).

In this thesis, I deal with the Class I Cys-based tyrosine phosphatases only. As I successfully implemented method of Burridge and Nelson for detection of phosphatase activities of nonreceptor protein tyrosine phosphatases in polyacrylamide gels (Burridge and Nelson, 1995), my experiments focused almost exclusively on this phosphatase subfamily. Those known to be expressed in mast cells and basophils are shown in fig. 2. The details regarding their interaction partners and their role in mast cell physiology were described by us in (Heneberg and Dráber, 2002b) just one year before start of my Ph.D. studies, thus I advert to that paper instead of unwinding the long story again.

## 3.5 ACTIN CYTOSKELETON

Actin is the most abundant eukaryotic cell protein constituting approximately 5 %, in muscle cells even 20% of its total protein content. Generally, it controlls the cell shape, migration, and spatiotemporal distribution of most of the cellular organels. Actin exists in two forms – a globular monomer called G-actin and filamenous polymer called F-actin. In the presence of high salts, G-actin polymerize into F-actin. Actin polymerization may be dysregulated by number of drugs. The most frequently used are cytochalasins and latrunculins disrupting actin filaments, or phalloidins and jasplakinolide stabilizing filaments.

All the drugs mentioned above are of the natural origin. Cytochalasins, a group of cell-permeable fungal metabolites, functionally resemble capping proteins as they block the barbed end of actin filaments causing their shortening (Cooper, 1987). Latrunculins were isolated first from the Red Sea sponge *Latrunculia magnifica* currently called *Negombata magnifica*. Latrunculins sequester monomeric actin by mimicking the activity of monomer sequestering proteins. It was suggested that latrunculin A binds to actin in the cleft between subdomains 2 and 4 of actin (Ayscough *et al.*, 1997), which blocks adenine nucleotide exchange on actin and binding of thymosine $\beta_4$. Phallotoxins are a group of bicyclic heptapeptides present in mushrooms. Phalloidin itself is a very toxic polypeptide isolated mainly from *Amanita phalloides* (*Agaricaceae*) called death cup, causing fatal liver, kidney and central nerve system damage. It binds to actin filaments much more tightly than to actin monomers and shifts the equilibrium between filaments and monomers toward filaments. Fluorescent derivatives of phalloidin have been extremely useful in fluorescence microscopy of cellular actin *in vitro* (Cooper, 1987) even though phalloidin is unable to permeate the cell membranes directly, only using pinocytosis or after artificial permeabilization (Meier-Abt *et al.*, 2004). The last mentioned drug, jasplakinolide, is a potent inducer of actin polymerization both *in vitro* and *in vivo*. It promotes both actin polymerization, and stabilizes existing actin filaments. Compared to phalloidin, jasplakinolide doesn`t stabilize actin oligomers and it can enter directly through the cellular membranes (Spector *et al.*, 1999).

In immune cells, actin polymerization is essential for mechanical properties and changes of the cell shape, but it is also involved in formation of the immunological synapse and cellular movement (Acuto and Cantrell, 2000). The first evidence that the most abundant microfilamentous structures in the cortical cytoplasm of mast cells are actin filaments emerged as early as in 1975 (Rohlich, 1975). Later it was shown that filamentous actin is present in the cortical region forming also a net-like structure surrounding granules and degranulation pores in stimulated mast cells. Patches of actin were observed also in the microvili (Tasaka *et al.*, 1986), as well as in activation-induced membrane ruffles. The amount of F-actin is increased by FcεRI- as well as by Thy-1-driven RBL cell activation (paper 1, fig. 1; Apgar, 1994). In isolated BMMC, a short few-seconds-lasting period of actin depolymerization forerun the long phase of actin polymerization similar to those of RBL cells (Heneberg, unpubl.).

Based on the results from T-cells, it seems, that adaptor proteins LAT and NTAL are responsible for the proper actin polymerization through binding of Gads and SLP-76, and further through activation of PLCγ1, binding of Nck and Vav (which activates Rho family G proteins), and for at all through promoting the interaction of Nck with WASP. WASP is a complex multidomain adaptor molecule containing sites for binding of many molecules including actin and the Arp2/3 complex, and thus enabling the initiation of actin polymerization (Bunnell *et al.*, 2001;Pivniouk *et al.*, 2003). The

importance of adaptors LAT and NTAL in initiation of actin polymerization was further corroborated using mice deficient in LAT and NTAL genes, in which the actin polymerization is impaired (Heneberg, unpubl.).

### 3.6 STAT3 IN CELL SIGNALING

A feature of many cytokines is that they engage the class of non-tyrosine-kinase cell surface receptors, which signal to the cell nucleus by activation of the JAK-STAT. Upon cytokine-induced receptor activation, monomeric cytosolic STATs are thought to be recruited to the cytoplasmic tail of the respective plasma membrane receptor, tyrosine phosphorylated by JAK family kinases, then they depart from the receptor by an unknown mechanism, dimerize, and translocate to the nucleus. In the nuclear compartment pY-STATs bind target DNA motifs and other transcription factors and thus modulate gene expression. But more recently, a couple of papers evolved (Yeung *et al.*, 1998;Lackmann *et al.*, 1998;Ndubuisi *et al.*, 1999;Sehgal, 2000) reporting that STAT proteins were present in the cytosol of mammalian cells not as free monomers but in the form of high molecular mass complexes of size 200-400 kDa and 1,000-2,000 kDa. E.g. (Ndubuisi *et al.*, 1999) shown that in human hepatoma Hep3B cells ~5-10% of total cellular STAT3 and significant amounts of pY-STAT3 were associated with a cytoplasmic membrane fraction. Later the same group showed that STATs associated with cytoplasmic membranes represent STATs contained in plasma membrane raft microdomains (Sehgal *et al.*, 2002), which is now more than controversial as our group reported in a paper included in this thesis (paper 5) exclusion of STAT3 from detergent resistant membranes.

Previous studies showed that removal of cholesterol by MβCD inhibits IL-6-induced tyrosine phosphorylation of STAT3. This was taken as an important evidence that lipid rafts are involved in IL-6 signaling (Sehgal *et al.*, 2002;Shah *et al.*, 2002). Cytokine IL-6 belongs to a family of mediators involved in the regulation of acute phase response to injury and infections (Heinrich *et al.*, 1998;Heinrich *et al.*, 2003). Dysregulation of IL-6-mediated signaling contributes to the onset and/or maintenance of several pathologies such as inflammatory bowel disease, rheumatoid arthritis or various types of cancer (Kishimoto, 2005a;Kishimoto, 2005b). IL-6 exerts its action by binding to the corresponding receptor composed of the 80 kDa ligand binding subunit (gp80, CD126) and the signal-transducing subunit (gp130, CD130). The binding leads to dimerization of gp130 and activation of protein-tyrosine kinases, JAK1&2 and Tyk2, which are constitutively associated with gp130. In turn, gp130 becomes tyrosine phosphorylated at its cytoplasmic tail and recruits transcription factors, STAT1 and STAT3. STAT3 is then phosphorylated on Y705 which is located in the conserved SH2 domain allowing homodimerization as well as heterodimerization (Taniguchi, 1995;Smith and Crompton, 1998;Haan *et al.*, 1999;O'Rourke and Shepherd, 2002;Shi *et al.*, 2006). During translocation to the nucleus, STAT3 is phosphorylated on a serine, a process which is indispensable

for full transcriptional activity. In the nucleus the STAT3 dimer binds to specific class II IL-6 responsive elements and activates the transcription of the target genes including genes of acute phase proteins (Heinrich *et al.*, 2003).

More recently, STAT3 was reported to be present in complexes with the Lyn kinase and PAG transmembrane adaptor protein in several B-cell lines and corresponding lymphoma tissues. But this association doesn`t seem to be general, as many other B-cell lines do not contain such a signalosomes. It is possible that STAT3 interaction with Lyn and PAG is responsible for the oncogenic potential of the Lyn kinase, as STAT3 might be one of prominent mediators of the signal between Lyn and cellular nucleus (Chakraborty *et al.*, 1999;Holtick *et al.*, 2005;Contri *et al.*, 2005;Sprangers *et al.*, 2006).

# 4 AIMS

The aim of this thesis was ***to contribute to elucidate some of the mechanisms of the cell signaling*** on the model of mast cells, basophils, and hepatocytes. First experiments corresponded to the topics of my master degree thesis dealing with the cloning and characterization of nonreceptor protein tyrosine phosphatases in mast cells and basophils, later I switched to more broad field of signaling through newly discovered adaptor proteins LAT and NTAL, to the communication between differen GPI-anchored proteins, surface receptors, and in part also to the role of signal transducer STAT3. Using the wide methodical background I focused to the following particular aims:

1. **To determine the role of actin in mast cell signaling *via* FcεRI and surface GPI-anchored proteins** (papers 1, 4, and 7) , focusing on:

   *identification of the phosphatase activities in immunoprecipitates of actin-associated proteins, use of FRET and actin polymerization inhibitors to understand fine topography of signaling molecules, detection of the F-actin in resting and activated cells with dysregulated expression of adaptor NTAL*

2. **To analyze the role of adaptor NTAL in mast cell signaling *via* FcεRI and Thy-1** (papers 2, 4, and 7), focusing on:

   *detection of the phosphatase activities in immunoprecipitates from NTAL$^{-/-}$ and wild-type mast cells using the phosphatase in-gel assay, flow cytometry analyses of FcεRI on NTAL$^{-/-}$ and wild-type mast cells, some of the blotting experiments, design and drawing of the signaling scheme of NTAL, LAT and Thy-1, some of the blotting experiments, flow cytometry experiments*

3. **To describe a role of reactive oxygen and nitrogen species in the regulation of mast cell PTPs** (paper 3), focusing on:

   *new aspects of the mast cell signaling using reactive oxide and nitrogen species - manuscript design and writing including design and drawing of all the schemes*

4. **To analyze the spatiotemporal distribution of surface glycoprotein Thy-1 at different levels of resolution** (paper 4), focusing on:

   *manuscript design an writing, all the flow-cytometry-based experiments including FRET analyses, Fab fragments preparation, labeling of antibodies with FITC, TRITC, and biotin, statistical analysis, design and drawing of the concluding signaling scheme*

5. **To analyze a topography of STAT3 in the signaling of freshly isolated hepatocytes and HepG2 cells** (paper 5), focusing on:

   *detection of the topography of STAT3 on IL-6-treated hepatocytes using confocal microscopy, detection of changes in the IL-6 receptor expression on MβCD-treated HepG2 cells using flow cytometry, detection of changes in the distribution of lysosomes and acidic organelles in both HepG2 cells and hepatocytes using flow cytometry*

6. **To verify that our new method for isolation of plasma membrane sheets from nonadherent cells doesn`t lead to the unintentional cell activation** (paper 6), focusing on:

   *verification that the newly created method doesn`t induce any cellular activation*

7. **To screen for the nonreceptor protein tyrosine phosphatases in mast cells and basophils and to show involvement of phosphatase PTP20 in the mast cell signalling** (paper 8), focusing on:

   *manuscript design and writing, most of the immunoprecipitation and blotting experiments, RT-PCR-based detection of new phosphatase molecules in BMMC and RBL cells, phosphatase in-gel assay, kinase assay, monoclonal and polyclonal antibody design, immunization, cloning, selection, and characterization, sucrose density gradients, sepharose gradient*

The aims and the respective papers are ordered chronologically as they were published during my Ph.D. studies. As the aims were usually solved by a group of people and their results constitute compact and indivisible entity, the contribution of the thesis author is shown below each particular aim, but the aims are presented in their whole coverage.

# 5 METHODS

During my Ph.D. studies I used a wide range of methods both used commonly at the Department of Signal Transduction or newly introduced by myself during my stay at the department. Here I show just a brief overview of methods I used. For the detailed informations regarding particular methods please check the Material and methods chapters of the papers enclosed.

### *1. Mast cell isolation and cultivation*

Rat basophilic leukemia cell line RBL-2H3, and mast cells (BMMC) derived from freshly isolated mice bone marrow were cultivated in complete media alone (RBL-2H3, Dráberová and Dráber, 1991) or in complete media supplemented with recombinant growth factors IL-3 and SCF (BMMC, Volná *et al.*, 2004). Occasionally some other cell lines were used (papers 1-8).

### *2. Measurement of mast cell degranulation*

Detection of the β-glucuronidase released into supernatant (Surviladze *et al.*, 2001). 20 µl aliquots of the supernatant were mixed with 60 µl of 40 µM 4-methylumbelliferyl β-D-glucuronide. After 60 min incubation at 37°C, the reaction was stopped by adding 200 µl of ice-cold 0.2 M glycine buffer, pH 10.0, and fluorescence was determined in microtiter plate reader Fluorostar (SLT Labinstruments GmbH, Grödig, Austria) with 365 nm excitation and 460 nm emission filters. Total cell content of the enzyme was evaluated in supernatants from cells lysed in 0.1% Triton X-100 (paper 2).

### *3. Immunoprecipitation, SDS page, immunoblotting*

Detection of the protein immunoprecipitated using protein-specific antibodies bound to protein A/G/L using SDS page followed by a western blot (Laemmli, 1970). Immunoreactivity was detected by ECL (Amersham Pharmacia, Little Chalfont, UK) on X-ray film and/or quantified by Luminiscent Image Analyzer LAS-3000 (Fuji Photo Film Co., Tokyo, Japan) (papers 1, 2, 6 & 8).

### *4. Phosphatase in-gel assay*

Highly specific enzymatic assay detecting even traces of activity of nonreceptor protein tyrosine phosphatases (paper 1, Burridge and Nelson, 1995). The assay is performed in somewhat modified polyacrylamide gel allowing to detect the exact molecular weight of the desired phosphatase and to see ladders of phosphatases associated with other molecules

during coprecipitation experiments. It was the first published usage of this method in the Czech Republic (papers 1, 2 & 8).

***5. Kinase assay***

Detection of the tyrosine kinase activity (Tolar *et al.*, 1997) of the precipitated protein tyrosine kinases (paper 8).

***6. Sucrose density gradient***

Sucrose density gradients (Hutchcroft *et al.*, 1992) used for analysis of association of the analyzed adaptor molecules, protein kinases and phosphatases (paper 8).

***7. Sepharose gradient***

Gradient used for the fractionation of the multimolecular complexes (Dráberová and Dráber, 1993). Used to proof that phosphatase PTP20 is present in different complexes than Lyn (paper 8).

***8. Confocal and fluorescence microscopy***

Used for detection of distribution of STAT3 and phosho-STAT3 in rat hepatocytes, and its changes following the cell activation (paper 5). Distribution of PTP20 in RBL cells and its changes following the aggregation of FcεRI, Thy-1, or TEC-21 (paper 8).

***9. Flow cytometry***

FcεRI level detection in differeciating bone marrow mast cells as an indicator of their maturity (paper 2), experiments with FcεRI and Thy-1 on RBL cells (paper 4), detection of IL-6 expression on HepG2 cells and hepatocytes (paper 5), detection of changes in polymeric actin content (paper 7).

***10. Fluorescence resonance energy transfer***

FRET efficiency between FITC- and TRITC-conjugated cell-bound antibodies was detected. Donor fluorescence of double-labeled samples was compared with fluorescence of samples where the acceptor antibody was replaced by non-labeled antibody to compensate for any competition between the donor and acceptor antibodies. FRET efficiency was calculated from the fractional decrease of the donor fluorescence in the presence of the acceptor. Forward and side angle light scattering were used to gate out debris and dead cells. Calculated values

for FRET efficiency were expressed as the ratio of the number of excited donor molecules, tunneling their excitation energy to the acceptor, to the number of all excited molecules. It was the first usage of this method in the Department of Signal Transduction (paper 4).

### *11. Monoclonal antibody design, immunization, cloning, selection, and characterization*

Monoclonal antibody against PTP20 was generated, characterized and transmitted to the company Exbio, s.r.o. for commercial use (paper 8, transfer protocols in chapter 6.9).

### *12. Polyclonal antibody design, immunization, and characterization*

Panel of rabbit polyclonal antibodies was prepared against some of the phosphatase molecules (paper 8).

# 6 RESULTS

**6.1**

**Tolarová, H.; Dráberová, L.; Heneberg, P. & Dráber, P. (2004):**

**Involvement of filamentous actin in setting the threshold for degranulation in mast cells.**

**European Journal of Immunology 34(6): 1627-1636.**

# Involvement of filamentous actin in setting the threshold for degranulation in mast cells

**Helena Tolarová, Lubica Dráberová, Petr Heneberg and Petr Dráber**

Department of Signal Transduction, Institute of Molecular Genetics, Academy of Sciences of the Czech Republic, Prague, Czech Republic

Previous studies using cytochalasins and latrunculin B, inhibitors of actin polymerization, showed that filamentous (F)-actin had a negative regulatory role in Fcε receptor I (FcεRI) signaling. How F-actin is involved in regulating the activation of mast cells is unknown. In this study we investigated the role of F-actin in mast cell activation induced by aggregation of the glycosylphosphatidylinositol (GPI)-anchored proteins Thy-1 and TEC-21, and compared it to activation via FcεRI. Pretreatment of rat basophilic leukemia cells with latrunculin B inhibited the Thy-1-induced actin polymerization and elevated the Thy-1-mediated secretory and calcium responses. Inhibition of actin polymerization followed by Thy-1 aggregation resulted in an increased tyrosine phosphorylation of Syk, phospholipase Cγ (PLCγ), Gab2 and linker for activation of T cells (LAT) adapters, and some other signaling molecules. Enzymatic activities of phosphatidylinositol 3-kinase, PLCγ, and phosphatase SHP-2 were also upregulated, but tyrosine phosphorylation of ezrin was inhibited. Similar changes were observed in FcεRI-activated cells. Significant changes in intracellular distribution, tyrosine phosphorylation, and/or enzymatic activities of signaling molecules occurred in latrunculin-pretreated cells before cell triggering. The combined data suggest that actin polymerization is critical for setting the thresholds for mast cell signaling via aggregation of both FcεRI and GPI-anchored proteins.

| | |
|---|---|
| Received | 6/2/04 |
| Revised | 17/3/04 |
| Accepted | 31/3/04 |

**Key words:** Mast cell / Signal transduction / Fc receptor / Protein kinase / Phosphatase

## 1 Introduction

Aggregation of the Fcε receptor I (FcεRI) on mast cells and basophils, as well as other immunoreceptors on other cell types, by natural ligands or Ab initiates tyrosine phosphorylation of the receptor subunits, recruitment of signaling molecules, and their translocation to various compartments of the cell [1]. In addition to enzymes, such as kinases and phosphatases, other molecules play a critical role in this process, including adapters and components of the cytoskeleton.

Previous studies have shown that pretreatment of rat basophilic leukemia (RBL) cells, which have been extensively used as a model for analysis of mast cell activation, with inhibitors of actin polymerization, such as cytochalasin D and latrunculin B, enhances the FcεRI-mediated $Ca^{2+}$ mobilization and degranulation [2, 3]. Cytochalasin D, which inhibits actin polymerization by capping the barbed end of actin filaments and preventing their elongation [4], enhanced both the early and the late events in FcεRI-induced mast cell signaling [2]. In contrast, latrunculin, which inhibits actin polymerization by sequestering the monomeric actin [5], had no effect on degranulation induced by activation of the cells with A23187 and PMA or pervanadate, suggesting that it acts mainly on early stages of FcεRI signaling [2]. Further experiments showed an increased tyrosine phosphorylation of FcεRI and Syk in latrunculin-pretreated and Ag-stimulated cells, and suggest that filamentous (F)-actin negatively regulates the interaction of aggregated FcεRI with Lyn kinase and thus the initiation of signaling pathways [2].

Mast cells and RBL cells can also be activated by aggregation of the glycosylphosphatidylinositol (GPI)-anchored proteins Thy-1 and TEC-21 [6–8]. This activation is independent of the surface expression of FcεRI [9] and tyrosine phosphorylation of FcεRI subunits [8], and

[DOI 10.1002/eji.200424991]

**Abbreviations:** **$[Ca^{2+}]_i$:** Concentration of free cytoplasmic $Ca^{2+}$ **F-actin:** Filamentous actin **GEM:** Glycosphingolipid-enriched membrane microdomains **GPI:** Glycosylphosphatidylinositol **HRP:** Horseradish peroxidase **$IP_3$:** Inositol 1,4,5-triphosphate **LAT:** Linker for activation of T cells **PI3K:** Phosphatidylinositol 3-kinase **$PIP_3$:** Phosphatidylinositol 3,4,5-triphosphate **PLCγ:** Phospholipase Cγ **RBL:** Rat basophilic leukemia **SH2:** Src homology-2

 

seems to reflect indirect interactions of these proteins with Lyn kinase within the glycosphingolipid-enriched membrane microdomains (GEM) [8, 10]. It has been suggested that these microdomains are also involved in FcεRI signaling [11].

To gain more insight in the role of actin filaments in mast cell signaling, we investigated early activation events initiated by aggregation of Thy-1 or TEC-21 in latrunculin-pretreated cells, and compared them to those induced by aggregation of FcεRI. Since increased calcium and secretory responses in latrunculin-pretreated cells occurred within seconds after Ag exposure, we also analyzed the changes in subcellular distribution and other properties of the signaling molecules immediately preceding the mast cell triggering and sensitization with Ab.

## 2 Results

### 2.1 Enhanced Thy-1-mediated secretory and calcium responses in latrunculin-pretreated cells

Previous studies showed that inhibition of F-actin polymerization correlated with enhanced calcium and secretory responses in Ag-activated RBL-2H3 cells, and suggested that GEM could be involved in this process [2, 3]. Because the Thy-1 glycoprotein seems to be one of the major protein components of the exoplasmic leaflet of GEM in RBL cells and since its aggregation also induces cell activation, we decided to find out whether the Thy-1-mediated secretory response is also promoted by latrunculin. First we determined the changes in F-actin polymerization in Thy-1-activated cells. For these experiments the biotinylated anti-Thy-1.1 mAb-sensitized RBL cells were pre-incubated without or with 0.5 μM latrunculin and then exposed to streptavidin to induce Thy-1 aggregation. Data presented in Fig. 1A show that aggregation of Thy-1 caused a rapid increase in the level of detergent-insoluble F-actin with a maximum attained at 1 min (1.8-fold increase), followed by a slow decline to basal levels. There was an approximately 25% inhibition of detergent-insoluble F-actin basal levels in latrunculin-pretreated cells, and Thy-1 aggregation induced only a moderate increase in the amount of F-actin. Interestingly, the Thy-1 aggregation induced a prompter and more extensive formation of detergent-insoluble F-actin than aggregation of FcεRI-IgE complexes with TNP-BSA (Fig. 1B).

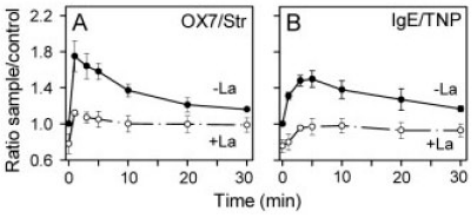


*Fig. 1.* Actin polymerization in latrunculin-pretreated and Thy-1- or FcεRI-activated cells. RBL cells in suspension were sensitized with biotinylated anti-Thy-1 (OX7) mAb (A) or TNP-specific IgE (B), and then exposed (+La) or not (-La) to latrunculin (0.5 μM, 15 min, 37°C). The cells were activated for the indicated time intervals with (A) streptavidin (Str, 10 μg/ml) or (B) TNP-BSA (TNP, 1 μg/ml). The amount of F-actin was determined by flow cytofluorometry. Means ± SD were calculated from three independent experiments.

In accordance with published data [2], 0.5 μM latrunculin alone did not cause any degranulation in RBL cells. Only weak and variable secretory responses were observed in OX7-sensitized and latrunculin-pretreated cells. However, an exposure to latrunculin followed by Thy-1 aggregation resulted in a dramatic degranulation response. Thus, although in control cells the Thy-1 activation for 5 min released approximately 14% of β-glucuronidase, more than 50% was released in latrunculin-pretreated and Thy-1-activated cells. Significant differences between control and latrunculin-pretreated cells were already noticeable at the first time interval analyzed (1 min), indicating that very early activation events are affected (Fig. 2A). Although the extent of degranulation in control cells was lower in Thy-1-activated than in FcεRI-

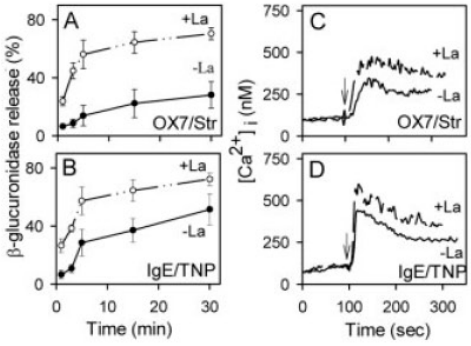


*Fig. 2.* Degranulation and calcium responses. RBL cells were sensitized with biotinylated OX7 mAb (A, C) or TNP-specific IgE (B, D), and then exposed (+La) or not (–La) to latrunculin. The cells were activated with streptavidin (A, C) or TNP-BSA (B, D). The activators were added at time 0 min (A, B) or as indicated by arrows (C, D). The amount of β-glucuronidase released into supernatant (A, B) and $[Ca^{2+}]_i$ (C, D) were determined at various time intervals. Means ± SD were calculated from three to four experiments performed in duplicates (A, B). Representatives of four to six independent experiments are shown in (C, D).

activated cells, the secretory responses in latrunculin-pretreated cells were comparable (Fig. 2A, B).

The differences between control and latrunculin-pretreated cells were confirmed by measurements of free cytoplasmic $Ca^{2+}$ ($[Ca^{2+}]_i$). Again, aggregated Thy-1 induced a quicker and more extensive calcium response in latrunculin-pretreated cells than in control cells (Fig. 2C). However, in contrast to the secretory response, the calcium response in latrunculin-pretreated cells was lower in Thy-1- than in Ag-stimulated cells (Fig. 2D). The enhanced secretory and calcium responses in latrunculin-pretreated cells were not specific for Thy-1- or FcεRI-induced activation, because they were also observed in RBL cells stimulated via TEC-21 glycoprotein (not shown). These data suggest that pretreatment with latrunculin generally enhances the activation induced via FcεRI and GPI-anchored proteins.

### 2.2 Is FcεRI involved in latrunculin-elevated Thy-1 signaling?

The similarity between secretory and calcium responses in latrunculin-pretreated cells triggered by means of Thy-1, TEC-21, or FcεRI suggested that in the absence of stimulated actin polymerization it might be FcεRI that is involved in Thy-1-mediated signaling. Physical interaction between FcεRI and GPI-anchored proteins was analyzed by equilibrium ultracentrifugation in sucrose gradients. Most of the Thy-1 glycoprotein from cells solubilized with 1% Triton X-100 (Fig. 3A) or 0.06% Triton X-100 (not shown) was found in low-density fractions of sucrose gradient (fractions 3–10, corresponding to 15–30% sucrose). A significant amount of Thy-1 was also detected in fraction 23 containing cytoskeleton/nuclear remnants. After pretreatment of the cells with latrunculin, the proportion of Thy-1 in low-density fractions increased and the peak showed a slight shift to the high-density fractions; a corresponding decrease of Thy-1 content in high-density fractions was observed.

In contrast to Thy-1, the majority of FcεRI in unstimulated cells either untreated (Fig. 3B) or pretreated with latrunculin (not shown) was found in high-density fractions. After FcεRI aggregation most of the receptors were associated with low-density fractions, and latrunculin had no significant effect on this distribution except that there was a reduced amount of FcεRI associated with fraction 23. As described before [3, 8, 11], association of aggregated FcεRI with low-density fractions was only observed in cells solubilized with 0.06% Triton X-100. Interestingly, there was no increased association of FcεRI with low-density fractions in cells pretreated with latrunculin, activated via Thy-1, and solubilized in 0.06%

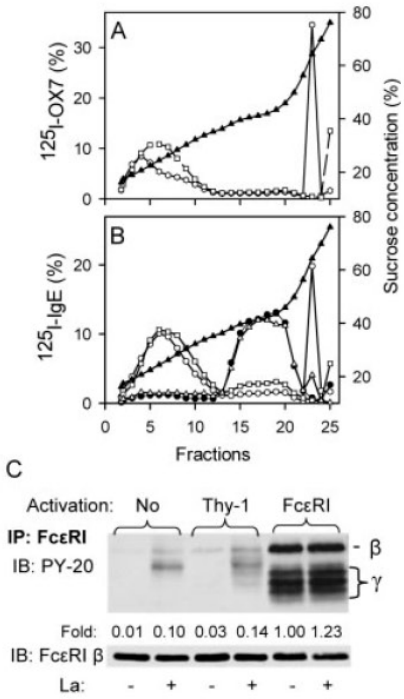


*Fig. 3.* Sucrose density gradient profiles and tyrosine phosphorylation of FcεRI. (A) RBL cells were incubated (squares) or not (circles) with latrunculin, then exposed to $^{125}$I-OX7 mAb (0.1 μg/ml) for 5 min, and lysed in a lysis buffer containing 1% Triton X-100. (B) $^{125}$I-IgE-primed cells were pretreated (open squares) or not (circles) with latrunculin, then stimulated (open squares and circles) or not (filled circles) with rabbit anti-IgE (10 μg/ml) for 5 min, and lysed in a lysis buffer containing 0.06% Triton X-100. Alternatively, $^{125}$I-IgE-primed cells were incubated with latrunculin and then with biotinylated OX7 mAb (5 μg/ml) for 10 min at 37°C. After washing, Thy-1-OX7 complexes were aggregated by streptavidin (10 μg/ml) for 5 min at 37°C followed by lysis in 0.06% Triton X-100 (open triangles). Total cell lysates were fractionated by ultracentrifugation for 4 h. Points show the percentage of total cpm present in individual fractions (left axes) and sucrose concentrations (filled triangles, right axes). Data represent a typical experiment from three performed. (C) Control (–) or latrunculin-pretreated (+) cells were unstimulated (No) or stimulated with biotinylated OX7 and streptavidin (Thy-1), or with IgE and TNP-BSA complexes (FcεRI), and lysed in lysis buffer containing 0.2% Triton X-100. FcεRI was immunoprecipitated (IP) and analyzed by immunoblotting (IB) with HRP-PY-20 mAb, followed by stripping and immunoblotting with anti-FcεRI **β** subunit. The positions of FcεRI **β** and **γ** subunits and the fold induction of FcεRI **β** subunit tyrosine phosphorylation, corrected for the amount of FcεRI **β** subunit and normalized to FcεRI-activated but latrunculin-untreated cells, are also shown. A typical result from four experiments performed is presented.

 

Triton X-100 (Fig. 3B, open triangles). These data suggested that F-actin polymerization had no effect on physical association of aggregated Thy-1 with FcεRI. Thus the enhanced calcium/secretory responses observed in latrunculin-pretreated and Thy-1-activated cells cannot be simply explained by an increased physical association of FcεRI with GEM.

Tyrosine phosphorylation of the β and γ subunits of FcεRI is the earliest known event occurring after FcεRI engagement, and is enhanced by inhibitors of actin polymerization [2, 3]. To determine the extent of tyrosine phosphorylation of β and γ subunits under different conditions, FcεRI was immunoprecipitated from control or latrunculin-pretreated cells which were either nonsensitized and non-activated or activated via Thy-1 or FcεRI, and then solubilized with 0.2% Triton X-100, which preserves the association of FcεRI subunits. Immunoblotting analyses showed that latrunculin alone induced a weak increase in tyrosine phosphorylation of FcεRI β subunit in non-activated or Thy-1-activated cells (Fig. 3C). In contrast, FcεRI-activated cells exhibited strong tyrosine phosphorylation of both FcεRI subunits, further elevated by latrunculin exposure. These data indicate that latrunculin causes an increase in tyrosine phosphorylation of FcεRI subunits not only in activated but also in non-activated cells. The possibility that latrunculin might potentiate the secretory response independently of FcεRI was also supported by data showing 2.2±0.3-fold increase (mean ± SD, $n$=4) of β-glucuronidase release from Thy-1-activated (30 min) RBL-γ⁻c.1 cells, defective in the expression of surface FcεRI [9], after pretreatment with latrunculin.

### 2.3 Early activation pathways

The rapid increase in calcium and secretory responses in latrunculin-pretreated and Thy-1-, TEC-21- or FcεRI-activated cells suggested that latrunculin affected the early biochemical events common for all these activation pathways. In an attempt to determine which pathways are primarily affected, we first analyzed tyrosine phosphorylation of Syk. This kinase becomes rapidly phosphorylated in Thy-1- [12], TEC-21- [8] or FcεRI- [13] activated RBL cells, and has already been shown to exhibit an increased tyrosine phosphorylation in latrunculin-pretreated and FcεRI-activated cells [2]. Immunoblotting analysis showed that phosphorylation of Syk was slightly increased by latrunculin alone, *i.e.* in non-activated cells (Fig. 4A, B, 0 min). This increase was not attributable to the binding of anti-Thy-1 or IgE to the cells because a similar increase in Syk phosphorylation was also observed in latrunculin-treated but nonsensitized cells (not shown). Thy-1-mediated tyrosine phosphorylation of

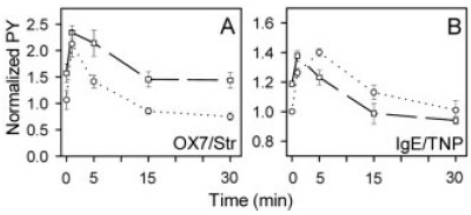


*Fig. 4.* Tyrosine phosphorylation of Syk and LAT. RBL cells were sensitized with biotinylated OX7 (A) or TNP-specific IgE (B), exposed or not to latrunculin and activated with streptavidin (A) or TNP-BSA (B), for the indicated time intervals. The cells were lysed in a buffer containing 1% Triton (for Syk) or 1% n-dodecyl β-D-maltoside (for LAT). Syk and LAT were immunoprecipitated and analyzed by immunoblotting with HRP-PY-20 and with the corresponding protein-specific Ab. Values of tyrosine-phosphorylated Syk (squares; means ± SD, $n$=3) and LAT (circles; means ± SD, $n$=4) were corrected for the total amount of proteins, and normalized to values obtained in latrunculin-untreated cells analyzed at identical time intervals.

Syk was enhanced by latrunculin with a peak at 1 min after cell triggering. At later time intervals the difference between control and latrunculin-pretreated cells diminished but remained significant even after 30 min.

Next, we analyzed changes in phosphorylation of the Syk substrate, linker for activation of T cells (LAT). Tyrosine phosphorylation of this adapter molecule in non-stimulated cells was identical in both control and latrunculin-pretreated cells. After Thy-1 triggering the phosphorylation of LAT was enhanced by latrunculin; this stimulatory effect was transient (peak at 1 min) and disappeared after 15 min. In FcεRI-activated cells (Fig. 4B), latrunculin had a similar effect on Syk and LAT, except that the enhanced Syk phosphorylation was more transient and the enhanced LAT phosphorylation extended for more than 15 min. We also analyzed the effect of latrunculin on Lyn kinase activity. However, in three independent immunocomplex kinase assays with enolase as a substrate we saw no change in Lyn kinase activity (not shown). These data suggested that rather than inducing changes in Lyn kinase activity, latrunculin might affect Lyn topography with respect to its substrates.

### 2.4 Changes in cellular distribution and properties of signaling molecules

In further experiments we investigated the spatial distribution and properties of signaling molecules in cells sequentially solubilized with saponin and Triton X-100. In this procedure, the cells are first permeabilized on ice

 

with saponin, free cytoplasmic components are washed away, and the cellular ghosts are subsequently solubilized in Triton X-100. Our previous results showed that the procedure solubilized the plasma membrane components more efficiently than other methods routinely used for extraction of membrane proteins, and allowed a better assessment of the formation of large macromolecular complexes in the course of FcεRI signaling [14, 15].

Using this method we first analyzed the distribution and tyrosine phosphorylation of phospholipase Cγ (PLCγ), whose activity seems to be negatively regulated by F-actin, as suggested by an increased amount of inositol 1,4,5-triphosphate ($IP_3$) produced in latrunculin-pretreated and Thy-1- or FcεRI-activated cells (Fig. 5A, B). We found that both the tyrosine phosphorylation and the amount of PLCγ1 and PLCγ2 associated with saponin-permeabilized cells were increased in Thy-1-activated cells (Fig. 5C). Interestingly, latrunculin alone (0 min) induced an increased association of both enzymes with cellular ghosts. In Thy-1-activated cells, latrunculin further enhanced the phosphorylation of PLCγ1, particularly 30 s after Thy-1 triggering, but had no effect on PLCγ2. Increased association of PLCγ1 and PLCγ2 with macromolecular complexes was also observed in latrunculin-pretreated and IgE-sensitized cells (0 min).

These experiments were extended to several other signaling molecules [paxillin, ezrin, phosphatidylinositol 3-kinase (PI3K), Gab2 adapter and SHP-2 phosphatase] which are involved in mast cell signaling and could potentially be affected by F-actin. Paxillin is a 68-kDa cytoskeletal protein that accumulates at focal adhesion sites. It has already been shown that aggregation of FcεRI in RBL cells results in increased tyrosine phosphorylation of paxillin and its cytoplasmic redistribution [16]. In Thy-1- or FcεRI-activated cells paxillin showed an increased association with large macromolecular complexes (Fig. 6). Latrunculin alone (0 min) also enhanced this association. In FcεRI-activated cells pretreatment with latrunculin increased tyrosine phosphorylation of paxillin, suggesting an increased activity and/or changes in topography of the corresponding kinases. Interestingly, aggregation of Thy-1 induced more dramatic changes in the distribution of paxillin than did FcεRI aggregation.

Tyrosine phosphorylation of ezrin, a compound which functions as a linker between the actin skeleton and integral plasma membrane proteins [17], was strongly inhibited by pretreatment with latrunculin in both Thy-1- and FcεRI-activated cells. This inhibition was not attributable to a decreased amount of ezrin immunoprecipitated from saponin/Triton X-100-solubilized cells, as inferred from the results of immunoblotting with anti-ezrin Ab (Fig. 6).

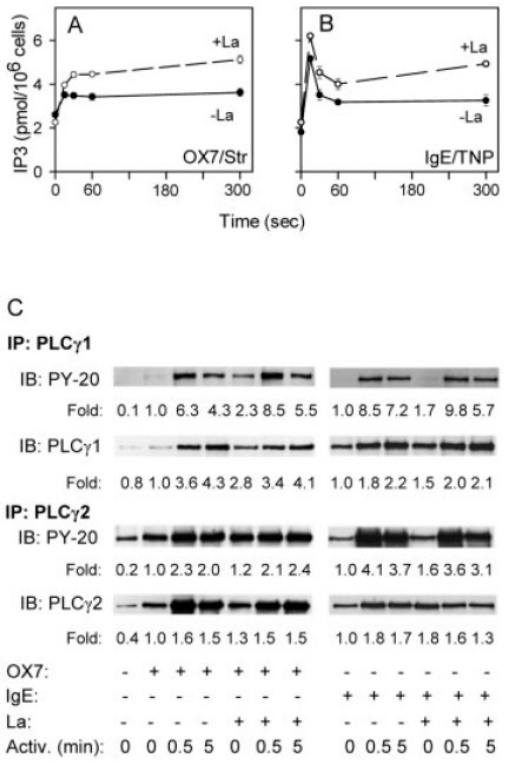


*Fig. 5.* Enzymatic activity, tyrosine phosphorylation, and cytoplasmic location of PLCγ. (A, B) RBL cells were sensitized, exposed (+La) or not (–La) to latrunculin and activated via Thy-1 (A) or FcεRI (B). Samples were collected at indicated time intervals after triggering and the amount of $IP_3$ was determined. Means ± SD of two independent experiments performed in duplicates are presented. (C) The cells were sensitized or not with biotinylated OX7 or IgE, exposed or not to latrunculin and activated (Activ.) with streptavidin (OX7) or TNP-BSA (IgE) for the indicated time intervals. Then the cells were permeabilized with saponin, and the "empty cells" solubilized with 1% Triton X-100. PLCγ1 and PLCγ2 were immunoprecipitated from postnuclear supernatants and analyzed by immunoblotting with HRP-PY-20 and the corresponding protein-specific Ab. Relative amounts of the immunoprecipitated PLCγ1 and PLCγ2 and their tyrosine phosphorylations were determined by densitometry analysis of the corresponding immunoblots and normalized to sensitized but non-activated cells. Typical results from three to five experiments are shown.

Early activation events in mast cells are dependent on the activity of PI3K. PI3K catalyzes the synthesis of phosphatidylinositol 3,4,5-triphosphate ($PIP_3$) and phos-

 

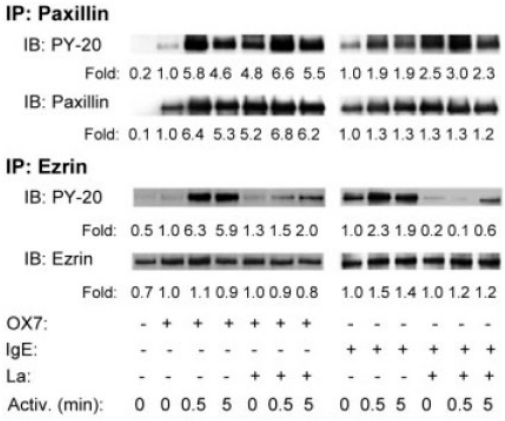


*Fig. 6.* Tyrosine phosphorylation and cytoplasmic location of paxillin and ezrin. The cells were sensitized with biotinylated OX7 or IgE, exposed to latrunculin, and activated via Thy-1 or FcεRI as shown. At the indicated time intervals the cells were extracted by saponin/Triton X-100. Paxillin and ezrin were immunoprecipitated and analyzed by immunoblotting with HRP-PY-20 and anti-paxillin or anti-ezrin Ab. Relative amounts of the immunoprecipitated proteins and their tyrosine phosphorylation were determined by densitometry and normalized to sensitized but non-activated cells. Typical results from two to four experiments are shown.

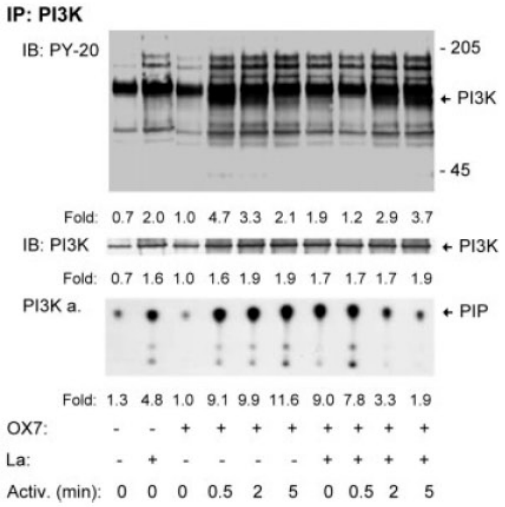


*Fig. 7.* PI3K immunocomplexes from Thy-1-activated cells. The cells were sensitized with biotinylated OX7, exposed to latrunculin, and/or activated via Thy-1 as shown. At the indicated time intervals the cells were extracted with saponin/Triton X-100, and the proteins immunoprecipitated with Ab specific for the p85 subunit of PI3K. The immunoprecipitates were divided into two parts. One part was analyzed by immunoblotting with HRP-PY-20 and anti PI3K-p85. The second part was analyzed for PI3K activity (PI3 K a.) using thin-layer chromatography and phosphatidylinositol (PI) as a substrate; position of [$^{32}$P]PI (PIP) is indicated by arrow. Relative amounts of the immunoprecipitated proteins, their tyrosine phosphorylations, and PI3K activity were determined and normalized to OX7-sensitized, latrunculin untreated and streptavidin-non-activated cells. Typical results from at least four experiments performed are shown.

phatidylinositol 3,4-biphosphate, and functionally interacts with Gab2, SHP-2, and several other proteins [18]. We therefore monitored in control and Thy-1-activated cells the subcellular distribution of PI3K, its enzymatic activity, and the tyrosine phosphorylation of both PI3K and associated molecules (Fig. 7). When PI3K was immunoprecipitated from control (nonsensitized) saponin/Triton X-100-solubilized cells, its amount significantly rose after an exposure of the cells to latrunculin (2.3±0.4-fold increases, mean ± SD, $n$=4). Furthermore, latrunculin alone reproducibly increased the amount of tyrosine-phosphorylated proteins associated with PI3K and the enzymatic activity of PI3K as detected by immunocomplex kinase assay. Enzymatic activity of PI3K in OX7-sensitized cells was increased ninefold after pretreatment of the cells with latrunculin (0 min). Aggregation of Thy-1-biotinylated OX7 complexes with streptavidin induced no further increase in PI3K activity; in fact it reduced it, especially at later time intervals (2 and 5 min). PI3K complexes isolated from IgE-sensitized cells exhibited similar properties, namely that PI3K activity remained low in IgE-sensitized cells and was dramatically increased by latrunculin pretreatment even in the absence of FcεRI aggregation (not shown).

Previous studies showed that multiple signaling molecules could be assembled by Gab2 scaffolding protein [18]. Tyrosine-phosphorylated Gab2 provides the binding sites for Src homology-2 (SH2) domain-containing proteins, including the p85 subunit of PI3K, PLCγ, and phosphatase SHP-2. Gab2 immunoprecipitation experiments showed a rapid association of Gab2 with macromolecular complexes in Thy-1-activated cells at all time intervals studied (Fig. 8). Latrunculin alone (in nonsensitized and non-activated cells) promoted association of Gab2 with saponin-permeabilized cells, but reduced its association with the complexes after Thy-1 triggering. The PI3K activity associated with immunoprecipitated Gab2 was increased by latrunculin in both non-activated and Thy-1-activated cells.

To determine whether there are any changes in phosphatases associated with Gab2, we probed the Gab2 immunocomplexes by immunoblotting and in-gel phosphatase assay. Data presented in Fig. 8 (bottom) show that latrunculin alone significantly enhanced the amount of

 

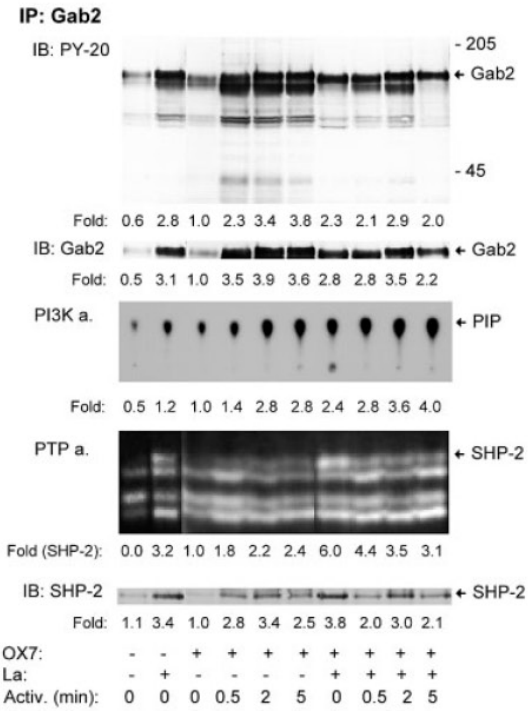


*Fig. 8.* Gab2 immunocomplexes from Thy-1-activated cells. The cells were sensitized with biotinylated OX7, exposed to latrunculin, and/or activated via Thy-1 as shown. At the indicated time intervals the cells were extracted with saponin/Triton X-100, and the proteins immunoprecipitated (IP) with anti-Gab2 Ab. The immunoprecipitates were divided into three parts. One part was analyzed by immunoblotting (IB) with HRP-PY-20, anti-Gab2, and anti-SHP-2. The second part was analyzed for PI3K activity (PI3K a.), and the third part was analyzed by in-gel assay for the presence of a phosphatase activity (PTP a.). Relative amounts of the immunoprecipitated proteins, their tyrosine phosphorylations, and enzymatic activities were determined and normalized to OX7-sensitized, latrunculin-untreated and non-activated cells. Typical results from at least two experiments are shown.

SHP-2 immunoprecipitated with Gab2, and also increased the activity of a phosphatase with molecular weight corresponding to SHP-2. Immunodepletion experiments confirmed that this was indeed SHP-2. The phosphatase activity associated with Gab2, namely SHP-2, was elevated in OX7-sensitized cells and was further enhanced after Thy-1 aggregation. In OX7-sensitized and latrunculin-pretreated cells, SHP-2 phosphatase activity was further enhanced, but declined slightly after Thy-1 triggering (Fig. 8). Gab2 immunocomplexes isolated from IgE-sensitized but non-activated cells also exhibited an increased amount of Gab2 and enhanced activity of PI3K and SHP-2 after exposure to latrunculin (not shown).

## 3 Discussion

Data presented in this study indicate that pretreatment of RBL cells with latrunculin caused a significant decrease in the basal level of F-actin, and comparably inhibited actin polymerization induced by aggregation of both Thy-1 and FcεRI. Inhibition of actin polymerization correlated with increased calcium and secretory responses not only in FcεRI-activated cells, as has already been described [2], but also in Thy-1-activated cells, supporting thus the notion that these two activation pathways employ similar signaling modules [7, 19]. The relatively low secretory and calcium responses in Thy-1-activated cells could be an outcome of more stringent regulation of Thy-1 by F-actin; when actin polymerization is inhibited and the amount of F-actin reduced, the differences between Thy-1 and FcεRI activation pathways disappear.

The similarity between Thy-1- and FcεRI-mediated activation pathways in latrunculin-pretreated cells could imply that FcεRI is involved in both these activation pathways. However, our finding that a pretreatment with latrunculin followed by Thy-1 aggregation did not enhance the association of the receptor with GEM suggests that Thy-1 is not physically associated with FcεRI under these conditions and that Thy-1 could initiate mast cell signaling in the absence of FcεRI. This conclusion is supported by the results of our previous studies in which Thy-1-mediated activation of RBL cells was observed even in the absence of FcεRI expression [9, 12], and by the finding of an increased Thy-1-mediated activation of latrunculin-pretreated FcεRI-defective cells (this study). Interestingly, latrunculin alone induced a weak tyrosine phosphorylation of FcεRI β subunit (Fig. 3C, see also [2]), suggesting that microfilaments are involved in this process. Our finding that latrunculin pretreatment did not change the activity of Lyn kinase as determined by immunocomplex kinase assays is consistent with a key role of Lyn topography in initiation of cell signaling.

Latrunculin dramatically affected, although in an opposite manner, the distribution and tyrosine phosphorylation of two cytoskeletal proteins, paxillin and ezrin. Paxillin was poorly immunoprecipitated from control saponin-permeabilized cells, but its amount significantly increased after FcεRI triggering (Fig. 6). It is remarkable that paxillin redistribution was observed not only in activated cells (with elevated F-actin levels), but also in cells pretreated with latrunculin alone (with reduced F-actin levels), a clear indication of a complex regulatory role of

 

F-actin in this process. Increased binding of paxillin to activated and permeabilized cells could reflect an interaction of Lyn-SH2 domain with tyrosine-phosphorylated paxillin [20]. It is tempting to speculate that this *trans* interaction could locally increase the Lyn kinase activity by blocking the *cis* interaction of Lyn-SH2 domain with Lyn C-terminal phosphotyrosine [21], and could thus contribute to enhanced tyrosine phosphorylation of FcεRI and subsequent signaling molecules.

In contrast to paxillin, ezrin failed to exhibit any substantial changes in its association with large complexes in the course of Thy-1 or FcεRI signaling, and this association was not affected by F-actin levels. On the other hand, tyrosine phosphorylation of ezrin dramatically increased in Thy-1-/FcεRI-activated cells and was almost completely blocked by latrunculin. Ezrin, as well as other members of the ezrin/radixin/moesin (ERM) family of proteins, can mediate the anchoring of some transmembrane proteins to the actin skeleton. ERM proteins interact with the plasma membrane proteins through their N-terminal domain, and with the actin cytoskeleton through their C-terminal domain. The decreased phosphorylation of ezrin in latrunculin-pretreated cells suggests that ezrin is a negative regulator of Thy-1/FcεRI signaling in mast cells. This conclusion is strengthened by the results of studies on B cell receptor activation documenting an increased tyrosine phosphorylation of ezrin accompanied by an inhibition of Syk tyrosine phosphorylation and calcium mobilization response [22].

Several lines of evidence presented in this study show that actin filaments contribute to spatial distribution and/or functional properties of other signaling molecules, including PI3K, Gab2, and SHP-2. PI3K catalyzes the synthesis of $PIP_3$, which is involved in recruiting the molecules with pleckstrin homology to the plasma membrane. Importantly, the activity of PI3K associated with macromolecular complexes was dramatically increased in cells pretreated with latrunculin alone, reaching levels observed in Thy-1-/FcεRI-activated cells. Although the activity of PI3K in latrunculin-pretreated cells was not further enhanced by Thy-1/FcεRI triggering, the high initial activity levels may be sufficient to promote strong and rapid activation responses. It has been shown that the p85 subunit of PI3K from epithelial cells interacted with tyrosine-phoshorylated ezrin, and that this interaction increased the PI3K enzymatic activity [23]. Tyrosine phosphorylation of ezrin is inhibited in latrunculin-pretreated cells (see above), and PI3K could therefore preferentially bind to another substrate, *e.g.* Gab2, an event which would presumably result in an enhanced PI3K activity. In fact, we have found that inhibition of actin polymerization led to an increased association of Gab2 with large signaling complexes and that these complexes were enriched of PI3K and SHP-2 (Fig. 8).

An important question is how the actin filaments regulate the activation via GPI-anchored proteins and FcεRI. A previous study [3] showed that inhibition of actin polymerization stimulated FcεRI-mediated tyrosine phosphorylation of several substrates, sustained for many tens of minutes; this implied that actin polymerization regulated the kinetics of Ag-induced tyrosine phosphorylation by modulating the lifetime of FcεRI-Lyn interactions. In contrast, our work shows that inhibition of actin polymerization with latrunculin induced a formation of signaling complexes even in non-activated cells. This leads us to postulate that latrunculin-induced changes in topography and/or activity of signaling molecules before cell triggering are responsible, at least in part, for prompter and more extensive activation observed after Thy-1/TEC-21 or FcεRI engagement. It should be noted that formation of signaling assemblies was observed not only in OX7- or IgE-sensitized cells, but also in nonsensitized cells; these findings exclude the possibility that latrunculin potentiated the formation of signaling complexes initiated by Thy-1 dimers or FcεRI oligomers produced by IgE aggregates present in IgE preparations.

Adhesion of mast cells to the extracellular matrix is essential for their development and function in allergic responses, as well as for innate immunity [24]. These interactions provide bi-directional signals resulting on one hand in the induction of mast cell proliferation and activation and, on the other hand, in the release of mediators from activated mast cells affecting the outcomes of inflammatory reactions. Experimental findings which are presented here and are complementary to previously published results (for references see Sect. 1), namely that cell adherence modulates the activation of RBL cells [25], that the engagement of surface receptors enhances actin polymerization, and that inhibition of actin polymerization increases the readiness of the cells to become activated, support the concept that actin filaments contribute to the setting of dynamic threshold for mast cell signaling. This notion is also supported by our unpublished data indicating that latrunculin enhances FcεRI-mediated secretory and calcium responses in mouse bone marrow-derived mast cells.

## 4 Materials and methods

### 4.1 Ab and reagents

The origins of mAb specific for Thy-1.1 (0X7), Syk kinase, Lyn kinase, LAT adaptor, TEC-21, FcεRI β subunit, and TNP-specific IgE (IGEL b4 1) have been described previously [8,

 

15]. Polyclonal Ab specific for Syk, Lyn, LAT and IgE were prepared by immunizing rabbits with the corresponding recombinant proteins. Rabbit anti-IgE Ab was affinity-purified on Sepharose 4B with immobilized IGEL b4 1. Ab were biotinylated with EZ-Link™ Sulfo-NHC-LC-Biotin (Pierce, Rockford, IL). Polyclonal Ab specific for Gab2, ezrin, PLCγ1, PLCγ2, and SHP-2 were purchased from Santa Cruz Biotechnology (Santa Cruz, CA). Ab specific for paxillin and phospho-Tyr (PY-20) conjugated to horseradish peroxidase (HRP), as well as HRP-conjugated anti-mouse and anti-rabbit IgG were purchased from Transduction Laboratories (Lexington, KY). Rabbit Ab specific for the p85 subunit of PI3K was obtained from Upstate Biotechnology (Lake Placid, NY). Fura-2-AM and streptavidin were purchased, respectively, from Molecular Probes (Eugene, OR) and Serva (Heidelberg, Germany). All other chemicals were obtained from Sigma-Aldrich (St. Louis, MO).

### 4.2 Cell stimulation, immunoprecipitation, and immunoblotting

RBL cells (subclone 2H3) and mutant cells (RBL-γ⁻c.1) defective in the surface expression of FcεRI [9] were cultured as previously described [7]. For activation, cells were harvested, resuspended in culture medium, and sensitized or not in suspension with IgE (IGEL b4 1; ascites ultracentrifuged at 100,000×g for 1 h; diluted 1:1,000), biotinylated anti-Thy-1.1 (3 μg/ml), or biotinylated anti-TEC-21 (3 μg/ml). After 30 min at 37°C, the cells were washed and resuspended to a concentration of $5\times10^6$/ml in buffered saline solution containing 20 mM Hepes pH 7.4, 135 mM NaCl, 5 mM KCl, 1.8 mM $CaCl_2$, 5.6 mM glucose, 1 mM $MgCl_2$, and 0.1% BSA, followed by incubation for 15 min in the presence or absence of latrunculin B (0.5 μM).

IgE-sensitized cells were then activated by exposure to TNP-BSA (1 μg/ml); the cells sensitized with biotinylated Ab were activated by exposure to streptavidin (10 μg/ml). After activation, the cells were solubilized and analyzed by SDS polyacrylamide gel electrophoresis (PAGE) [15]. In some experiments the cells were incubated for 5 min on ice in PBS containing 0.1% saponin, 5 mM $MgCl_2$, and 1 mM $Na_3VO_4$, and then extracted for 15 min on ice in lysis buffer supplemented with 1% Triton X-100. Immunoblots were quantified by Luminescent Image Analyzer LAS-3000 (Fuji Photo Film Co., Tokyo, Japan).

### 4.3 In-gel phosphatase assay

Anti-Gab2 precipitates were prepared from $10^7$ cells. In-gel phosphatase assays were performed as described [26] with some modifications. Briefly, the substrate poly$(Glu_4Tyr)_n$ was radiolabeled with [γ-$^{32}$P]ATP (ICN, Irvine, CA) using recombinant human cSrc expressed as a glutathione S-transferase fusion protein in *Escherichia coli*, kindly provided by Dr. F. D. Böhmer (Jena, Germany). The substrate was incorporated into 10% SDS-PAGE (acrylamide/bisacrylamide 30:0.8). Following electrophoresis, the SDS was removed and proteins were renatured by incubation in 6 M guanidine hydrochloride followed by incubation in buffers containing 0.04% Tween-20 and 0.3% 2-mercaptoethanol. Final renaturation step was carried out in a buffer containing 50 mM Tris-HCl (pH 8.0), 0.3% 2-mercaptoethanol, 1 mM EDTA, and 0.04% Tween-20. Protein tyrosine phosphatase activities were detected in autoradiographs of dried gels as regions from which the $^{32}$P had been selectively removed. Quantification was performed by Fuji Bio-Imaging Analyzer Bas 5000 (Fuji Photo Film Co.).

### 4.4 Other methods

Details on sucrose density gradient ultracentrifugation and determination of PI3K activity and total amounts of $IP_3$ and F-actin were previously described [15]. $[Ca^{2+}]_i$ were measured using Fura-2 fluorescence probe [27].

**Acknowledgements:** We thank H. Mrázová and R. Budovičová for excellent technical assistance. This work was supported by project LN00A026 (Center of Molecular and Cellular Immunology) from the Ministry of Education, Youth and Sports of the Czech Republic, grants 204/03/0594 and 301/03/0596 from the Grant Agency of the Czech Republic, grants A7052006 and A5052310 from the Grant Agency of the Academy of Sciences of the Czech Republic, and grant NB6758–3/01 from the Ministry of Health of the Czech Republic. The research of P. H. was supported in part by Research goal No. 002 from the Third Faculty of Medicine, Charles University, Prague, and the research of P. D. was supported by an International Research Scholar's Award from Howard Hughes Medical Institute.

## References

1 **Kinet, J. P.,** The high-affinity IgE receptor (FcεRI): from physiology to pathology. *Annu. Rev. Immunol.* 1999. **17:** 931–972.

2 **Frigeri, L. and Apgar, J. R.,** The role of actin microfilaments in the down-regulation of the degranulation response in RBL-2H3 cells. *J. Immunol.* 1999. **162:** 2243–2250.

3 **Holowka, D., Sheets, E. D. and Baird, B.,** Interactions between FcεRI and lipid raft components are regulated by the actin cytoskeleton. *J. Cell Sci.* 2000. **113:** 1009–1019.

4 **Cooper, J. A.,** Effects of cytochalasin and phalloidin on actin. *J. Cell Biol.* 1987. **105:** 1473–1478.

5 **Coue, M., Brenner, S. L., Spector, I. and Korn, E. D.,** Inhibition of actin polymerization by latrunculin A. *FEBS Lett.* 1987. **213:** 316–318.

6 **Dráberová, L.,** The involvement of Thy-1 antigen in the activation of rat mast cells. *Eur. J. Immunol.* 1989. **19:** 1715–1720.

7 **Dráberová, L. and Dráber, P.,** Functional expression of the endogenous Thy-1 gene and the transfected murine Thy-1.2 gene in rat basophilic leukemia cells. *Eur. J. Immunol.* 1991. **21:** 1583–1590.

 

8 **Hálová, I., Dráberová, L. and Dráber, P.,** A novel lipid raft-associated glycoprotein, TEC-21, activates rat basophilic leukemia cells independently of the type 1 Fcε receptor. *Int. Immunol.* 2002. **14:** 213–223.

9 **Dráberová, L. and Dráber, P.,** Thy-1-mediated activation of rat basophilic leukemia cells does not require co-expression of the high-affinity IgE receptor. *Eur. J. Immunol.* 1995. **25:** 2428–2432.

10 **Dráberová, L. and Dráber, P.,** Thy-1 glycoprotein and src-like protein-tyrosine kinase p53/p56lyn are associated in large detergent-resistant complexes in rat basophilic leukemia cells. *Proc. Natl. Acad. Sci. USA* 1993. **90:** 3611–3615.

11 **Field, K. A., Holowka, D. and Baird, B.,** Compartmentalized activation of the high affinity immunoglobulin E receptor within membrane domains. *J. Biol. Chem.* 1997. **272:** 4276–4280.

12 **Tolar, P., Dráberová, L. and Dráber, P.,** Protein tyrosine kinase Syk is involved in Thy-1 signaling in rat basophilic leukemia cells. *Eur. J. Immunol.* 1997. **27:** 3389–3397.

13 **Hutchcroft, J. E., Geahlen, R. L., Deanin, G. G. and Oliver, J. M.,** FcεRI-mediated tyrosine phosphorylation and activation of the 72-kDa protein-tyrosine kinase, PTK72, in RBL-2H3 rat tumor mast cells. *Proc. Natl. Acad. Sci. USA* 1992. **89:** 9107–9111.

14 **Dráberová, L., Amoui, M. and Dráber, P.,** Thy-1-mediated activation of rat mast cells: the role of Thy-1 membrane microdomains. *Immunology* 1996. **87:** 141–148.

15 **Dráberová, L., Dudková, L., Boubelík, M., Tolarová, H., Šmíd, F. and Dráber, P.,** Exogenous administration of gangliosides inhibits FcεRI-mediated mast cell degranulation by decreasing the activity of phospholipase Cγ. *J. Immunol.* 2003. **171:** 3585–3593.

16 **Hamawy, M. M., Swaim, W. D., Minoguchi, K., de Feijter, A. W., Mergenhagen, S. E. and Siraganian, R. P.,** The aggregation of the high affinity IgE receptor induces tyrosine phosphorylation of paxillin, a focal adhesion protein. *J. Immunol.* 1994. **153:** 4655–4662.

17 **Das, V., Nal, B., Roumier, A., Meas-Yedid, V., Zimmer, C., Olivo-Marin, J. C., Roux, P., Ferrier, P., Dautry-Varsat, A. and Alcover, A.,** Membrane-cytoskeleton interactions during the formation of the immunological synapse and subsequent T cell activation. *Immunol. Rev.* 2002. **189:** 123–135.

18 **Xie, Z. H., Ambudkar, I. and Siraganian, R. P.,** The adapter molecule Gab2 regulates FcεRI-mediated signal transduction in mast cells. *J. Immunol.* 2002. **168:** 4682–4691.

19 **Dráberová, L. and Dráber, P.,** Cross-linking of Thy-1 glycoproteins or high-affinity IgE receptors induces mast cell activation via different mechanisms. *Immunology* 1993. **80:** 103–109.

20 **Minoguchi, K., Kihara, H., Nishikata, H., Hamawy, M. M. and Siraganian, R. P.,** Src family tyrosine kinase Lyn binds several proteins including paxillin in rat basophilic leukemia cells. *Mol. Immunol.* 1994. **31:** 519–529.

21 **Huse, M. and Kuriyan, J.,** The conformational plasticity of protein kinases. *Cell* 2002. **109:** 275–282.

22 **Rozsnyay, Z., Sarmay, G. and Gergely, J.,** Rapid desensitization of B-cell receptor by a dithiol-reactive protein tyrosine phosphatase inhibitor: uncoupling of membrane IgM from Syk inhibits signals leading to Ca2+ mobilization. *Immunol. Lett.* 1995. **44:** 149–156.

23 **Gautreau, A., Poullet, P., Louvard, D. and Arpin, M.,** Ezrin, a plasma membrane-microfilament linker, signals cell survival through the phosphatidylinositol 3-kinase/Akt pathway. *Proc. Natl. Acad. Sci. USA* 1999. **96:** 7300–7305.

24 **Mekori, Y. A. and Metcalfe, D. D.,** Mast cells in innate immunity. *Immunol. Rev.* 2000. **173:** 131–140.

25 **Hamawy, M. M., Oliver, C., Mergenhagen, S. E. and Siraganiam, R. P.,** Adherence of rat basophilic leukemia (RBL-2H3) cells to fibronectin-coated surfaces enhances secretion. *J. Immunol.* 1992. **149:** 615–621.

26 **Burridge, K. and Nelson, A.,** An in-gel assay for protein tyrosine phosphatase activity: detection of widespread distribution in cells and tissues. *Anal. Biochem.* 1995. **20:** 56–64.

27 **Surviladze, Z., Dráberová, L., Kovářová, M., Boubelík, M. and Dráber, P.,** Differential sensitivity to acute cholesterol lowering of activation mediated via the high-affinity IgE receptor and Thy-1 glycoprotein. *Eur. J. Immunol.* 2001. **31:** 1–10.

**Correspondence:** Petr Dráber, Department of Signal Transduction, Institute of Molecular Genetics, Academy of Sciences of the Czech Republic, Vídeňská 1083, 142 20 Prague 4, Czech Republic
Fax: +42–02–4147–0339
e-mail: draberpe@biomed.cas.cz

 

**6.2**

**Volná, P.; Lebduška, P.; Dráberová, L.; Šímová, Š., Heneberg, P.; Boubelík, M.; Bugajev, V.; Malissen, B.; Wilson, B.S.; Hořejší, V.; Malissen, M. & Dráber, P. (2004):**

**Negative regulation of mast cell signaling and function by the adaptor LAB/NTAL.**

**Journal of Experimental Medicine 200(8): 1001-1013.**

The Journal of Experimental Medicine

# Negative Regulation of Mast Cell Signaling and Function by the Adaptor LAB/NTAL

Petra Volná,[1] Pavel Lebduška,[1] Lubica Dráberová,[1] Šárka Šímová,[1] Petr Heneberg,[1] Michael Boubelík,[1] Viktor Bugajev,[1] Bernard Malissen,[2] Bridget S. Wilson,[3] Václav Hořejší,[1] Marie Malissen,[2] and Petr Dráber[1]

[1]*Institute of Molecular Genetics, Academy of Sciences of the Czech Republic, 142 20 Prague 4, Czech Republic*
[2]*Centre d'Immunologie de Marseille-Luminy, INSERM–CNRS–Université de la Méditerranée, 13288 Marseille Cedex 9, France*
[3]*Department of Pathology and Cancer Research, University of New Mexico Health Sciences Center, Albuquerque, NM 87131*

## Abstract

Engagement of the Fcε receptor I (FcεRI) on mast cells and basophils initiates signaling pathways leading to degranulation. Early activation events include tyrosine phosphorylation of two transmembrane adaptor proteins, linker for activation of T cells (LAT) and non–T cell activation linker (NTAL; also called LAB; a product of *Wbscr5* gene). Previous studies showed that the secretory response was partially inhibited in bone marrow–derived mast cells (BMMCs) from LAT-deficient mice. To clarify the role of NTAL in mast cell degranulation, we compared FcεRI-mediated signaling events in BMMCs from NTAL-deficient and wild-type mice. Although NTAL is structurally similar to LAT, antigen-mediated degranulation responses were unexpectedly increased in NTAL-deficient mast cells. The earliest event affected was enhanced tyrosine phosphorylation of LAT in antigen-activated cells. This was accompanied by enhanced tyrosine phosphorylation and enzymatic activity of phospholipase C γ1 and phospholipase C γ2, resulting in elevated levels of inositol 1,4,5-trisphosphate and free intracellular $Ca^{2+}$. NTAL-deficient BMMCs also exhibited an enhanced activity of phosphatidylinositol 3-OH kinase and Src homology 2 domain–containing protein tyrosine phosphatase-2. Although both LAT and NTAL are considered to be localized in membrane rafts, immunogold electron microscopy on isolated membrane sheets demonstrated their independent clustering. The combined data show that NTAL is functionally and topographically different from LAT.

Key words: mast cell • signal transduction • Fcε receptor • calcium mobilization • adapter molecules

## Introduction

Mast cells play a pivotal role in initiating acute inflammatory and immediate allergic reactions. The binding of multivalent antigen (Ag) to receptor-bound IgE and subsequent aggregation of the Fcε receptor I (FcεRI) provide the trigger for mast cell activation, resulting in a release of histamine, serotonin, and other preformed inflammatory mediators, as well as de novo synthesis and subsequent secretion of arachidonic acid metabolites and a variety of inflammatory cytokines. These signal transduction pathways are initiated by the engagement of protein tyrosine kinases of the Src and Syk families. Src family kinase Lyn phosphorylates immunoreceptor tyrosine-based activation motifs present on FcεRI β and γ subunits. This leads to a recruitment and subsequent activation of Syk kinase, which phosphorylates

Address correspondence to Petr Dráber, Institute of Molecular Genetics, Academy of Sciences of the Czech Republic, Vídeňská 1083, 142 20 Prague 4, Czech Republic. Phone: 420-241-062-468; Fax: 420-241-470-339; email: draberpe@biomed.cas.cz; or Marie Malissen, Centre d'Immunologie de Marseille-Luminy, INSERM–CNRS–Univ. Med., Parc Scientifique de Luminy, 13288 Marseille Cedex 9, France. Phone: 33-491269402; Fax: 33-491269430; email: malissen@ciml.univ-mrs.fr

*Abbreviations used in this paper:* Ag, antigen; BMMC, BM-derived mast cell; BSS, buffered saline solution; $[Ca^{2+}]_i$, concentration of free intracellular calcium; ES, embryonic stem; FcεRI, Fcε receptor I; HRP, horseradish peroxidase; IP3, inositol 1,4,5-trisphosphate; LAT, linker for activation of T cells; MAP, mitogen-activated protein; NTAL, non–T cell activation linker; PI, phosphatidylinositol; PI3K, PI 3-OH kinase; PLC, phospholipase C; PS, phosphatidylserine; SCF, stem cell factor; SH, Src homology.

 J. Exp. Med. © The Rockefeller University Press • 0022-1007/2004/10/1001/13 $8.00
Volume 200, Number 8, October 18, 2004 1001–1013
http://www.jem.org/cgi/doi/10.1084/jem.20041213

several downstream signaling molecules, including the linker for activation of T cells (LAT). Phosphorylated LAT recruits a number of signaling molecules containing Src homology (SH)2 domains, such as adaptor protein Grb2 and phospholipase C (PLC)γ1 and PLCγ2. An important intermediate is phosphatidylinositol (PI) 3-OH kinase (PI3K), which catalyzes the synthesis of PI 3,4-bisphosphate and PI 3,4,5-trisphosphate. These phospholipids contribute to recruitment to the plasma membrane of Akt and PLCγ and other molecules containing pleckstrin homology domains. PLCγ catalyzes the cleavage of the lipid substrate PI 4,5-bisphosphate into diacylglycerol, an activator of protein kinase C, and inositol 1,4,5-trisphosphate (IP3), a ligand for the IP3 receptor $Ca^{2+}$ channel in the ER membrane that initiates a rise in cytoplasmic $Ca^{2+}$ levels. This is followed by a more sustained influx of extracellular calcium through $Ca^{2+}$ channels in the plasma membrane. Many of these events rely on formation of multimolecular signaling complexes that propagate the activation signal from aggregated FcεRI (1).

Recently, we have found that mast cells express a LAT-related transmembrane adaptor protein, the non–T cell activation linker (NTAL) (2). NTAL, also called LAB (3), was also found to be expressed in other cell types, such as B lymphocytes, NK cells, and monocytes but not in T lymphocytes. NTAL resembles LAT in general organization, consisting of a short extracellular domain, a single hydrophobic transmembrane domain, and a cytoplasmic tail with multiple tyrosine phosphorylation sites and two potential palmitoylation sites. The two acylation sites are likely responsible for partitioning of NTAL into detergent-resistant membrane microdomains, also called lipid rafts (4). NTAL is rapidly tyrosine phosphorylated upon engagement of FcεRI, FcγRI, or B cell receptor (2, 3). Functional similarity between LAT and NTAL was suggested by experiments in which ectopically expressed NTAL could partially restore some aspects of T cell receptor signaling in LAT-deficient cells (2). Furthermore, NTAL expressed in T cells could in part rescue the T cell development in $LAT^{-/-}$ mice (3, 5). An important functional role of NTAL in immunoreceptor signaling was suggested by experiments in which a diminution of NTAL expression by silencing RNA oligonucleotides resulted in a reduction of B cell receptor–mediated activation of mitogen-activated protein (MAP) kinase in A20 cell line (3), as well as in a reduced degranulation in FcεRI-activated human mast cells (6).

Using a genetic approach, Saitoh et al. showed that mast cell effector functions were impaired but not completely inhibited in BM-derived mast cells (BMMCs) from LAT-deficient mice (7). Accordingly, low levels of PLCγ activation and calcium response were detected in LAT-deficient BMMCs, suggesting the existence of alternative pathways. One alternative pathway independent of Lyn kinase and LAT phosphorylation but dependent on Fyn kinase and Gab2 adaptor has been described recently (8). In this study, we analyzed the signaling events in BMMCs from NTAL-deficient mice and compared them with those observed in WT mice or mice deficient in both NTAL and LAT linkers. Furthermore, we analyzed the respective topography of NTAL and LAT on membrane sheets isolated from nonactivated and activated mast cells.

## Materials and Methods

*Antibodies and Reagents.* The following mAbs have been used: anti-Syk (9), anti-LAT (10), anti-FcεRI β subunit (JRK) (11), anti-NTAL (NAP-07) (2), TNP-specific IgE mAb (IGEL b4 1) (12), and DNP-specific IgE mAb (13). Polyclonal antibodies specific for Syk, LAT, NTAL, and IgE have been prepared by common procedures after immunizing rabbits with the corresponding proteins or their fragments (14). Polyclonal antibodies specific for PLCγ1, PLCγ2, ERK 1, phospho-ERK (specific for phosphorylated Tyr 204), Grb2, SH2-containing protein tyrosine phosphatase (SHP)-2, and horseradish peroxidase (HRP)–conjugated donkey anti–goat IgG, goat anti–mouse IgG, and goat anti–rabbit IgG were obtained from Santa Cruz Biotechnology, Inc. Rabbit anti-PI3K p85 subunit antibody (a mixture of equal amounts of antisera against the intact p85 subunit and the N-SH2 region of PI3K) was obtained from Upstate Biotechnology. Phospho-Tyr–specific mAb (PY-20) conjugated to HRP was purchased from Transduction Laboratories. Biotinylated rat anti–mouse c-kit, FITC-labeled rat anti–mouse IgE antibody, and phycoerythrin-labeled streptavidin were from BD Biosciences. Goat anti–mouse IgG and anti–rabbit IgG conjugated to colloidal gold particles of 10- and 5-nm were obtained from Amersham Biosciences. Fura-2-AM and $^{45}Ca$ (37 MBq; specific activity 566 MBq/mg $Ca^{2+}$) were purchased from Molecular Probes and MP Biomedicals, Inc., respectively. All other chemicals were obtained from Sigma-Aldrich.

*Vector Construction.* The targeting construct used for disruption of the *Ntal* gene is shown in Fig. 1 b. It should be noted that the official name of the gene is *Wbscr5*. The 5′ homologous sequences correspond to a gene segment encompassing nucleotide positions 79680–81447 (sequence data available from GenBank/EMBL/DDBJ under accession no. AF139987). The 3′ homologous sequences correspond to a gene segment encompassing nucleotide positions 87023–91726 (sequence data available from GenBank/EMBL/DDBJ under accession no. AF139987). In the engineered vector, the sequence containing exons 2–9 of the *Ntal* gene and coding for amino acids 1–121 of the NTAL protein was replaced by a lox P–flanked neomycin-resistance gene ($neo^r$). Finally, the targeting construct was abutted to a thymidine kinase expression cassette and linearized.

*Isolation of Recombinant Embryonic Stem Cell Clones and Production of Mutant Mice.* After electroporation of CK35 129/CV embryonic stem (ES) cells (15) and selection in G418 and gancyclovir, colonies were screened for homologous recombination by Southern blot analysis. The 5′ single copy probe corresponded to a 400-bp EcoRI–XbaI fragment. When tested on EcoRI-digested DNA, it hybridized either to a 8-kb WT fragment or to a 2.5-kb recombinant fragment. The presence of an appropriate homologous recombination event at the 3′ side was assessed using a 1051-bp XbaI–EcoRI fragment. When tested on HindIII-digested DNA, it hybridized either to a 9.5-kb WT fragment or to a 6.7-kb recombinant fragment. A neo probe was also used to ensure that adventitious nonhomologous recombination events had not occurred in the selected clones. Among the recombinant ES cell clones, one was found capable of germline transmission. The resulting mutant mouse line was first bred to Deleter mice (16) to eliminate the lox

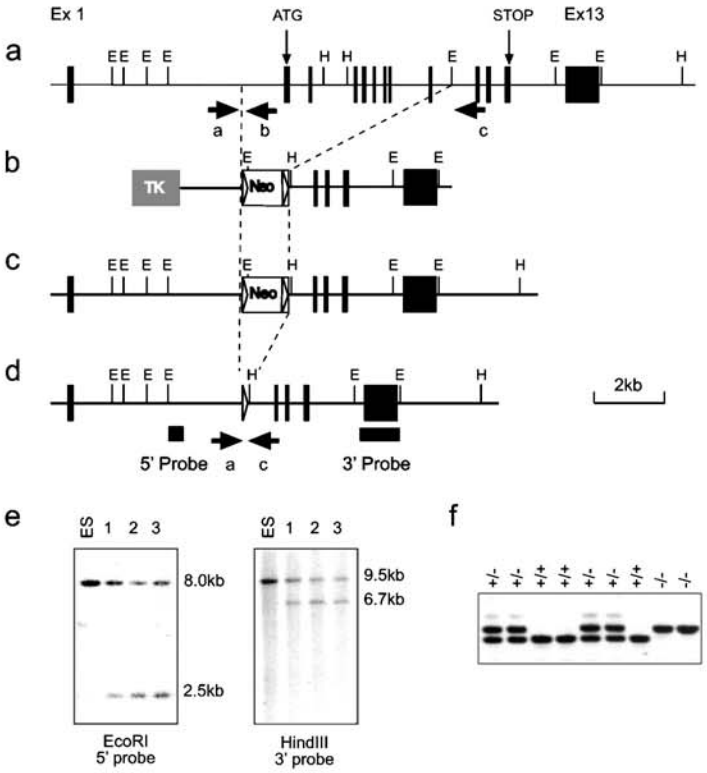


**Figure 1.** Generation and identification of *Ntal*-deficient mice. (a–d) Schematics of the *Ntal* knock-out strategy. (a) Partial restriction map of the WT *Ntal* gene. Exons are shown as filled boxes. The restriction sites are EcoRI (E) and Hind III (H). The exons containing the initiation (start) and the stop codon are specified. (b) Targeting vector used for the deletion of exons 2–9. Shaded or open boxes correspond to the thymidine kinase expression cassette (TK) and to the lox P–flanked neo$^r$ cassette, respectively. Lox P sites are shown as triangles. (c) Structure of the targeted allele after homologous recombination. (d) Final structure of the targeted allele after removal of the neo$^r$ gene via cre-mediated recombination. The 5′ and 3′ single copy probes used to verify 5′ and 3′ targeting events are indicated, and the position of the PCR primers used to genotype the resulting mice are indicated by arrows. (e) Southern blot analysis of three recombinant ES cell clones including the one that gave germline transmission (clone 1). DNA was digested as specified and hybridized with the 5′ or 3′ single copy probe. (f) PCR genotyping of *Ntal*-deficient and -proficient littermates using primers indicated in panel d.

P–flanked neomycin cassette and intercrossed to produce homozygous mutant mice. Screening of mice for the presence of the *Ntal*-null mutation was performed by PCR using the following oligonucleotides: a: 5′-CTACGGAGCTGAGTGTTCTCA-3′, b: 5′-GAACGGCTAGAACTACACAGAG-3′, c: 5′-GAGAGGAGGATAAAGTGGACCTC-3′. WT *Ntal* allele is visualized as a 383-bp fragment using the a-b pair of oligonucleotides, whereas the intended mutation is visualized as a 450-bp fragment using the a-c pair of oligonucleotides. Production of LAT$^{-/-}$ mice has been described (17). NTAL$^{-/-}$ and LAT$^{-/-}$ mice were bread to generate the NTAL$^{-/-}$/LAT$^{-/-}$ strain. All mice were maintained and used in accordance with the Institute of Molecular Genetics guidelines.

*Cells.* BMMCs were isolated from the femurs and tibias of the 6–10-wk-old mice. The cells were incubated for 4–8 wk in suspension cultures in freshly prepared culture media (RPMI-1640 supplemented with 20 mM Hepes, pH 7.5, 100 U/ml penicillin, 100 μg/ml streptomycin, 100 μM MEM nonessential amino acids, 1 mM sodium pyruvate, 17% FCS, 41 μM 2-ME) supplemented with IL-3 (20 ng/ml; PeproTech EC) and stem cell factor (SCF; 40 ng/ml; PeproTech EC). No discernible differences in growth properties and morphology were detected among BMMCs derived from NTAL$^{+/+}$, NTAL$^{+/-}$, NTAL$^{-/-}$, LAT$^{-/-}$, and NTAL$^{-/-}$/LAT$^{-/-}$ mice. Before activation, BMMCs were cultured for 16 h in culture medium without SCF, followed by incubation for 3–4 h in SCF- and IL-3–free medium supplemented with anti-TNP IgE (1 μg/ml). The cells were then washed in buffered saline solution (BSS) containing 20 mM Hepes, pH 7.4, 135 mM NaCl, 5 mM KCl, 1.8 mM $CaCl_2$, 5.6 mM glucose, 1 mM $MgCl_2$, and 0.1% BSA (BSS-BSA), and challenged with various concentrations of TNP-BSA.

*Flow Cytometry Analyses of FcεRI and Phosphatidylserine Expression.* Flow cytometry analyses of FcεRI in unfractioned freshly isolated peritoneal mast cells (c-kit positive) and BMMCs were performed as described (18) except that in the first incubation step the cells were exposed to TNP-specific IgE. To determine externalization of phosphatidylserine (PS), cells were exposed to FITC-labeled annexin V (Alexis) and then analyzed using FACSCalibur and CellQuest software (Beckton Dickinson) as described (19).

*Passive Systemic Anaphylaxis and Degranulation.* Mice were sensitized by i.v. tail vein injection of TNP-specific IgE (3 μg/mouse) and 24 h later challenged by i.v. tail vein injection with TNP-BSA (500 μg/mouse) or vehicle (PBS). After 1.5 min, the animals were killed, blood samples were obtained by cervical puncture, and serum was isolated. Serum histamine concentrations were determined according to the manufacturer's protocol using a histamine radioimmunoassay kit (Immunotech). Statistical significance of differences among particular groups was determined using Student's *t*-test. The degree of degranulation was determined by measuring the release of β-glucuronidase from anti-TNP IgE-sensitized and TNP-BSA–activated cells as described (20).

*Immunoprecipitation and Immunoblotting.* Activated and control cells were lysed in ice cold lysis buffer (50 mM Tris-HCl, pH 7.4, 150 mM NaCl, 2 mM EDTA, 10 mM β-glycerophosphate, 1 mM $Na_3VO_4$, 1 mM PMSF, 1 μg/ml aprotinin, 1 μg/ml leupeptin) supplemented with 1% NP-40 and 1% *n*-dodecyl β-D-maltoside (for LAT, and NTAL immunoprecipitation or for ERK immunoblotting) or 0.2% Triton X-100 (for FcεRI immunoprecipitation). In some experiments, association of the proteins under study with large macromolecular complexes was analyzed

in cells permeabilized with 0.1% saponin in PBS, thus releasing free cytoplasmic components, and the cellular ghosts were extracted for 15 min on ice in a lysis buffer supplemented with 1% Triton X-100 (21). Proteins in postnuclear supernatants were immunoprecipitated with the corresponding antibodies bound to UltraLink-immobilized protein A (Pierce Chemical Co.) and analyzed by immunoblotting as described (9). Some proteins were analyzed by direct immunoblotting of SDS-PAGE–fractionated cell lysates. Immunoblots were quantified by Luminescent Image Analyzer LAS 3000 (Fuji Photo Film Co.).

*Sucrose Gradients.* Cells were solubilized in lysis buffer containing 1% Brij 96 and fractionated by sucrose density gradient ultracentrifugation as described (20).

*Measurements of Intracellular $Ca^{2+}$ Concentrations and $^{45}Ca$ Uptake.* Concentrations of free intracellular calcium $[Ca^{2+}]_i$ were determined using Fura-2-AM as a reporter. BMMCs were sensitized with anti-TNP IgE (1 μg/ml) at 37°C in culture medium supplemented with 2% FCS but devoid of SCF and IL-3. After 3–4 h, the cells were washed and resuspended at a concentration $5 \times 10^6$/ml in BSS-BSA supplemented with Fura-2-AM and probenecid at a final concentration of 1 μg/ml and 2.5 mM, respectively. After 30 min, the cells were washed in BSS-BSA supplemented with probenecid and immediately before measurement briefly centrifuged and resuspended in BSS-BSA. Calcium mobilization was determined using luminescence spectrometer LS-50B (PerkinElmer). Uptake of extracellular calcium was determined as before (22) except that the radioactivity was measured in 10 ml scintillation liquid (EcoLite; ICN Biomedicals) in QuantaSmart TM counter.

*Immune Complex PI3K, PLCγ and Syk Kinase Assays, and IP3 Determination.* PI3K and PLCγ activities and IP3 concentrations were determined as described previously (21). Syk kinase activity was determined by in vitro kinase assay (9).

*In-gel Phosphatase Assay.* SHP-2 immunoprecipitates were prepared and analyzed by in-gel phosphatase assay as described (23).

*Electron Microscopy.* Cells were left overnight to settle on 15-mm round-glass coverslips in the presence or absence of anti-DNP IgE (1 μg/ml). IgE-sensitized cells were activated by DNP-BSA (1 μg/ml), and membrane sheets were obtained and processed as described (24). FcεRI, NTAL, and LAT were labeled by sequential incubation with the corresponding primary antibodies followed by gold-conjugated secondary reagents diluted 1:20 from commercial stocks. Samples were postfixed in 2% glutaraldehyde in PBS, washed in PBS, and then stained with 1% $OsO_4$ in 0.1 M cacodylate buffer, 1% tannic acid, and 1% uranyl acetate. Samples were examined using a Hitachi 600 transmission electron microscope. Gold particles distribution was analyzed using software developed at the University of New Mexico (25). Clusters of particles of the same type were analyzed using the Hopkins and Ripley's statistics (25). In each of two independent experiments, ~30 $\mu m^2$ of plasma membranes from activated and resting cells were analyzed.

## Results

*Enhanced Degranulation in $NTAL^{-/-}$ Mast Cells.* To explore the role of NTAL in mast cell physiology, we generated knock-out mice with a lox P sequence that replaced a central segment of the *Ntal* gene containing exons 2–9 (Fig. 1). Mice homozygous for this mutation, $Ntal^{-/-}$, were born at the expected Mendelian frequencies and were deprived of detectable NTAL protein (see next paragraph). First, we

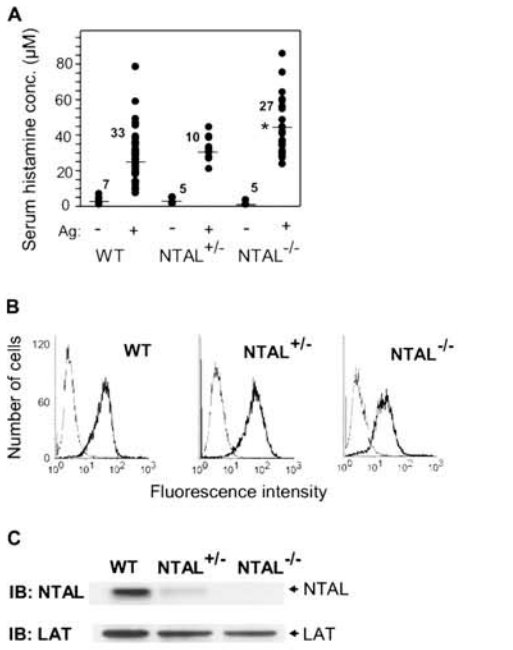


**Figure 2.** Enhanced passive systemic anaphylaxis in $NTAL^{-/-}$, and FcεRI and NTAL expression in BMMCs. (A) WT, $NTAL^{+/-}$, and $NTAL^{-/-}$ mice were sensitized with TNP-specific IgE, challenged with TNP-BSA (+) or with PBS alone (−), and the serum histamine levels were determined. Numbers above the mean bars indicate the numbers of mice in each group. The asterisk indicates a significant increase ($P < 0.01$) of histamine levels in $NTAL^{-/-}$ mice compared with WT mice. (B) BMMCs from WT, $NTAL^{+/-}$, and $NTAL^{-/-}$ mice were stained for surface FcεRI by sequential exposure to anti-TNP IgE (1 μg/ml, thick line) or PBS alone (thin line) followed by anti–mouse IgG–FITC conjugate. The samples were analyzed by flow cytometry. (C) NTAL expression levels in lysates from BMMCs were determined by immunoblotting (IB) using anti-NTAL mAb followed by anti–mouse IgG–HRP conjugate. As a control for protein loading the membrane was also developed with rabbit anti-LAT followed by anti–rabbit IgG–HRP conjugate.

analyzed the effect of NTAL on passive anaphylactic reaction in vivo. In controls, the basal level of serum histamine was identical in WT, $NTAL^{+/-}$, and $NTAL^{-/-}$ mice (Fig. 2 A). After challenge with Ag, the serum histamine levels were enhanced in all mice, although the levels were significantly higher in $NTAL^{-/-}$ mice. The observed increase in serum histamine was not attributable to elevated numbers of mast cells in $NTAL^{-/-}$ mice, as inferred from similar numbers of mast cells in peritoneal lavage of WT, $NTAL^{+/-}$, and $NTAL^{-/-}$ mice (2.5% ± 1.1%, mean ± SD, $n = 9$). Furthermore, peritoneal mast cells (c-kit positive) from $NTAL^{-/-}$ and WT mice did not differ in the amount of surface FcεRI as determined by flow cytometry (not depicted). These data suggested that the observed increase in serum histamine levels in $NTAL^{-/-}$ cells could reflect negative regulation of mast cell signaling by NTAL.

To investigate the underlying mechanism responsible for the enhanced degranulation response in $NTAL^{-/-}$ mice, BMMCs from WT, $NTAL^{+/-}$, or $NTAL^{-/-}$ mice were

obtained by growing BM cells for 4–8 wk in the presence of IL-3 and SCF. The cells expressed comparable amount of FcεRI (Fig. 2 B) and LAT (Fig. 2 C) and the expected amount of NTAL (Fig. 2 C). The cells were sensitized with TNP-specific IgE and activated with various doses of Ag. Data presented in Fig. 3 A indicate that FcεRI-mediated degranulation was significantly increased in NTAL$^{-/-}$ cells compared with NTAL$^{+/-}$ cells and WT cells, although the total amount of β-glucuronidase present in the cells was similar (not depicted). The most dramatic difference between WT and NTAL$^{-/-}$ cells was observed at suboptimal concentration of Ag (10 ng/ml). Under these conditions, the NTAL$^{-/-}$ cells released 40 ± 2% of the total β-glucuronidase (mean ± SD, $n$ = 12) compared with a maximum of 22 ± 2% ($n$ = 12) in WT cells. These data were confirmed in four independent BMMC isolates in each group. Even at optimal (100 ng/ml) and supraoptimal (500 and 1,000 ng/ml) doses of Ag, the response in NTAL$^{-/-}$ BMMCs was significantly higher. When the cells were stimulated with ionophore A23187, the differences between WT and NTAL$^{-/-}$ cells disappeared (not depicted), suggesting that NTAL affects early receptor-specific activation events which precede the calcium response.

An important feature of the degranulation process in mast cells is PS externalization (19). In nonstimulated cells, PS is found almost exclusively in the inner leaflet of the plasma membrane. FcεRI-dependent degranulation leads to an exposure of PS on the plasma membrane, detectable by binding of FITC-labeled annexin V to intact cells. Cytofluorometric analyses showed that the number of annexin V binding sites increased in WT cells with a maximum reached at 100 ng/ml (Fig. 3 C). Activated NTAL$^{-/-}$ cells exhibited higher PS externalization than activated WT cells, and again the most dramatic difference was observed at a suboptimal dose of Ag (10 ng/ml). As expected (19), no PS externalization in WT or NTAL$^{-/-}$ cells was observed in the absence of extracellular $Ca^{2+}$ (not depicted).

*Tyrosine Phosphorylation of LAT Is Enhanced in NTAL$^{-/-}$ BMMCs.* Next we assessed the tyrosine phosphorylation of several proteins known to be involved in the initial stages of FcεRI signaling. When total lysates from Ag-activated cells were analyzed by immunoblotting with PY-20 mAb, the most significant difference between WT and NTAL$^{-/-}$ cells was the absence in NTAL$^{-/-}$ cells of a 30-kD phosphorylated protein corresponding in molecular weight to NTAL (Fig. 3 D). Furthermore, NTAL$^{-/-}$ cells exhibited an increased tyrosine phosphorylation of a 38-kD protein, corresponding to LAT (see end of this paragraph). If the IgE receptor was immunoprecipitated from control and Ag-activated cells, increased tyrosine phosphorylation of FcεRI β and γ subunits was observed in both WT and NTAL$^{-/-}$ cells after cell triggering, and no significant difference in the extent and/or dynamics of tyrosine phosphorylation was observed between these two groups (Fig. 4 A). Neither did the Syk kinase immunoprecipitated from the whole cell lysate exhibit any significant differences in amount, tyrosine phosphorylation, and kinase activity between WT and NTAL$^{-/-}$ cells (not depicted). However, when Syk was immunoprecipitated from cells first permeabilized with saponin in order to release free cytoplasmic components and then solubilized with Triton X-100, increased amounts of Syk and its phosphorylated form were precipitated from activated NTAL$^{-/-}$ cells relative to WT cells. This difference, which apparently reflects enhanced association of Syk with as yet unidentified plasma membrane component(s), was more pronounced at later stages (5 min) after FcεRI triggering (Fig. 4 B). The most dramatic difference observed in

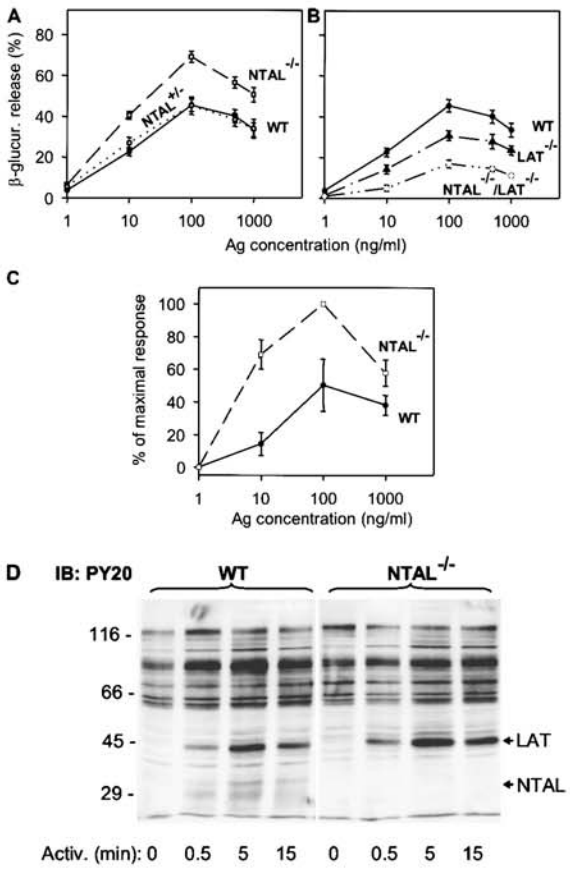


**Figure 3.** Enhanced degranulation, PS externalization, and tyrosine phosphorylation in NTAL$^{-/-}$ cells. BMMCs were sensitized with anti-TNP IgE (1 μg/ml) and then stimulated with Ag (TNP-BSA). (A and B) β-Glucuronidase released into supernatant from cells stimulated for 30 min with various concentrations of Ag. Data represent mean ± SD ($n$ = 12 for WT and NTAL$^{-/-}$ cells; $n$ = 4 for NTAL$^{+/-}$ cells; $n$ = 6 for LAT$^{-/-}$ and NTAL$^{-/-}$/LAT$^{-/-}$ cells). (C) Externalization of PS in WT and NTAL$^{-/-}$ BMMCs stimulated for 30 min with various concentrations of Ag was determined by flow cytometry after surface staining of the cells with FITC-labeled annexin V. Data were normalized to maximal values in each assay and represent means ± SD ($n$ = 3). (D) Cells were activated with 100 ng/ml TNP-BSA for the indicated time intervals, solubilized in 1% NP-40 and 1% $n$-dodecyl-β-D-maltoside, and the postnuclear supernatants were size fractionated by SDS-PAGE. The extent of tyrosine phosphorylation was determined by immunoblotting with PY-20–HRP conjugate. Positions of molecular weight standards, LAT and NTAL, are indicated on the left and right, respectively. A typical experiment from three performed is shown.

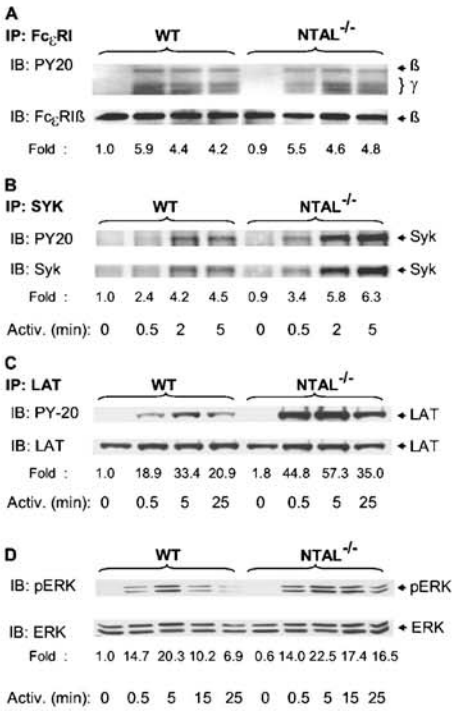


**Figure 4.** Tyrosine phosphorylation of FcεRI, Syk, LAT, and ERK. BMMCs from WT and NTAL$^{-/-}$ cells were sensitized with anti-TNP IgE and stimulated with TNP-BSA (100 ng/ml) for the indicated time intervals. The cells were solubilized in lysis buffer containing 0.2% Triton X-100 (A), 1% NP-40, and 1% *n*-dodecyl-β-D-maltoside (C and D) or by sequential treatment with 0.1% saponin and 1% Triton X-100 (B). FcεRI (A), Syk (B), and LAT (C) were immunoprecipitated (IP) from postnuclear supernatants with the corresponding antibodies. The immunoprecipitates were resolved by SDS-PAGE and analyzed by immunoblotting using PY-20–HRP conjugate (top). After stripping, the same membranes were reblotted with protein-specific antibodies (bottom). Phosphorylated ERK (pERK) and ERK were determined by immunoblotting in size-fractionated whole cell lysates using anti-pERK antibody, followed by stripping and immunoblotting with ERK-specific antibody (D). Fold inductions of protein tyrosine phosphorylation, normalized to nonactivated WT cells and corrected for the amount of the protein in each immunoprecipitate, are also indicated. A typical result from two to four experiments performed is presented.

NTAL$^{-/-}$ cells was an increased tyrosine phosphorylation of LAT at all time intervals analyzed (0.5–25 min; Fig. 4 C). It should be noted, however, that we were unable to coimmunoprecipitate Syk with LAT from either activated WT or NTAL$^{-/-}$ cells.

Next we examined whether NTAL is involved in FcεRI-mediated Ras–MAP kinase signaling pathway. Activation of MAP kinases was detected in total cellular lysates by immunoblotting with anti–phospho-ERK. Data in Fig. 4 D show that FcεRI-mediated tyrosine phosphorylation of the ERK was comparable in WT and NTAL$^{-/-}$ cell at early time intervals (0.5 and 5 min), but in NTAL$^{-/-}$ cells it exhibited a slower decline at later stages of activation (15 and 25 min).

*NTAL Negatively Regulates the PI3K Activity.* Early biochemical events in FcεRI-activated mast cells are dependent on the activity of PI3K, which functionally interacts with Gab2 and several other signaling proteins (26, 27). Therefore, we monitored the subcellular distribution and enzymatic activity of PI3K in WT and NTAL$^{-/-}$ BMMCs. PI3K was immunoprecipitated from saponin/Triton X-100–solubilized cells, and its amount was quantified by immu-

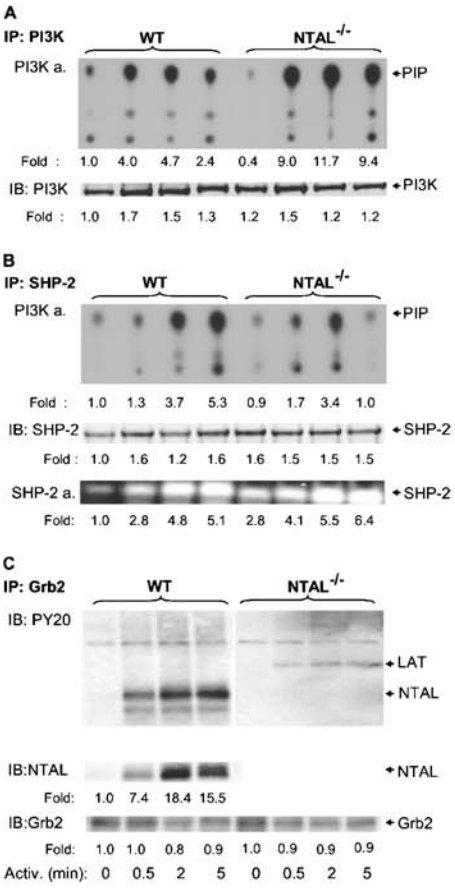


**Figure 5.** PI3K, SHP-2, and Grb2 immunocomplexes. BMMCs from WT and NTAL$^{-/-}$ mice were activated with TNP-BSA (100 ng/ml) for the indicated time intervals, solubilized with saponin/Triton X-100, and PI3K, SHP-2, and Grb2 immunocomplexes were isolated by immunoprecipitation with the corresponding antibodies. (A) PI3K immunoprecipitates were analyzed for (a) PI3K activity (PI3K a.) using PI as a substrate and TLC (position of [$^{32}$P]PI [PIP] is indicated by arrow) and (b) the amount of immunoprecipitated PI3K by immunoblotting with anti–PI3K-p85. (B) SHP-2 immunoprecipitates were analyzed for (a) SHP-2–associated PI3K activity by PI3K assay, (b) the amount of SHP-2 by immunoblotting with anti–SHP-2 antibody, and (c) SHP-2 enzymatic activity by in-gel phosphatase assay (SHP-2 a.). (C) Grb2 immunoprecipitates were analyzed by immunoblotting for the presence of tyrosine-phosphorylated proteins, NTAL and Grb2. Relative amounts of the immunoprecipitated proteins, their tyrosine phosphorylations, and/or enzymatic activities were normalized to nonactivated WT cells. Representative data from two to four experiments performed are shown.

noblotting. Enzymatic activity of PI3K in the immune complexes was determined using PI as a substrate, and the expected product [$^{32}$P]PI (PIP) was detected by autoradiography. Similar to a previous study performed with RBL-2H3 cells (23), we observed an activation-induced increase in recovery of PI3K from saponin-permeabilized WT BMMCs (Fig. 5 A), consistent with translocation of PI3K to the plasma membrane. The changes in the distribution of PI3K were accompanied by an enhanced PI3K enzymatic activity with peak at 2 min after FcεRI triggering. In nonactivated NTAL$^{-/-}$ cells, the enzymatic activity of PI3K was slightly lower than in WT cells. However, 0.5 min after FcεRI triggering the PI3K activity was 2.5-fold higher in NTAL$^{-/-}$ and remained higher at all time intervals analyzed.

One of the proteins interacting with PI3K is the ubiquitously expressed nonreceptor tyrosine phosphatase SHP-2 (28). Because SHP-2 regulates PI3K activity (29), we further compared the SHP-2–associated PI3K activity in WT and NTAL$^{-/-}$ cells. SHP-2 was immunoprecipitated from saponin/Triton X-100–solubilized cells, and the enzymatic activity of SHP-2–coprecipitated PI3K was determined. Data presented in Fig. 5 B show that PI3K enzymatic activity was elevated after FcεRI triggering in both WT and NTAL$^{-/-}$ cells but was more rapidly down-regulated in NTAL$^{-/-}$ cells at later time intervals (5 min). Total enzymatic activity of SHP-2 phosphatase, as detected by in-gel assay, was higher in nonactivated NTAL$^{-/-}$ than in WT cells (2.8 ± 0.3-fold increase, $n = 3$) and remained higher after FcεRI triggering at all time intervals analyzed.

*NTAL Is a Major Tyrosine Phosphorylated Target of Grb2.* 5 of the total 10 consensus tyrosine phosphorylation sites in NTAL, and in LAT, are of the YXN type (where X is any amino acid), and are thus potential binding sites for the SH2 domain of the cytoplasmic adaptor Grb2. Anti-NTAL immunoblotting of Grb2 immunoprecipitates showed an enhanced association of NTAL and Grb2 after FcεRI engagement in WT BMMCs (Fig. 5 C). Among the tyrosine-phosphorylated proteins in activated WT cells, NTAL was a major Grb2 target, as determined by PY-20 immunoblotting. Interestingly, more tyrosine-phosphorylated protein of 38 kD, presumably LAT, was bound to Grb2 in NTAL$^{-/-}$ cells compared with WT cells.

*Enhanced PLCγ Activity and Calcium Response in NTAL$^{-/-}$ BMMCs.* The observed increase in tyrosine phosphorylation of LAT implied elevated levels of PLCγ activity in NTAL$^{-/-}$ cells, and we therefore evaluated the properties of immunoisolated PLCγ. Data presented in Fig. 6 A indicate that tyrosine phosphorylation of PLCγ1 was indeed enhanced; 2 and 5 min after Ag triggering the enhancement was, respectively, 4.8- and 4-fold higher in NTAL$^{-/-}$ cells than in WT cells. Tyrosine phosphorylation of PLCγ2 isolated from NTAL$^{-/-}$ cells was also enhanced (Fig. 6 B). Next, we analyzed the PLCγ enzymatic activity. PLCγ2 was immunoprecipitated, and its enzymatic activity, resulting in the production of [$^3$H]IP3 from P[$^3$H]IP2 substrate, was determined. As shown in Fig. 6 C, PLCγ activity in FcεRI-activated cells was significantly higher in NTAL$^{-/-}$ cells than in WT cells. The enhanced PLCγ activity in NTAL$^{-/-}$ cells resulted in higher accumulation of IP3, the critical PLCγ metabolite (Fig. 6 D).

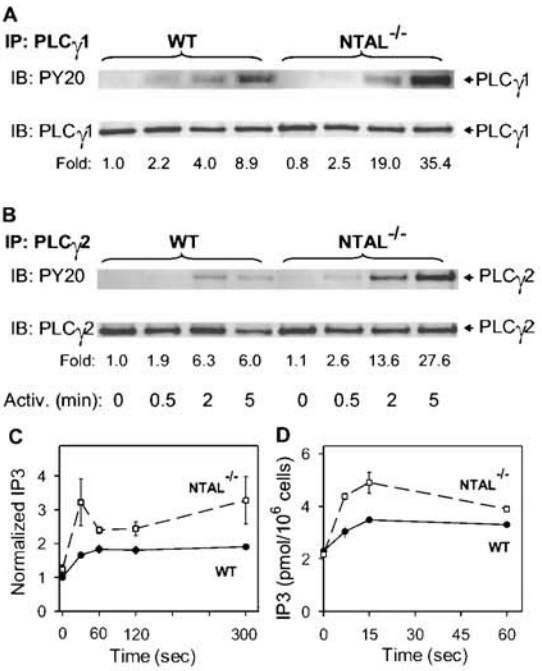


**Figure 6.** Tyrosine phosphorylation and enzymatic activity of PLCγ. BMMCs from WT and NTAL$^{-/-}$ mice were activated for the indicated time intervals with TNP-BSA (100 ng/ml). (A and B) The cells were solubilized with saponin/Triton X-100, and PLCγ1 (A) and PLCγ2 (B) were immunoprecipitated and analyzed by immunoblotting using phosphotyrosine-specific PY-20–HRP conjugate (top). Subsequently, after stripping the same membranes were reblotted with anti-PLCγ1 (A) and anti-PLCγ2 (B) (bottom). Representative data from two experiments performed are shown. (C) The cells were lysed in 1% Triton X-100, and enzymatic activity of the immunoprecipitated PLCγ2 was measured by immune complex PLCγ assay; the data were normalized to nonactivated WT cells. (D) IP3 levels were determined by $^3$H-radioreceptor assay kit as described in Materials and Methods. Data in C and D represent means ± SD ($n$ = 3–4).

Since an enhanced activity of PLCγ and production of IP3 are prerequisites for FcεRI-mediated calcium responses, we also estimated the $[Ca^{2+}]_i$ in WT and NTAL$^{-/-}$ cells. After an exposure of IgE-sensitized and Fura-2–loaded cells to low concentrations of Ag (5 or 10 ng/ml) in the presence of extracellular $Ca^{2+}$, only a small increase in $[Ca^{2+}]_i$ was observed in WT cells, whereas the response was markedly enhanced in NTAL$^{-/-}$ cells (Fig. 7, A and B). At a higher concentration of Ag (100 ng/ml), the difference between WT and NTAL$^{-/-}$ cells was less dramatic, due to enhanced calcium response in WT cells but remained significant (Fig. 7 C). An elevated calcium response was also observed in NTAL$^{-/-}$ cells activated in the absence of extracellular $Ca^{2+}$ (Fig. 7 D).

FcεRI-mediated increase in $[Ca^{2+}]_i$ in the presence of extracellular $Ca^{2+}$ reflects not only a transient release of in-

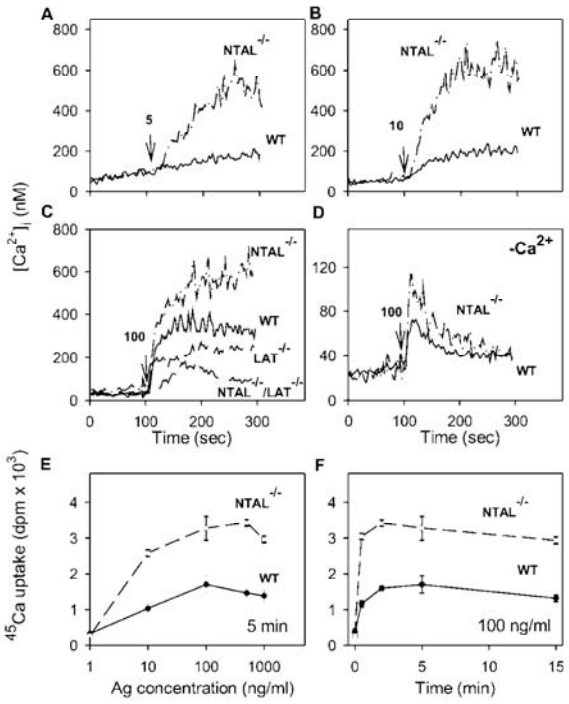


**Figure 7.** $Ca^{2+}$ mobilization and extracellular $^{45}Ca$ uptake. (A–D) IgE-sensitized BMMCs were loaded with Fura-2-AM and stimulated with various concentrations of TNP-BSA (5 ng/ml [A], 10 ng/ml [B], or 100 ng/ml [C and D]) added at the time point indicated by arrows, in the presence (A–C) or absence (D) of 1.0 mM extracellular $Ca^{2+}$. The $Ca^{2+}$ mobilization was monitored by spectrofluorometry in WT and $NTAL^{-/-}$ (A–D) and at a single concentration of TNP-BSA (100 ng/ml) also in $LAT^{-/-}$ and $NTAL^{-/-}/LAT^{-/-}$ (C) BMMCs. Representative data from at least three to five experiments are shown. (E and F) Uptake of calcium from extracellular medium was measured in IgE-sensitized WT and $NTAL^{-/-}$ cells activated in the presence of extracellular $^{45}Ca^{2+}$ (1 mM) for 5 min with various concentrations of TNP-BSA (E) or activated with 100 ng/ml of TNP-BSA for various time intervals (F). Data in E and F represent means ± SD ($n$ = 3–6).

tracellularly stored $Ca^{2+}$ but also a more sustained influx of $Ca^{2+}$ from the extracellular medium through incompletely characterized store-operated channels in the plasma membrane (30). To determine whether NTAL has any effect on the influx of extracellular $Ca^{2+}$, we measured the uptake of $^{45}Ca$ from the extracellular medium. In nonactivated cells, the uptake of $^{45}Ca$ was low and there was no difference between WT and $NTAL^{-/-}$ cells. When the cells were exposed to increasing concentrations of TNP-BSA, the $^{45}Ca$ uptake rose in WT cells and even more so in $NTAL^{-/-}$ cells. The enhancement of $^{45}Ca$ uptake in $NTAL^{-/-}$ cells was observed at all concentrations of Ag used (up to 1 μg/ml; Fig. 7 E) and at all time intervals analyzed (up to 15 min; Fig. 7 F).

*Impaired Secretory and Calcium Responses in $NTAL^{-/-}/LAT^{-/-}$ BMMCs.* Although LAT and NTAL are structurally similar adaptor molecules, their absence has dramatically different consequences on FcεRI-mediated events in BMMCs. In $LAT^{-/-}$ cells, the secretory and $Ca^{2+}$ responses are partially inhibited (7), whereas in $NTAL^{-/-}$ the same responses are potentiated (see Figs. 3–7). To determine the properties of cells defective simultaneously in both these adaptor proteins, we prepared $NTAL^{-/-}/LAT^{-/-}$ mice and examined their BMMCs. When the cells were solubilized and analyzed by immunoblotting, no proteins reactive with anti-NTAL– and anti-LAT–specific Abs were detected (not depicted). The $NTAL^{-/-}/LAT^{-/-}$ BMMCs differed from the cells expressing both adaptor proteins neither in their growth properties nor in their expression of surface FcεRI. Data presented in Fig. 3 B indicate that $NTAL^{-/-}/LAT^{-/-}$ cells exhibited lower secretory response than $LAT^{-/-}$ cells. Similarly, calcium response in $NTAL^{-/-}/LAT^{-/-}$ cells was lower than in $LAT^{-/-}$ cells (Fig. 7 C). It should be noted that although they were dramatically reduced, the secretory and calcium responses were not completely inhibited. Furthermore, there was no significant difference in degranulation and calcium responses induced by the ionophore A23187 in WT, $LAT^{-/-}$, and $NTAL^{-/-}/LAT^{-/-}$ BMMCs (not depicted), demonstrating that degranulation itself does not depend on the presence of these linker proteins.

*Different Membrane Topography of NTAL and LAT in Resting and Activated Cells.* Both NTAL and LAT partition into lipid rafts, as can be inferred from their detergent resistance and association with buoyant density fractions of sucrose gradient (2). However, a direct comparison of the distribution of these two adaptors in sucrose gradients has not been reported. Data presented in Fig. 8 indicate that in WT cells both LAT and NTAL are located predominantly in low density fractions of sucrose gradient (fractions 1–4). In Ag-activated cells, the amount of LAT in these fractions was decreased, and tyrosine-phosphorylated LAT was found

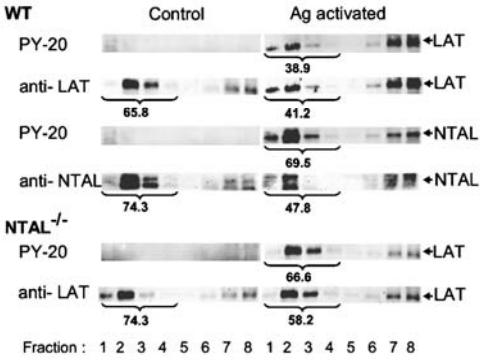


**Figure 8.** Distribution of NTAL and LAT in sucrose gradients. BMMCs from WT or $NTAL^{-/-}$ mice were sensitized with TNP-specific IgE and activated or not with TNP-BSA (100 ng/ml) for 5 min. The cells were solubilized in a lysis buffer containing 1% Brij 96, and the whole cell lysates were fractionated by sucrose density gradient ultracentrifugation. Individual fractions were collected and analyzed by immunoblotting for the presence of NTAL and LAT and their phosphorylated forms (PY-20). Percentage of NTAL and LAT and their phosphorylated forms in low density fractions (fraction 1–4) is indicated by numbers under fractions.

predominantly in high density fractions. Although the amount of NTAL in low density fractions also decreased in activated cells (from 74.3 to 47.8%), most of the tyrosine-phosphorylated NTAL was found in lipid rafts fractions (69.5%). Compared with WT cells, NTAL$^{-/-}$ cells exhibited higher amount of LAT in low density fractions in both nonactivated and activated cells. This difference was even more pronounced when the distribution of tyrosine-phosphorylated LAT was analyzed (38.9 versus 66.6%). These data suggested that at least a fraction of LAT and NTAL could associate with different lipid-containing structures in plasma membrane.

To throw more light on the topography of LAT and NTAL, we isolated membrane sheets from an adherent mast cell line, RBL-2H3, which also possesses the two adaptor proteins (unpublished data), and analyzed their topography by immunogold electron microscopy. In resting cells, both NTAL and LAT were found in small clusters that distributed independently of FcεRI β subunits (Fig. 9, A and C). Based on the Hopkins test, these clusters were significantly different from random patterns. After FcεRI aggregation, the FcεRI β subunits accumulated predominantly in osmiophilic regions of the plasma membrane, thus confirming previously published data (24, 31). Clusters of both NTAL and LAT were often found in the vicinity of aggregated FcεRI, without forming mixed aggregates with them (Fig. 9, B and D).

Finally, we attempted to find out whether NTAL and LAT form mixed aggregates before and/or after FcεRI aggregation. To this end, we double labeled membrane sheets for LAT and NTAL, using combinations of 5- and 10-nm gold particles (Fig. 10). The labeling with 5-nm gold particles was consistently more abundant, regardless of whether the target was LAT or NTAL. This difference reflects technical aspects of the assay, since smaller gold particles more efficiently label target molecules than large gold particles. In nonactivated cells, LAT and NTAL each formed small clusters which did not mix. The visual observations that LAT and NTAL fail to mix were confirmed using the Ripley's statistical test (not depicted). Importantly, clusters of these transmembrane adaptors can often be seen in or near osmiophilic patches of activated membranes, but again no mixing of NTAL and LAT molecules was observed. Thus, NTAL and LAT are located in distinct, nonoverlapping regions of the plasma membrane in both nonactivated and activated cells.

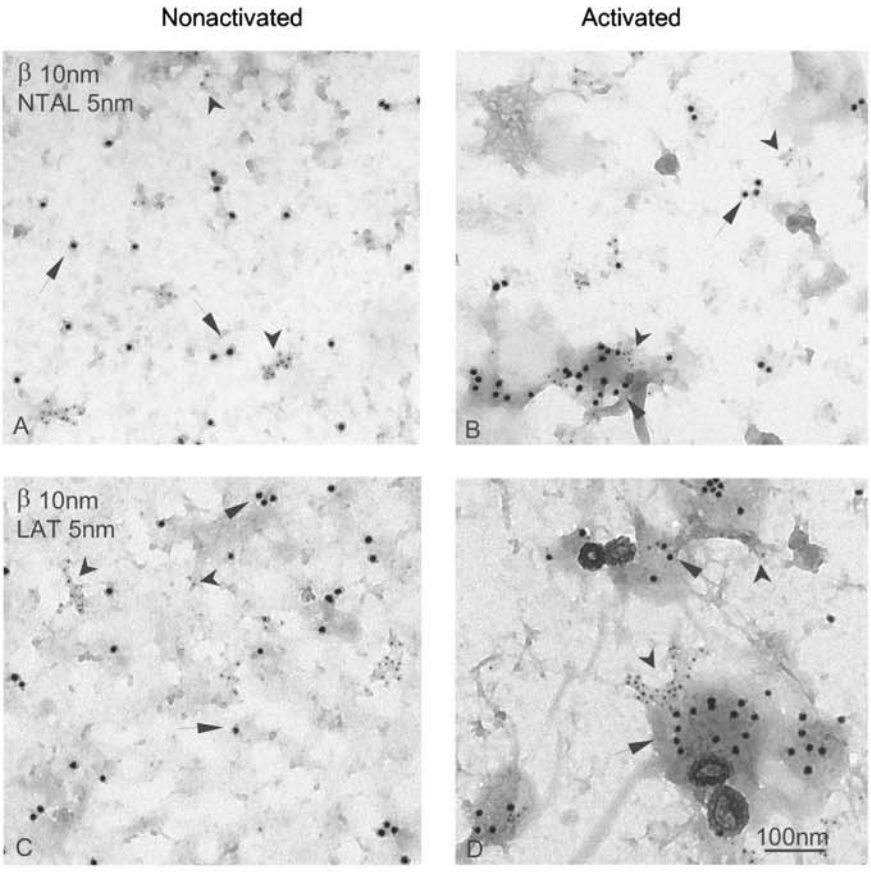


**Figure 9.** Membrane topography of NTAL, LAT, and FcεRI β subunit in nonactivated and Ag-activated cells. Membrane sheets were prepared from IgE-sensitized RBL-2H3 cells exposed for 2 min to PBS alone (A and C) or DNP-BSA in PBS (1 μg/ml; B and D), and double labeled from the cytoplasmic side of the plasma membrane for FcεRI β subunit (10-nm gold particles, arrows; A–D), NTAL (5-nm gold particles, arrowheads; A and B), or LAT (5-nm gold particles, arrowheads; C and D).

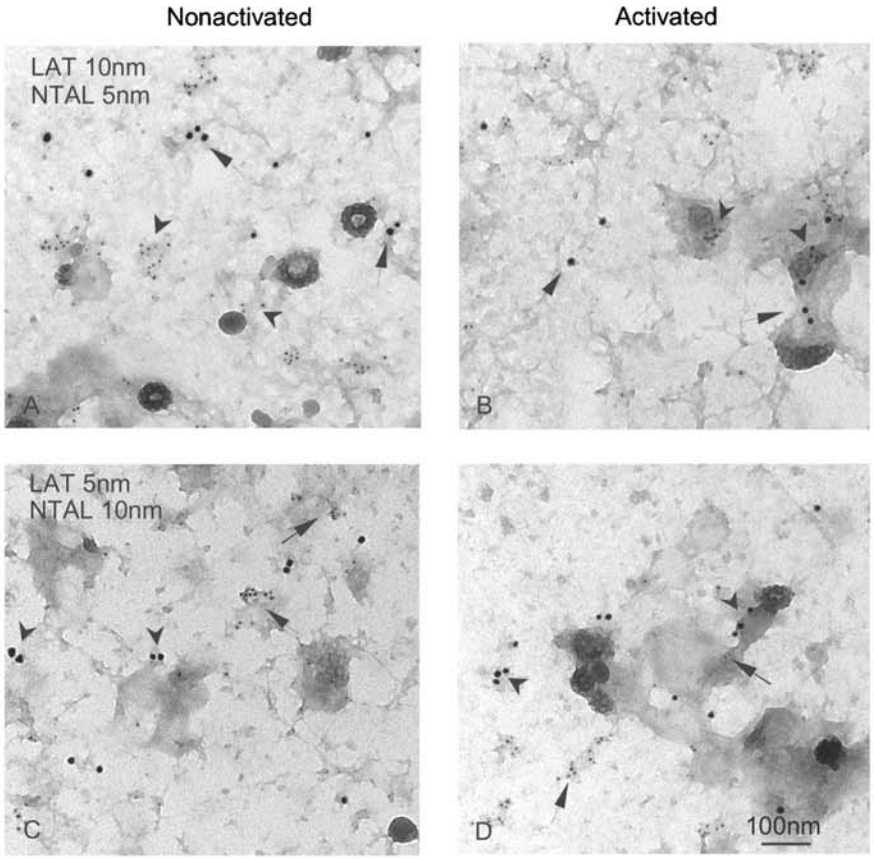


**Figure 10.** Different localization of NTAL and LAT clusters. Membrane sheets were prepared from nonactivated (A and C) and DNP-BSA–activated (1 μg/ml; B and D) RBL-2H3 cells and double-labeled from the inside for LAT (arrows), marked with 10-nm (A and B) or 5-nm (C and D) gold particles, and NTAL (arrowheads) marked with 5-nm (A and B) or 10-nm (C and D) gold particles.

## Discussion

The structural similarity of NTAL and LAT suggested that those two proteins could have similar functions. This notion was supported by their expression pattern. Whereas NTAL is expressed in B cells, which lack LAT, the reverse is true for LAT. Studies with LAT-deficient mice revealed a complete block in T cell development (17, 32), and LAT-negative T cell lines showed a complete block in TCR signaling (33, 34). Importantly, transfection of NTAL into LAT-deficient cells or mice partially restored the defects (2, 3, 5). Mast cells express both these proteins, and LAT deficiency had no effect either on mast cell development in vivo or maturation of mast cells in vitro (7). However, BMMCs from $LAT^{-/-}$ mice exhibited defects in pathways known to be downstream of Lyn and Syk kinase activation. These included FcεRI-mediated tyrosine phosphorylation of PLCγ, production of IP3, release of $Ca^{2+}$ from internal stores, and degranulation. Importantly, though the mast cell effector functions were impaired, they were not completely inhibited (7). These data together with enhanced tyrosine phosphorylation of NTAL in FcεRI-activated mast cells (2) and normal development of $NTAL^{-/-}$ mast cells under in vivo and in vitro conditions (this study) suggested that NTAL could be the missing adaptor protein responsible for the remaining signaling activity noted in LAT-deficient cells. However, several lines of evidence presented in this study indicate that NTAL, unlike LAT, has a negative regulatory role in FcεRI-mediated activation in mouse mast cells. First, $NTAL^{-/-}$ mice compared with WT mice exhibited an enhanced passive anaphylactic response. This systemic reaction reflects the activity of mast cells and was found reduced in $LAT^{-/-}$ cells (7). Second, BMMCs from $NTAL^{-/-}$ mice exhibited an enhanced degranulation. Third, several proteins in FcεRI-activated $NTAL^{-/-}$ cells exhibited an enhanced tyrosine phosphorylation and/or modified subcellular distribution. These proteins included Syk kinase, LAT, ERK, and PLCγ. Fourth, FcεRI-activated $NTAL^{-/-}$ cells exhibited an enhanced activity of PLCγ and PI3K, producing increased levels of IP3 and PI 3,4,5-trisphosphate, respectively. Finally, $NTAL^{-/-}$ phenotype was associated with a dramatic increase in calcium response in Ag-activated cells. This enhancement was mostly pronounced at suboptimal concentrations of the Ag and was observed even in the absence of extracellular calcium, suggesting that the enhanced release of calcium from intracellular stores contributes at least in part to this phenomenon. Thus, the conclusion based on our data seems to indicate that FcεRI-

mediated signaling events in BMMCs are negatively regulated by NTAL.

How could NTAL be involved in negative regulation of PLCγ and downstream signaling pathways? We propose that the inhibitory role of NTAL could result from its competition with LAT in lipid rafts. Furthermore, it should be noted that a major difference between LAT and NTAL is in the absence of the tyrosine residue responsible for interaction with PLCγ in the latter. In the absence of NTAL, more LAT is located in lipid rafts (Fig. 8) and is tyrosine phosphorylated (Fig. 4 C), resulting in (a) an increased recruitment of PLCγ into complexes formed around aggregated FcεRI, (b) enhanced tyrosine phosphorylation and enzymatic activities of PLCγ, (c) elevated production of IP3 and $[Ca^{2+}]_i$, and (d) more potent degranulation. Alternatively, NTAL could have a negative regulatory role in FcεRI signaling by indirect binding of phosphatases. In T cells, TCR ligation induces binding of Grb2 with SHP-2, and this interaction presumably brings the phosphatase into juxtaposition to its potential substrates (35). In stimulated mast cells, phosphorylated NTAL is a major binder of Grb2 (Fig. 5 C), and therefore, it is possible that in the absence of NTAL Grb2–phosphatase complexes are not properly targeted, and down-regulating signaling pathways are less effective. It should be mentioned that these two hypotheses are not mutually exclusive: in the absence of NTAL, more tyrosine-phosphorylated LAT in lipid rafts (Fig. 8) could better serve as a substrate for signaling molecules, and at the same time the signaling molecules could be more active due to the absence on NTAL-bound protein tyrosine phosphatases.

Our experiments with BMMCs defective in both adaptor proteins, NTAL and LAT, surprisingly reveal that NTAL, besides its negative regulatory role, may potentially also have a positive role in FcεRI signaling. Clearly, NTAL in the absence of LAT cannot play the above described inhibitory (competitive) role and it may take over, albeit with lower efficiency, some of the functions of LAT, just as it was observed in T cells (2, 3, 5). Which of these two functions would prevail could possibly depend on qualitative and/or quantitative differences in the composition of the signaling assemblies induced by FcεRI aggregation. These differences could explain why a diminution of NTAL expression by silencing RNA oligonucleotides in human mast cells resulted in an opposite phenotype (reduction of FcεRI-mediated secretory and calcium responses [6]) compared with that observed in $NTAL^{-/-}$ BMMCs (this study). In this context, it should be noted that profiles of tyrosine-phosphorylated proteins in human and mouse mast cells are very different (6). Furthermore, the influence of different tissue origins and cell culture conditions used for growth of human and mouse mast cells could also play a role.

Mast cell degranulation involves two signaling pathways proximal to FcεRI. Lyn-dependent pathway, which involves transmembrane adaptor LAT, serves as both kinetic accelerator and negative regulator of signaling, whereas Fyn-dependent pathway is essential for degranulation (8). Experiments with human mast cells suggested that NTAL could represent the transmembrane adaptor involved in the Fyn-dependent pathway (6). However, our findings that NTAL in mouse BMMCs is not essential for degranulation (Fig. 3) and that tyrosine phosphorylation of NTAL is not dependent on Fyn kinase activity but at least partially depends on Lyn kinase activity (unpublished data) suggest that NTAL is not involved in the Fyn-dependent pathway. Rather, NTAL could contribute in part to the complexity of Lyn-dependent regulatory mechanisms of mast cell signaling.

Although both NTAL and LAT are structurally similar molecules partitioning into lipid rafts in detergent-solubilized cells, a detailed analysis of their distribution on sucrose gradients indicate that they differ in physical properties, particularly in activated cells. Thus, ~60% of tyrosine-phosphorylated LAT was found in high density fractions of sucrose gradient, whereas a larger fraction (~70%) of phosphorylated NTAL was found in low density fractions (Fig. 8). These data suggest that the two molecules do not occupy the same regions of the plasma membrane. This was confirmed by electron microscopy analysis on membrane sheets. Previously, it has been shown that LAT in resting cells is found in clusters which do not mix with dispersed clusters of FcεRI β subunits (24, 31). We have confirmed these results and demonstrated that NTAL was also found in clusters that were similar in size to LAT clusters. Interestingly, NTAL clusters were topographically separated from LAT clusters. Aggregation of FcεRI induced a redistribution of the receptor into distinct areas of the plasma membrane that are characterized by their dark staining with osmium, proximity of clathrin-coated pits, and accumulation of several signaling molecules (24, 31). Although NTAL and LAT were often found in the vicinity of these aggregates, they did not form mixed aggregates.

In conclusion, our data indicate that at least in murine mast cells, NTAL mostly negatively regulates the activation through FcεRI. Therefore, it can be speculated that the absence, reduced expression, or mutations in this adaptor protein might be a contributing factor in an increased sensitivity to allergens.

We thank H. Mrázová, D. Lorenčíková, and M. Dráber for technical assistance, and Dr. J. Rivera for kindly providing the FcεRI β chain–specific antibody.

This work was supported by project LN00A026 (Center of Molecular and Cellular Immunology) from the Ministry of Education, Youth and Sports of the Czech Republic, grants 204/03/0594 and 301/03/0596 from the Grant Agency of the Czech Republic, and grant A5052310 from the Grant Agency of the Academy of Sciences of the Czech Republic. The generation of NTAL-deficient mice was supported by Institut National de la Santé et de la Recherche Médicale, Centre National de la Recherche Scientifique, and Plate-forme Rassemblement Inter Organismes. The research of P. Heneberg was supported in part by Research goal no. 002 from the 3rd Faculty of Medicine, Charles University, Prague, and the research of P. Dráber was supported by an International Research Scholar's Award from Howard Hughes Medical Institute.

The authors have no conflicting financial interests.

*Submitted: 18 June 2004*
*Accepted: 31 August 2004*

## References


1. Kinet, J.P. 1999. The high-affinity IgE receptor (FcεRI): from physiology to pathology. *Annu. Rev. Immunol.* 17:931–972.
2. Brdička, T., M. Imrich, P. Angelisová, N. Brdičková, O. Horváth, J. Špička, I. Hilgert, P. Lusková, P. Dráber, P. Novák, et al. 2002. Non-T cell activation linker (NTAL): a transmembrane adaptor protein involved in immunoreceptor signaling. *J. Exp. Med.* 196:1617–1626.
3. Janssen, E., M. Zhu, W. Zhang, S. Koonpaew, and W. Zhang. 2003. LAB: a new membrane-associated adaptor molecule in B cell activation. *Nat. Immunol.* 4:117–123.
4. Harder, T., and K.R. Engelhardt. 2004. Membrane domains in lymphocytes—from lipid rafts to protein scaffolds. *Traffic.* 5:265–275.
5. Janssen, E., M. Zhu, B. Craven, and W. Zhang. 2004. Linker for activation of B cells: a functional equivalent of a mutant linker for activation of T cells deficient in phospholipase C-γ1 binding. *J. Immunol.* 172:6810–6819.
6. Tkaczyk, C., V. Horejsi, I. Shoko, P. Draber, L.E. Samelson, A.B. Satterthwaite, D.H. Nahm, D.D. Metcalfe, and A.M. Gilfillan. 2004. NTAL phosphorylation is a pivotal link between the signaling cascades leading to human mast cell degranulation following kit activation and FcεRI aggregation. *Blood.* 104:207–214.
7. Saitoh, S., R. Arudchandran, T.S. Manetz, W. Zhang, C.L. Sommers, P.E. Love, J. Rivera, and L.E. Samelson. 2000. LAT is essential for FcεRI-mediated mast cell activation. *Immunity.* 12:525–535.
8. Parravicini, V., M. Gadina, M. Kovarova, S. Odom, C. Gonzalez-Espinosa, Y. Furumoto, S. Saitoh, L.E. Samelson, J.J. O'Shea, and J. Rivera. 2002. Fyn kinase initiates complementary signals required for IgE-dependent mast cell degranulation. *Nat. Immunol.* 3:741–748.
9. Tolar, P., L. Dráberová, and P. Dráber. 1997. Protein tyrosine kinase Syk is involved in Thy-1 signaling in rat basophilic leukemia cells. *Eur. J. Immunol.* 27:3389–3397.
10. Tolar, P., M. Tumová, and P. Dráber. 2001. New monoclonal antibodies recognizing the adaptor protein LAT. *Folia Biol. (Praha).* 47:215–217.
11. Rivera, J., J.-P. Kinet, J. Kim, C. Pucillo, and H. Metzger. 1988. Studies with a monoclonal antibody to the β subunit of the receptor with high affinity for immunoglobulin E. *Mol. Immunol.* 25:647–661.
12. Rudolph, A.K., P.D. Burrows, and M.R. Wabl. 1981. Thirteen hybridomas secreting hapten-specific immunoglobulin E from mice with $Ig^a$ or $Ig^b$ heavy chain haplotype. *Eur. J. Immunol.* 11:527–529.
13. Liu, F.-T., J.W. Bohn, E.L. Ferry, H. Yamanoto, C.A. Molinaro, L.A. Sherman, N.R. Klinman, and D.H. Katz. 1980. Monoclonal dinitrophenyl-specific murine IgE antibody: preparation, isolation, and characterization. *J. Immunol.* 124:2728–2737.
14. Kovářová, M., P. Tolar, R. Arudchandran, L. Dráberová, J. Rivera, and P. Dráber. 2001. Structure-function analysis of Lyn kinase association with lipid rafts and initiation of early signaling events after Fcε receptor I aggregation. *Mol. Cell. Biol.* 21:8318–8328.
15. Kress, C., S. Vandormael-Pournin, P. Baldacci, M. Cohen-Tannoudji, and C. Babinet. 1998. Nonpermissiveness for mouse embryonic stem (ES) cell derivation circumvented by a single backcross to 129/Sv strain: establishment of ES cell lines bearing the Omd conditional lethal mutation. *Mamm. Genome.* 9:998–1001.
16. Schwenk, F., U. Baron, and K. Rajewsky. 1995. A cre-transgenic mouse strain for the ubiquitous deletion of loxP-flanked gene segments including deletion in germ cells. *Nucleic Acids Res.* 23:5080–5081.
17. Nunez-Cruz, S., E. Aguado, S. Richelme, B. Chetaille, A.M. Mura, M. Richelme, L. Pouyet, E. Jouvin-Marche, L. Xerri, B. Malissen, and M. Malissen. 2003. LAT regulates γδ T cell homeostasis and differentiation. *Nat. Immunol.* 4:999–1008.
18. Yamaguchi, M., C.S. Lantz, H.C. Oettgen, I.M. Katona, T. Fleming, I. Miyajima, J.P. Kinet, and S.J. Galli. 1997. IgE enhances mouse mast cell FcεRI expression in vitro and in vivo: evidence for a novel amplification mechanism in IgE-dependent reactions. *J. Exp. Med.* 185:663–672.
19. Demo, S.D., E. Masuda, A.B. Rossi, B.T. Throndset, A.L. Gerard, E.H. Chan, R.J. Armstrong, B.P. Fox, J.B. Lorens, D.G. Payan, et al. 1999. Quantitative measurement of mast cell degranulation using a novel flow cytometric annexin-V binding assay. *Cytometry.* 36:340–348.
20. Surviladze, Z., L. Dráberová, M. Kovářová, M. Boubelík, and P. Dráber. 2001. Differential sensitivity to acute cholesterol lowering of activation mediated via the high-affinity IgE receptor and Thy-1 glycoprotein. *Eur. J. Immunol.* 31:1–10.
21. Dráberová, L., L. Dudková, M. Boubelík, H. Tolarová, F. Šmíd, and P. Dráber. 2003. Exogenous administration of gangliosides inhibits FcεRI-mediated mast cell degranulation by decreasing the activity of phospholipase Cγ. *J. Immunol.* 171:3585–3593.
22. Dráberová, L. 1990. Cyclosporin A inhibits rat mast cell activation. *Eur. J. Immunol.* 20:1469–1473.
23. Tolarová, H., L. Dráberová, P. Heneberg, and P. Dráber. 2004. Involvement of filamentous actin in setting the threshold for degranulation in mast cells. *Eur. J. Immunol.* 34:1627–1636.
24. Wilson, B.S., J.R. Pfeiffer, and J.M. Oliver. 2000. Observing FcεRI signaling from the inside of the mast cell membrane. *J. Cell Biol.* 149:1131–1142.
25. Wilson, B.S., S.L. Steinberg, K. Liederman, J.R. Pfeiffer, Z. Surviladze, J. Zhang, L.E. Samelson, L.H. Yang, P.G. Kotula, and J.M. Oliver. 2004. Markers for detergent-resistant lipid rafts occupy distinct and dynamic domains in native membranes. *Mol. Biol. Cell.* 15:2580–2592.
26. Gu, H., K. Saito, L.D. Klaman, J. Shen, T. Fleming, Y. Wang, J.C. Pratt, G. Lin, B. Lim, J.-P. Kinet, and B.G. Neel. 2001. Essential role for Gab2 in the allergic response. *Nature.* 412:186–190.
27. Xie, Z.H., I. Ambudkar, and R.P. Siraganian. 2002. The adapter molecule Gab2 regulates FcεRI-mediated signal transduction in mast cells. *J. Immunol.* 168:4682–4691.
28. Wu, C.J., D.M. O'Rourke, G.S. Feng, G.R. Johnson, Q. Wang, and M.I. Greene. 2001. The tyrosine phosphatase SHP-2 is required for mediating phosphatidylinositol 3-kinase/Akt activation by growth factors. *Oncogene.* 20:6018–6025.
29. Zhang, S.Q., W.G. Tsiaras, T. Araki, G. Wen, L. Minichiello, R. Klein, and B.G. Neel. 2002. Receptor-specific regulation of phosphatidylinositol 3′-kinase activation by the protein tyrosine phosphatase Shp2. *Mol. Cell. Biol.* 22:4062–4072.
30. Putney, J.W., Jr., L.M. Broad, F.J. Braun, J.P. Lievremont, and G.S. Bird. 2001. Mechanisms of capacitative calcium entry. *J. Cell Sci.* 114:2223–2229.
31. Wilson, B.S., J.R. Pfeiffer, Z. Surviladze, E.A. Gaudet, and

J.M. Oliver. 2001. High resolution mapping of mast cell membranes reveals primary and secondary domains of FcεRI and LAT. *J. Cell Biol.* 154:645–658.
32. Zhang, W., C.L. Sommers, D.N. Burshtyn, C.C. Stebbins, J.B. DeJarnette, R.P. Trible, A. Grinberg, H.C. Tsay, H.M. Jacobs, C.M. Kessler, et al. 1999. Essential role of LAT in T cell development. *Immunity*. 10:323–332.
33. Finco, T.S., T. Kadlecek, W. Zhang, L.E. Samelson, and A. Weiss. 1998. LAT is required for TCR-mediated activation of PLCγ1 and the Ras pathway. *Immunity*. 9:617–626.
34. Zhang, W., B.J. Irvin, R.P. Trible, R.T. Abraham, and L.E. Samelson. 1999. Functional analysis of LAT in TCR-mediated signaling pathways using a LAT-deficient Jurkat cell line. *Int. Immunol.* 11:943–950.
35. Tailor, P., T. Jascur, S. Williams, M. von Willebrand, C. Couture, and T. Mustelin. 1996. Involvement of Src-homology-2-domain-containing protein-tyrosine phosphatase 2 in T cell activation. *Eur. J. Biochem.* 237:736–742.

**6.3**

**Heneberg, P. & Dráber, P. (2005):**

**Regulation of Cys-based protein tyrosine phosphatases *via* reactive oxygen and nitrogen species in mast cells and basophils.**

**Current Medicinal Chemistry 12(16): 1859-1871.**

# Regulation of Cys-Based Protein Tyrosine Phosphatases *Via* Reactive Oxygen and Nitrogen Species in Mast Cells and Basophils

P. Heneberg[1,2] and P. Dráber*,[1]

[1]*Department of Signal Transduction, Institute of Molecular Genetics, Academy of Sciences of the Czech Republic, Prague, Czech Republic*

[2]*3rd Medical Faculty, Charles University, Prague, Czech Republic*

**Abstract:** Activation of mast cells and basophils is accompanied by the production of reactive oxygen and nitrogen species that regulate diverse signaling pathways leading to the release of inflammatory mediators and production of a variety of cytokines. Although the functional pathways of reactive oxygen and nitrogen species *in vivo* are not completely understood, some novel metabolic pathways can be envisioned based on recent findings that protein tyrosine phosphatases can be regulated by reversible oxidation. In this review, we describe major sources and targets of reactive oxide and nitrogen species in mast cells and basophils. Direct and indirect regulations of class I and II Cys-based protein tyrosine phosphatases (LMW-PTP, PTEN, PTP-PEST, SHP-2, PTP1B, PTPα, PTPε, DEP-1, TC45, SHP-1, HePTP and LAR) are discussed. The combined data highlight the role of redox-regulated protein tyrosine phosphatases as targets in the development of new ways of therapeutic intervention in allergies and inflammatory diseases.

**Keywords**: Mast Cell, Basophils, IgE Receptor, Tyrosine Phosphatase, Hydrogen Peroxide, Superoxide, Nitric Oxide, Redox-regulation.

## INTRODUCTION

A mounting evidence supports the concept that reactive oxygen species (ROS) are involved in a variety of cell activation pathways. The NADPH oxidase complex has been found in many phagocytic and non-phagocytic cells including mast cells and basophils, and direct sensors of the ROS and reactive nitric species (RNS) have been proposed in these cells [1]. Typically, 1-5% of electrons from the mitochondrial respiratory chain are diverted to the formation of superoxide by ubiquinone-dependent reduction [2]. However, the molecular mechanism of ROS and RNS signaling in various cell types is only partially understood. One of the potential targets of ROS and RNS are the protein tyrosine phosphatases (PTPs), which have been shown to become inactivated after treatments enhancing the concentrations of ROS or RNS.

Mast cells are highly specialized secretory cells distributed widely throughout the tissues, particularly in the proximity to blood vessels, nerves and epithelia. Antigen-mediated aggregation of the high affinity IgE receptor (FcεRI) on the surface of mast cells induces within minutes, the secretion of preformed allergy mediators like β-hexosaminidase, histamine, serotonin, proteoglycans and proteases. Later on, the cells synthesize mRNA for multiple cytokines including interleukin (IL)-2 – IL-6, IL-8 and interferon (INF)-γ. Besides that, they also produce IL-1, granulocyte macrophage-colony stimulating factor, macrophage inflammatory protein-1α and β, monocytic chemotactic protein-1, and tumor necrosis factor (TNF)-α [3].

*Address correspondence to this author at the Department of Signal Transduction, Institute of Molecular Genetics, Academy of Sciences of the Czech Republic, Vídeňská 1083, CZ-142 20 Prague 4 – Krč, Czech Republic; Tel: +420-241062468; Fax: +420-241 470 339; E-mail: draberpe@biomed.cas.cz

0929-8673/05 $50.00+.00 

Recent progress has defined the molecular pathways involved in the stimulation of mast cells, and has shown the importance of protein tyrosine kinases (PTKs) and PTPs in this process. More than ten PTPs have been identified and characterized in mast cells and basophils; some of them are involved directly in the FcεRI-mediated activation pathways [4-7].

Recently, Suzuki *et al.* found that FcεRI-mediated activation of bone marrow mast cells (BMMC) and rat basophilic leukemia cells (RBL) was accompanied by the production of ROS involved in the release of inflammatory mediators [8]. Other studies described that some mast cell populations also expressed several nitric oxide synthase (NOS) isoforms [9], and that nitric oxide (NO) controlled, at least in part, mast cell survival, proliferation and activation [10]. Thus, it seems that the NO pathways play an exocrine as well as autocrine regulatory role in mast cell physiology. The functional pathways of ROS and RNS signaling *in vivo* remains incompletely understood. However, because it is known that reversible oxidation is one of the main regulatory mechanisms of many PTPs [11], one can imagine novel links in cellular signaling *via* these critical regulators.

In this review, we describe the major sources and targets of ROS and RNS in mast cells and basophils. Emphasis is put on the potential involvement of ROS and RNS in the inhibition of PTPs, and thus in the setting of a threshold for activation *via* FcεRI and other surface receptors.

## ENDOGENOUS ROS PRODUCTION

ROS such as superoxide, hydrogen peroxide and hydroxyl radical are small diffusible molecules produced in virtually every cell type by the action of a broad range of enzymes. Previous studies disputed the ability of mast cells to produce ROS [12], arguing that isolated mast cells used

in most experiments were contaminated with a small fraction of macrophages, which are known to produce 30-times more ROS than mast cells. These objections were refuted in recent studies which demonstrated that RBL cells produced ROS upon FcεRI aggregation and released them into the extracellular space [13,14]. ROS production in RBL cells could be inhibited by diphenyleneiodonium (DPI; a broad-spectrum inhibitor of flavoprotein-containing oxidoreductases) or antioxidants; the inhibition results in the suppression of IgE-mediated release of histamine release leukotriene $C_4$ [15,16] (Fig. (**1**)). Production of ROS in FcεRI-activated cells is dependent on the dose of antigen, with the maximum effect at > 30 ng TNP-BSA/ml, and attains its peak level about 5 min after FcεRI triggering. [8]. Antigen-activated BMMC show a more prominent increase of ROS, even surpassing that observed in RBL cells [8]. FcεRI-mediated ROS production in mast cells is facilitated by NOX (NADPH oxidases) and DUOX (dual domain oxidases) families. The predominant ROS produced in FcεRI-triggered RBL cells is $H_2O_2$. An increase in $H_2O_2$ production is observable within 2 min after stimulation with the peak at about 10 min [8]. Low levels of superoxide are also released from the cells [12].

The oxidative burst is abrogated by selective inhibitors of the Src family kinases, Syk kinase, and phosphoinositide 3-kinase (PI3K) [8]. Syk and PI3K have been shown to be involved in intracellular signaling, leading to $H_2O_2$ production in phagocytic and non-phagocytic cells [17,18]. In neutrophils, two pools of PI3K exist, one localized in the plasma membrane and the other in the membranes of granules. The release of superoxide is independent of PI3K, whereas intracellular production of this radical depends on the enzyme [18].

## ENDOGENOUS RNS PRODUCTION

NO is a 30 Da uncharged molecule carrying an unpaired electron, classifying it as a radical. It is able to diffuse into and out of the cells and between cellular compartments. NOS-mediated NO synthesis requires L-arginine as a sole nitrogen donor and co-factor. Cellular arginine levels are dependent on a variety of synthesis and transport mechanisms including uptake from extracellular fluid, intracellular protein breakdown and endogenous synthesis. Two basic factors necessary to activate NOS are the presence of L-arginine and the availability of an electron donor tetrahydrobiopterin, generated from GTP in a process utilizing a couple of enzymes with the important role of GTP cyclohydrolase I [9].

FcεRI-mediated activation of mucosal and serosal mast cells, as well as CD8-mediated activation of serosal mast cells, results in the production of the inducible isoform of NOS (iNOS) [19]. Low levels of iNOS mRNA and NO production are observed in long-term stem cell factor (SCF)-treated BMMC undergoing maturation into connective tissue mast cells [19]. Expression of iNOS in mast cells is upregulated not only after FcεRI-mediated activation [19], but also after an exposure of the cells to various mediators, including TNF-α and IL-1β [20] (Fig. (**2**)). Surprisingly, IL-10 is the only cytokine downregulating the constitutive and inducible NO production by mast cells. This effect is

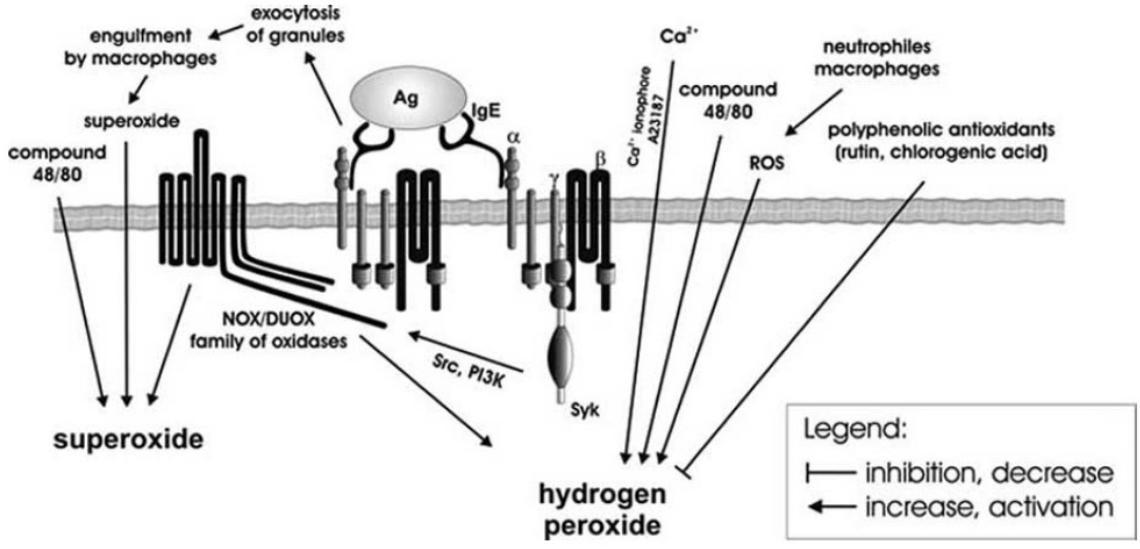


**Fig. (1).** Sources of ROS in mast cells. Aggregation of FcεRI by multivalent antigen leads to tyrosine phosphorylation of FcεRI subunits, followed by phosphorylation and activation of Syk kinase and numerous other substrates. Activated Syk, together with Src family kinases and PI3K are responsible for further transfer of the signal to the NOX /DUOX family and other substrates. Subsequent exocytosis of secretory granules could lead to their engulfment by macrophages followed by the release of superoxide. Superoxide generated by macrophages is capable of penetrating the plasma membrane and modifying certain signaling pathways. Superoxide can also be produced directly in mast cells in response to FcεRI-aggregation or stimulation with compound 48/80. Production of $H_2O_2$ in mast cells can be stimulated by the antigen-mediated activation, $Ca^{2+}$ ionophore A23187 or compound 48/80. ROS can be also produced by neutrophiles or macrophages and further processed intracellularly. ROS production can be inhibited by polyphenolic antioxidants, including rutin or chlorogenic acid.

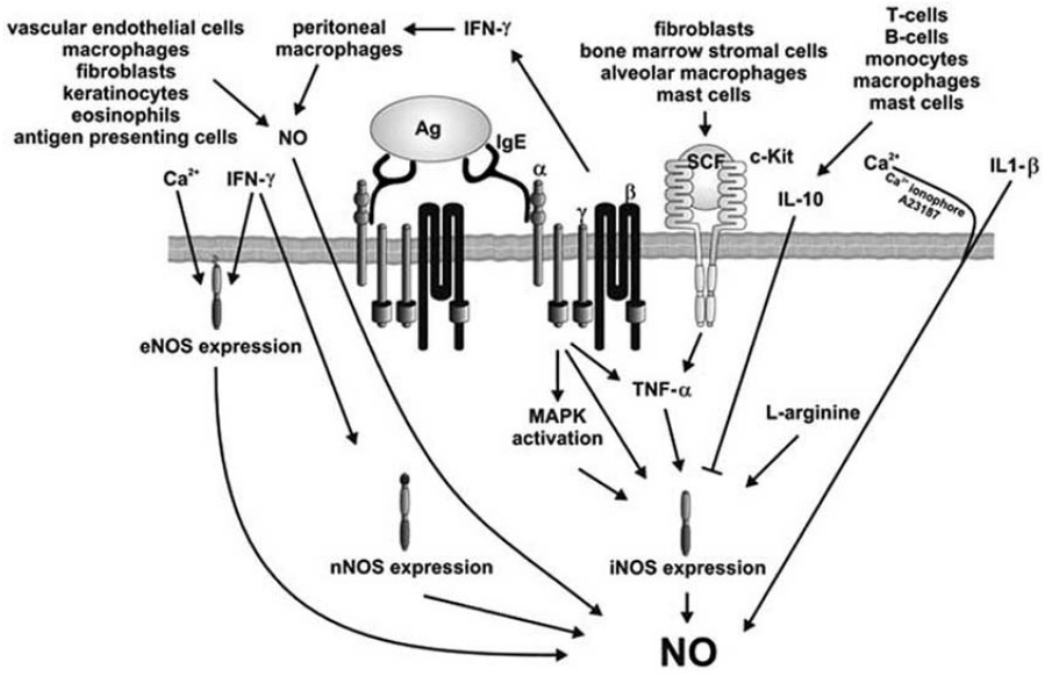


**Fig. (2).** Sources of NO in mast cells. Aggregation of FcεRI by multivalent antigen leads to the production of NO through the expression of iNOS. iNOS expression can be enhanced by three distinct pathways involving TNF-α, MAPK activation or a special pathway, which includes neither TNF-α nor MAPK. Another pathway leading to NO production is *via* cKit. This pathway is initiated by binding the SCF (produced by fibroblasts and other cell types) to c-Kit, followed by production of TNF-α and enhanced expression of iNOS. iNOS expression can be inhibited by IL-10 produced by T- and B-cells, monocytes, macrophages and mast cells. Aggregation of FcεRI also leads to the release of IFN-γ, which is capable of inducing NO production in macrophages. IFN-γ could also enhance NO production *via* two other NOS isoforms, e-NOS and nNOS. Enhanced concentration of free cytoplasmic calcium ions also leads to an enhanced production of NO *via* eNOS. NO production is also enhanced in cells exposed to IL1-β, together with $Ca^{2+}$ ionophore. Extracellular NO, produced by macrophages and some other cells types, can penetrate the cell membrane. Not all the pathways are present in all mast cell types. Symbols are explained in Fig. (**1**).

likely to be important in mast cell biology, since these cells are capable releasing IL-10 [21]. Interestingly, in human epithelial cells, iNOS can be suppressed by action of IL-4, IL-13 and glucocorticoids [22].

The mechanism of iNOS activation seems to be biphasic; the early phase, induced immediately after FcεRI triggering, is responsible for the induction of initial iNOS mRNA synthesis. The late phase of iNOS mRNA synthesis reflects the FcεRI-mediated production and release of TNF-α, which dose-dependently upregulates the sustained synthesis of iNOS mRNA. The role of TNF-α in regulation of iNOS mRNA expression is accentuated by the finding that SCF enhances both TNF-α synthesis and iNOS expression [10,21]. Another signal for iNOS synthesis might come from the FcεRI-mediated activation of MAP kinases, which have already been shown to induce iNOS expression in other cellular systems [23].

In human basophils, endogenous NO synthesis is also stimulated by relaxin, a peptide hormone produced mainly by the corpus luteum during pregnancy and prominently influencing the cardiovascular system. Previous data showed that relaxin inhibited the histamine release from activated mast cells and basophils [24]. This inhibitory effect seems to be mediated by RNS, because the effect of relaxin on FcεRI-mediated mast cell activation could be mitigated by incubation of the cells with NOS inhibitor, $N^{\omega}$-monomethyl-L-arginine (L-NMMA), or with 1*H*-[1,2,4]oxadiazolo-[4,3-α]quinoxalin-1-one, an inhibitor of the NO physiological target guanylate cyclase [25].

It should be mentioned that the regulation of mast cell signaling is affected not only by NO, but also by RNS generated from NO *via* its reaction with $O_2$ or $O_2^-$. Main targets of NO are the PTPs, guanylate cyclase, NOS, cyclooxygenase, carbon centered radicals and lipid radicals. NO also regulates the $Cl^-$ secretion, which in turn may influence the FcεRI-mediated histamine release [9]. RNS have three main mechanisms of action – nitration (nitrotyrosine, nitroguanosine), oxidation (DNA strand breaks, lipid peroxidation, and hydroxylation) and nitrosation (nitrosamines, *S*-nitrosothiols). For example, the *S*-nitrosation of p21Ras leads to an enhanced level of TNF through p21Ras involvement in the growth factor signal pathways. Examples of RNS commonly found *in vivo* in mast cells are peroxynitrite anion ($ONOO^-$) and dinitrogentrioxide ($N_2O_3$) [9].

Expression and translational regulation of NOS in mast cells, regulation of their function by NO, regulation of ion channels, release of mediators and modulation of mast cell

adhesion and survival have been already reviewed [9]. Production of RNS and NO in *in vivo*-derived mast cells has also been surveyed [26,27]. However, it should be mentioned that production of RNS in mast cells is controversial and that several papers from Coleman's group showed that antigen activated human and rodent mast cells are unable to generate detectable levels of intracellular NO [28-30]. These contradictions should be solved in near future .

## MAST CELLS AS A TARGET FOR ROS

Previous experiments indicated that pervanadate generated from a combination of $H_2O_2$ and $Na_3VO_4$ concomitantly induced protein tyrosine phosphorylation, formation of inositol 1,4,5-trisphosphate, an increase in calcium influx, and histamine secretion in RBL and mast cells, thus mimicking the action of crosslinked FcεRI [31] (Fig. (**3**)).

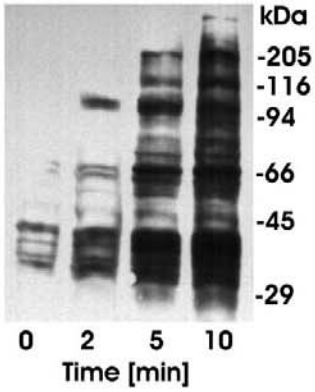


**Fig. (3).** Tyrosine phosphorylated proteins in cells pretreated with 10 mM pervanadate. RBL cells were exposed to pervanadate for the indicated time intervals, lysed, size fractionated by polyacrylamide gel electrophoresis, and analyzed for the presence of phosphotyrosine residues by immunoblotting with PY-20 antibody labeled with horseradish peroxidase. From [32] with permission from Wiley-VCH Publishers, Inc.

Although the inhibitory effect of pervanadate on PTPs has been known for long and several reports on the use of pervanadate for mast cell activation have been published (see e.g.[32]), the molecular mechanism of the action of pervanadate remained enigmatic. It has been shown only recently that DPI inhibits ROS synthesis in RBL cells and suppresses in a dose-dependent manner, the FcεRI-mediated histamine and β-hexosaminidase release. It is surprising that ebselen, a glutathione peroxidase mimetic agent scavenging peroxides, had no influence on this process. The blockade of ROS, both by DPI and by ebselen, also impaired the release of $LTC_4$ [8]. It should be mentioned in this connection that degranulation in rat peritoneal mast cells, but not RBL cells, was induced by chemically derived superoxide [33], potassium superoxide [34], and $H_2O_2$ [35]. Degranulation in RBL cells was observed only at relatively high concentrations of $H_2O_2$ (2 mM), which are probably toxic [12]. It is important to note that intracellular concentrations of $H_2O_2$ during FcεRI-mediated signaling vary from 1nM to a maximum of 700 nM [1]. When applied extracellularly, a gradient of $H_2O_2$ is rapidly established across the plasma membrane resulting in an intracellular concentration 7-10 fold below that found in the extracellular space [36,37]. The maximal extracellular concentration of $H_2O_2$ in mammalian tissues is usually around 2-4 μM [38], which could bring intracellular levels up to 700 nM. Even higher concentrations of ROS (10-100 μM) may be reached in the immediate vicinity of activated macrophages, suggesting that high concentrations of ROS might be physiologically relevant [39-41].

The calcium response in FcεRI-activated RBL cells is impaired, though not completely inhibited, by both DPI and ebselen. Complete inhibition of calcium response occurs in the presence of $La^{3+}$ ions, which block the calcium influx, or if the store-operated calcium entry is blocked by its antagonists [8]. DPI and ebselen reduced the increase of FcεRI-mediated tyrosine phosphorylation of phospholipase C (PLC)γ1 by 71% and 47 % respectively and that of PLCγ2 by, 90% and 57 % respectively, [8]. This in turn could cause an inhibition of store-operated calcium entry. Another molecule involved in the calcium flux pathways is the transmembrane adaptor protein LAT which binds PLCγ. DPI and ebselen suppressed the FcεRI-mediated tyrosine phosphorylation of LAT by, 66 and 53 % respectively, [8]. It has been shown that LAT deficiency considerably impairs multiple signaling events including calcium flux, degranulation and cytokine production in BMMC [42,43], and that LAT-deficient mast cells resemble those with blocked ROS production [8]. The combined data suggest that tyrosine phosphorylation of LAT, PLCγ and some other substrates is ROS dependent in RBL cells. These data could be explained by postulating that PTKs involved in FcεRI-mediated signaling are downregulated by the ROS. Alternatively, it is possible that some PTPs are upregulated under these conditions [11].

Several other proteins are affected by ROS. The best known examples are peroxidases and catalases, which specifically react with $H_2O_2$. This reactivity reflects in part the presence of active site residues like Cys-thiolate, selenocysteine, ferric heme or vanadate [1]. Cys-thiolates are also used by Cys-proteases, thiol-disulfide reductases, dehydrogenases, dual specificity phosphatases and PTPs [1]. ROS also oxidize the transcription factors such as the nuclear factor κ-B [44], activator protein 1 [45], hypoxia-inducible factor [46], p53 [47], and p21Ras [48]. The effect of ROS on the PTP-mediated signaling will be described below.

## MAST CELLS AS A TARGET FOR RNS

NO radicals can modify target molecules by three major ways. First, NO can induce *S*-nitrosylation of thiol groups of free aminoacids, peptides or proteins. Second, it is also capable of donating electrons allowing reactions with transition of metals such as iron, copper or zinc. Finally, NO can react with other radicals, and the process results in the formation of peroxynitrite, tyrosyl or tryptophanyl radicals (reviewed in [49]).

In all their locations, mast cells are in close contact with other NO-producing cells, such as macrophages, fibroblasts, keratinocytes, and vascular endothelial cells [10]. Vane and

collaborators first reported an inhibitory action of NO on histamine release from mast cells [50,51]. The authors showed that exogenous NO was able to induce apoptosis and impaired mast cell survival and proliferation. Importantly, the cytocidal effects of NO were blocked by the presence of SCF in the growth medium [10,52]. At the molecular level, exogenous NO induces a rapid increase of cGMP levels that preceed an accumulation of cAMP in mast cells. This can then result in a decrease of intracellular calcium and subsequent inhibition of the PKC-dependent proliferation pathway, which might explain the NO-mediated inhibition of mast cell proliferation [10].

NO, either exogenous or endogenous, is an effective modulator of the release after antigen challenge of vasoactive mediators that have a protective role against allergic and anaphylactic reactions. The release of histamine from BMMC can be inhibited by incubation with sodium nitroprusside, an exogenous NO donor, and enhanced by the treatment with NOS inhibitor, L-NMMA [24]. Sodium nitroprusside also inhibits the release of β-hexosaminidase and TNF-α from BMMC [10]. However, when cell lines (C1.MC/C57.1 or RBL) or isolated mast cells were used, no NO-mediated regulation of secretory responses was observed [29,53]. Furter studies showed that NO generated from *S*-nitrosoglutathione inhibited the FcεRI-mediated serotonin release from mouse and rat peritoneal mast cells [53]. Herman and co-workers showed that NO-mediated regulation of histamine and tryptase release could also be observed in human skin mast cells [54], and Coleman found that an addition of RNS to cultured RBL cells inhibited antigen-induced cytokine mRNA expression, in particular, mRNA for IL-4, IL-6 and TNF-α [55].

Different NO donors have a different mechanism of action, which might in part explain the inconsistency of results in different studies. Thus, sodium nitroprusside and 3-morpholinosydnonimine-HCl spontaneously release the NO intracellularly or extracellularly, respectively, while $NaNO_2$ and $NaNO_3$ require intracellular bioactivators. Lipopolysaccharides are inducers of NOS, and L-arginine in contrast to D-arginine, is the natural precursor for NO formation [56]. However, the effects of NO donors described above are not consistent and vary with different cell types. Thus, BMMC and peritoneal mast cells seem to be sensitive to NO donors, whereas mast cell-derived cell lines and some mast cell populations do not show any response to NO.

Various mast cell types differ in their sensitivity to NOS inhibitors. For example, inhibitors of NO-production ($N^{\omega}$-nitro-L-arginine, sodium nitroprusside, aminoguanidine and methylene blue) have little effect on either basal or induced histamine release from rat peritoneal mast cells [56], but can affect the NO production and cGMP levels in purified rat peritoneal mast cells [50]. Another inhibitor of NO production, hemoglobin, inhibited the histamine release from rat mast cells activated by antigen-IgE complexes or A23187 ionophore, but was inactive after activation by means of compound 48/80 [56]. Interestingly, IFN-γ was able to potentiate the NO production and inhibit the FcεRI-mediated secretory function of mouse peritoneal mast cells [28]. The combined data indicate that NO-regulated pathways modulate the secretory responses of mast cells, and this capability in turn determines the outcomes of various physiological and pathological responses, including immune [57] and nasal airway response [58]. Important molecular targets of NO are various kinases, including p21ras, PKB, SEK1, JNK1, JNK2, SAPK, Erk1, Erk2, PI3K, Jak3, Tyk2, STAT5, Src, Raf-1 kinase, FAK and creatine kinase (reviewed in [49]), and PTPs (this review).

## EFFECTS OF ROS ON THE ACTIVITY OF PTPS

PTPs denote a large family of enzymes encoded by 107 genes, 99 of which represent the class I Cys-based PTPs [59]. Several Cys-based PTPs, which are known to be regulated by ROS and/or RNS, are reported in Fig. (**4**); biochemical properties and functions of PTPs present in mast cells and basophils have recently been reviewed [5]). It is known that the Cys in catalytic domain of PTPs is highly susceptible to oxidation *in vitro*, and it has been speculated that this could play a role in cells exposed to oxidizing agents. Unlike most of other Cys residues, which remain protonated at the physiological pH (pKa>8.0), the Cys residue in catalytic domain of PTPs is extremely reactive and rapidly forms a thiolate anion at physiological pH (pKa<6.0). This is a necessary step for the catalytic activity of PTPs requiring the phosphocysteine intermediate. The high reactivity of catalytic Cys required for enzymatic activity of PTPs, in turn renders this Cys vulnerable to oxidation [60]. Using iodoacetic acid (capable of irreversibly alkylating reactive Cys residues except for those previously oxidized to their sulphenic acid derivative), one can discriminate the oxidized and hence inactive PTPs from those reduced and active molecules [11]. An important advance in the understanding of ROS action on PTPs is marked by the finding that oxidation of PTP1B does not result in formation of a stable sulfenic acid derivative, but rather becomes rapidly transformed into a sulfenyl amine ring involving the adjacent serine residue [61]. This form is resistant to further irreversible oxidation commonly occurring in the case of sulfenic acid, and is readily reduced back to free cysteinyl, a catalytically active form. It now seems likely that reversible redox regulation of PTPs plays a dominant role in setting the level of tyrosine phosphorylation in cells; this regulation seems to be physiologically important [59].

Unlike other known second messengers, ROS are not directly recognized by a sensor protein; instead, they modulate intracellular protein phosphorylation by reversible modification of downstream effectors [62]. All PTPs contain one essential Cys residue in the signature active-site motif Cys-Xaa-Xaa-Xaa-Xaa-Xaa-Arg that exists as a thiolate anion at neutral pH [63]. This thiolate anion contributes to the formation of a thiol phosphate intermediate. Oxidation of the active-site Cys of PTPs leads to enzymatic inactivation; yet, this modification can be reversed with thiol compounds [62,63].

The transient negative regulation of PTPs oxidants produced in response to PTK-ligand stimulation represents a strategy that has been adopted by cells, in order to promote PTK signaling by avoiding its prompt inactivation by means of PTPs [62]. The functional relevance of ROS-mediated PTP inhibition has been demonstrated by blocking ROS accumulation. For instance, blocking ROS production,

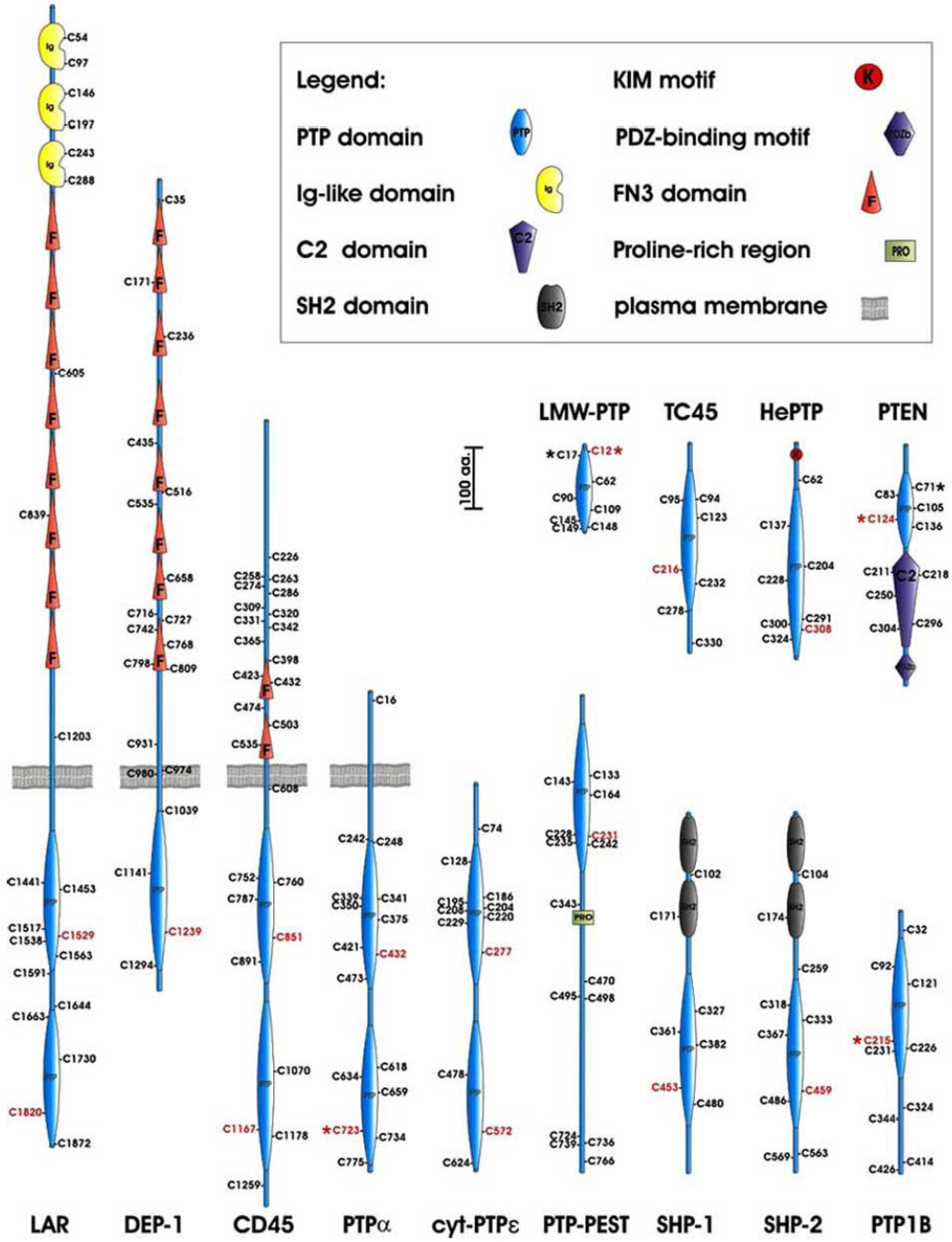


**Fig. (4).** Cys-based PTPs known to be regulated by ROS and RNS. Schematic domain structure, approximate length of the molecules and positions of cysteins are indicated. Cysteins present in the catalytic sites are in red; asterisks denote cysteins known to form disulfide bonds regulated *via* ROS or RNS. The following domains/motifs are indicated: PTP catalytic domain (PTP domain); immunoglobulin (Ig)-like domain; $Ca^{2+}$-binding site (C2 domain); Src homology 2 (SH2) domain recognizing phosphotyrosine motifs; kinase interaction motif (KIM); PDZ-binding motif recognizing PDZ domains; fibronectin type 3 (FN3) domain; proline rich region.

either by catalase pre-treatment or inhibition of the NADPH oxidase by DPI, in platelet-derived growth factor (PDGF)-stimulated cells, led to the reduction of PDGF receptor (PDGFR) tyrosine phosphorylation and PTP redox inhibition with very similar kinetics [64]. The combined data suggest that ROS produced after cell triggering may be considered as intracellular second messengers entagled in cell transduction pathways.

The involvement of ROS has also been proposed as a causal aspect preceding the intracellular G-protein-coupled receptor-mediated receptor PTK transactivation. Interestingly, activation of different G-protein-coupled receptors led to the generation of $H_2O_2$, suggesting that subsequent inactivation of PTPs could contribute to intracellular G-protein-coupled receptor-induced transactivation of receptor PTKs. Thus, PTP redox inhibition seems to have an important role in intracellular receptor PTK transactivation pathways initiated by G-protein-coupled receptors. This concept is corroborated by findings that prevention of $H_2O_2$ accumulation by antioxidants blocks the stimulation of receptor PTK and the activation of ERK in cells treated with lysophosphatidic acid, angiotensin II, or serotonin [65-67].

$H_2O_2$ reacts with the active-site Cys-thiolate in PTPs to generate the Cys-sulfenic acid, followed by a reaction with the adjacent backbone amide to generate the sulfenyl-amide. A kinetic analysis revealed that the second-order rate constants for the reaction of PTPs LAR and PTP1 with $H_2O_2$ are of the order of 10 $M^{-1}s^{-1}$; four orders of magnitude lower than that observed for the bacterial $H_2O_2$ sensor OxyR [63]. The reaction occurring in PTPs exposed to ROS are summarized in Fig. (**5**).

The reduced form of the active site Cys-SH can be oxidized by various ROS or RNS to Cys-SOH. During the redox regulation of PTP1B, glutathionylation of active site Cys has been observed. This process is assumed to protect Cys-SOH from further oxidation, which can lead to the formation of irreversible cysteine-sulfinic acid Cys-$SO_2H$ and cysteine-sulfonic acid Cys-$SO_3H$ [68]. However, Rhee's group has recently found that sulfinic acid can be rapidly reduced back to the catalytically active thiol form [69]. Cys-SOH produced by ROS can also undergo another type of modification. It can be rapidly converted to a previously unknown sulfenylamide intermediate, in which the sulfur atom of the catalytic Cys is covalently linked to the main chain nitrogen of an adjacent residue [61,70]. It has been proposed that the function of the sulfenylamide intermediate is to protect the active site Cys residue of PTP1B from irreversible further oxidation [71].

In case of the phosphatase and tensin homolog (PTEN) and low molecular weight (LMW)-PTP, a reversible disulfide bond is formed between the active site Cys and the neighboring Cys by a mechanism different from that effective in the regulation of PTP1B and other. The presence of a disulfide bond partner Cys of the active site Cys, which may be located either near to or distant from the active site Cys in

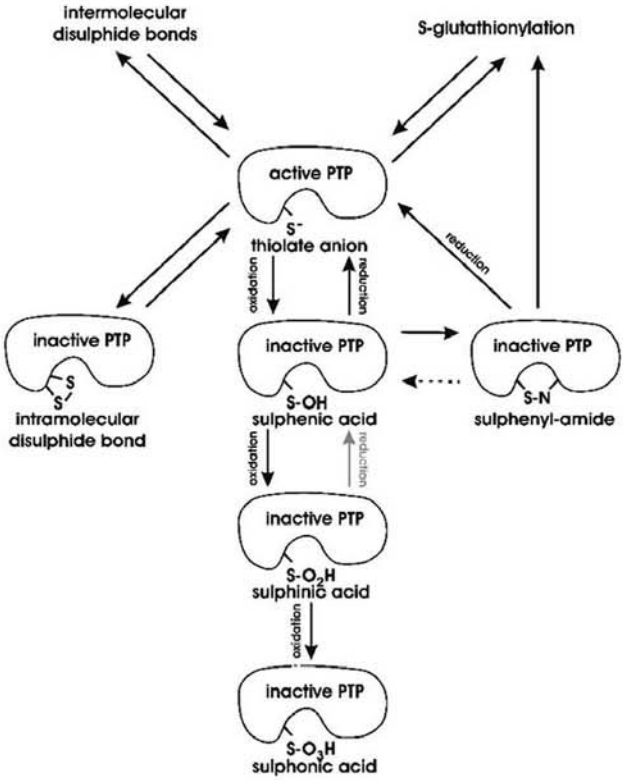


**Fig. (5).** A model for the regulation of PTP activity by oxidation. Catalytic cystein of active PTPs is in the thiolate anion form under physiological conditions due to low $pK_a$. Oxidation leads to sulphenic acid formation, which is reversible. Further oxidation leads to the irreversible sulphinic and sulphonic acid formation. Recently, sulphinic acid has been shown to be able to revert to sulphenic acid, at least in the case of *S. cerevisieae* protein sulphiredoxide [112], but this mechanism has not been confirmed in PTPs. Sulphenic acid can be prevented from its oxidation by its rapid conversion to cyclic sulphenyl-amide. Sulphenyl-amide cannot be further oxidized, but can be reduced to the active thiolate anion form in response to thiols. Other regulatory pathways involve formation of inter- and intra-molecular disulphide bonds and S-glutathionylation. Only the reduced thiolate anion form is enzymatically active.

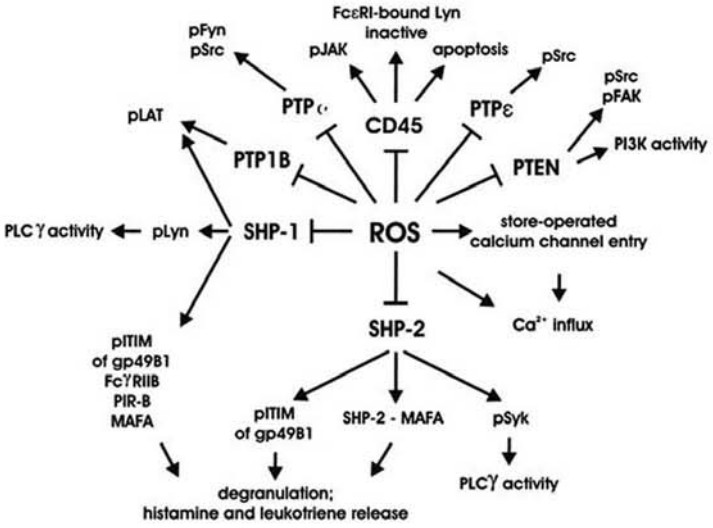


**Fig. (6).** Schematic presentation of biological effects of ROS on the regulation of Cys-based PTPs in mast cells and basophils (see the text for detailed explanation).

primary sequence, may confer efficiency in the redox regulation of phosphatases as well as protection of Cys-SOH from further oxidation [71]. Despite the fact that redox regulation mechanisms differ among PTPs, it seems likely that the redox regulation in PTPs has the same purpose of protecting Cys-SOH from further oxidation. The PTP-mediated effects of ROS in mast cells are shown in Fig. (**6**).

## EFFECTS OF RNS ON THE ACTIVITY OF PTPS

A recent study demonstrated that in hypoxic animals, the activity of membrane-associated PTPs decreased by 55%. This decrease could be blocked by adding the neural (n)NOS inhibitor 7-nitro-indazole sodium salt. On the other hand, in the same hypoxic animals, the activity of cytosolic PTPs increased up to 243% [72]. Focusing on non-receptor PTPs, it was found that the amount of PTP1B, SHP-1 and SHP-2 increased in hypoxic animals, to 419%, 251%, and 206% respectively, of the protein level found in normoxic piglets, and returned back after treatment with the NOS blocker, 7-nitroindazole sodium salt. Interestingly, phosphorylation of many proteins including Bcl-2 changed in hypoxic animals, suggesting an involvement of NO-induced PTPs in the regulation of hypoxic neuronal injuries in the newborn [72].

Expression of IFN-γ, TNF-α and iNOS has been found to be upregulated *in vivo* in *tc-ptp*$^{-/-}$ mice. A significant increase could be detected as early as 3 days after birth, prior to the onset of any overt disease [73]. The increased expression of iNOS mRNA was also reflected at the protein level in liver and salivary gland, where no detectable iNOS was present in the corresponding *tc-ptp*$^{+/+}$ tissues. iNOS was present in thymus of both *tc-ptp*$^{+/+}$ and *tc-ptp*$^{-/-}$ mice. In spleen cells of 14-day-old *tc-ptp*$^{-/-}$ mice, the maximum level of NO production was at least 3-fold higher than in wild-type splenocytes [73]. Effects of NO and RNS on PTP activity and other mast cell activation-related events are schematically shown in Fig. (**7**).

## CLASS I AND II CYS-BASED PHOSPHATASE MOLECULES REGULATED BY ROS AND RNS

Currently, several phosphatases have been shown to be either directly or indirectly regulated *via* ROS or RNS. These include LMW-PTP, PTEN, PTP-PEST, Src homology phosphatase (SHP)-2, PTP1B, PTPα, PTPε, DEP-1, TC45, SHP-1, hematopoietic (He)PTP, and leukocyte antigen-related tyrosine phosphatase (LAR). In the following paragraphs, we describe the known mechanisms of redox regulation of these phosphatases, as well as the consequences of this regulation for the outcome of signal transduction pathways present in mast cells and basophils.

### LMW-PTPS

LMW-PTPs, about 18-kDa cytoplasmic enzymes with almost ubiquitous expression, are involved in the regulation of cellular growth rate [74]. Presence of different isoforms of LMW-PTPs is also responsible for atopy predisposition [75]. LMW-PTPs are activated by phosphorylation on $Tyr^{131}$ and $Tyr^{132}$. Phosphorylation depends on localization of the enzyme. The pool of LMW-PTPs associated with cytoskeleton is specifically phosphorylated by the Src kinase and affects cell adhesion, spreading and migration by controlling the phosphorylation level of p190Rho-GAP. Cytoskeleton-unbound pool of LMW-PTP does not act on p190Rho-GAP, but directly dephosphorylates PDGFR [76]. LMW-PTP is inactivated by $H_2O_2$ and NO, but is protected from inactivation by DPI. This finding suggests that $H_2O_2$ reacts with the active site [77,78]. Only two of eight Cys residues present in LMW-PTP are modified by the exposure to $H_2O_2$, namely $Cys^{12}$ and $Cys^{17}$, causing the formation of intramolecular disulfide bond and inhibition of enzyme activity. The activity of the enzyme is completely restored after treatment with low molecular weight thiols, such as dithiothreitol or reduced glutathione [77,78]. *In vivo* LMW-PTP reactivation is attained upon removal of ROS; this

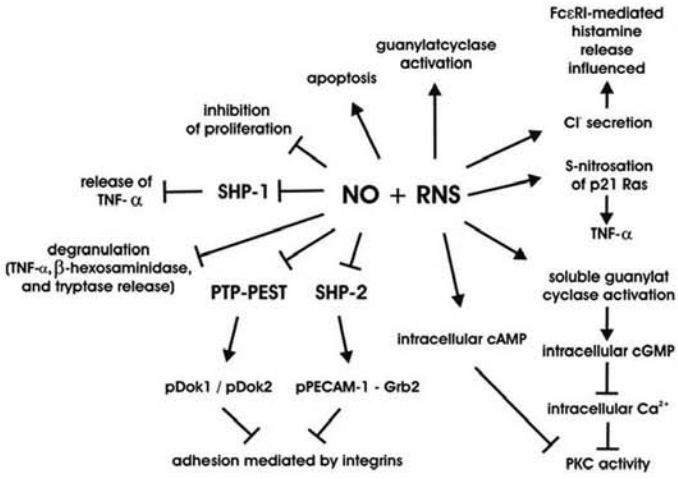


**Fig. (7).** Schematic presentation of biological effects of NO and RNS on mast cells and basophils with the highlighted potential role of protein tyrosine phosphatases (see the text for detailed explanation).

appears to be under the control of the glutaredoxin/glutathione/glutathione reductase/NADPH system. Upon PDGF treatment, almost 80% of LMW-PTP is oxidized and inhibited within 10 min, but after 45 min, almost 70% of the phosphatase becomes reduced and recovers its catalytic activity [79]. LMW-PTP acts on PDGFR by dephosphorylation of the $Tyr^{857}$ in the kinase domain, $Tyr^{716}$ which serves as the Grb2 binding site, and $Tyr^{751}$ which is the PI3K binding site [79]. Downregulation of LMW-PTP by ROS is a necessary step in integrin-mediated cell spreading [80].

## PTEN

PTEN is one of the ubiquitously expressed key regulators of cell growth and apoptosis. The 54-kDa PTEN protein contains an N-terminal phosphatase domain with specificity toward both phosphatidylinositol-3,4,5-trisphosphate (PI-3,4,5-$P_3$) and, to a lesser degree, tyrosine phosphorylated proteins. The most important effect of PTEN is its lipid phosphatase activity, which, by reducing the PI-3,4,5-$P_3$ levels, suppresses protein kinase B (PKB)/Akt phosphorylation and activation. Suppression of PKB/Akt makes it possible for forkhead transcription factors to up regulate the cell cycle inhibitor p27, which arrests cells in G1 [81]. Enzymatic activity of PTEN reduces Erk activation by dephosphorylating Shc, and thus inhibiting the association of Shc with Grb2/Sos complexes [82]. PTEN has also been shown to directly bind to focal adhesion kinase (FAK) and to reduce its tyrosine phosphorylation, and thus the ability of the cells to form focal adhesions, to migrate, and to respond to integrin-induced cell spreading [83].

Recent work has demonstrated an exposure of cells to $H_2O_2$ induced oxidation of PTEN in a time-dependent and $H_2O_2$ concentration-dependent manner [84]. The active site $Cys^{124}$ and $Cys^{71}$ form a disulfide bond under these conditions. The oxidative inactivation of PTEN *in vivo* by either exogenously or endogenously produced $H_2O_2$ increased the concentration of PIP3 and activated downstream signaling events such as cell proliferation through Akt activation; these signaling events were reversed by an exposure of the cells to antioxidants [85]. The decreased oxidative inactivation of PTEN could result in the forkhead activation and in subsequent activation of antioxidant enzymes such as catalase. This is affected by a decreased Akt activation in $p66^{Shc}$-null cells having reduced concentrations of oxidants [86].

## PTP-PEST

PTP-PEST is expressed abundantly in various hematopoietic cell types, including mast cells and basophils. It is a negative regulator of B- and T-cell activation being capable of dephosphorylating Shc, Cas, Pyk2 and FAK and preventing activation of the Ras signaling cascade. Two residues in the catalytic domain, $Cys^{231}$ and $Arg^{237}$, are critical for its phosphatase activity.The role of PTP-PEST in immunoreceptor signaling has recently been reviewed [87].

The enzymatic activity of PTP-PEST is increased by NO. This explains the NO-induced inhibition of cell motility in primary cultures of dedifferentiated aortic muscle cells. The inhibitory effect of NO requires cGMP as a second messenger. Using this pathway, NO induces dephosphorylation of p130cas mediated by PTP-PEST, which is followed by dissociation of p130cas from the adaptor protein Crk, leading to an inhibition of cell motility [86,88]. Recent data suggest that there is an additional messenger operative between NO and PTP-PEST, perhaps cGMP, which is necessary for the NO-mediated inhibition [86,88].

## SHP-2

SHP-2 is a cytoplasmic phosphatase which is abundantly expressed in mast cells and basophils. The role of SHP-2 in mast cell physiology has been recently reviewed [5]. It includes two N-terminal SH2 domains and a C-terminal hydrophilic domain containing several phosphorylation

sites. Enzymatic activity of SHP-2 is regulated *via* different mechanisms, including those mediated by ROS. A recent study by Meng and co-workers brought evidence for the role of PTP inhibition by $H_2O_2$ in physiological signaling [11]. SHP-2 becomes rapidly oxidized in PDGF-stimulated cells. The time course of oxidation coincided with that of autophosphorylation of the PDGFR. Furthermore, the recruitment of SHP-2 into a complex with the activated PDGFR is essential for oxidation and inactivation of the molecule. Importantly, only SHP-2 activity associated with the receptor was altered by $H_2O_2$, and activation of the same cells with EGF, which also induces ROS production, did not result in SHP-2 inhibition. These and other data suggest that the PDGFR-induced transient oxidation and inactivation of SHP-2 is specific, reversible and directly connected to the generation of $H_2O_2$ [11].

SHP-2 has also been identified as a pivotal signal transduction element in NO-stimulated vascular smooth muscle cells [89]. NO transiently increases the SHP-2 expression in these cells, and this is probably related to cGMP signaling pathways [89]. This upregulation has been shown to stimulate the cellular motility using the pathway involving RhoA, which is downstream of SHP-2 [90]. For this effect, Gab1 and PI3K are also required [91]. Based on these data, it is possible to speculate that SHP-2 is regulated by ROS and NO in activated mast cells.

### PTP1B

Ubiquitously expressed PTP1B contains 6 Cys residues, which based on crystal structure analysis of the protein, do not appear to form disulfide bonds [92]. The essential $Cys^{215}$ present in the active site has a $pK_a$ value of 5.4. Additionally, $Cys^{121}$ is also essential for enzymatic activity of this molecule [93]. $Cys^{215}$ is specifically targeted by $H_2O_2$ or alternatively by alendronate and pervanadate. It is probable that the sulfenate anion Cys-$SO^-$ in PTP1B is stabilized by a salt bridge to $Arg^{221}$. The oxidized PTP1B can be reactivated by means of thioredoxin, glutaredoxin or GSH systems *in vitro*. Thioredoxin has the highest efficiency in this system, suggesting that it is the major electron donor for PTP1B reduction in cells [94]. Oxidative inactivation of PTP1B has also been shown *in vivo* in epidermal growth factor (EGF)- or insulin-triggered cells [94].

Acidic aminoacids participate selectively in nitrosylation reactions suggesting that the (K/R/H)C(D/E) sequence is a consensus motif for nitrosylation [95]. PTP1B was found to be inhibited by NO donors in A431 and Jurkat cells in a reversible manner by oxidizing Cys residues. Full-length PTP1B contains 10 Cys residues, out of which 4 are flanked by basic aminoacids. Inhibition of PTP1B by NO is associated with increased phosphorylation of EGF receptors [96]. In this connection, it should also be noted that NO-mediated attenuation of insulin-stimulated cell motility is associated with increased PTP1B activity [97].

### PTPα

PTPα is a transmembrane PTP containing two conserved intracellular PTP domains (D1 and D2) separated by a spacer region. We have recently found that mRNA for PTPα is expressed in both BMMC and RBL cells (unpublished data). Interestingly, Src and Fyn kinase activity is reduced to <50% in fibroblasts derived from *PTPα*$^{-/-}$ mice [98]. The activity of PTPα, as well as some other PTP receptors like PTPε or CD45, is regulated by dimerization, which in the case of PTPα is dependent on the helix-loop-helix wedge structure in the juxtamembrane region with the catalytic site on the opposite monomer. PTPα dimerizes constitutively *in vivo*, and this dimerization causes inhibition of the enzymatic activity of this molecule [99].

Under *in vitro* conditions, only the D2 domain of PTPα can undergo oxidation by $H_2O_2$ [100]. The intermolecular disulfide bond forms on the catalytic $Cys^{723}$ in this domain, and this process depends on $H_2O_2$ concentration and time [101]. Treatment of cell lysates with dithiothreitol abolished the intermolecular disulfide bonds, but stable dimer formation remained intact, suggesting a role of other intrinsic properties of the protein. Cells treated with $H_2O_2$ show enhanced formation of PTPα dimers [101].

It is likely that the reversible conformational change in PTPα-D2 is caused by the formation of cyclic sulfenyl amide, which reportedly induces conformational changes in the catalytic site [61,70]. Cyclic sulfenylamide formation leads to the opening of the catalytic pocket, making it more shallow and rendering the catalytic Cys better accessible to the formation of an intermolecular disulfide bond with the thiolate anion $Cys^{723}$ from the dyad-related PTPα monomer. Intermolecular disulfide bonds between PTPα-D2s engage both monomers in the dimer in an active conformation and at the same time, protect the agent against irreversible further oxidation [101].

### PTPε

PTPε is expressed in a variety of endothelial cells and leukocytes including granulocytes. The two most prevalent forms of PTPε are the non-receptor type (cyt-PTPε) and the receptor type (RPTPε). cyt-PTPε dephosphorylates and inactivates the voltage-gated potassium channels, Kv1.5 and Kv2.1. PTPε is involved in numerous signaling pathways including JAK-STAT signaling, suppression of proliferation, insulin signaling and Src activation [102].

cyt-PTPε is unique among non-receptor phosphatases in that it forms dimers and higher-order associations under *in vivo* conditions. Dimerization of cyt-PTPε is enhanced by oxidative stress. Dimerization also occurs after EGF receptor triggering. Dimers of PTPε are detectable in the absence of $H_2O_2$; however, after treatment of the cells with $H_2O_2$ interactions between PTPε, molecules are significantly increased in the absence of enhanced cyt-PTPε phosphorylation. The ability of cyt-PTPε to dimerize is not affected by dithiothreitol or β-mercaptoethanol, implying that the intermolecular disulfide bonds are not major stabilizers in this process. The intermolecular binding is mediated through the D2 PTP domain, mainly *via* residues 360 to 380 and 621 to 643 [102]; these data suggest that D2 PTP domain has a negative regulatory role in PTPs.

### DEP-1

DEP-1 is a receptor PTP which contains only one phosphatase domain in contrast to two PTP domains of

previously discussed other receptor PTPs, the PTPα and PTPε. Its molecular mass varies between 180 and 250 kDa because of heavy glycosylation. It is expressed throughout the hematopoietic system and in a wide variety of tissues. Transient transfection of DEP-1 leads e.g. to TCR-mediated Erk activation and reduced tyrosine phosphorylation [103]. PLCα and LAT are also potential downstream targets of this molecule [104]. DEP-1 regulates diverse processes such as cell proliferation, adhesion, motility and cytoskeletal organization [103]. Using an antibody specific for oxidized form of PTPs, Persson *et al.* [100] showed that catalytic Cys of DEP-1 could be oxidized by pervanadate. $H_2O_2$-mediated DEP-1 oxidation was reversible, similarly as in other PTPs [100].

## OTHER PTPS

Among other ROS- and RNS-regulated PTPs, an important role is played by TC45, a nuclear T cell PTP. In insulin-activated cells, TC45 moves from the nucleus to the cytoplasm and dephosphorylates several cytoplasmic substrates. It binds to the insulin receptor β-subunit and downregulates the insulin-induced signaling pathways [105]. It has been recently shown that TC45, like the PTP1B, is rapidly and transiently oxidized in this signaling pathway [106].

Other phosphatases regulated by $H_2O_2$ are CD45 [107,108], and SHP-1 [109]. Overexpression of SHP-1 moderately reduces the $H_2O_2$-induced Erk phosphorylation and substantially inhibits JNK phosphorylation [110]. Overexpression of another non-receptor phosphatase, HePTP, suppresses $H_2O_2$-induced Erk and p38 phosphorylation, but not JNK phosphorylation. HePTP directly dephosphorylates MAPK at the activation loop containing Tyr residue [110]. $H_2O_2$-mediated regulation of LAR *in vitro* has also been reported [63]. Generally, redox regulation of these molecules was not studied in detail up till now, and the research ought to be focused on specification of the exact role of ROS and RNS in signaling accomplished by these very important signal transduction mediators.

## CONCLUDING REMARKS

Although the enhanced tyrosine phosphorylation of numerous substrates in $H_2O_2$ pre-treated cells was described almost two decades ago [111], the physiological relevance was unclear until recent years when reversible inactivation of PTP1B by $H_2O_2$ was convincingly demonstrated [94]. Modulation of enzyme activity by disulfide bond formation seems to be a universal mechanism of protein redox regulation in PTPs. The oxidation products of reactive cysteines in PTPs are Cys-SOH, glutathiolylated Cys, a disulfide bond with the neighboring Cys, and most recently found sulfenyl-amide intermediate. While there exist very diverse oxidized species of Cys and oxidation modes to produce them, it seems that the chance of a stable existence of Cys-SOH is excluded. Previous data have shown the probable irreversibility of Cys-$SO_2$H form, but Woo *et al.* found that the Cys-$SO_2$H form of peroxiredoxin was rapidly reduced to form a catalytically active thiol species [69]. Furthermore, it has been shown that sulfredoxin could also reduce the Cys-$SO_2$H form of peroxiredoxin using ATP and magnesium in yeast [112]. The reversibility of Cys-$SO_2$H as another possible mechanism in PTPs should therefore still be kept in mind and should be verified *in vivo*.

The finding that activated mast cells are capable of producing ROS and RNS (Fig.(**1** and **2**)) suggests that these cells may undergo ROS- and RNS-mediated regulation of PTPs involved in FcεRI-mediated signaling. In this connection, it should be noted that NO gas was detected in exhaled breath of asthmatics [113], and that NO generated by NOS in lungs could exert combined beneficial and harmful effects in asthma development [55]. The combined data highlight the potential role of redox-regulated PTPs in allergy, asthma and inflammatory diseases and could lead to further research on generation of new causal treatments based on targeting redox-regulated PTPs involved in signal transduction pathways.

Clearly, the evolving complex of regulatory pathways offers great expectations for the development of new therapeutic interventions in inflammatory states. By regulating the production of ROS and RNS in mast cells, it may be possible to finely tune up mast cell functions under pathological conditions, including asthma and allergies. This promising therapeutic potential of novel drugs regulating the production of ROS and RNS in mast cells is hampered by the fact that not only are they responsible for undesirable hypersensitivity reactions, but they also act as important sensors of infection and injury through innate recognition receptors. Furthermore, it is unlikely that these drugs would be specific for mast cells, because ROS and RNS targets are found in numerous cell types in the body. The favorable prospect of these drugs would be dramatically increased by their targeting into specific sites in the body. Aerosolization of the drugs and targeting mast cells-mediated pulmonary diseases is a promising example (for recent review see [114]) . A similar approach using RNA interference techniques could also be used for targeting enzymes involved in generation of ROS and RNS [115].

## ACKNOWLEDGEMENTS

This work was supported by project 1M6837805001 (Center of Molecular and Cellular Immunology) and project 1P040E158 from Ministry of Education, Youth and Sports of the Czech Republic, grants 204/03/0594 and 301/03/0596 from the Grant Agency of the Czech Republic, project AVOZ50520514 and grant A5052310 from the Grant Agency of the Academy of Sciences of the Czech Republic, and grant NR8079-3/2004 from the Ministry of Health of the Czech Republic. The research of P. H. was supported in part by Research goal MSM0021620814 from the 3rd Faculty of Medicine, Charles University, Prague, and the research of P. D. was supported by an International Research Scholar's Award from Howard Hughes Medical Institute.

## LIST OF ABBREVIATIONS

ROS = Reactive oxygen species

RNS = Reactive nitric species

PTP = Protein tyrosine phosphatase

FcεRI = High affinity IgE receptor
IL = Interleukin
IFN = Interferon
TNF = Tumor necrosis factor
PTK = Protein tyrosine kinases
BMMC = Bone marrow mast cells
RBL = Rat basophilic leukemia
NOS = Nitric oxide synthase
NO = Nitric oxide
DPI = Diphenyleneiodonium
NOX = NADPH oxidases
DUOX = Dual domain oxidases
PI3K = Phosphoinositide 3-kinase
iNOS = Inducible isoform of NOS
SCF = Stem cell factor
L-NMMA = $N^{\omega}$-monomethyl-L-arginine
PLC = phospholipase C
PDGF = Platelet-derived growth factor
PDGFR = PDGF receptor (PDGFR
PTEN = Phosphatase and tensin homologue
LMW = Low molecular weight
SHP = Src homology phosphatase
LAR = Leukocyte antigen-related tyrosine phosphatase
PI-3,4,5-$P_3$ = Phosphatidylinositol-3,4,5-trisphosphate
PKB = Protein kinase B
FAK = Focal adhesion kinase
EGF = Epidermal growth factor

## REFERENCES


[1] Stone, J.R. *Arch. Biochem. Biophys.*, **2004**, *422*, 119.
[2] Cadenas, E.; Davies, K.J. *Free Radic. Biol. Med.*, **2000**, *29*, 222.
[3] Marshall, J.S.; Jawdat, D.M. *J. Allergy Clin. Immunol.*, **2004**, *114*, 21.
[4] Murakami, K.; Sato, S.; Nagasawa, S.; Yamashita, T. *Int. Immunology*, **2000**, *12*, 169.
[5] Heneberg, P.; Dráber, P. *Int. Arch. Allergy Immunol.*, **2002**, *128*, 253.
[6] Tolarová, H.; Dráberová, L.; Heneberg, P.; Dráber, P. *Eur. J. Immunol.*, **2004**, *34*, 1627.
[7] Volna, P.; Lebduska, P.; Draberova, L.; Simova, S.; Heneberg, P.; Boubelik, M.; Bugajev, V.; Malissen, B.; Wilson, B.S.; Horejsi, V.; Malissen, M.; Draber, P. *J. Exp. Med.*, **2004**, *200*, 1001.
[8] Suzuki, Y.; Yoshimaru, T.; Matsui, T.; Inoue, T.; Niide, O.; Nunomura, S.; Ra, C. *J. Immunol.*, **2003**, *171*, 6119.
[9] Forsythe, P.; Gilchrist, M.; Kulka, M.; Befus, A.D. *Int. Immunopharmacol.*, **2001**, *1*, 1525.
[10] Bidri, M.; Feger, F.; Varadaradjalou, S.; Ben Hamouda, N.; Guillosson, J.J.; Arock, M. *Int. Immunopharmacol.*, **2001**, *1*, 1543.
[11] Meng, T.C.; Fukada, T.; Tonks, N.K. *Mol. Cell*, **2002**, *9*, 387.
[12] Swindle, E.J.; Hunt, J.A.; Coleman, J.W. *J. Immunol.*, **2002**, *169*, 5866.
[13] Matsui, T.; Suzuki, Y.; Yamashita, K.; Yoshimaru, T.; Suzuki-Karasaki, M.; Hayakawa, S.; Yamaki, M.; Shimizu, K. *Biochem. Biophys. Res. Commun.*, **2000**, *276*, 742.
[14] Yoshimaru, T.; Suzuki, Y.; Matsui, T.; Yamashita, K.; Ochiai, T.; Yamaki, M.; Shimizu, K. *Clin. Exp. Allergy*, **2002**, *32*, 612.
[15] Yamashita, K.; Suzuki, Y.; Matsui, T.; Yoshimaru, T.; Yamaki, M.; Suzuki-Karasaki, M.; Hayakawa, S.; Shimizu, K. *Biochem. Biophys. Res. Commun.*, **2000**, *274*, 603.
[16] Chen, S.; Gong, J.; Liu, F.; Mohammed, U. *Immunology*, **2000**, *100*, 471.
[17] Fernandez, R.; Suchard, S.J. *J. Immunol.*, **1998**, *160*, 5154.
[18] Karlsson, A.; Nixon, J.B.; McPhail, L.C. *J. Leukoc. Biol.*, **2000**, *67*, 396.
[19] Bidri, M.; Ktorza, S.; Vouldoukis, I.; Le Goff, L.; Debre, P.; Guillosson, J.J.; Arock, M. *Eur. J. Immunol.*, **1997**, *27*, 2907.
[20] Hogaboam, C.M.; Befus, A.D.; Wallace, J.L. *J. Immunol.*, **1993**, *151*, 3767.
[21] Lin, T.J.; Befus, A.D. *J. Immunol.*, **1997**, *159*, 4015.
[22] Berkman, N.; Robichaud, A.; Robbins, R.A.; Roesems, G.; Haddad, E.B.; Barnes, P.J.; Chung, K.F. *Immunology*, **1996**, *89*, 363.
[23] Xu, X.; Malave, A. *Life Sci.*, **2000**, *67*, 3221.
[24] Masini, E.; Bani, D.; Bigazzi, M.; Mannaioni, P.F.; Bani-Sacchi, T. *J. Clin. Invest*, **1994**, *94*, 1974.
[25] Bani, D.; Baronti, R.; Vannacci, A.; Bigazzi, M.; Sacchi, T.B.; Mannaioni, P.F.; Masini, E. *Int. Immunopharmacol.*, **2002**, *2*, 1195.
[26] Gilchrist, M.; Savoie, M.; Nohara, O.; Wills, F.L.; Wallace, J.L.; Befus, A.D. *J. Leukoc. Biol.*, **2002**, *71*, 618.
[27] Gilchrist, M.; McCauley, S.D.; Befus, A.D. *Blood*, **2004**, *104*, 462.
[28] Eastmond, N.C.; Banks, E.M.; Coleman, J.W. *J. Immunol.*, **1997**, *159*, 1444.
[29] Deschoolmeester, M.L.; Eastmond, N.C.; Dearman, R.J.; Kimber, I.; Basketter, D.A.; Coleman, J.W. *Immunology*, **1999**, *96*, 138.
[30] Swindle, E.J.; Metcalfe, D.D.; Coleman, J.W. *J. Biol. Chem.*, **2004**, *279*, 48751.
[31] Teshima, R.; Ikebuchi, H.; Nakanishi, M.; Sawada, J. *Biochem. J.*, **1994**, *302*, 867.
[32] Amoui, M.; Dráberová, L.; Tolar, P.; Dráber, P. *Eur. J. Immunol.*, **1997**, *27*, 321.
[33] Menon, I.A.; Shirwadkar, S.; Ranadive, N.S. *Biochem. Cell Biol.*, **1989**, *67*, 397.
[34] Akagi, M.; Katakuse, Y.; Fukuishi, N.; Kan, T.; Akagi, R. *Biol. Pharm. Bull.*, **1994**, *17*, 732.
[35] Peden, D.B.; Dailey, L.; DeGraff, W.; Mitchell, J.B.; Lee, J.G.; Kaliner, M.A.; Hohman, R.J. *Am. J. Physiol*, **1994**, *267*, L85.
[36] Antunes, F.; Cadenas, E. *FEBS Lett.*, **2000**, *475*, 121.
[37] Seaver, L.C.; Imlay, J.A. *J. Bacteriol.*, **2001**, *183*, 7182.
[38] Kulagina, N.V.; Michael, A.C. *Anal. Chem.*, **2003**, *75*, 4875.
[39] Nathan, C.F.; Root, R.K. *J. Exp. Med.*, **1977**, *146*, 1648.
[40] Keisari, Y.; Braun, L.; Flescher, E. *Immunobiol.*, **1983**, *165*, 78.
[41] Droge, W. *Physiol Rev.*, **2002**, *82*, 47.
[42] Saitoh, S.; Arudchandran, R.; Manetz, T.S.; Zhang, W.; Sommers, C.L.; Love, P.E.; Rivera, J.; Samelson, L.E. *Immunity.*, **2000**, *12*, 525.
[43] Saitoh, S.I.; Odom, S.; Gomez, G.; Sommers, C.L.; Young, H.A.; Rivera, J.; Samelson, L.E. *J. Exp. Med.*, **2003**, *198*, 831.
[44] Schreck, R.; Rieber, P.; Baeuerle, P.A. *EMBO J.*, **1991**, *10*, 2247.
[45] Okuno, H.; Akahori, A.; Sato, H.; Xanthoudakis, S.; Curran, T.; Iba, H. *Oncogene*, **1993**, *8*, 695.
[46] Wang, G.L.; Jiang, B.H.; Semenza, G.L. *Biochem. Biophys. Res. Commun.*, **1995**, *216*, 669.
[47] Rainwater, R.; Parks, D.; Anderson, M.E.; Tegtmeyer, P.; Mann, K. *Mol. Cell Biol.*, **1995**, *15*, 3892.
[48] Lander, H.M.; Ogiste, J.S.; Pearce, S.F.; Levi, R.; Novogrodsky, A. *J. Biol. Chem.*, **1995**, *270*, 7017.
[49] Schindler, H.; Bogdan, C. *Int. Immunopharmacol.*, **2001**, *1*, 1443.
[50] Mannaioni, P.F.; Masini, E.; Pistelli, A.; Salvemini, D.; Vane, J.R. *Int. J. Tissue React.*, **1991**, *13*, 271.
[51] Masini, E.; Mannaioni, P.F.; Pistelli, A.; Salvemini, D.; Vane, J. *Biochem. Biophys. Res. Commun.*, **1991**, *177*, 1178.
[52] Park, S.J.; Jun, C.D.; Choi, B.M.; Lee, E.J.; Kim, H.R.; Cho, H.W.; Chung, H.T. *Biochem. Mol. Biol. Int.*, **1996**, *40*, 721.
[53] Koranteng, R.D.; Dearman, R.J.; Kimber, I.; Coleman, J.W. *Inflamm. Res.*, **2000**, *49*, 240.
[54] Jorens, P.G.; van Overveld, F.J.; Bult, H.; Vermeire, P.A.; Herman, A.G. *Agents Actions*, **1993**, *38*, 100.
[55] Coleman, J.W. *Clin. Exp. Immunol.*, **2002**, *129*, 4.
[56] Peh, K.H.; Moulson, A.; Wan, B.Y.; Assem, E.K.; Pearce, F.L. *Eur. J. Pharmacol.*, **2001**, *425*, 229.
[57] Zidek, Z.; Masek, K. *Int. J. Immunopharmacol.*, **1998**, *20*, 319.

[58] Dear, J.W.; Scadding, G.K.; Foreman, J.C. *Br. J. Pharmacol.*, **1995**, *116*, 1720.
[59] Alonso, A.; Sasin, J.; Bottini, N.; Friedberg, I.; Friedberg, I.; Osterman, A.; Godzik, A.; Hunter, T.; Dixon, J.; Mustelin, T. *Cell*, **2004**, *117*, 699.
[60] Xu, D.; Rovira, I.I.; Finkel, T. *Dev. Cell*, **2002**, *2*, 251.
[61] Salmeen, A.; Andersen, J.N.; Myers, M.P.; Meng, T.C.; Hinks, J.A.; Tonks, N.K.; Barford, D. *Nature*, **2003**, *423*, 769.
[62] Chiarugi, P.; Cirri, P. *Trends Biochem. Sci.*, **2003**, *28*, 509.
[63] Denu, J.M.; Tanner, K.G. *Biochemistry*, **1998**, *37*, 5633.
[64] Chiarugi, P.; Cirri, P.; Taddei, M.L.; Talini, D.; Doria, L.; Fiaschi, T.; Buricchi, F.; Giannoni, E.; Camici, G.; Raugei, G.; Ramponi, G. *J. Cell Sci.*, **2002**, *115*, 2219.
[65] Daub, H.; Weiss, F.U.; Wallasch, C.; Ullrich, A. *Nature*, **1996**, *379*, 557.
[66] Greene, E.L.; Houghton, O.; Collinsworth, G.; Garnovskaya, M.N.; Nagai, T.; Sajjad, T.; Bheemanathini, V.; Grewal, J.S.; Paul, R.V.; Raymond, J.R. *Am. J. Physiol. Renal. Physiol.*, **2000**, *278*, F650.
[67] Ushio-Fukai, M.; Alexander, R.W.; Akers, M.; Lyons, P.R.; Lassegue, B.; Griendling, K.K. *Mol. Pharmacol.*, **1999**, *55*, 142.
[68] Barrett, W.C.; DeGnore, J.P.; Konig, S.; Fales, H.M.; Keng, Y.F.; Zhang, Z.Y.; Yim, M.B.; Chock, P.B. *Biochemistry*, **1999**, *38*, 6699.
[69] Woo, H.A.; Chae, H.Z.; Hwang, S.C.; Yang, K.S.; Kang, S.W.; Kim, K.; Rhee, S.G. *Science*, **2003**, *300*, 653.
[70] van Montfort, R.L.; Congreve, M.; Tisi, D.; Carr, R.; Jhoti, H. *Nature*, **2003**, *423*, 773.
[71] Cho, S.H.; Lee, C.H.; Ahn, Y.; Kim, H.; Kim, H.; Ahn, C.Y.; Yang, K.S.; Lee, S.R. *FEBS Lett.*, **2004**, *560*, 7.
[72] Ashraf, Q.M.; Haider, S.H.; Katsetos, C.D.; Delivoria-Papadopoulos, M.; Mishra, O. *Neurosci. Lett.*, **2004**, *362*, 108.
[73] Heinonen, K.M.; Nestel, F.P.; Newell, E.W.; Charette, G.; Seemayer, T.A.; Tremblay, M.L.; Lapp, W.S. *Blood*, **2004**, *103*, 3457.
[74] Raugei, G.; Ramponi, G.; Chiarugi, P. *Cell Mol. Life Sci.*, **2002**, *59*, 941.
[75] Bottini, N.; Mao, X.Q.; Borgiani, P.; Saccucci, P.; Stefanini, L.; Greco, E.; Fontana, L.; Shirakawa, T.; Hopkin, J.M. *Allergy*, **2002**, *57*, 10.
[76] Chiarugi, P.; Cirri, P.; Taddei, L.; Giannoni, E.; Camici, G.; Manao, G.; Raugei, G.; Ramponi, G. *J. Biol. Chem.*, **2000**, *275*, 4640.
[77] Caselli, A.; Camici, G.; Manao, G.; Moneti, G.; Pazzagli, L.; Cappugi, G.; Ramponi, G. *J. Biol. Chem.*, **1994**, *269*, 24878.
[78] Caselli, A.; Marzocchini, R.; Camici, G.; Manao, G.; Moneti, G.; Pieraccini, G.; Ramponi, G. *J. Biol. Chem.*, **1998**, *273*, 32554.
[79] Chiarugi, P.; Fiaschi, T.; Taddei, M.L.; Talini, D.; Giannoni, E.; Raugei, G.; Ramponi, G. *J. Biol. Chem.*, **2001**, *276*, 33478.
[80] Nimmual, A.S.; Taylor, L.J.; Bar-Sagi, D. *Nat. Cell Biol.*, **2003**, *5*, 236.
[81] Li, D.M.; Sun, H. *Cancer Res.*, **1997**, *57*, 2124.
[82] Gu, J.; Tamura, M.; Pankov, R.; Danen, E.H.; Takino, T.; Matsumoto, K.; Yamada, K.M. *J. Cell Biol.*, **1999**, *146*, 389.
[83] Tamura, M.; Gu, J.; Takino, T.; Yamada, K.M. *Cancer Res.*, **1999**, *59*, 442.
[84] Lee, S.R.; Yang, K.S.; Kwon, J.; Lee, C.; Jeong, W.; Rhee, S.G. *J. Biol. Chem.*, **2002**, *277*, 20336.
[85] Leslie, N.R.; Bennett, D.; Lindsay, Y.E.; Stewart, H.; Gray, A.; Downes, C.P. *EMBO J.*, **2003**, *22*, 5501.
[86] Nemoto, S.; Finkel, T. *Science*, **2002**, *295*, 2450.
[87] Mustelin, T.; Tasken, K. *Biochem. J.*, **2003**, *371*, 15.
[88] Lin, Y.; Ceacareanu, A.C.; Hassid, A. *Am. J. Physiol. Heart Circ. Physiol.*, **2003**, *285*, H710.
[89] Brown, C.; Lin, Y.; Hassid, A. *Am. J. Physiol. Heart Circ. Physiol.*, **2001**, *281*, H1598.
[90] Chang, Y.; Ceacareanu, B.; Dixit, M.; Sreejayan, N.; Hassid, A. *Circ. Res.*, **2002**, *91*, 390.
[91] Dixit, M.; Zhuang, D.; Ceacareanu, B.; Hassid, A. *Circ. Res.*, **2003**, *93*, e113.
[92] Barford, D.; Flint, A.J.; Tonks, N.K. *Science*, **1994**, *263*, 1397.
[93] Guan, K.L.; Deschenes, R.J.; Qiu, H.; Dixon, J.E. *J. Biol. Chem.*, **1991**, *266*, 12964.
[94] Lee, S.R.; Kwon, K.S.; Kim, S.R.; Rhee, S.G. *J. Biol. Chem.*, **1998**, *273*, 15366.
[95] Stamler, J.S.; Toone, E.J.; Lipton, S.A.; Sucher, N.J. *Neuron*, **1997**, *18*, 691.
[96] Li, S.; Whorton, A.R. *Arch. Biochem. Biophys.*, **2003**, *410*, 269.
[97] Sreejayan, N.; Lin, Y.; Hassid, A. *Arterioscler. Thromb. Vasc. Biol.*, **2002**, *22*, 1086.
[98] Skelton, M.R.; Ponniah, S.; Wang, D.Z.; Doetschman, T.; Vorhees, C.V.; Pallen, C.J. *Brain Res.*, **2003**, *984*, 1.
[99] Jiang, G.; den Hertog, J.; Su, J.; Noel, J.; Sap, J.; Hunter, T. *Nature*, **1999**, *401*, 606.
[100] Persson, C.; Sjoblom, T.; Groen, A.; Kappert, K.; Engstrom, U.; Hellman, U.; Heldin, C.H.; den Hertog, J.; Ostman, A. *Proc. Natl. Acad. Sci. U.S.A.*, **2004**, *101*, 1886.
[101] van der Wijk, T.; Overvoorde, J.; den Hertog, J. *J. Biol. Chem.*, **2004**, *279*, 44355.
[102] Toledano-Katchalski, H.; Tiran, Z.; Sines, T.; Shani, G.; Granot-Attas, S.; den Hertog, J.; Elson, A. *Mol. Cell Biol.*, **2003**, *23*, 5460.
[103] Kellie, S.; Craggs, G.; Bird, I.N.; Jones, G.E. *J. Cell Sci.*, **2004**, *117*, 609.
[104] Baker, J.E.; Majeti, R.; Tangye, S.G.; Weiss, A. *Mol. Cell Biol.*, **2001**, *21*, 2393.
[105] Galic, S.; Klingler-Hoffmann, M.; Fodero-Tavoletti, M.T.; Puryer, M.A.; Meng, T.C.; Tonks, N.K.; Tiganis, T. *Mol. Cell Biol.*, **2003**, *23*, 2096.
[106] Meng, T.C.; Buckley, D.A.; Galic, S.; Tiganis, T.; Tonks, N.K. *J. Biol. Chem.*, **2004**, *279*, 37716.
[107] Secrist, J.P.; Burns, L.A.; Karnitz, L.; Koretzky, G.A.; Abraham, R.T. *J. Biol. Chem.*, **1993**, *268*, 5886.
[108] Fialkow, L.; Chan, C.K.; Rotin, D.; Grinstein, S.; Downey, G.P. *J. Biol. Chem.*, **1994**, *269*, 31234.
[109] Cunnick, J.M.; Dorsey, J.F.; Mei, L.; Wu, J. *Biochem. Mol. Biol. Int.*, **1998**, *45*, 887.
[110] Lee, K.; Esselman, W.J. *Free Radic. Biol. Med.*, **2002**, *33*, 1121.
[111] Hayes, G.R.; Lockwood, D.H. *Proc. Natl. Acad. Sci. U.S.A.*, **1987**, *84*, 8115.
[112] Biteau, B.; Labarre, J.; Toledano, M.B. *Nature*, **2003**, *425*, 980.
[113] Kharitonov, S.A.; Yates, D.; Robbins, R.A.; Logan-Sinclair, R.; Shinebourne, E.A.; Barnes, P.J. *Lancet*, **1994**, *343*, 133.
[114] Lusková, P.; Dráber, P. *Curr. Pharm. Des*, **2004**, *10*, 1727.
[115] Caplen, N.J. *Gene Ther.*, **2004**, *11*, 1241.

**6.4**

**Heneberg, P.; Lebduška, P.; Dráberová, L.; Korb, J. & Dráber, P. (2006):**

**Topography of plasma membrane microdomains and its consequences for mast cell signaling.**

**European Journal of Immunology 36(10): 2795-2806.**

European Journal of Immunology **Leukocyte signaling**

# Topography of plasma membrane microdomains and its consequences for mast cell signaling

*Petr Heneberg[1,2], Pavel Lebduška[1], L'ubica Dráberová[1], Jan Korb[1] and Petr Dráber[1]*

[1] Institute of Molecular Genetics, Academy of Sciences of the Czech Republic, Prague, Czech Republic
[2] Center for Research in Diabetes, Metabolism and Nutrition, Third Faculty of Medicine, Charles University, Prague, Czech Republic

Thy-1 (CD90) is a glycoprotein bound to the plasma membrane by a GPI anchor. Aggregation of Thy-1 in mast cells and basophils induces activation events independent of the expression of Fcε receptor I (FcεRI). Although we and others have previously suggested that plasma membrane microdomains called lipid rafts are implicated in both Thy-1 and FcεRI signaling, properties of these microdomains are still poorly understood. In this study we used rat basophilic leukemia cells and their transfectants expressing both endogenous Thy-1.1 and exogenous Thy-1.2 genes and analyzed topography of the Thy-1 isoforms and Thy-1-induced signaling events. Light microscopy showed that both Thy-1 isoforms were in the plasma membrane distributed randomly and independently. Electron microscopy on isolated membrane sheets and fluorescence resonance energy transfer analysis indicated cross-talk between Thy-1 isoforms and between Thy-1 and FcεRI. This cross-talk was dependent on actin filaments. Thy-1 aggregates colocalized with two transmembrane adaptor proteins, non-T cell activation linker (NTAL) and linker for activation of T cells (LAT), which had been shown to inhabit different membrane microdomains. Thy-1 aggregation led to tyrosine phosphorylation of these two adaptors. The combined data indicate that aggregated GPI-anchored proteins can attract different membrane proteins in different clusters and thus can trigger different signaling pathways.

Received 12/4/06
Revised 13/7/06
Accepted 22/8/06

[DOI 10.1002/eji.200636159]

**Key words:** Actin · Adaptor proteins · Mast cell · Thy-1 glycoprotein

## Introduction

Aggregation of the Thy-1 gp (CD90) induces activation of mast cells [1, 2], which is independent of the surface expression of Fcε receptor I (FcεRI) [3]. It has been suggested that this activation is caused by an association of the GPI-anchored Thy-1 with sterol- and sphingolipid-enriched membrane microdomains called lipid rafts. Microdomains of this composition can be isolated by sucrose density gradient ultracentrifugation after solubilization of cells with Triton X-100 or other nonionic detergents [4, 5]. Biochemical studies of isolated detergent-resistant membranes (DRM) showed that they are rich not only in GPI-anchored proteins, but also in palmitoylated Src family protein tyrosine kinases [6, 7] and palmitoylated transmembrane adaptor proteins, including linker for activation of T cells (LAT) [8] and non-T cell activation linker (NTAL) [9]. Importantly, in nonactivated mast cells, the FcεRI is excluded from DRM, whereas in FcεRI-activated cells most of the receptor is associated with DRM in a cholesterol-dependent manner [10–12]. These findings

**Correspondence:** Dr. Petr Dráber, Department of Signal Transduction, Institute of Molecular Genetics, Academy of Sciences of the Czech Republic, Vídeňská 1083, CZ-142 20 Prague 4, Czech Republic
Fax: +420-241470339
e-mail: draberpe@biomed.cas.cz

**Abbreviations:** **BRA:** bivariate Ripley's analysis · **BSS:** buffered salt solution · **DRM:** detergent-resistant membranes · **F-actin:** filamentous actin · **FcεRI:** Fcε receptor I · **FRET:** fluorescence resonance energy transfer · **GαM:** goat anti-mouse · **LAT:** linker for activation of T cells · **NTAL:** non-T cell activation linker · **PM:** plasma membrane · **RαM:** rabbit anti-mouse · **RBL:** rat basophilic leukemia · **RFI:** relative fluorescence intensity · **TRITC:** tetramethylrhodamine isothiocyanate

suggested that FcεRI-mediated activation is initiated through association of the aggregated FcεRI with membrane microdomains possessing signal transduction machinery. However, solubilization of the cells with detergents could produce artifacts and misleading results [13]. Other approaches are therefore required to understand the fundamental mechanism by which clustering of membrane receptors initiates tyrosine phosphorylation of numerous substrates.

In an attempt to understand topography of plasma membrane (PM) components, EM on isolated PM sheets has been used. These studies showed that aggregated FcεRI accumulate in osmiophilic membrane regions together with several signaling molecules but with no preference for colocalization with Thy-1 or other proteins considered to be localized in lipid rafts [14, 15]. Based on these results, Wilson and co-authors suggested that the observed FcεRI aggregates could represent the true signal transduction organizing units [14]. However, we recently found that mAb-mediated FcεRI dimerization induces strong cell activation response in the absence of formation of the large signaling assemblies around FcεRI aggregates [12]. Thus, FcεRI signal transduction units could be much smaller than previously thought [14, 16], and their molecular topography and changes during the course of mast cell activation remain enigmatic.

In this study we used rat basophilic leukemia (RBL) cells and their transfectants expressing both the endogenous Thy-1.1 and transfected Thy-1.2 genes to analyze the topography of Thy-1 isoforms and some other signaling proteins. The techniques included light microscopy, fluorescence resonance energy transfer (FRET) and EM on isolated PM sheets. The role of filamentous actin (F-actin) in Thy-1-mediated signaling and in cross-talk between Thy-1, FcεRI and the adaptor proteins LAT and NTAL was also investigated.

## Results

### Clusters of Thy-1 isoforms move independently in the plasma membrane

We previously isolated RBL-derived cells, RBL-gT1.2/1, expressing the murine Thy-1.2 gene [2]. FACS analysis showed that all RBL-gT1.2/1 cells express FcεRI and both Thy-1.1 and Thy-1.2 (Fig. 1A). Immunoblotting examination revealed that RBL-gT1.2/1 cells express less Thy-1.1 gp than RBL cells (Fig. 1B), implying a mechanism regulating the amount of total Thy-1 produced. Using RBL-gT1.2/1 cells we analyzed topography of Thy-1.1 and Thy-1.2 by three different approaches. In the first series of experiments using immunofluorescence microscopy on cells fixed with 4% paraformaldehyde before staining, both Thy-1.1 and Thy-1.2 were found homogenously distributed over the cell surface (Fig. 1Ca–c). Aggregation of Thy-1.1 by OX7 Ab and FITC-conjugated goat anti-mouse (GαM) IgG induced formation of patches (after 10 min at 37°C, Fig. 1Cd) and caps (after 60 min at 37°C; Fig. 1Cj) of Thy-1.1, whereas Thy-1.2 remained diffusely distributed over the cell surface (Fig. 1Ce, k). Similarly, in the reverse experiment, cells with patches and caps of cross-linked Thy-1.2 (Fig. 1Ch, n) exhibited diffuse staining of Thy-1.1 (Fig. 1Cg, m). These results suggest that Thy-1.1 and Thy-1.2 gp move in the plane of the PM independently.

Next we examined topography of Thy-1 isoforms using EM on immunogold-labeled PM sheets isolated from RBL-gT1.2/1 cells. As the isolation of membrane sheets is not compatible with strong fixation, we fixed the cells with 2% paraformaldehyde, allowing effective isolation of membrane sheets but unlikely to completely inhibit the formation of small Thy-1 aggregates. Under these conditions we found that both Thy-1.1 and Thy-1.2 were localized mostly in small autonomous clusters (Fig. 2 and 3). When Thy-1.1 was aggregated with OX7 mAb and 10 nm gold-labeled GαM IgG (GαM-gold-10 nm) followed by fixation with 2% paraformaldehyde and blocking remaining free IgG-binding sites, Thy-1.2 showed significant colocalization with Thy-1.1 at distances larger than ~40 nm as detected by bivariate Ripley's analysis (BRA; Fig. 2B). Importantly, under the same experimental conditions, much stronger Thy-1.1 homoassociation was detected (Fig. 2C). Interestingly, although the size of Thy-1 clusters was smaller in prefixed cells than in cells fixed after Thy-1 labeling, the distance between individual gold labels in the clusters remained unchanged (Fig. 3A–D). Furthermore, we confirmed recent data [15] that aggregation of Thy-1 does not lead to its enhanced colocalization with FcεRI (Fig. 3E, F). These EM data support the concept that aggregated Thy-1 isoforms can move relatively independently in the plane of the PM and are localized in membrane regions with no preference for FcεRI.

Finally, we studied the topography of Thy-1 isoforms by measuring FRET efficiency. When Thy-1.1 and Thy-1.2 were labeled, respectively, with OX7-FITC and 1aG4-tetramethylrhodamine isothiocyanate (TRITC), we observed intense energy transfer leading to a decrease in relative fluorescence intensity (RFI) of 1aG4-TRITC by –26.51±0.45% (Fig. 4A). Interestingly, when both Thy-1.1-OX7-FITC and Thy-1.2–1aG4-TRITC complexes were aggregated by rabbit anti-mouse (RαM) IgG, only a small decrease of RFI (–1.06±0.47%) was observed, suggesting existence of the preformed clusters. Furthermore, when the Thy-1.2 on the cells was labeled with 1aG4-FITC and 1aG4-TRITC at a ratio 5:1, the RFI remained the same after aggregation of the Thy-1-Ab

 

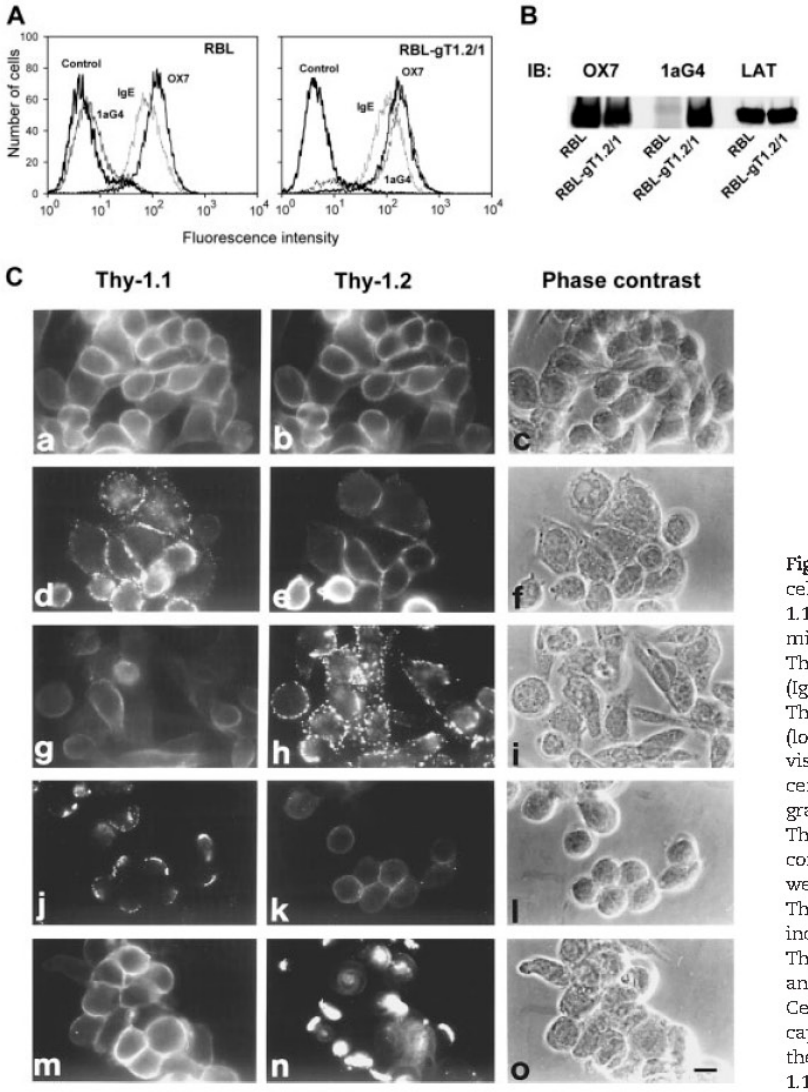


**Figure 1.** Properties of RBL and RBL-gT1.2/1 cells and independent movement of Thy-1.1 and Thy-1.2 as detected by light microscopy. (A) FACS analysis of surface Thy-1.1 (OX7), Thy-1.2 (1aG4) and FcεRI (IgE). (B) Immunoblotting (IB) analysis of Thy-1.1 (OX7), Thy-1.2 (1aG4) and LAT (loading control). (C) Thy-1.1 and Thy-1.2 visualized by indirect immunofluorescence on RBL-gT1.2/1 cells. The micrographs show staining for Thy-1.1 (left), Thy-1.2 (middle) and phase contrast of the corresponding fields (right). (a–c) Cells were fixed and then stained to visualize Thy-1.1 and Thy-1.2. (d–i) Cells were incubated for 10 min to induce patches of Thy-1.1 (d–f) or Thy-1.2 (g–i) and then fixed and stained for Thy-1.2 or Thy-1.1. (j–o) Cells were incubated for 60 min to induce caps of Thy-1.1 (j–l) or Thy-1.2 (m–o) and then fixed and stained for Thy-1.2 or Thy-1.1 (bar represents 10 μm).

complexes with RαM IgG (+1.57±3.05%). These data strengthen the results of EM studies indicating that the short-range distances between Thy-1 in its clusters do not dramatically change during the course of Ab-induced Thy-1 aggregation.

In the above experiments, we used whole IgG class mAb capable of dimerizing the target antigens. The observed FRET between Thy-1.1 and Thy-1.2 could thus reflect small changes in topography of the target molecules induced by their dimerization and movement into the same clusters, a situation that has been observed in another system [17]. In order to determine whether Ab-induced dimerization does indeed contribute to FRET, we labeled Thy-1.1 with either monovalent OX7(Fab)-FITC or dimerizing OX7($IgG_1$)-FITC probes. Thy-1.2 was labeled with 1aG4($IgG_3$)-TRITC, and FRET was analyzed by flow cytometry (Fig. 4B). At the time indicated by an arrow in Fig. 4B, Thy-1.2–1aG4-TRITC complexes were aggregated with nonlabeled isotype-specific anti-$IgG_3$. Monomeric Thy-1.1, labeled with OX7(Fab)-FITC, remained scattered throughout the whole cell surface after Thy-1.2 aggregation (not shown), which resulted in significantly enhanced RFI of 1aG4-TRITC (Fig. 4B, thick line), reflecting decreased FRET. However, dimeric Thy-1.1, labeled with OX7($IgG_1$)-FITC, was dragged into Thy-1.2 clusters, resulting in decreased RFI values of TRITC-labeled 1aG4 (Fig. 4B, thin line). These data indicate that dimerization of Thy-1.1 results in its enhanced association with Thy-1.2 aggregates.

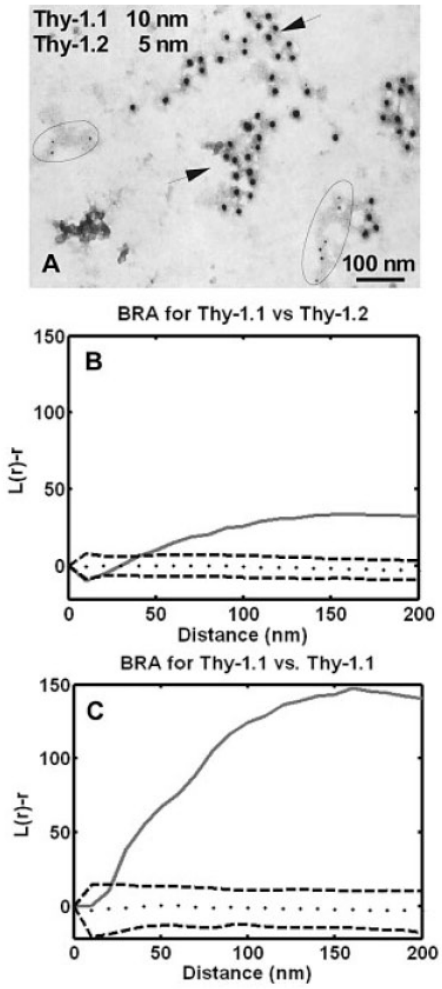


**Figure 2.** Topography of Thy-1.1 and Thy-1.2 as detected by EM. (A) Thy-1.1 in RBL-gT1.2/1was aggregated with OX7 mAb and GαM-gold-10 nm (arrows). The cells were fixed, free IgG binding sites were blocked with mouse IgG, and Thy-1.2 was labeled with biotinylated 1aG4 mAb followed by streptavidin-gold-5 nm (inside ellipses). (B) BRA of Thy-1.2 colocalization with aggregated Thy-1.1. (C) As a positive control, BRA is also shown for colocalization of the aggregated Thy-1.1 (labeled as above) with the remaining free Thy-1.1 in fixed cells (detected with biotinylated OX7 and streptavidin-gold-5 nm). Significant colocalization ($p<0.01$) of the proteins is shown as the position of the L-value curve (solid line) above boundaries (dashed lines) predicted for the random distribution of gold-labeled particles at a corresponding distance. Each graph represents approximately 35 $\mu m^2$ of the RBL PM from two independent experiments.

## Thy-1 topography is regulated by F-actin

Distribution of PM components is regulated at least in part by submembraneous cytoskeleton [18]. In further experiments we therefore examined by means of FRET the changes in Thy-1 distribution in cells pretreated with inhibitors of actin polymerization, latrunculin B or cytochalasin D. Preincubation of RBL-gT1.2/1 cells with latrunculin for 15 min resulted in a significant increase in energy transfer between Thy-1.2–1aG4-TRITC and Thy-1.2–1aG4-FITC (Fig. 5A, column 2). These data probably reflect the formation of small Ab-Thy-1 clusters after F-actin fence removal. The homo-FRET values obtained in latrunculin-pretreated cells did not further increase by aggregation of Ab-dimerized Thy-1 with RαM IgG (Fig. 5A, column 3), suggesting that the intermolecular distances between Thy-1 remain constant even after extensive Thy-1 aggregation.

However, when Thy-1.2 was labeled with 1aG4-TRITC and Thy-1.1 with OX7-biotin-FITC, latrunculin and cytochalasin caused a decrease in the energy transfer (Fig. 5B, columns 2 and 3), which could be explained by more diffuse distribution of Thy-1.1 and Thy-1.2 dimers after F-actin fence removal. Aggregation of the Thy-1.1-OX7-biotin-FITC complexes with streptavidin caused a small but significant decrease in FRET efficiency between Thy-1.1 and Thy-1.2 (Fig. 5B, column 4). Interestingly, aggregation of Thy-1.1-OX7-biotin-FITC by streptavidin completely abolished the effect of both latrunculin and cytochalasin described above and caused, in fact, significant increase of FRET values compared to control cells (Fig. 5B, columns 5 and 6). Thus, the formation of large Thy-1.1 aggregates in cells lacking F-actin fence caused co-clustering of Thy-1.1 and Thy-1.2.

## Cross-talk between Thy-1 and FcεRI

Biochemical studies with detergent-solubilized cells implied that FcεRI-mediated activation is initiated by coalescence of aggregated FcεRI with DRM [10, 12] and that F-actin is involved in this process [19, 20]. However, EM observations failed to discern any significant increase in association between Thy-1 and aggregated FcεRI [12, 15]. To elucidate these discrepancies, we further investigated the topography of Thy-1 and FcεRI by means of FRET, a method with 1–10 nm resolution. When FcεRI was dimerized by 5.14 mAb, enhanced FRET efficiency between Thy-1.1-OX7-FITC and FcεRI-IgE-TRITC complexes was observed (Fig. 6A, column 2). An even higher increase in FRET was determined after aggregation of FcεRI-IgE-TRITC complexes with multivalent antigen (TNP-BSA; Fig. 6A, column 3). These data confirm the results of biochemical studies documenting that FcεRI aggregation is indeed accompanied by movement of FcεRI aggregates into Thy-1-enriched domains [19]. As the pretreatment of cells with actin polymerization inhibitors enhanced FRET efficiency between Thy-1 and FcεRI even in control cells with nonaggregated FcεRI (Fig. 6A, columns 4 and 7), F-actin

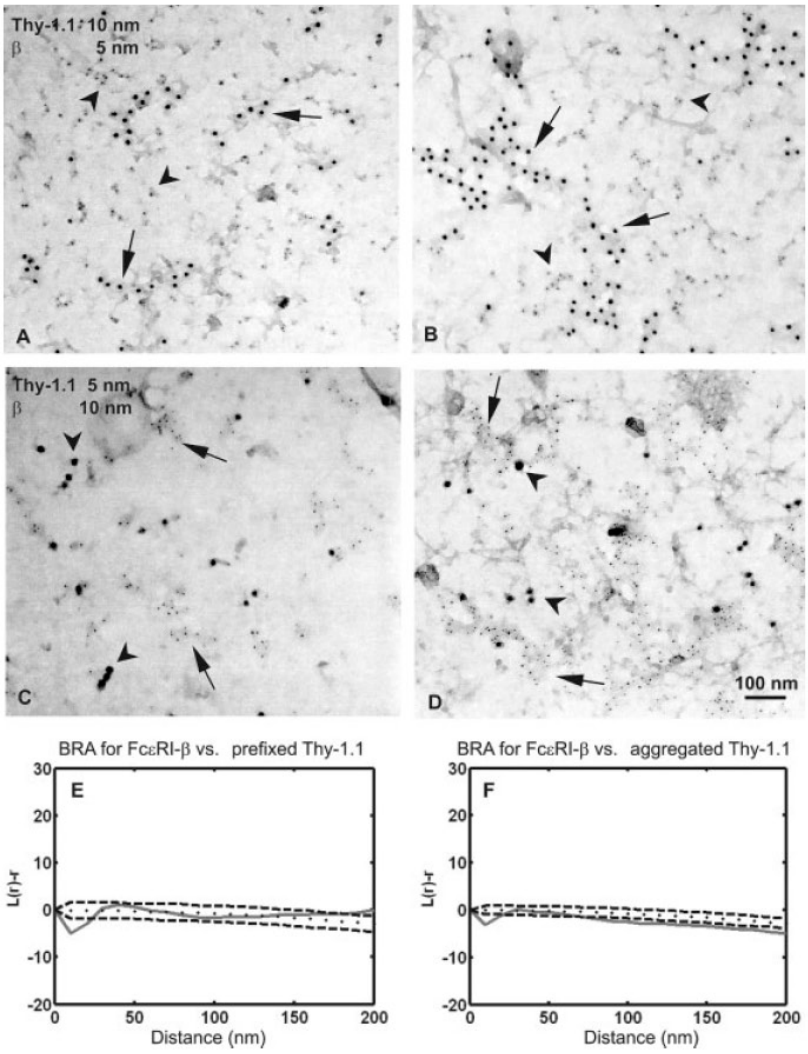


**Figure 3.** Topography of Thy-1.1 and FcεRI as detected by EM. RBL-2H3 cells were fixed before (A, C) or after (B, D) antibody-mediated Thy-1.1 aggregation. Thy-1.1 (arrows) was labeled on whole cells using 10 nm (A, B) or 5 nm (C, D) gold particles conjugated to OX7 mAb; FcεRI (arrowheads) was labeled on the cytoplasmic face of the PM sheets using the JRK antibody and secondary GαM-gold-5 nm (A, B) or –10 nm (C, D). BRA of colocalization of FcεRIβ subunit and nonaggregated (E) or aggregated (F) Thy-1.

could serve as a possible fence in confining FcεRI and Thy-1 in distinct membrane microdomains. Dimerization of FcεRI by 5.14 mAb in the presence of both inhibitors led to enhanced FRET between Thy-1 and FcεRI (Fig. 6A, columns 5 and 8). However, because latrunculin alone enhanced FRET efficiency by 10%, the observed difference (Fig. 6A, columns 4 and 5) was insignificant. After aggregation of FcεRI with TNP-BSA, there was even higher FRET efficiency in latrunculin-pretreated cells (Fig. 6A, columns 5 and 6, $p<0.01$), whereas in cytochalasin-pretreated cells, no further increase was observed (Fig. 6A, columns 8 and 9).

Because Thy-1 and FcεRI triggerings induce some common early activation events [21], it was important to determine whether Thy-1 aggregation has any effect on FcεRI homoassociation and whether F-actin is involved in this process. TNP-specific IgE was covalently modified either with TRITC or FITC, and the cells were labeled with both these FcεRI probes at a molar ratio 1:1. Then the cells were activated or not with dimerizing OX7 mAb or by extensive Thy-1 aggregation with Thy-1-OX7-biotin-streptavidin complexes. Data presented in Fig. 6B indicate that Thy-1 dimerization results in a small but significant enhancement of FRET, reflecting homoassociation of the FcεRI (Fig. 6B, column 2). Extensive Thy-1 aggregation had smaller effect (Fig. 6B, column 3). Pretreatment of the cells with latrunculin significantly enhanced FcεRI homo-FRET efficiency (Fig. 6B, column 4). Dimerization of Thy-1.1 and, namely, extensive Thy-1.1 aggregation in the presence of latrunculin resulted in further enhancement of IgE homoassociations (Fig. 6B, columns 5 and 6). Similar enhancement of FRET efficiencies was observed in cells pretreated with cytochalasin, except that extensive

 

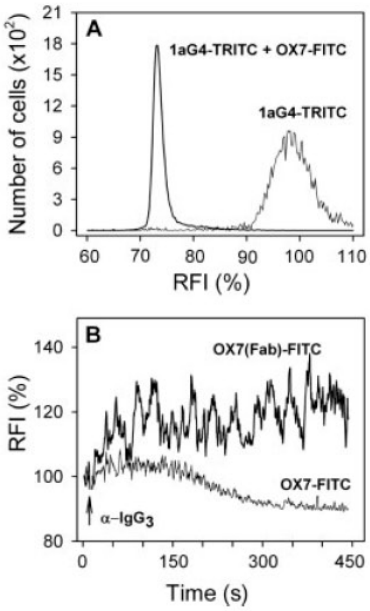


**Figure 4.** FRET between Thy-1.1 and Thy-1.2. (A) Representative RFI measured in RBL-gT1.2/1 cells by flow cytometry after binding of 1aG4-TRITC alone or 1aG4-TRITC and OX7-FITC. (B) Dimerization of Thy-1.1 results in its enhanced association with Thy-1.2 aggregates. Thy-1.1 was labeled either with Fab fragments of OX7-FITC or the whole OX7-FITC. Thy-1.2 was labeled with 1aG4-TRITC, and RFI were determined at various time intervals after aggregation of the Thy-1.2–1aG4-TRITC complexes with isotype-specific anti-$IgG_3$. Typical experiment from three performed is shown.

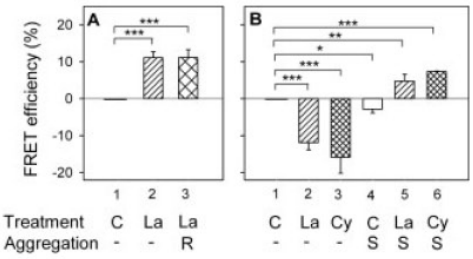


**Figure 5.** Different regulation of Thy-1 homo-FRET and hetero-FRET by F-actin. (A) Homo-FRET between Thy-1.2–1aG4-TRITC and Thy-1.2–1aG4-FITC. (B) Hetero-FRET between Thy-1.2–1aG4-TRITC and Thy-1.1-OX7-biotin-FITC. The cells were pretreated with latrunculin (La; 0.5 μM), cytochalasin B (Cy; 4 μM) or vehicle (C; 0.2% DMSO). In some experiments Thy-1 aggregation was induced by RαM IgG (R) or streptavidin (S). Data were normalized to vehicle-pretreated cells in column 1 (*$p<0.05$, **$p<0.01$, ***$p<0.001$).

aggregation of Thy-1 was less potent (Fig. 6B, columns 7–9). These data indicate that Thy-1 aggregation as well as actin polymerization affect the topography of FcεRI.

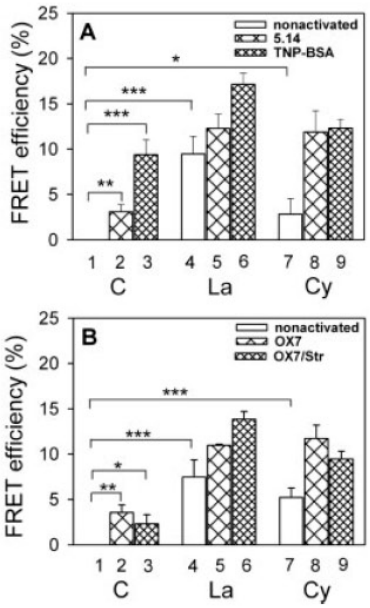


**Figure 6.** F-actin is involved in FRET cross-talk between Thy-1 and FcεRI. (A) FRET between Thy-1.1-OX7-FITC and FcεRI-IgE-TRITC was analyzed in RBL cells preincubated for 15 min with latrunculin (La; 0.5 μM), cytochalasin (Cy; 4 μM) or vehicle (C; 0.2% DMSO). IgE-TRITC-sensitized cells were nonactivated (1, 4, 7) or activated with 5.14 mAb (2, 5 ,8) or TNP-BSA (3, 6, 9) for 2 min, and the RFI was immediately evaluated by FACS. (B) RBL cells were either untreated or treated with latrunculin or cytochalasin and subsequently labeled with IgE-TRITC and IgE-FITC. Then the cells were either nonactivated (1, 4, 7) or activated for 5 min by Thy-1 dimerization with biotinylated OX7 (10 μg/mL; 2, 5, 8) or by extensive Thy-1 aggregation through biotinylated OX7-streptavidin complexes (3, 6, 9) (*$p<0.05$), **$p<0.01$, ***$p<0.001$).

## Cross-talk between Thy-1 and the adaptor proteins LAT and NTAL

EM on PM sheets showed that LAT and NTAL are located in distinct regions of the PM [22] and that aggregated Thy-1 colocalizes with LAT [15]. To determine whether Thy-1 also colocalizes with NTAL, we used RBL cells fixed before or after Thy-1 labeling with OX7 mAb and GαM-IgG-gold-10 nm (Fig. 7 and 8). Colocalization of Thy-1 with both LAT and NTAL was occasionally observed in cells fixed before Thy-1 staining (Fig. 7A, C and 8A, C), in which NTAL and LAT are distributed in separate domains (Fig. 8E). Colocalization of both adaptors with Thy-1 was strongly enhanced after Thy-1 aggregation (Fig. 7B, D and 8B, D). Under these conditions colocalization of LAT and NTAL was observed only at distances larger than the size of LAT/NTAL clusters (Fig. 8F).

The observed colocalization of Thy-1 with NTAL and LAT could have functional consequences for initial

 

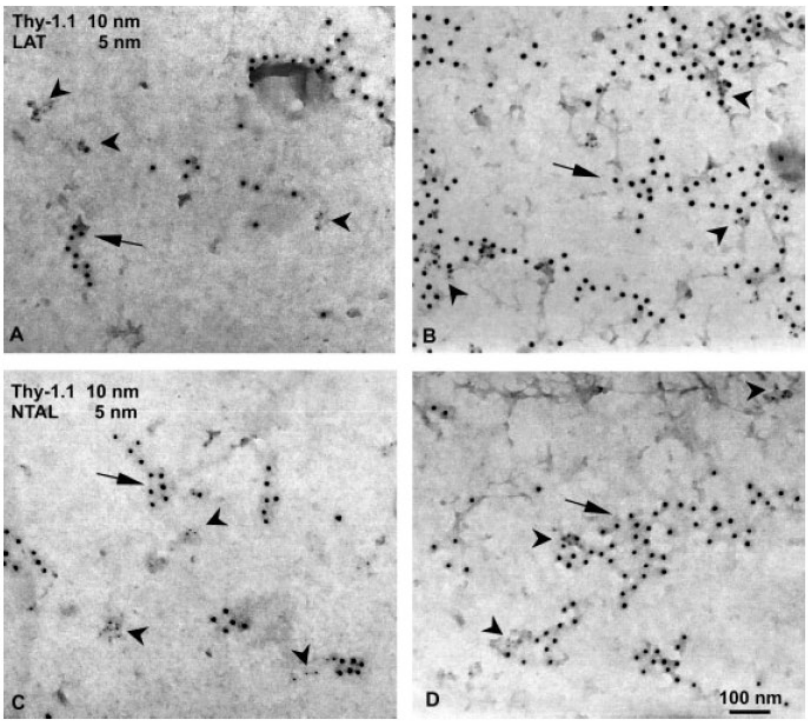


**Figure 7.** Colocalization of LAT and NTAL adaptors with Thy-1 clusters. Membrane topography of Thy-1.1 and adaptor proteins LAT (A, B) or NTAL (C, D) was determined in cells stained with OX7 Ab and GαM-gold-10 nm after fixation with 2% paraformaldehyde (A, C) or before fixation to induce formation of Thy-1 aggregates (B, D). Adaptors were detected with the corresponding mAb and GαM-gold-5 nm. Arrows indicate Thy-1.1; arrowheads mark LAT (A, B) or NTAL (C, D).

stages of Thy-1-induced cell activation. We therefore examined protein tyrosine phosphorylation in control and Thy-1-activated cells. The cells were lysed in 0.5% Triton X-100 and fractionated by sucrose density gradient ultracentrifugation. In nonactivated cells the major tyrosine phosphorylated protein found in DRM (fractions 1–5) is Lyn kinase, forming a typical 53/55 kDa double band (Fig. 9A, Control). Exposure of the cells to latrunculin alone resulted in weak tyrosine phosphorylation of a protein in DRM with Mr of 38 kDa, corresponding to LAT, and several other proteins in non-DRM high density fractions of the sucrose gradient (Fig. 9A, 0/La, fractions 6–9). After Thy-1-mediated activation induced by biotinylated OX7-streptavidin complexes, enhanced tyrosine phosphorylation in DRM was observed in proteins with Mr of NTAL (30 kDa) and LAT (Fig. 9A, OX7/0/Str). Aggregation of Thy-1 in the presence of latrunculin further enhanced tyrosine phosphorylation of both NTAL- and LAT-like proteins (Fig. 9A, OX7/La/Str). Further analysis showed that Syk kinase was excluded from DRM, whereas Lyn, LAT, NTAL and Thy-1 were included, as expected. Direct evidence that both NTAL and LAT are phosphorylated in Thy-1-activated cells was obtained by immunoprecipitation experiments. Thy-1 dimerization by OX7 alone induced 3.6- and 2.9-fold increases in tyrosine phosphorylation of LAT and NTAL, respectively (Fig. 9B, C). The extent of tyrosine phosphorylation was further enhanced by more extensive Thy-1 aggregation and rose even more after inhibition of actin polymerization by latrunculin. Immunoprecipitation experiments showed that latrunculin alone induced modest but reproducible dose-dependent tyrosine phosphorylation of LAT, NTAL and Syk, with peak effect at a concentration 0.5 μM (Fig. 9D).

## Discussion

RBL-gT1.2/1 cells expressing both the endogenous Thy-1.1 and the transfected Thy-1.2 were used to analyze the topography of Thy-1 isoforms with three methods differing in their resolution power. Although both rat Thy-1.1 and mouse Thy-1.2 are anchored to PM through the GPI anchor and differ only in a limited number of aminoacids (82% identity), immunofluorescence microscopy showed that both isoforms are distributed in the PM randomly and are aggregated independently. These data suggest that Thy-1 domains are very small, under the resolution limit of light microscopy, and/or that forces that keep GPI-anchored molecules in the putative domains are weaker than forces leading to their antibody-mediated aggregation. Using EM on immunogold-labeled PM sheets isolated from cells fixed before labeling, we confirmed previous data [15] that Thy-1 is distributed in small clusters independently of FcεRI.

 

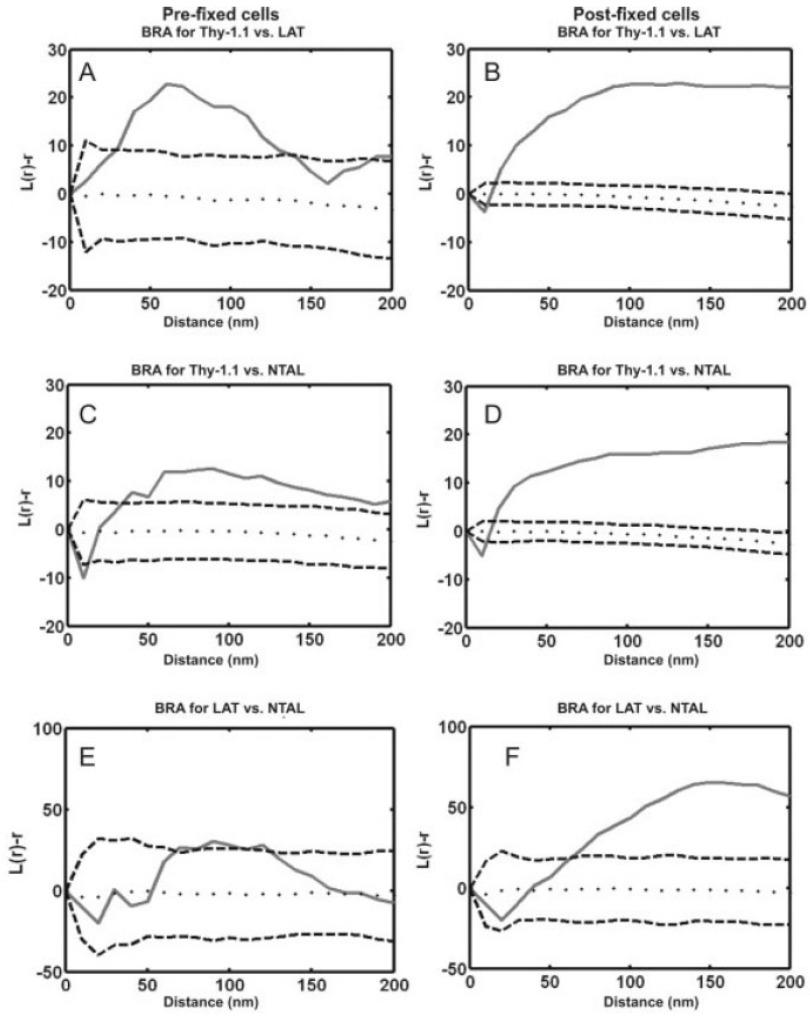


**Figure 8.** BRA of Thy-1.1 colocalization with LAT or NTAL in cells labeled for Thy-1 after fixation (A, C) or before fixation to induce formation of Thy-1 aggregates (B, D). BRA of LAT colocalization with NTAL in cells with nonaggregated (E) or aggregated (F) Thy-1.

However, based on these results, we cannot exclude the possibility that these clusters are induced, or that their size is enhanced, by the antibodies used for Thy-1 detection because isolation of PM sheets is incompatible with strong fixing conditions that ensure complete blocking of GPI-anchored protein movement. Antibody-induced aggregation of Thy-1 resulted in coalescence of smaller Thy-1 clusters into larger domains, as expected, yet the density of gold label in Thy-1 clusters was not enhanced; this suggests that distances between individual molecules were kept constant.

In an attempt to understand protein-protein interactions in the PM of living cells, we employed FRET-based analyses between one type of molecules (homo-FRET) or different molecules (hetero-FRET). FRET is unique in generating fluorescence signals sensitive to molecular conformations, associations and intermolecular distances in the range of 1–10 nm [23]. We found no dramatic changes in FRET efficiencies between immunolabeled Thy-1.2 and Thy-1.1 dimers after their aggregation with anti-IgG Ab. This implies that intermolecular distances do not dramatically change in the course of Thy-1 aggregation and in this sense support the results obtained by EM showing that density of gold-labeled Thy-1 in clusters is similar in cells with extensively aggregated Thy-1 (fixed after labeling) and cells fixed before Thy-1 labeling.

Previous studies suggested that segregation of lipid microdomains might be regulated by submembraneous cytoskeleton [19, 24]. Our data indicate that F-actin is involved in formation of Thy-1 clusters in PM. When polymerization of F-actin was disrupted with latrunculin, both Thy-1 isoforms distributed more randomly, as reflected in lower energy transfer between immunolabeled Thy-1.1 and Thy-1.2. These effects were almost abolished if biotinylated Thy-1.1 was crosslinked with

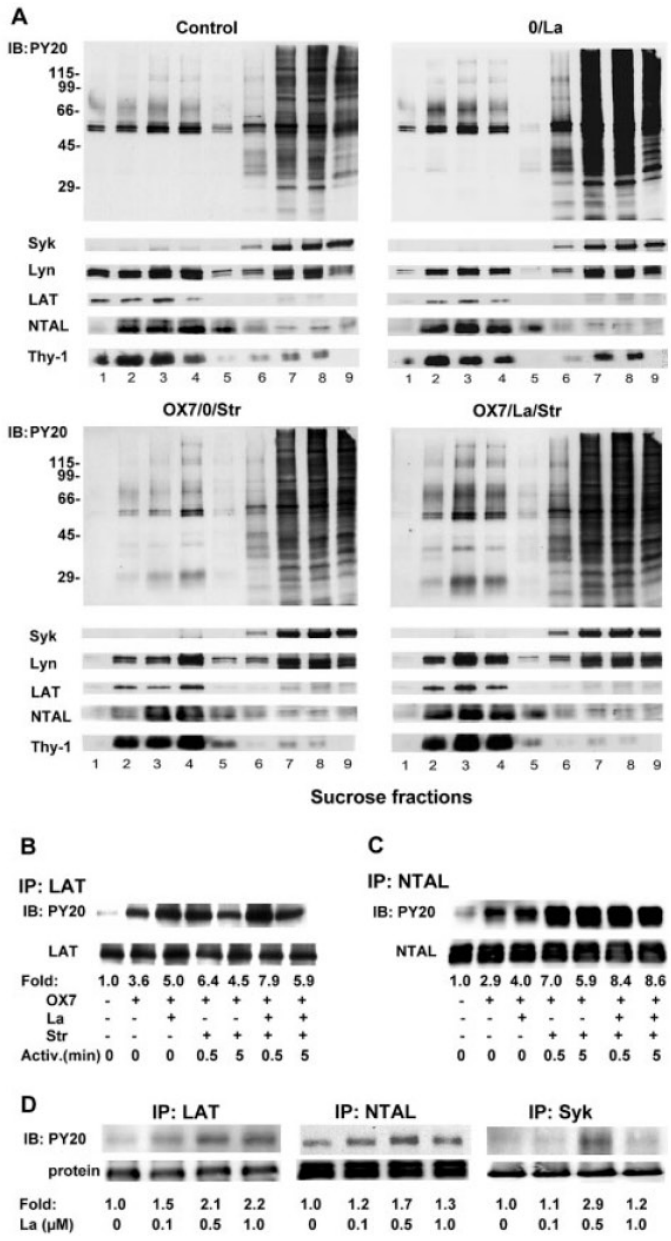


**Figure 9.** Tyrosine phosphorylation of NTAL and LAT in Thy-1-activated cells. (A) The cells were nonactivated (Control) or activated through Thy-1 aggregation by exposure to OX7-biotin-streptavidin (Str) complexes (OX7/0/Str). Alternatively, cells were preincubated for 15 min with latrunculin (La) and then activated in the presence of latrunculin alone (0/La) or together with OX7-biotin-streptavidin complexes (OX7/La/Str). After 5 min of incubation, the cells were solubilized, and the lysates were fractionated by sucrose density gradient ultracentrifugation. Individual fractions [1 (top) – 9 (bottom)] were collected and analyzed by immunoblotting for the presence of tyrosine phosphorylated proteins (PY-20), Syk, Lyn, LAT, NTAL and Thy-1. Numbers on the left indicate the position of Mr standards in kDa. (B–D) Extent of tyrosine phosphorylation of LAT, NTAL and Syk was determined in cells activated under different conditions as specified. The cells were solubilized and the proteins immunoprecipitated and analyzed by immunoblotting. Extent of tyrosine phosphorylation was determined by densitometry and normalized to the untreated cells and the amount of protein immunoprecipitated (Fold). A typical experiment from at least three performed in each group is shown.

streptavidin, suggesting that under these conditions cluster formation is driven by the crosslinking antibodies rather than F-actin. Thus, F-actin is crucial for the spatial distribution of Thy-1 in membrane microdomains, whereas external agents take the helm in activated cells.

Inhibition of actin polymerization leads to significant enhancement of the secretory response induced through FcεRI [25] or Thy-1 [20]. Our finding that inhibitors of actin polymerization enhance FRET efficiency between FcεRI and Thy-1.1 suggests that the decreased level of F-actin leads to loss of exclusion of the FcεRI from Thy-1 in nonactivated cells. Thus, F-actin could be the main regulator responsible for physical separation of signal transduction PM molecules. We noticed a significant difference in the effects of two inhibitors of actin polymerization, latrunculin B and cytochalasin D, which are distinct in their mode of action [26]. Latrunculin sequesters actin monomers by preventing actin polymerization and effectively disrupts both actin stress fibers and cortical actin filaments. In contrast, cytocha-

 

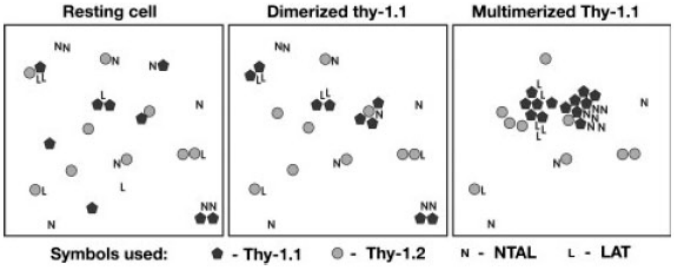


**Figure 10.** Schematic model of Thy-1 aggregation and interaction with transmembrane adaptors. In resting cells, both Thy-1.1 and Thy-1.2 reside scattered as single molecules or small patches of several molecules. After Thy-1.1 dimerization, Thy-1.2 remains scattered mostly independently of Thy-1.1. After Thy-1.1 multimerization, most of Thy-1.2 remains randomly scattered. However, aggregated Thy-1.1 forms large patches, recruiting transmembrane adaptors LAT and NTAL, occupying different membrane regions.

lasin binds to the barbed (growing) ends of actin filaments and prevents their elongation. Stronger inhibition of actin polymerization by latrunculin could explain why it was more potent in experiments measuring FRET efficiencies in this study.

By FACS analysis we found significantly increased FRET efficiency between Thy-1 and FcεRI after antigen-mediated FcεRI aggregation. Based on these data, we propose that at least a fraction of Thy-1 must edge towards FcεRI. However, the observed photobleaching (9.38%) after 1 min activation of the cells suggests that only a fraction of the Thy-1 was closer to aggregated FcεRI in activated cells. This finding is consistent with the results obtained by EM demonstrating that Thy-1 is not completely excluded from electron-dense patches where aggregated FcεRI accumulate [14].

Aggregated Thy-1 colocalizes with another lipid raft marker, LAT [15], which is structurally and functionally similar to NTAL. Surprisingly, LAT and NTAL are localized in different membrane microdomains in both nonactivated and activated cells [22]. Using EM we found that both LAT and NTAL colocalize with Thy-1 clusters, even though these adaptors did not form mixed clusters. Interestingly, extensive Thy-1 aggregation led to closer proximity of LAT and NTAL clusters. A schematic model of the distribution of Thy-1 isoforms, NTAL and LAT in nonactivated and Thy-1-activated cells is shown in Fig. 10. Because the two adaptors could be involved in different signaling pathways [27], our data suggest that these pathways could be affected by Thy-1 aggregation. Here we present evidence that Thy-1 aggregation induces tyrosine phosphorylation of the two adaptor proteins. Although pretreatment with latrunculin did not affect association of several signaling proteins (Lyn, LAT, NTAL and Thy-1) with DRM, it enhanced tyrosine phosphorylation of LAT, NTAL and even Syk, which is not considered to be associated with lipid rafts. It should be noted, however, that Syk could be recruited to lipid rafts through its binding to lipid raft-residing molecules such as Lyn [28] or aggregated FcεRI [10, 12]. The combined data support the notion that actin cytoskeleton is involved in setting the threshold for activation of mast cells through various pathways.

## Materials and methods

### Cells, antibodies and reagents

The origin and culture conditions for RBL cells (subclone 2H3) and Thy-1.2 transfectants (RBL-gT1.2/1) have been described [2]. The following mAb were used: MRC OX7 (OX7; $IgG_1$) recognizing Thy-1.1, F7D5 (IgM) and 1aG4 ($IgG_3$) directed against Thy-1.2 (their origins have been described [7]) and 5.14 ($IgG_1$) directed to the FcεRIα subunit [29]. The origins of IGEL b4 1 (IgE) recognizing TNP, JRK specific for the FcεRIβ subunit and antibodies against NTAL, LAT and Syk have been described [22]. GαM IgG-FITC and GαR IgM-LRSC (lissamine-rhodamine sulfonyl chloride) were obtained from Jackson Laboratories (West Grove, PA). HRP-conjugated anti-phosphotyrosine antibody PY20, RαM IgG and isotype-specific GαM $IgG_3$ were purchased from Sigma (St. Louis, MO). GαM-gold-10 nm and GαM-gold-5 nm were obtained from Amersham Biosciences (Uppsala, Sweden), and streptavidin-gold-5 nm was from Pelco International (Redding, CA). Fab fragments were prepared using ImmunoPure Fab Preparation Kit (Pierce, Rockford, IL). Fluorescence dyes FITC or TRITC (both from Sigma) were dissolved in DMSO at a concentration 10 mg/mL and then mixed with mAb (1:10 vol:vol). Reaction mix (1 mL containing ~2 mg antibody) was incubated for 1 h at room temperature and stopped by adding 0.1 mL 1.5 M hydroxylamine, pH 8.5. The conjugate was dialyzed against PBS and stored at –20°C. Some antibodies were biotinylated with ImmunoPure NHS-LC-biotin (Pierce) according to the manufacturer's instructions. All other reagents used were from Sigma.

### Immunofluorescence microscopy

Cells were grown on coverslips to semiconfluence. The coverslips were transferred on ice, and all procedures were

 

performed at 0°C unless stated otherwise. For antibody dilution and cell washing, ice-cold PBS and culture medium containing 10% FCS (5:1) was used. To visualize Thy-1, the cells were incubated for 30 min with antigen-specific antibody (1:100 diluted OX7 or F7D5), washed and incubated for 30 min with the class-specific secondary reagents GαM IgG-FITC or GαM IgM-LRSC (lissamine-rhodamine sulfonyl chloride), washed and incubated at 37°C for 10 or 60 min to induce patching or capping of the target gp. Then the cells were washed in PBS, pH 7.4, fixed in 4% paraformaldehyde in PBS for 20 min at 23°C, washed sequentially with 0.1 M glycine in PBS, PBS, and culture medium containing 10% FCS and then stained for a second antigen, using the two-step procedure as described above. In some experiments, the cells were first fixed and then stained on ice with the primary antibodies (OX7 and F7D5) followed by a mixture of the class-specific secondary antibodies. After staining, the cells were fixed once more in 4% paraformaldehyde for 10 min, washed, mounted in 0.1% *p*-phenylendiamine in 50% glycerol in PBS pH 8.0 and examined with an Orthoplan (Zeiss) fluorescence microscope.

### Electron microscopy

PM sheets were isolated, labeled and analyzed by EM as described [12, 15]. For labeling of both Thy-1 isoforms on the same membrane sheets, the cells were grown on coverslips and incubated for 15 min at room temperature with OX7 mAb (1 μg/mL) followed by 10 min incubation at 37°C with GαM-gold-10 nm; antibodies were diluted in buffered salt solution (BSS: 20 mM Hepes pH 7.4, 135 mM NaCl, 5 mM KCl, 1.8 mM $CaCl_2$, 5.6 mM glucose, 1 mM $MgCl_2$) supplemented with 0.1% BSA. Then the cells were fixed for 7 min in 2% paraformaldehyde in PBS at room temperature, and the remaining free IgG binding sites were blocked for 5 min in BSS-0.1% BSA with 5% normal mouse serum. Thy-1.2 gp (or Thy-1.1 gp) was detected by 15 min incubation with biotinylated 1aG4 (or OX7) in PBS-5% mouse serum. After a final 10 min incubation with streptavidin-gold-5 nm, the PM sheets were isolated and further processed.

### FRET

The cells ($10^6$) were incubated in 1 mL BSS-0.1% BSA with fluorescently tagged antibodies at saturating concentration for 30 min in the dark. Unbound antibodies were removed by washing the cells twice in BSS-0.1% BSA, and the cells were measured immediately by FACSCalibur (Becton Dickinson) to determine FRET efficiency between FITC- and TRITC-conjugated antibodies as described [30]. Donor fluorescence of double-labeled samples was compared with that of samples where the acceptor antibody was replaced by non-labeled antibody to compensate for any competition between the donor and acceptor antibodies. FRET efficiency was calculated from the fractional decrease of the donor fluorescence in the presence of the acceptor. Forward and side angle light scattering were used to gate out debris and dead cells. Calculated values for FRET efficiency were expressed as the ratio of the number of excited donor molecules, tunneling their excitation energy to the acceptor, to the number of all excited molecules.

### Cell activation, sucrose gradients and immunoblotting

RBL cells were harvested, resuspended in BSS-0.1% BSA and sensitized with biotinylated OX7 at a final concentration 10 mg/mL for 30 min at 37°C. After washing the cells were activated for 5 min at 37°C with streptavidin (10 mg/mL). In some experiments the cells were exposed for 15 min before activation to latrunculin (0.5 mM). Activated and control cells were lysed in ice-cold lysis buffer containing 0.5% Triton X-100 and fractionated by sucrose density gradient. Individual fractions from the gradient were analyzed by SDS-PAGE followed by immunoblotting as described [5]. In some experiments the cells were activated as specified in the Results, and LAT and NTAL were immunoprecipitated and analyzed as described [22].

### Statistical analysis

Statistical analysis of colocalization of antigens on PM sheets was evaluated by BRA using the $L(r)$-$r$ function as described [15]. $L(r)$-$r$ function maps the expected value of the Ripley's $K$ function defined similarly to the univariate function to radius $r$ and to 0. Unless further specified, FRET data represent mean ± SD from at least three independent experiments. Statistical significance of inter-group differences was calculated by the unpaired Student's $t$-test.

**Acknowledgements:** This work was supported by project 1 M6837805001 (Center of Molecular and Cellular Immunology) from the Ministry of Education, Youth and Sports of the Czech Republic, grant IAA5052310 from the Grant Agency of the Academy of Sciences of the Czech Republic, grants S301521904 and 301/06/0361 from the Grant Agency of the Czech Republic and Institutional project AVOZ50520514. The research of P. D. and P. H. were supported by an International Research Scholar's award from the Howard Hughes Medical Institute and by Research goal MSM0021620814 from the 3rd Faculty of Medicine (Charles University, Prague), respectively.

## References

1 **Dráberová, L.**, The involvement of Thy-1 antigen in the activation of rat mast cells. *Eur. J. Immunol.* 1989. **19:** 1715–1720.

2 **Dráberová, L. and Dráber, P.**, Functional expression of the endogenous Thy-1 gene and the transfected murine Thy-1.2 gene in rat basophilic leukemia cells. *Eur. J. Immunol.* 1991. **21:** 1583–1590.

3 **Dráberová, L. and Dráber, P.**, Thy-1-mediated activation of rat basophilic leukemia cells does not require co-expression of the high-affinity IgE receptor. *Eur. J. Immunol.* 1995. **25:** 2428–2432.

4 **Brown, D. A. and Rose, J. K.**, Sorting of GPI-anchored proteins to glycolipid-enriched membrane subdomains during transport to the apical cell surface. *Cell* 1992. **68:** 533–544.

5 **Surviladze, Z., Dráberová, L., Kubínová, L. and Dráber, P.**, Functional heterogeneity of Thy-1 membrane microdomains in rat basophilic leukemia cells. *Eur. J. Immunol.* 1998. **28:** 1847–1858.

 

6 **Štefanová, I., Hořejší, V., Ansotegui, I. J., Knapp, W. and Stockinger, H.,** GPI-anchored cell-surface molecules complexed to protein tyrosine kinases. *Science* 1991. **254:** 1016–1019.

7 **Dráberová, L. and Dráber, P.,** Thy-1 glycoprotein and src-like protein-tyrosine kinase p53/p56$^{lyn}$ are associated in large detergent-resistant complexes in rat basophilic leukemia cells. *Proc. Natl. Acad. Sci. USA* 1993. **90:** 3611–3615.

8 **Zhang, W., Sloan-Lancaster, J., Kitchen, J., Trible, R. P. and Samelson, L. E.,** LAT: the ZAP-70 tyrosine kinase substrate that links T cell receptor to cellular activation. *Cell* 1998. **92:** 83–92.

9 **Brdička, T., Imrich, M., Angelisová, P., Brdičková, N., Horváth, O., Šička, J., Hilgert, I. *et al.*,** Non-T cell activation linker (NTAL): a transmembrane adaptor protein involved in immunoreceptor signaling. *J. Exp. Med.* 2002. **196:** 1617–1626.

10 **Field, K. A., Holowka, D. and Baird, B.,** Compartmentalized activation of the high affinity immunoglobulin E receptor within membrane domains. *J. Biol. Chem.* 1997. **272:** 4276–4280.

11 **Sheets, E. D., Holowka, D. and Baird, B.,** Critical role for cholesterol in Lyn-mediated tyrosine phosphorylation of FcεRI and their association with detergent-resistant membranes. *J. Cell Biol.* 1999. **145:** 877–887.

12 **Dráberová, L., Lebduška, P., Hálová, I., Tolar, P., Štokrová, J., Tolarová, H., Korb, J. *et al.*,** Signaling assemblies formed in mast cells activated *via* Fcε receptor I dimers. *Eur. J. Immunol.* 2004. **34:** 2209–2219.

13 **Munro, S.,** Lipid rafts: elusive or illusive? *Cell* 2003. **115:** 377–388.

14 **Wilson, B. S., Pfeiffer, J. R., Surviladze, Z., Gaudet, E. A. and Oliver, J. M.,** High resolution mapping of mast cell membranes reveals primary and secondary domains of FcεRI and LAT. *J. Cell Biol.* 2001. **154:** 645–658.

15 **Wilson, B. S., Steinberg, S. L., Liederman, K., Pfeiffer, J. R., Surviladze, Z., Zhang, J., Samelson, L. E. *et al.*,** Markers for detergent-resistant lipid rafts occupy distinct and dynamic domains in native membranes. *Mol. Biol. Cell* 2004. **15:** 2580–2592.

16 **Simons, K. and Toomre, D.,** Lipid rafts and signal transduction. *Nat. Rev. Mol. Cell Biol.* 2000. **1:** 31–39.

17 **Harder, T., Scheiffele, P., Verkade, P. and Simons, K.,** Lipid domain structure of the plasma membrane revealed by patching of membrane components. *J. Cell Biol.* 1998. **141:** 929–942.

18 **Kwik, J., Boyle, S., Fooksman, D., Margolis, L., Sheetz, M. P. and Edidin, M.,** Membrane cholesterol, lateral mobility, and the phosphatidylinositol 4,5-bisphosphate-dependent organization of cell actin. *Proc. Natl. Acad. Sci. USA* 2003. **100:** 13964–13969.

19 **Holowka, D., Sheets, E. D. and Baird, B.,** Interactions between FcεRI and lipid raft components are regulated by the actin cytoskeleton. *J. Cell Sci.* 2000. **113:** 1009–1019.

20 **Tolarová, H., Dráberová, L., Heneberg, P. and Dráber, P.,** Involvement of filamentous actin in setting the threshold for degranulation in mast cells. *Eur. J. Immunol.* 2004. **34:** 1627–1636.

21 **Dráberová, L. and Dráber, P.,** Cross-linking of Thy-1 glycoproteins or high-affinity IgE receptors induces mast cell activation *via* different mechanisms. *Immunology* 1993. **80:** 103–109.

22 **Volná, P., Lebduška, P., Dráberová, L., Šímová, Š., Heneberg, P., Boubelík, M., Bugajev, V. *et al.*,** Negative regulation of mast cell signaling and function by the adaptor LAB/NTAL. *J. Exp. Med.* 2004. **200:** 1001–1013.

23 **Jares-Erijman, E. A. and Jovin, T. M.,** FRET imaging. *Nat. Biotechnol.* 2003. **21:** 1387–1395.

24 **Harder, T. and Simons, K.,** Clusters of glycolipid and glycosylphosphatidylinositol-anchored proteins in lymphoid cells: accumulation of actin regulated by local tyrosine phosphorylation. *Eur. J. Immunol.* 1999. **29:** 556–562.

25 **Frigeri, L. and Apgar, J. R.,** The role of actin microfilaments in the down-regulation of the degranulation response in RBL-2H3 cells. *J. Immunol.* 1999. **162:** 2243–2250.

26 **Spector, I., Shochet, N. R., Blasberger, D. and Kashman, Y.,** Latrunculins–novel marine macrolides that disrupt microfilament organization and affect cell growth: I. Comparison with cytochalasin D. *Cell Motil. Cytoskeleton* 1989. **13:** 127–144.

27 **Gilfillan, A. M. and Tkaczyk, C.,** Integrated signalling pathways for mast-cell activation. *Nat. Rev. Immunol.* 2006. **6:** 218–230.

28 **Amoui, M., Dráberová, L., Tolar, P. and Dráber, P.,** Direct interaction of Syk and Lyn protein tyrosine kinases in rat basophilic leukemia cells activated *via* type I Fcε receptor. *Eur. J. Immunol.* 1997. **27:** 321–328.

29 **Baniyash, M., Alkalay, I. and Eshhar, Z.,** Monoclonal antibodies specific to the α-subunit of the mast cell's FcεR block IgE binding and trigger histamine release. *J. Immunol.* 1987. **138:** 2999–3004.

30 **Dornan, S., Sebestyen, Z., Gamble, J., Nagy, P., Bodnar, A., Alldridge, L., Doe, S. *et al.*,** Differential association of CD45 isoforms with CD4 and CD8 regulates the actions of specific pools of p56lck tyrosine kinase in T cell antigen receptor signal transduction. *J. Biol. Chem.* 2002. **277:** 1912–1918.


 

**6.5**

**Dráber, P.; Dráberová, L.; Heneberg, P.; Šmíd, F.; Farghali, H. & Dráber, P. (2007):**

**Preformed STAT3 transducer complexes in human HepG2 cells and rat hepatocytes.**

**Cellular Signalling 19(11): 2400-2412.**

Available online at www.sciencedirect.com
ScienceDirect
Cellular Signalling 19 (2007) 2400–2412
CELLULAR SIGNALLING
www.elsevier.com/locate/cellsig

# Preformed STAT3 transducer complexes in human HepG2 cells and rat hepatocytes

Peter Dráber [a], Lubica Dráberová [a], Petr Heneberg [a,b], František Šmíd [c], Hassan Farghali [d], Petr Dráber [a,*]

[a] Institute of Molecular Genetics, Academy of Sciences of the Czech Republic, Prague, Czech Republic
[b] Center for Research in Diabetes, Metabolism and Nutrition, 3rd Faculty of Medicine, Charles University, Prague, Czech Republic
[c] Institute of Clinical Biochemistry and Laboratory Diagnostics, 1st Medical Faculty, Charles University, Prague, Czech Republic
[d] Institute of Pharmacology, 1st Medical Faculty, Charles University, Prague, Czech Republic

Received 14 July 2007; accepted 24 July 2007
Available online 1 August 2007

**Abstract**

Interleukin 6 (IL-6) is a pleiotropic cytokine that mediates a variety of functions, including induction of the acute-phase response in hepatocytes. IL-6 initiates its action by binding to its cell surface receptor, followed by activation of Janus kinases and tyrosine phosphorylation of the signal transducer and transcription factor (STAT) 3. Although it has been suggested that cholesterol- and sphingolipid-enriched membrane domains, called lipid rafts, and caveolin are involved in this process, their roles in the earliest stages of IL-6-mediated signaling are far from being understood. Here we show that pretreatment of HepG2 hepatoma cells with methyl-β-cyclodextrin (MβCD), which removes cholesterol and destroys lipid rafts, inhibited tyrosine phosphorylation of STAT3 in IL-6-activated, but not PV-activated cells. Furthermore, when the cells were lysed under conditions preserving lipid rafts, no IL-6- or PV-induced phosphorylation of STAT3 was observed. Although most of the STAT3 was found in large MβCD-resistant assemblies in both non-activated and IL-6-activated cells, its association with lipid rafts was weak or undetectable. The extent of IL-6-induced tyrosine phosphorylation of STAT3 was comparable in cells expressing low or high levels of caveolin. Similar STAT3 transducer complexes were observed in freshly isolated rat hepatocytes. The combined data suggest that STAT3 tyrosine phosphorylation occurs in preformed transducer complexes that can be activated in the absence of intact lipid rafts or caveolin.


*Keywords:* Cytokine signaling; Lipid rafts; Interleukin-6; Caveolin; Cholesterol; Cyclodextrin

## 1. Introduction

The cytokine interleukin 6 (IL-6) belongs to a family of mediators involved in the regulation of acute phase response to injury and infections [1–4]. Dysregulation of IL-6-mediated signaling contributes to the onset and/or maintenance of several pathologies such as inflammatory bowel disease, rheumatoid arthritis or various types of cancer [5,6]. IL-6 exerts its action by binding to the corresponding receptor composed of the 80 kDa ligand binding subunit (gp80, CD126) and the signal-transducing subunit (gp130, CD130). The binding leads to dimerization of gp130 and activation of protein-tyrosine kinases, Janus kinase (JAK) 1, JAK2 and Tyk2, which are constitutively associated with gp130. In turn, gp130 becomes tyrosine phosphorylated at its cytoplasmic tail and recruits transcription factors, the signal transducer and activator of transcription

*Abbreviations:* BSA, bovine serum albumin; BSS, buffered salt solution; DMSO, dimethyl sulfoxide; DRM, detergent-resistant membrane; FCS, fetal calf serum; FITC, fluorescein isothiocyanate; GPI, glycosylphosphatidylinositol; HRP, horseradish peroxidase; IgG, immunoglobulin G; IL-6, interleukin 6; JAK, Janus kinase; mAb, monoclonal antibody; MβCD, methyl-β-cyclodextrin; PAGE, polyacrylamide gel electrophoresis; PBS, phosphate-buffered saline; PMSF, phenylmethylsulfonyl fluoride; PTP, protein tyrosine phosphatase; PV, pervanadate/$H_2O_2$; pSTAT, tyrosine phosphorylated STAT; SDS, sodium dodecyl sulphate; SH2, Src homology 2; STAT, signal transducer and activator of transcription.

* Corresponding author. Department of Signal Transduction, Institute of Molecular Genetics, Academy of Sciences of the Czech Republic, Vídeňská 1083, 142 20 Prague 4, Czech Republic. Tel.: +420 241 062 468; fax: +420 241 062 214.
*E-mail address:* draberpe@biomed.cas.cz (P. Dráber).

0898-6568/$ - see front matter © 2007 Elsevier Inc. All rights reserved.
doi:10.1016/j.cellsig.2007.07.018

(STAT) 1 and STAT3. STAT3 is then phosphorylated on tyrosine 705 which is located in the conserved Src homology 2 (SH2) domain allowing homodimerization as well as heterodimerization [7]. During translocation to the nucleus, STAT3 is phosphorylated on a serine, a process which is indispensable for full transcriptional activity. In the nucleus the STAT3 dimer binds to specific class II IL-6 responsive elements and activates the transcription of the target genes including genes of acute phase proteins [4,8].

Cell fractionation studies using Hep3B human hepatoma cells showed that STAT3 was present in cytosol in the form of high molecular weight complexes [9]. In these cells, a significant fraction of STAT 3, approximately 10%, was found in detergent-resistant membranes (DRMs), suggesting an association with lipid rafts [10], newly called membrane rafts [11], whose composition, size, dynamics and functions remain incompletely understood [11,12]. Upon cell activation by IL-6 or orthovanadate, tyrosine phosphorylated STAT3 (pSTAT3) was found in DRMs, which also contained caveolin and heat shock protein 90. Exposure of Hep3B cells to methyl-β-cyclodextrin (MβCD), widely used to deplete cellular cholesterol and disrupt plasma membrane microdomains [13,14], inhibited the IL-6-induced STAT3 signaling [15,16]. These data suggested that signaling through specialized caveolin-containing lipid rafts may be a general mechanism operating at the level of plasma membrane whereby cytokines and growth factors activate STAT species (the "raft-STAT signaling hypothesis" [15,16]). Other studies using other tumor-derived cells, however, showed that caveolin was dispensable for some IL-6-mediated signaling events [17]. Furthermore, it has been reported that cholesterol depletion triggers shedding of IL-6 receptor; that could be an alternative explanation for the loss of responsiveness to IL-6 in cholesterol-depleted cells [18]. Thus, the role of lipid rafts and caveolin in early stages of IL-6-triggered signaling is unclear.

In this study we analyzed the cellular distribution and tyrosine phosphorylation of STAT3 in IL-6- and pervanadate/$H_2O_2$ (PV)-activated human hepatoma HepG2 cells which do not express caveolin [19,20], and their transfectants expressing caveolin. We also examined the sensitivity of IL-6- and PV-induced STAT3 phosphorylation to cholesterol removal by MβCD, and association of STAT3 with DRMs as determined by density gradient ultracentrifugation. Most of the previously published data aimed to understand the role of lipid rafts in hepatocyte signaling were based on studies of human hepatoma cell lines [15,21–24]. As hepatoma cells grown for many generations under *in vitro* conditions differ in their properties from hepatocytes [25,26], we also present first data regarding the localization of STAT3 in membrane microdomains in freshly isolated rat hepatocytes.

## 2. Materials and methods

### 2.1. Antibodies and reagents

Mouse monoclonal antibodies (mAbs) specific for Tyr 705 phosphorylated STAT3 (pSTAT3; sc-8059), rabbit polyclonal anti-STAT3 (sc-7179), horseradish peroxidase (HRP)- and fluorescein isothiocyanate (FITC)-conjugated goat anti-mouse immunoglobulin G (IgG) and goat anti-rabbit IgG were obtained from Santa Cruz Biotechnology (Santa Cruz, CA). Rabbit anti-caveolin antibody was purchased from BD Biosciences (Heidelberg, Germany). Mouse mAb specific for CD59 was provided by Dr. Hořejší (Institute of Molecular Genetics, Prague). Mouse anti-human CD126 (IL-6 receptor; clone B-R6) mAb and recombinant human IL-6 were obtained from Serotec (Oxford, UK) and Biosource International (Camarillo, CA), respectively. Cy3-conjugated donkey anti-rabbit IgG was from Jackson ImmunoRes (West Grove, PA). LysoTracker Red DND-99 and jasplakinolide were from Molecular Probes (Eugene, OR). Cell-Tak was purchased from BD Biosciences, Bedfort, MA; MβCD and all other chemicals were obtained from Sigma-Aldrich (St. Louis, MO).

### 2.2. Cell culture

The human hepatoma HepG2 cells were obtained from American Type Culture Collection, Rockville, MD. The cells were grown in RPMI-1640 medium supplemented with 10% (v/v) heat-inactivated fetal cal serum (FCS; BioClot, GmbH, Aidenbach, Germany), antibiotics and extra D-glucose (2.5 mg/ml). They were maintained at 37 °C in an atmosphere of 5% $CO_2$ in air. Cell cultures were mycoplasma free as verified by the Hoechst staining method [27].

### 2.3. Isolation of rat hepatocytes

Hepatocytes were isolated from male albino rats, weighing between 220 and 260 g, by the collagenase perfusion method [28] with minor modifications as described [29]. Viability of isolated hepatocytes, assessed by trypan blue exclusion, was between 80% and 90%. Hepatocytes were used in experiments within 3–7 h after isolation. All protocols for animal use were approved by the Animal Care and Use Committee, Institute of Molecular Genetics, Prague.

### 2.4. Cholesterol depletion and measurement

To remove cholesterol, cells were incubated with 12.5 mM MβCD in buffered salt solution (BSS; 20 mM HEPES, pH 7.4, 135 mM NaCl, 5 mM KCl, 1.8 mM $CaCl_2$, 1 mM $MgCl_2$, 5.6 mM glucose) supplemented with 0.1% bovine serum albumin (BSA) at 37 °C for various time intervals. Control cells were incubated with 12.5 mM cholesterol-saturated MβCD, prepared as described [30]. Cellular cholesterol was determined by means of microenzymatic fluorescence assay [31].

### 2.5. Flow cytometry

To determine the surface expression of IL-6 receptor, HepG2 cells were incubated with or without 12.5 MβCD for 30 min, followed by washing and fixation with 4% paraformaldehyde for 15 min on ice. After washing the cells were labeled for 30 min with mouse anti-human CD126, washed again, and subsequently incubated with saturating concentration of FITC-labeled anti-mouse IgG antibody. Cells were examined by FACSCalibur (BD Biosciences) immediately after labeling. Statistical analysis was conducted using CellQuest Pro; the data were exported by FACS Assistant 1.1 to LGD files to form images in Sigma Plot.

Single-cell suspensions of HepG2 cells or freshly isolated rat hepatocytes were loaded into 96-well tissue cell culture plates and incubated with or without 0.5 nM IL-6 or 0.2 mM PV for the indicated time intervals. LysoTracker Red DND-99 at a final concentration 50 nM was added for the last 5 min of incubation. Cell fluorescence was assessed using FACS LSR II (BD Biosciences); images and statistical analyses were prepared using FlowJo software.

### 2.6. Confocal microscopy

For microscopical studies, freshly isolated hepatocytes were attached to coverslips coated with Cell-Tak (BD Biosciences) and incubated for 1 h in medium used for culturing of HepG2 cells. The cells were activated or not with 0.5 nM IL-6 for the indicated time intervals, fixed with 4% paraformaldehyde in PBS and then permeabilized with 0.1% Triton X-100. Rabbit anti-STAT3 and mouse anti-pSTAT3 were added to the cells for 60 min at saturating concentrations. Cy3-conjugated donkey anti-rabbit IgG (Jackson ImmunoRes) was used as a secondary antibody. The cells were immediately analyzed with Leica TCS NT/SP confocal system in conjunction with Leica DMR microscope

(Leica Microsystems GmbH, Wetzlar, Germany). In some experiments, the HepG2 cells and hepatocytes were activated or not with 0.5 nM IL-6 or 0.2 mM PV. LysoTracker Red DND-99 at final concentration 50 nM was added to the cells just before the addition of activators or BSS/BSA. After 88 min incubation at 37 °C with the activators and LysoTracker, cells were fixed with 4% paraformaldehyde, washed, and immediately analyzed.

### 2.7. Caveolin cDNA transfection

Full-length human cDNA for α and β isoforms of caveolin cloned into pcDNA.3.1 (+) vector (Invitrogen, San Diego, CA, USA) was obtained from Dr. Fujimoto [19] and transfected into HepG2 cells by a modified calcium phosphate-mediated gene transfection method [32]. Briefly, HepG2 cells were seeded into 10 cm tissue culture dishes. After 24 h, fresh culture medium was added, followed by adding 1 ml of DNA mix containing 18 μg CsCl-isolated pcDNA3.1-caveolin α/β and 2 μg selection vector pSTneoB [33] in BES buffer [125 mM $CaCl_2$, 25 mM HEPES (pH 7.0), 140 mM NaCl and 0.75 mM $Na_2HPO_4$]. Control cells were likewise transfected with DNA mix containing empty pcDNA3.1 (+) vector and pSTneoB. After 3.5 h incubation at 37 °C in 5% $CO_2$ in air, culture medium was removed and 25% dimethyl sulfoxide (DMSO) in BES buffer added. Four min later, DMSO was replaced with culture medium. Cells were trypsinized after 48 h and transferred into medium containing 800 μg/ml G418 (Geneticin, Invitrogen, Rockville, MD). After 12 days, colonies were picked up and expanded for further analysis.

### 2.8. Cell activation and preparation of cell lysates

HepG2 cells were grown to semi-confluence, washed twice with phosphate-buffered saline (PBS), and cultured for 20 h in medium supplemented with 0.1% FCS. The cells were harvested with PBS/0.02% EDTA/0.05% trypsin, washed twice with BSS/BSA and activated for the indicated time intervals at 37 °C by adding IL-6 at a final concentration of 0.5 nM. Alternatively, the cells were activated by PV which was freshly made by mixing sodium orthovanadate solution with $H_2O_2$ to get a final concentration of 10 mM for both components. After 15 min at room temperature the PV solution was diluted 1:50 directly into cell suspensions in BSS/BSA (final concentration of PV is 0.2 mM). Cell activation was stopped by transferring the tubes on ice and a brief centrifugation to pellet the cells. The sedimented cells were lysed in ice-cold lysis buffer [50 mM Tris–HCl, pH 7.5, 150 mM NaCl, 2 mM EDTA, 1 mM $Na_3VO_4$, 1 mM phenylmethylsulfonyl fluoride (PMSF), 1 μg/ml aprotinin, 1 μg/ml leupeptin] supplemented with detergents as described in Results. The mixture was incubated with occasional vortexing for 30 min on ice. The lysates were clarified by centrifugation at 12,000 ×*g* for 10 min and the postnuclear supernatants were used for further analysis. As indicated in Results, freshly isolated hepatocytes were used in some experiments instead of HepG2 cells.

### 2.9. In vitro kinase assay

To induce tyrosine phosphorylation in cellular lysates, $2\times10^6$ HepG2 cells or freshly isolated hepatocytes were lysed in 0.5 ml kinase lysis buffer (50 mM Tris–HCl, pH 7.5, 5 mM $MnCl_2$, 5 mM $MgCl_2$, 0.1 mM $Na_3VO_4$ and protease inhibitors as above) for 15 min on ice. ATP at a final concentration 100 μM was added to 400 μl aliquots of postnuclear supernatant and the samples were incubated without or with 0.2 mM PV or 0.5 nM IL-6 at 37 °C for 15 min. The reaction was stopped by adding 2× concentrated sodium dodecyl sulphate (SDS)-polyacrylamide gel electrophoresis (PAGE) sample buffer and boiling for 5 min.

### 2.10. Cell fractionation

Harvested cells ($20\times10^6$) were washed in BBS/BSA, activated as described in Results, resuspended in 1 ml extract lysis buffer (10 mM HEPES, pH 7.9, 10 mM NaCl, 3 mM $MgCl_2$, 1 mM dithiothreitol, 1 mM PMSF, and 0.1 mM $Na_3VO_4$) and disrupted by gentle cell breakage in a loose-fitting Dounce homogenizer. All cell fractionation steps were carried out on ice or at 4 °C. Nuclei were removed from the cell homogenate by low speed centrifugation (1000 rpm for 2 min in an Eppendorf centrifuge 5810R). The crude post-nuclear supernatant (800 μl) was further fractionated by centrifugation for 15 min at 14,000 ×*g* to yield the supernatant fraction (S15) and pelleted crude membrane fraction (P15). Pelleted material was resuspended in 200 μl of 1×SDS-PAGE sample buffer, whereas 100 μl of S15 was mixed with an equal amount of 2×SDS-PAGE sample buffer. 600 μl of S15 was further fractionated into pellet (P100) and cytosol (S100) fractions by centrifugation at 100,000 ×*g* for 60 min. The P100 fraction was resuspended in 200 μl of 1×SDS-PAGE sample buffer and 100 μl S100 was mixed with 100 μl 2×SDS-PAGE sample buffer. Fifty μl aliquots of the samples were loaded on the gel.

Association of STAT3 with DRMs was determined on cells ($15\times10^6$) activated as described in Results and lysed on ice in 0.8 ml lysis buffer (10 mM Tris–HCl, pH 8.0, 50 mM NaCl, 2 mM EDTA, 10 mM glycerophosphate, 1 mM $Na_3VO_4$, 1 mM PMSF, 0.5 U/ml aprotinin and 0.5 U/ml leupeptin) supplemented with 0.5% Brij-96 or 0.05% Triton X-100. Gradient was formed by addition of 0.5 ml of 80% sucrose stock solution to the bottom of a polyallomer tube (13×51 mm; Beckman Instruments, Palo Alto, CA) followed by 1.5 ml of 40% sucrose containing the cell lysate, 2 ml 30% sucrose and 1 ml 5% sucrose. Tubes were centrifuged for 4 h at 210,000 ×*g* at 4 °C using a SW 55 Ti rotor (Beckman Instruments). Ten fractions were collected from top of the gradient. The exact sucrose concentration (% w/v) in each fraction was determined by Abbe refractometer. Each fraction was mixed with equal amount of 2×SDS sample buffer and analyzed by SDS-PAGE.

In order to release free cytoplasmic molecules, cells were permeabilized by incubation for 5 min on ice in PBS containing 0.1% saponin, 5 mM $MgCl_2$ and 1 mM $Na_3VO_4$, centrifuged (15 s, 14,000 rpm, Eppendorf microcentrifuge, 4 °C), and the cellular ghosts were extracted for 15 min on ice in lysis buffer supplemented with 1% Triton X-100. All samples were resolved on 10% SDS-PAGE and analyzed by immunoblotting as described [34].

### 2.11. Gel chromatography

Gel chromatography experiments were performed as described before [35]. Briefly, samples of postnuclear supernatant from $10^7$ nonactivated or IL-6-activated cells in 300 μl of lysis buffer were applied to the top of a small column filled with Sepharose 4B [10 mm (diameter)×40 mm; Pharmacia, Sweden], and eluted with lysis buffer. Individual fractions (300 μl) were collected at 5 min intervals and further analyzed by immunoblotting.

### 2.12. Immunoblotting

Proteins (50 μl sample/well) were size-fractionated by SDS-PAGE under reducing conditions, except for CD59, and then electrotransferred to nitrocellulose membranes (BA 85, Schleicher and Schuell, Dassel, Germany) as described [36]. The membranes were blocked in blocking buffer (10 mM Tris–HCl, pH 7.5, 150 mM NaCl, 0.1% Tween 20, 3% BSA) and proteins detected with protein-specific antibodies followed by anti-Ig antibodies conjugated to HRP. The membrane-bound HRP was visualized with ECL Western blotting reagent (Amersham, Little Chalfont, UK) according to the manufacturer's instructions. In some experiments, the antibodies were stripped from the membranes by incubation for 10 min in $H_2O$, followed by 10 min in 0.2 M NaOH, and 2×10 min in $H_2O$, and the membranes were reprobed with other antibodies. Immunoblots were quantified by Luminescent Image Analyzer LAS-3000 (Fuji Photo Film Co., Tokyo) and further analyzed by AIDA image analyzer software (Raytest, Straubenhardt, Germany).

## 3. Results

### 3.1. Acute cholesterol lowering inhibits IL-6- but not PV-induced tyrosine phosphorylation of STAT3

In initial experiments we tested our hypothesis postulating that tyrosine phosphorylation of STAT3 in MβCD-pretreated cells would be inhibited in both IL-6- and PV-activated cells if lipid rafts were crucial for the formation of signaling assemblies required for STAT3 phosphorylation. On the other hand, if plasma

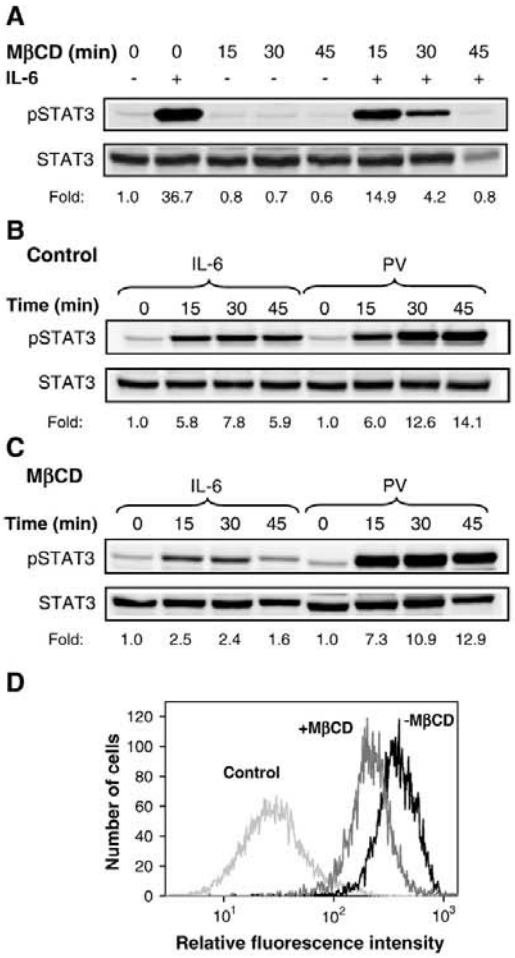


Fig. 1. Different sensitivity of IL-6- and PV-induced tyrosine phosphorylation of STAT3 to cholesterol removal in HepG2 cells. (A) Cells incubated in suspension without (0) or with 12.5 mM MβCD in BSS/BSA for the indicated time intervals, followed by 15 min activation without (−) or with (+) 0.5 nM IL-6. (B, C) Cells incubated in BSS/BSA alone (B) or in BSS/BSA supplemented with 12.5 mM MβCD (C) for 30 min and then activated for the indicated time intervals with 0.5 nM IL-6 or 0.2 mM PV. After activation the cells were solubilized in lysis buffer containing 1% NP-40 and their postnuclear supernatants were size fractionated by SDS-PAGE followed by immunoblotting with pSTAT3-specific antibody. STAT3 was determined by immunoblotting with anti-STAT3 antibody after stripping off the membranes. Relative amount of the pSTAT3 was determined by densitometry analysis of the corresponding immunoblots and normalized to control cells (nonactivated, MβCD untreated; Fold). (D) Flow cytometry analysis of IL-6 receptor expression in MβCD pretreated cells. Cells were incubated without (−) or with (+) 12.5 mM MβCD for 30 min at 37 °C, and IL-6 receptor expression was determined with anti-CD126 mAb followed by anti-mouse IgG-FITC conjugate. MβCD pretreated cells exposed to irrelevant IgG1 mAb served as a negative control. Typical results from at least 3 experiments performed are shown.

membrane cholesterol is required only for proper assembly of IL-6 receptor subunits and their interaction with preassembled transducer complex, then cholesterol removal will inhibit IL-6-but not PV-mediated STAT3 phosphorylation. Representative data in Fig. 1A show that pretreatment of HepG2 cells with MβCD had no effect on basal STAT3 tyrosine phosphorylation, but inhibited tyrosine phosphorylation induced by IL-6. The extent of inhibition of STAT3 phosphorylation was dependent on the length of exposure of the cells to MβCD and correlated with the decrease in the amount of cellular cholesterol. Incubation with 12.5 mM MβCD for 15 min, which reduced the content of cellular cholesterol by 43±3% (mean±SD; $n$=3), reduced STAT3 phosphorylation by 59±3%. Prolonged incubation for 30 min, reducing total cellular cholesterol by 55±4%, led to 89±4% inhibition of STAT3 phosphorylation. Almost complete inhibition of STAT3 tyrosine phosphorylation was observed after 45 min exposure to MβCD, resulting in 64±5% decrease in cellular cholesterol. When the cells were activated by PV, even higher and more protracted tyrosine phosphorylation of STAT3 was observed, compared to IL-6 triggered cells (Fig. 1B). Surprisingly, exposure to MβCD had no inhibitory effect on PV-induced phosphorylation of STAT3 (Fig. 1C).

The degree of cholesterol removed by MβCD from HepG2 cells consists with previously described levels of cholesterol

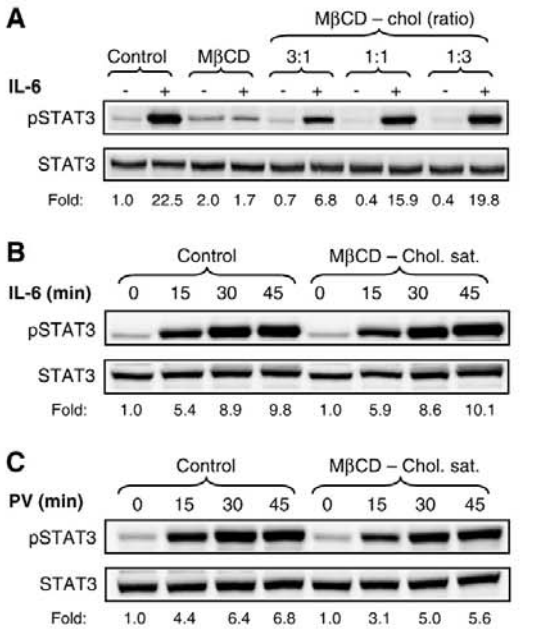


Fig. 2. Cholesterol-saturated MβCD does not inhibit IL-6-induced tyrosine phosphorylation of STAT3. (A) Cells incubated for 30 min with BSS/BSA alone (Control), or BSS/BSA supplemented with 12.5 mM MβCD or 12.5 mM MβCD mixed with cholesterol at various ratios, and then exposed for 15 min to BSS/BSA without (−) or with (+) 0.5 nM IL-6. (B, C) Cells incubated in BSS/BSA alone (Control) or in BSS/BSA supplemented with 12.5 mM MβCD saturated with cholesterol (MβCD-Chol. sat.), and then activated for the indicated time intervals with IL-6 (0.5 nM; B) or PV (0.2 mM; C). Relative amounts of pSTAT3 were determined by densitometry analysis of the corresponding immunoblots and normalized to control (nonactivated, MβCD untreated) cells (Fold). Typical results from at least 3 (A, B) or 2 (D) experiments performed are shown.

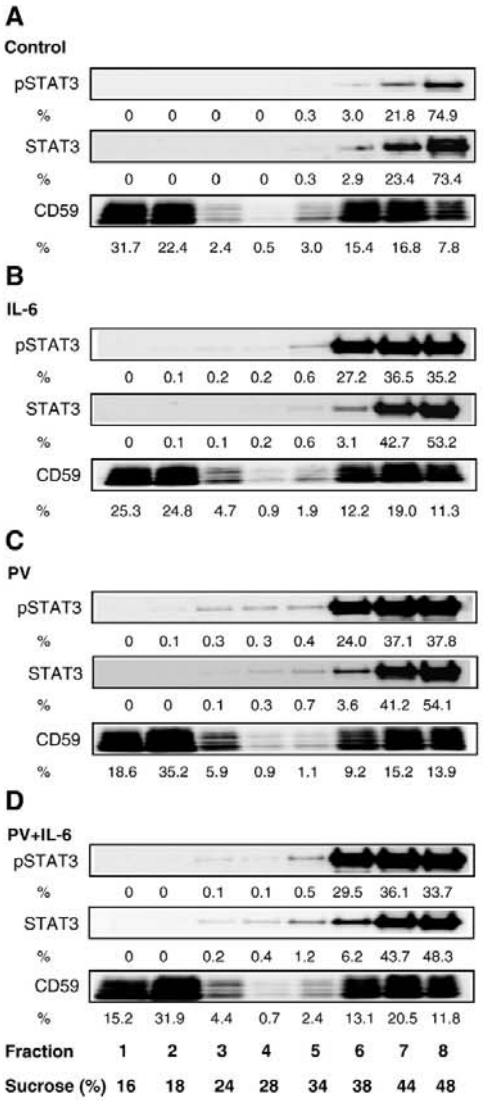


Fig. 3. STAT3 in HepG2 cells solubilized in Brij-96-containing lysis buffer is excluded from CD59-possessing DRMs. Nonactivated (Control) cells (A), or cells activated for 15 min with 0.5 nM IL-6 (B), 0.2 mM PV (C) or 0.5 nM IL-6 plus 0.2 mM PV (D) were solubilized in 0.5% Brij-96-containing lysis buffer and the whole lysates fractionated by sucrose density-gradient ultracentrifugation. Fractions were collected from top of the tube and the amount of pSTAT3, STAT3 and CD59 was determined by immunoblotting with the corresponding antibodies. Concentration of sucrose in individual fractions was determined by Abbe refractometer. Relative amounts of the proteins were determined by densitometry analysis of the immunoblots. A typical result from 3 experiments performed is shown.

depletion for a variety of cell types under similar conditions [13,37–39]. Removal of cholesterol decreases the expression of surface receptor [39,40] and induces the release of membrane vesicles [40–43]. To find out whether MβCD-treated cells still express the IL-6 receptor, we quantified it by flow cytometry. Data presented in Fig. 1D show that the number of IL-6 receptors on the cell decreased by 42±4% (mean±S.D., $n=3$) after treatment of HepG2 cells with 12.5 mM MβCD for 30 min. It should be noted, however, that the amount of receptors remaining on the cell surface after MβCD treatment was still relatively high.

The inhibitory effect of MβCD on IL-6-induced phosphorylation of STAT3 is attributable to cholesterol removal, since the inhibitory effect of MβCD correlated inversely with the extent of its saturation with cholesterol (Fig. 2A). Furthermore, pretreatment of cells with cholesterol-saturated MβCD had no inhibitory effect on STAT3 tyrosine phosphorylation in cells activated for different time intervals by either IL-6 (Fig. 2B) or PV (Fig. 2C).

### 3.2. Association of STAT3 with DRMs in detergent-solubilized HepG2 cells

Association of STAT3 with DRMs was evaluated using sucrose density gradient centrifugation of control and activated HepG2 cells solubilized under different conditions. Data presented in Fig. 3A show the distribution of STAT3 from cells solubilized with 0.5% Brij 96, which we had previously used as a gentle detergent preserving even weak association of proteins with DRMs [44]. In nonactivated control cells >99% of pSTAT3 and STAT3 was found in fractions 6–8 corresponding to 38%–48% of sucrose, where most of detergent soluble proteins and high density complexes are found (Fig. 3A). In fractions 1–3, corresponding to 16%–24% sucrose and marked by localization of >50% of glycosylphosphatidylinositol (GPI)-anchored glycoprotein CD59, no pSTAT3 and STAT3 was detected. In cells activated by IL-6, dramatic increase in the amount of pSTAT3 was observed, but again, a very small amount (<0.5%) of STAT3 and its phosphorylated form was found in fractions containing lipid raft components (Fig. 3B). In 2 more experiments we were unable

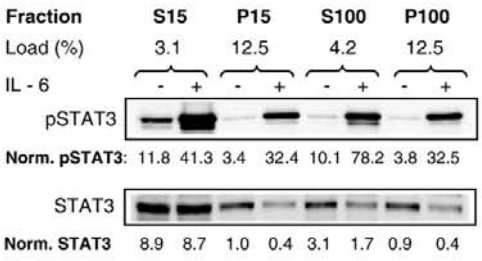


Fig. 4. Distribution of STAT3 and pSTAT3 in cell fractions. The cells were exposed for 15 min to BSS/BSA alone (−) or to 0.5 nM IL-6 (+) and then fractionated as described in Materials and methods into S15 supernatant, P15 pellet, S100 supernatant and P100 pellet. Fractions were size-separated by SDS-PAGE and pSTAT3 and STAT3 were determined by immunoblotting with the corresponding antibodies. The amount of pSTAT3 was normalized to the amount of STAT3 and total volume of individual fractions (Norm. pSTAT3). STAT3 amount was normalized to P15 fraction from unstimulated cells and total volume of individual fractions (Norm. STAT3). Relative amount of material loaded into the gel is also indicated [Load (%)].

to detect any STAT3 in lipid raft fractions. Similar distribution of pSTAT3 was observed in cells activated by PV (Fig. 3C) or mixture of PV and IL-6 which resulted in the highest tyrosine phosphorylation of STAT3 (Fig. 3D). Similarly, when the cells were solubilized in 0.05% Triton X-100, >99% of STAT3 and pSTAT3 was detectable in high-density fractions of sucrose gradient (not shown). These data indicate that in HepG2 cells very low or undetectable amount of STAT3 is associated with lipid rafts.

### 3.3. STAT3 forms large complexes in HepG2 cells

The above data suggest that lipid rafts are dispensable for STAT3 tyrosine phosphorylation in HepG2 cells. The next relevant question therefore was whether large fraction of STAT3 in HepG2 cells is indeed associated with plasma membrane structures and large complexes as was described for Hep3B cells [9]. Nonactivated or IL-6-activated HepG2 cells were homogenized in detergent-free lysis buffer and nuclei were removed by low-speed centrifugation. Postnuclear supernatant was centrifuged at 15,000 ×*g* for 15 min to yield supernatant fraction (S15), which contained large amount of STAT3, part of which was tyrosine phosphorylated even in nonactivated cells (Fig. 4). In IL-6-activated cells the amount of STAT3 was comparable to nonactivated cells, but exhibited enhanced tyrosine phosphorylation. P15 pellet contained about 10% of total cellular STAT3 and its amount was reduced to about 40% in IL-6-activated cells. Nevertheless, the amount of tyrosine phosphorylated STAT3 was increased more than 10 fold. Ultracentrifugation at 100,000 ×*g* of S15 supernatant yilded two fractions, S100, containing soluble STAT3 and pellet, P100. In both fractions the amount of STAT3 was reduced to about 50% in IL-6-activated cells, and there was a 2.4-fold increase in the amount of pSTAT3 in S100 compared to P100. These data indicate that STAT3 and its tyrosine phosphorylated form in HepG2 cells is found in large signaling complexes as well as in uncomplexed form in cytosol.

In an attempt to determine the fraction of STAT3 associated with large detergent-resistant complexes, nonactivated (control) cells or cells activated by IL-6 were solubilized in lysis buffer containing 0.5% Triton X-100. Postnuclear supernatants were rapidly size-fractionated by chromatography on Sepharose 4B using minicolumns as previously described [35], and the presence of STAT3 and pSTAT3 in individual fractions was detected by immunoblotting. CD59 in individual fractions was also detected to determine the size distribution of a typical lipid raft-associated protein. Data presented in Fig. 5A indicate that the elution peak of large complexes containing CD59 was found in fraction 5 in both nonactivated and IL-6-activated HepG2 cells. In nonactivated cells fraction 5 contained only a minute amount of STAT3 (0.2%); most of it was eluted in fractions corresponding to smaller complexes (<$10^6$ kDa). After treatment with IL-6 no dramatic increase in size of detergent-resistant STAT3 complexes was observed and the distribution of pSTAT3 corresponded to that of total STAT3. Pretreatment with MβCD resulted, as expected, in a decreased amount of large CD59-containing complexes, found in fraction 5, in both control and IL-6-activated cells (Fig. 5B). Tyrosine phosphorylation of STAT3 in IL-6-activated cells was also reduced but the size distribution of STAT3 complexes did not strikingly change. When the cells were solubilized in lysis buffer containing 0.5% Brij 96 (Fig. 5C), almost all CD59 was found in large complexes distributed over a broader peak (fractions 4–7). The shift towards higher molecular weight complexes was less conspicuous when the distribution of pSTAT3 or STAT3 was investigated, supporting the previous data that complexes containing GPI-anchored proteins are different from those possessing STAT3.

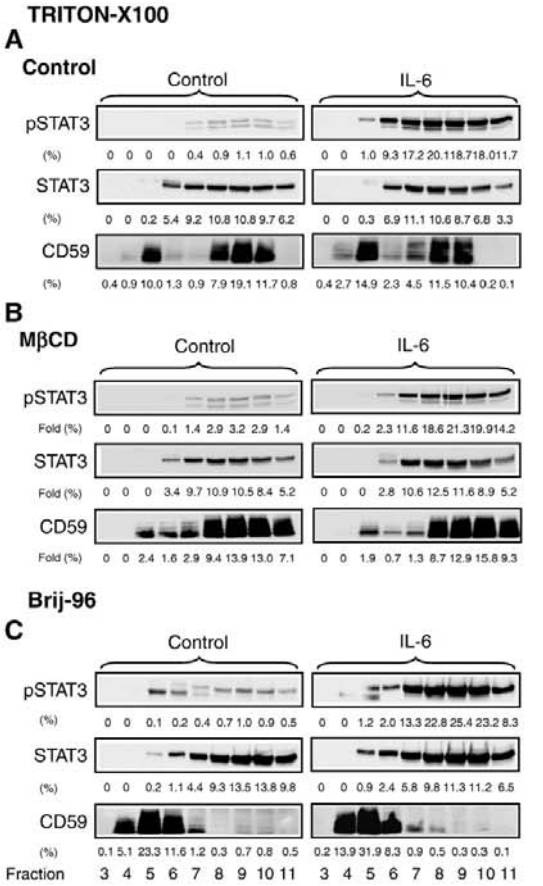


Fig. 5. Changes in association of STAT3 and its phosphorylated forms with large detergent-resistant complexes. Cells were preincubated for 30 min with BSS/BSA alone (A, C) or with BSS/BSA supplemented with 12.5 mM MβCD (B) and then incubated with BSS/BSA alone (control) or 0.5 nM IL-6. After 15 min the cells were solubilized in 0.5% Triton X-100 (A, B) or 0.5% Brij-96 (C) and postnuclear supernatants were size-fractionated by chromatography on Sepharose 4B. The amounts of pSTAT3, STAT3 and CD59 in individual fractions were determined by immunoblotting with the corresponding antibodies. Elution peaks of erythrocytes, IgM and albumin were at fractions 4, 6 and 9, respectively. Amounts of different proteins in individual fractions are expressed as percentage of signal determined by densitometry from both nonactivated and activated cells in each group. Two experiments were performed with similar results.

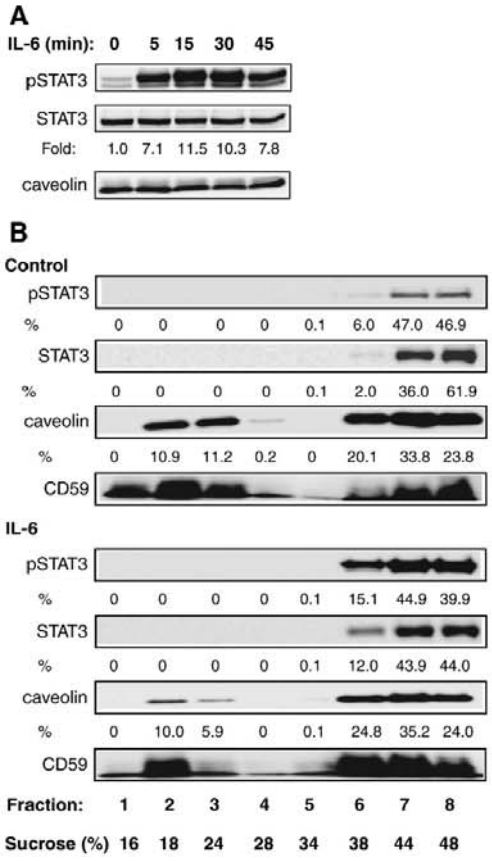


Fig. 6. Caveolin does not enhance association of STAT3 with DRMs. (A) HepG2-Cav1 cells activated with 0.5 nM IL-6 for the indicated time intervals, followed by immunoblotting analysis with antibodies specific for pSTAT3, STAT3 and caveolin. Relative amounts of pSTAT3 were determined by densitometry analysis of the corresponding immunoblots and normalized to nonactivated cells and amount of STAT3. (B) Nonactivated (Control) cells or cells activated for 15 min with 0.5 nM IL-6 (IL-6) solubilized in lysis buffer containing 0.05% Triton X-100. Whole cell lysates were fractionated by sucrose density-gradient ultracentrifugation. Fractions were collected from top of the tube and amounts of pSTAT3, STAT3 and caveolin were determined by immunoblotting. Protein amounts were expressed as percentages of signal determined by densitometry in individual fractions. A typical result from 3 experiments performed is shown.

### *3.4. Expression of caveolin in HepG2 cells does not enhance IL-6-mediated tyrosine phosphorylation of STAT3 and its association with DRMs*

It has been shown in Hep3B cells that approximately 10% of STAT3 is associated with DRMs containing caveolin [16]. Our finding that much smaller fraction of STAT3 is associated with DRMs in HepG2 cells, could be related to the absence of caveolin expression in these cells ([45] and see below). Therefore, we analyzed the properties of permanent transfectants of HepG2 cells expressing caveolin. When HepG2-Cav1 cells were activated by IL-6, a rapid increase in STAT3 tyrosine phosphorylation was observed (Fig. 6A). Density gradient ultracentrifugation of total cell lysates from nonactivated HepG2-Cav1 cells revealed that a significant part of caveolin was associated with low density fractions (Fig. 6B). As expected, the same fractions also contained GPI-anchored CD59 glycoprotein. However, there was no increase in association of STAT3 with these DRM fractions. After stimulation of HepG2-Cav1 cells with IL-6, an increased tyrosine phosphorylation of STAT3 in high density fractions was detectable with no evidence for enhanced association of STAT3 and pSTAT3 with DRM fractions. Similar results were obtained when the cells were solubilized with lysis buffer supplemented with 0.5% Brij-96 or 0.05% Triton X-100 (not shown). Thus an enhanced expression of caveolin did not result in enhanced association of STAT3 with DRMs.

Previously, we have described a simple and rapid method for estimating the formation of signaling assemblies in the course of cell activation [34,46]. The method is based on permeabilization

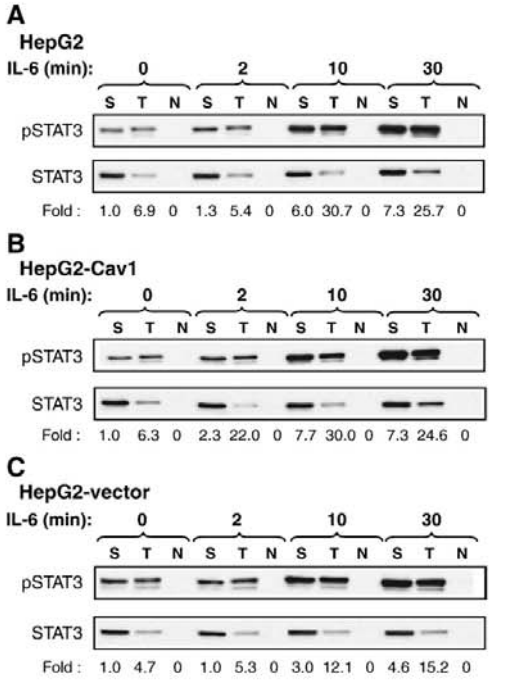


Fig. 7. Caveolin does not affect cellular distribution of STAT3 in IL-6 activated cells. HepG2 cells (A), caveolin-expressing transfectants HepG2-Cav1 (B) and transfected control cells expressing empty vector (C) were activated for different time intervals with 0.5 nM IL-6. The cells ($5\times10^6$) were centrifuged and resuspended in 0.2 ml of 0.1% saponin in PBS. After 15 min on ice cells were pelleted and supernatant (S) was saved. Pelleted cells were extracted for 20 min on ice in 0.2 ml lysis buffer containing 1% Triton X-100, spun down and supernatant (T) was used for further analysis. Remaining pelleted material was solubilized in 0.2 ml 1×SDS-sample buffer, centrifuged and supernatant (N) was also saved. The samples were size-fractionated by SDS-PAGE followed by immunoblotting with anti-pSTAT or anti-STAT antibodies. Tyrosine phosphorylation of STAT3 was normalized to the amount of STAT3 in saponin supernatant in nonactivated cells (Fold). Two experiments with similar results were performed.

of cells with cholesterol-sequestering reagent saponin, followed by separation of free cytoplasmic components, complete solubilization of cellular membranes including DRMs by nonionic detergents, and probing individual fractions by immunoblotting. Using this method we found that in control HepG2 cells (Fig. 7A; IL-6, 0 min) most of the STAT3 (~70%) was released from saponin-permeabilized cells; cellular ghost solubilized by Triton X-100 retained ~30% of STAT3. After exposure to IL-6, more STAT3 was found to be associated with large signaling assemblies. When pSTAT3 was analyzed and the data were normalized to the amount of STAT3, enhanced tyrosine phosphorylation of STAT3 (6.9 fold increase) in large signaling complexes was evident in nonactivated cells. After IL-6 triggering the amount of pSTAT3 increased in both soluble and insoluble form. Unexpectedly, after this two-step solubilization procedure only small (undetectable) amount of pSTAT3/STAT3 remained associated with cellular/nuclear remnants. When HepG2-Cav1 cells (Fig. 7B) or HepG2 cells transfected with vector alone (Fig. 7C) were analyzed, very similar picture was obtained, confirming previous data that the formation of STAT3 or pSTAT3 signaling assemblies is not affected by caveolin expression.

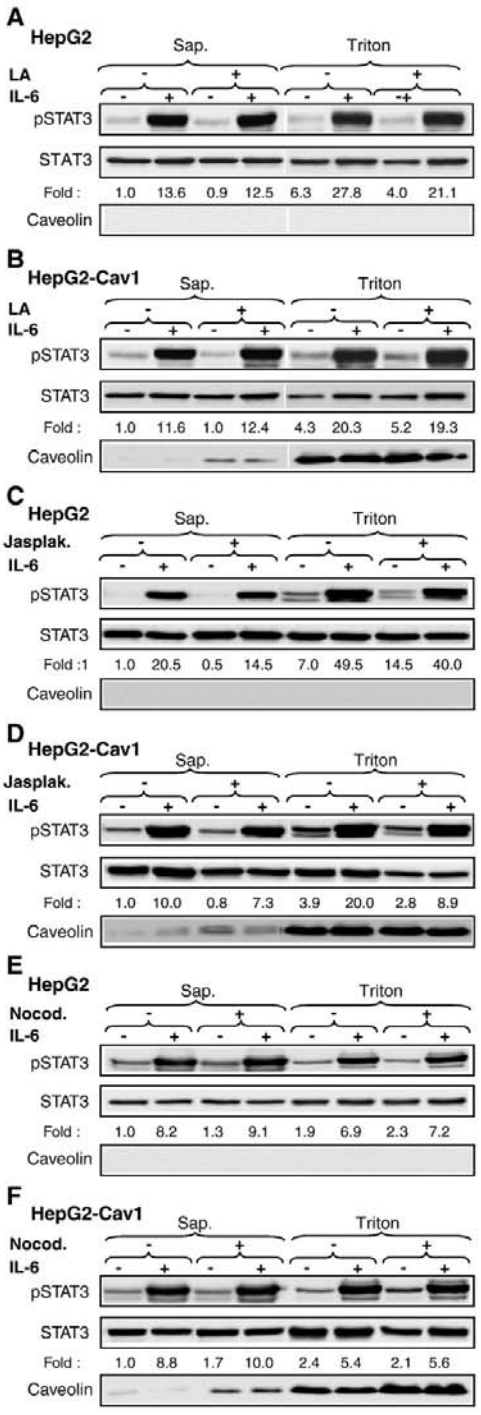


### 3.5. Role of cytoskeleton in the formation of STAT3 signaling assemblies

Experiments with cells sequentially solubilized with saponin and Triton X-100 showed that STAT3 is found in both soluble form (released from the saponin-permeabilized cells) and large signaling assemblies (released from saponin-permeabilized cellular ghosts after solubilization with Triton X-100). STAT3 could interact with microtubule-destabilizing protein stathmin and could thus contribute to stabilization of the tubular network [47]. Furthermore, STAT3 was shown to represent an essential effector pathway of Rho GTPases in regulating multiple cellular functions including actin cytoskeleton organization and cell migration [48]. To decide whether intact actin filaments and microtubules are required for STAT3 tyrosine phosphorylation and whether caveolin could contribute to the formation of STAT3 signaling assemblies, we analyzed STAT3 complexes in HepG2 and HepG2-Cav1 cells pretreated with inhibitors of actin and tubulin polymerization. The amount of STAT3 and pSTAT3 was determined by immunoblotting followed by densitometry. To exclude any biased interpretation, nonactivated and drug untreated cells were included in each experiment. When HepG2 cells were pretreated with an inhibitor of actin polymerization, latrunculin B, or vehicle alone (0.5% DMSO), no dramatic change was seen in the distribution of STAT3 and

Fig. 8. Involvement of filamentous actin and tubulin in formation of signaling assemblies containing STAT3 and pSTAT3. HepG2 cells (A, C, E) or HepG2-Cav1 cells (B, D, F) were pretreated (+) or not (−) for 15 min with 2.5 μM latrunculin B (LA; A, B) or 0.5 μM jasplakinolide (Jasplak., C, D), or for 14 h with 10 μM nocodazole (Nocod., E, F), and then activated (+) or not (−) with 0.5 nM IL-6. After 10 min the cells were permeabilized with 0.1% saponin, pelleted and supernatant (Sap.) was saved. The cell pellet was then extracted with 1% Triton X-100 in lysis buffer and supernatant (Triton) was further used. Samples were analyzed by immunoblotting for pSTAT3, STAT3 and caveolin. Tyrosine phosphorylation of STAT3 was normalized to the amount of STAT3 in saponin supernatant in nontreated and nonactivated cells (Fold). Two experiments with similar results were performed.

pSTAT3 either in soluble fraction (material released from saponin-permeabilized cells) or in insoluble fraction (material released from saponin-permeabilized ghosts with Triton X-100) (Fig. 8A). IL-6-mediated phosphorylation of STAT3 was likewise unaffected by this inhibitor (Fig. 8A). Similar distribution of STAT3 and pSTAT3 was observed in HepG2-Cav1, no matter whether pretreated or not with latrunculin (Fig. 8B). Interestingly, more caveolin was found in supernatant after saponin permeabilization in LA-pretreated cells, indicating that caveolin is stabilized in plasma membrane by filamentous-actin. Next we analyzed the effect of jasplakinolide, an inducer of actin polymerization and stimulator of actin nucleation. Jasplakinolide-pretreated HepG2 cells (Fig. 8C) and HepG2-Cav1 cells (Fig. 8D) showed normal distribution of STAT3 and pSTAT3 in saponin and Triton X-100 fractions. In cells pretreated with nocodazole, an inhibitor of tubulin polymerization, the only clear and reproducible effect of the drug was an enhanced amount of caveolin in both saponin and Triton X-100 fractions in HepG2-Cav1 cells (Fig. 8E and F). These data indicate that neither inhibition of actin or tubulin polymerization nor enhanced F-actin formation has any dramatic effect on IL-6-mediated STAT3 phosphorylation. Furthermore, they provide further evidence that caveolin is dispensable for STAT3 phosphorylation.

### 3.6. Association of STAT3 with DRMs in freshly isolated hepatocytes

All data presented so far were obtained with cultured HepG2 cells or their transfectants. It is known, however, that cultured tumor cells could substantially differ in lipidic composition from normal cells and consequently the properties of lipid rafts would also be different. To shed some light on STAT3 signaling assemblies in normal cells, freshly isolated rat hepatocytes were used in further studies. Hepatocytes have higher mean diameter (~20 μm) unlike ~8 μm in HepG2 cells. Furthermore, they have more lysosomes detectable by staining with LysoTracker Red DND-99. After activation of hepatocytes or HepG2 cells with IL-6 or PV, there were small changes in the distribution of LysoTracker red stained lysosomes (more dispersed staining), but the total amount of dye detected by flow cytometry was not dramatically changed (data not shown).

Based on confocal microscopy, only part of STAT3 is localized in close proximity of the plasma membrane in resting hepatocytes and, as previously shown in other cells [3,49], considerable amount of it is associated with nucleus (Fig. 9A). This fraction is largely, but transiently, increased following IL-6 triggering (Fig. 9B–C). Furthermore, in IL-6 stimulated cells, STAT3 is concentrated in numerous small dot-like structures within nucleus (Fig. 9, [3]). The phosphorylated form of STAT3 in resting cells was distributed mainly in nucleus (Fig. 9D). After IL-6 triggering, pSTAT3 was more abundant on the plasma membrane at all time intervals tested (5 and 20 min, Fig. 9E–F).

Data presented in Fig. 10A indicate that freshly isolated hepatocytes are capable of responding to both IL-6 and PV triggering by enhanced STAT3 phosphorylation. When nonactivated cells were solubilized in 0.5% Brij-96 and then fractionated by sucrose gradient ultracentrifugation, only very small amounts of STAT3 (0.8%) and pSTAT3 (0.6%) were associated with DRMs (fractions 1–3 in Fig. 10B). An increase in the amount of pSTAT3, but none in STAT3 was seen in DRM

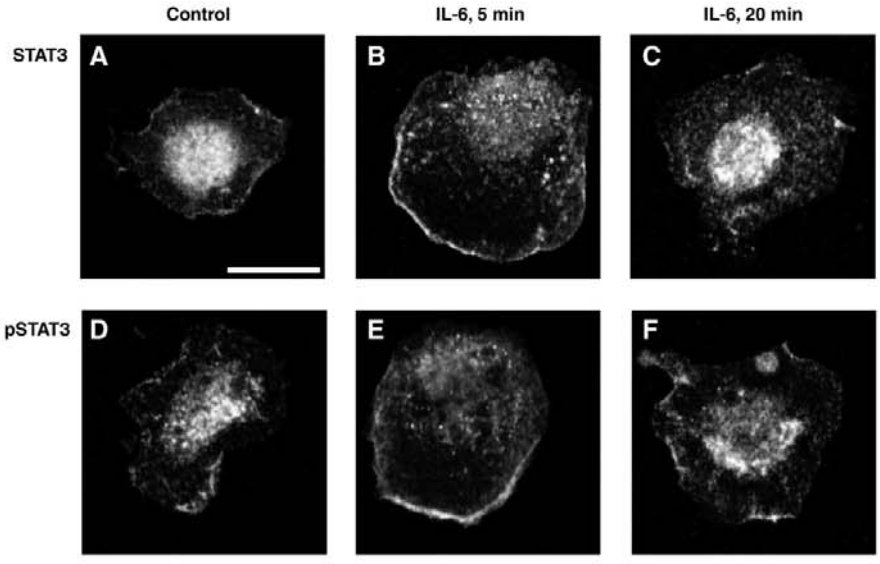


Fig. 9. STAT3 and pSTAT3 distribution in freshly isolated hepatocytes. STAT3 and pSTAT3 were detected by confocal laser scanning microscopy. Hepatocytes were incubated for 5 min with BSS/BSA alone (A, D), or activated with 0.5 nM IL-6 for 5 min (B, E) or 20 min (C, F). Photographs of typical cells are shown. Bar shown represents 10 μm.

fractions of cells activated with IL-6 for 15 min (Fig. 10C). In cells activated by PV (Fig. 10D) or PV plus IL-6 (Fig. 10E), there was only a slight increase in the amount of STAT3 and pSTAT3 in fractions containing DRMs (fractions 1–3). Thus the pattern of STAT3 and pSTAT3 distribution was in accordance with data obtained using HepG2 cells.

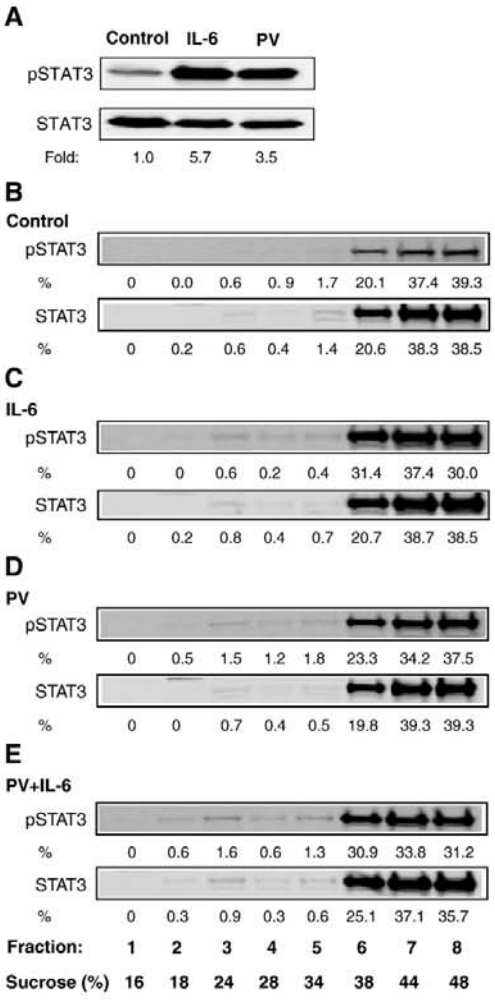


Fig. 10. Association of STAT3 with DRMs in freshly isolated hepatocytes. (A) Freshly isolated hepatocytes were exposed for 15 min to BSS/BSA alone (control), 0.5 nM IL-6 or 0.2 mM PV, solubilized in lysis buffer with 0.5% Brij-96 and analyzed by immunoblotting for pSTAT3 and STAT3. Tyrosine phosphorylation of STAT3 was normalized to the amount of STAT3 in nonactivated cells (Fold). (B–E) Nonactivated (control) cells (B), or cells activated for 15 min with 0.5 nM IL-6 (C), 0.2 mM PV (D) or 0.5 nM IL-6 plus 0.2 mM PV (E) were solubilized in 0.5% Brij-96 and the whole lysates fractionated by sucrose density-gradient ultracentrifugation. Fractions were collected from top of the tube and amounts of pSTAT3 and STAT3 were determined by immunoblotting. Concentration of sucrose in individual fractions was verified by Abbe refractometer. Relative amounts of proteins in individual fractions were determined by densitometry analysis of the corresponding immunoblots. A typical result from 3 experiments performed is shown.

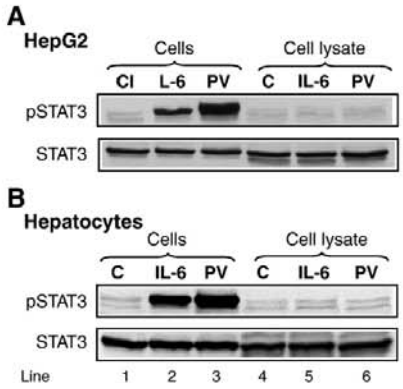


Fig. 11. Tyrosine phosphorylation of STAT3 requires cellular integrity. HepG2 cells (A) or freshly isolated rat hepatocytes (B) were either nonactivated (control; C) or activated with 0.5 nM IL-6 or 0.2 mM PV. After 15 min the cells were sedimented, lysed in 0.2% Triton X-100 in kinase buffer and postnuclear supernatants were isolated. Alternatively, the cells were first lysed in 0.2% Triton X-100 in kinase buffer and postnuclear supernatants were incubated for 15 min in the presence of 100 μM ATP alone (control; C) or together with 0.5 nM IL-6 or 0.2 mM PV. Postnuclear supernatants and kinase reaction mixes were combined with 2×SDS-PAGE sample buffer and analyzed by SDS PAGE and immunoblotting for pSTAT3 and STAT3. Typical data from two experiments performed is shown.

### *3.7. Tyrosine phosphorylation of STAT3 requires cellular integrity*

This was studied by means of a modified *in vitro* kinase assay, previously described for analysis of B cell receptor complexes [50]. Intact HepG2 cells (Fig. 11A) and freshly isolated hepatocytes (Fig. 11B) or their postnuclear supernatants in kinase buffer with Triton X-100 (preserving lipid rafts) were incubated for 15 min without activator or with 0.5 nM IL-6 or 0.2 mM PV. Then the cells were solubilized and all postnuclear supernatants analyzed by immunoblotting with pSTAT3- and STAT3-specific antibodies. These experiments failed to show any increase in tyrosine phosphorylation of STAT3 after adding IL-6 or PV to cell lysates. These data indicate that protein tyrosine kinases and their substrate, STAT3, are separated from each other in the lysate. It implies that STAT3 transducer complexes are disrupted upon exposure of the cells to Triton X-100, which, however, preserves lipid rafts.

## 4. Discussion

Previous studies showed that removal of cholesterol by MβCD inhibits IL-6-induced tyrosine phosphorylation of STAT3. This was taken as an important evidence that lipid rafts are involved in IL-6 signaling [15,16]. Further experiments showing association of STAT3 with lipid rafts in flotation fractions and the results of pull-down experiments, suggesting that STAT3 and caveolin interact within the plasma membrane, led to assumption that caveolin-containing lipid rafts play an important role in STAT3 signaling [15,16]. Several lines of evidence presented in this study suggest, however, that caveolin-containing lipid rafts are dispensable for STAT3

tyrosine phosphorylation. First, HepG2 cells do not express caveolin, but they still exhibit strong STAT3 tyrosine phosphorylation upon IL-6 triggering. Second, transfection of caveolin gene into HepG2 cells resulted in caveolin expression without any effect on IL-6-induced tyrosine phosphorylation. Third, flotation analyses showed that typical DRMs, containing GPI-anchored proteins, possess undetectable or only very low amount (<2%) of STAT3. There was no accumulation of pSTAT3 in DRMs in IL-6-activated cell even in cells with enhanced expression of caveolin. Fourth, after solubilization of the cells with nonionic detergents and size fractionation on Sepharose 4B, only a minute portion of STAT3 and pSTAT3 (<2%) was localized in fractions enriched in GPI-anchored protein CD59 and caveolin, which are considered to be typical protein components of lipid rafts. Fifth, pretreatment of the cells with MβCD decreased the size of complexes containing GPI-anchored protein CD59, as determined by flotation analysis, but had almost no effect on size distribution of STAT3 complexes. Finally, removal of cholesterol with MβCD resulted in a dramatic decrease in size of structures classified as lipid rafts but had no effect on PV-induced STAT3 tyrosine phosphorylation. Because PV acts by inhibiting phosphatases, the likely interpretation is that STAT3 transducer complexes are pre-associated. *In vitro* kinase assays, however, showed that STAT3 in postnuclear supernatant from cells solubilized by Triton X-100 was not phosphorylated by IL-6, neither by PV. Since the integrity of lipid rafts seems to be preserved under these solubilization conditions, these data suggest that STAT3 signaling assemblies are not dependent on intact lipid rafts, but rather on detergent-sensitive assemblies. It should be stressed, that several studies showed that acute removal of cholesterol by MβCD treatment not only destroyed lipid rafts, but had global effects on plasma membrane properties [12,39,51]. The inhibitory effect of MβCD on IL-6-mediated signaling may therefore be complex and cannot be taken as an evidence that lipid rafts are involved in this process.

Extensive changes caused by MβCD treatment were also documented in studies on IL-6 receptor exposure on the cell surface. Treatment of HepG2 cells with 12.5 mM MβCD for 30 min resulted in approximately 42% reduction in the amount of IL-6 receptor as detected by flow cytometry. This could possibly be related to decreased response to IL-6 in MβCD pretreated cells [18]. However, it is unlikely that the observed inhibition in IL-6 receptor expression is solely responsible for the observed inhibition of STAT3 phosphorylation. For flow cytofluorometry analyses the anti-IL-6 receptor mAb was used at almost saturating concentrations (10 μg/ml or 67 nM) but to induce STAT3 phosphorylation, IL-6 was used at approximately 0.5 nM. This is more than 100-fold lower then is concentration saturating binding of IL-6 to its receptor [52].

Treatment of cells with PV inhibits protein tyrosine phosphatases (PTPs), thereby modifying the intracellular equilibrium between dephosphorylation and phosphorylation rates [53,54]. The observed tyrosine phosphorylation of STAT3 in MβCD-pretreated and PV-activated cells suggest that signaling assemblies containing PTPs and protein tyrosine kinases are formed before cell triggering and that in resting cells the kinase activity could be counterbalanced by active PTPs. If activity of PTPs is blocked by PV, STAT3 is rapidly tyrosine phosphorylated, mimicking the situation after IL-6 receptor engagement. It is known that gp130 associates with ubiquitously expressed cytoplasmic PTP containing two N-terminal SH2 domains, SHP-2 [55]. However, this phosphatase is hardly responsible for enhanced phosphorylation of STAT3 by PV because SHP-2 binds to gp130 only after IL-6 triggering. Several other phosphatases, such as PTP1B, PTPε and SHP-1, have also been implicated in JAK/STAT signaling [56–58], but their function and association with preformed transduction complexes remain to be determined. Most recently, PTP receptor T has been shown to regulate Y705 phosphorylation of STAT3 [59]. Whether this is the phosphatase involved in dephosphorylation of Y705 in hepatocytes remains to be determined.

Although HepG2 cells do not express caveolin, a large portion of STAT3 (~50%) was found in complexes as determined by cell fractionation studies. These data were confirmed in experiments with saponin-permeabilized cells showing that approximately half of STAT3 was retained in permeabilized cellular ghosts. The amount of STAT3 associated with saponin-resistant cellular ghosts was not increased in HepG2-Cav1 cell expressing the transfected caveolin; this implies that caveolin is not involved in retention of STAT3 in lipid rafts and/or cellular debris. To decide whether or not cytoskeletal components are involved in formation of STAT3-containing assemblies we employed a pharmacological approach. It appears that neither inhibitor of actin polymerization (latrunculin B), nor enhancer of actin polymerization (jasplakinolide), nor inhibitor of microtubules formation (nocodazole) interfere with the retention of STAT3 with saponin-resistant cellular ghost and with IL-6-induced STAT3 tyrosine phosphorylation. Thus, intact actin filaments and microtubuli are dispensable for formation of STAT3 complexes and/or STAT3 tyrosine phosphorylation. A recent study showed that ~5% of cytoplasmic STAT3 was constitutively associated with purified early endosome fraction in human Hep3B cells, and that 15 min after IL-6 treatment up to two-thirds of cytoplasmic pSTAT3 could be associated with purified early endosomes [60]. These and other experiments suggest that the endocytic pathway is involved in IL-6/STAT3 signaling. Our finding of minute differences in association of STAT3 with saponin-permeabilized cellular ghosts in nonactivated and IL-6-activated HepG2 cells suggest that preformed large signaling assemblies merge with endosomes, or participate in their formation in the course of IL-6-mediated cell activation.

Most of the studies analyzing the role of membrane microdomains in STAT3 signaling were performed on hepatoma-derived cultured cells, such as Hep3B or HepG2. It is known, however, that tumor cells have different composition of membrane lipids, compared to normal cells, and could therefore exhibit different properties of plasma membrane microdomains [25,61]. The most significant changes associated with malignant transformation are changes in composition of glycosphingolipids, reflecting aberrant glycosylation. This could be caused by a defect in single or multiple glycosyltransferases and is often followed by accumulation of precursor lipids. Alternatively, tumor cells could exhibit glycosphingolipid biosynthesis pathways which are minor

or absent in non-transformed cells, resulting in formation of so called "neoglycosphingolipids". In HepG2 cells, the typical tumor-associated markers are sulfated and highly acidic glycosphingolipids, which are almost undetectable in normal liver tissue [25]. In this study we show for the first time that in nonactivated as well as IL-6-, PV- or IL-6+PV-activated freshly isolated hepatocytes, almost all STAT3 is localized in high density fraction and that only a small part of STAT3 (<2%) is found in flotation fractions. Furthermore, *in vitro* kinase assays with hepatocytes confirmed the previous results obtained with HepG2 cells that STAT3 signaling assemblies are sensitive to nonionic detergents which preserve DRMs. Thus, the conclusions drawn in this study from HepG2 cells can be extended to normal hepatocytes.

## 5. Conclusions

Our data indicate that tyrosine phosphorylation of STAT3 is not dependent on intact lipid rafts and caveolin. Rather, it seems to be dependent on preassociated transducer complexes, which are sensitive to nonionic detergents. These complexes are involved in regulating equilibrium between kinases and phosphatases. The topography of signaling molecules and the interplay between kinases and phosphatases in IL-6-mediated STAT3 triggering have to be critically reevaluated.

## Acknowledgements

We thank T. Fujimoto for providing caveolin cDNA expression vectors, and H. Mrázová, R. Budovičová and M. Dráber for their technical assistance. This work was supported by grants NB6758-3/01 and NR8079-3/2004 from the Ministry of Health of the Czech Republic, project 1M6838805001 (Center of Molecular and Cellular Immunology) from Ministry of Education, Youth and Sports of the Czech Republic and Institutional project AVOZ50520514. The research of P.D. and P.H. was supported in part by, respectively, an International Research Scholar's award from Howard Hughes Medical Institute and Research goal MSM0021620814 from the 3rd Faculty of Medicine (Charles University, Prague).

## References

[1] S. Akira, T. Taga, T. Kishimoto, Adv. Immunol. 54 (1993) 1.
[2] P.C. Heinrich, I. Behrmann, G. Muller-Newen, F. Schaper, L. Graeve, Biochem. J. 334 (1998) 297.
[3] A. Herrmann, U. Sommer, A.L. Pranada, B. Giese, A. Kuster, S. Haan, W. Becker, P.C. Heinrich, G. Muller-Newen, J. Cell Sci. 117 (2004) 339.
[4] P.C. Heinrich, I. Behrmann, S. Haan, H.M. Hermanns, G. Muller-Newen, F. Schaper, Biochem. J. 374 (2003) 1.
[5] S. Rose-John, J. Scheller, G. Elson, S.A. Jones, J. Leukoc. Biol. 80 (2006) 227.
[6] T. Kishimoto, Annu. Rev. Immunol. 23 (2005) 1.
[7] T. Taniguchi, Science 268 (1995) 251.
[8] W.J. Leonard, J.J. O'Shea, Annu. Rev. Immunol. 16 (1998) 293.
[9] M.I. Ndubuisi, G.G. Guo, V.A. Fried, J.D. Etlinger, P.B. Sehgal, J. Biol. Chem. 274 (1999) 25499.
[10] K. Simons, D. Toomre, Nat. Rev., Mol. Cell Biol. 1 (2000) 31.
[11] L.J. Pike, J. Lipid Res. 47 (2006) 1597.
[12] S. Munro, Cell 115 (2003) 377.
[13] E.P. Kilsdonk, P.G. Yancey, G.W. Stoudt, F.W. Bangerter, W.J. Johnson, M.C. Phillips, G.H. Rothblat, J. Biol. Chem. 270 (1995) 17250.
[14] P. Scheiffele, M.G. Roth, K. Simons, EMBO J. 16 (1997) 5501.
[15] P.B. Sehgal, G.G. Guo, M. Shah, V. Kumar, K. Patel, J. Biol. Chem. 277 (2002) 12067.
[16] M. Shah, K. Patel, V.A. Fried, P.B. Sehgal, J. Biol. Chem. 277 (2002) 45662.
[17] J. Kim, R.M. Adam, K.R. Solomon, M.R. Freeman, Endocrinology 145 (2004) 613.
[18] V. Matthews, B. Schuster, S. Schutze, I. Bussmeyer, A. Ludwig, C. Hundhausen, T. Sadowski, P. Saftig, D. Hartmann, K.J. Kallen, S. Rose-John, J. Biol. Chem. 278 (2003) 38829.
[19] T. Fujimoto, H. Kogo, R. Nomura, T. Une, J. Cell Sci. 113 (2000) 3509.
[20] Y. Fu, A. Hoang, G. Escher, R.G. Parton, Z. Krozowski, D. Sviridov, J. Biol. Chem. 279 (2004) 14140.
[21] T.A. Slimane, G. Trugnan, S.D. Van IJzendoorn, D. Hoekstra, Mol. Biol. Cell 14 (2003) 611.
[22] L.M. Camarota, J.M. Chapman, D.Y. Hui, P.N. Howles, J. Biol. Chem. 279 (2004) 27599.
[23] D. Rhainds, P. Bourgeois, G. Bourret, K. Huard, L. Falstrault, L. Brissette, J. Cell Sci. 117 (2004) 3095.
[24] A. Calzolari, C. Raggi, S. Deaglio, N.M. Sposi, M. Stafsnes, K. Fecchi, I. Parolini, F. Malavasi, C. Peschle, M. Sargiacomo, U. Testa, J. Cell Sci. 119 (2006) 4486.
[25] N. Hiraiwa, Y. Fukuda, H. Imura, K. Tadano-Aritomi, K. Nagai, I. Ishizuka, R. Kannagi, Cancer Res. 50 (1990) 2917.
[26] J. Chen, D.L. Clemens, A.I. Cederbaum, B. Gao, Clin. Biochem. 34 (2001) 203.
[27] T.R. Chen, Exp. Cell Res. 104 (1977) 255.
[28] P. Moldeus, J. Hogberg, S. Orrenius, Methods Enzymol. 52 (1978) 60.
[29] H. Farghali, E. Buchar, Z. Machkova, L. Kamenikova, K. Masek, Methods Find. Exp. Clin. Pharmacol. 8 (1986) 469.
[30] A.E. Christian, M.P. Haynes, M.C. Phillips, G.H. Rothblat, J. Lipid Res. 38 (1997) 2264.
[31] J.G. Heider, R.L. Boyett, J. Lipid Res. 19 (1978) 514.
[32] C. Chen, H. Okayama, Mol. Cell. Biol. 7 (1987) 2745.
[33] K. Katoh, Y. Takahashi, S. Hayashi, H. Kondoh, Cell Struct. Funct. 12 (1987) 575.
[34] L. Dráberová, L. Dudková, M. Boubelík, H. Tolarová, F. Šmíd, P. Dráber, J. Immunol. 171 (2003) 3585.
[35] L. Dráberová, P. Dráber, Proc. Natl. Acad. Sci. U. S. A. 90 (1993) 3611.
[36] L. Dráberová, P. Dráber, Eur. J. Immunol. 25 (1995) 2428.
[37] P.G. Yancey, W.V. Rodrigueza, E.P.C. Kilsdonk, G.W. Stoudt, W.J. Johnson, M.C. Phillips, G.H. Rothblat, J. Biol. Chem. 271 (1996) 16026.
[38] P. Keller, K. Simons, J. Cell Biol. 140 (1998) 1357.
[39] Z. Surviladze, L. Dráberová, M. Kovářová, M. Boubelík, P. Dráber, Eur. J. Immunol. 31 (2001) 1.
[40] E.D. Sheets, D. Holowka, B. Baird, J. Cell Biol. 145 (1999) 877.
[41] S. Ilangumaran, D.C. Hoessli, Biochem. J. 335 (1998) 433.
[42] C. Claas, C.S. Stipp, M.E. Hemler, J. Biol. Chem. 276 (2001) 7974.
[43] P. Gutwein, S. Mechtersheimer, S. Riedle, A. Stoeck, D. Gast, S. Joumaa, H. Zentgraf, M. Fogel, D.P. Altevogt, FASEB J. 17 (2003) 292.
[44] Z. Surviladze, L. Dráberová, L. Kubínová, P. Dráber, Eur. J. Immunol. 28 (1998) 1847.
[45] T. Fujimoto, Nagoya J. Med. Sci 63 (2000) 9.
[46] L. Dráberová, M. Amoui, P. Dráber, Immunology 87 (1996) 141.
[47] D.C. Ng, B.H. Lin, C.P. Lim, G. Hunag, T. Zhang, V. Poli, X. Cao, J. Cell Biol. 172 (2006) 245.
[48] M. Debidda, L. Wang, H. Zang, V. Poli, Y. Zheng, J. Biol. Chem. 280 (2005) 17275.
[49] T. Meyer, K. Gavenis, U. Vinkemeier, Exp. Cell Res. 272 (2002) 45.
[50] J. Wienands, O. Larbolette, M. Reth, Proc. Natl. Acad. Sci. U. S. A. 93 (1996) 7865.
[51] J. Kwik, S. Boyle, D. Fooksman, L. Margolis, M.P. Sheetz, M. Edidin, Proc. Natl. Acad. Sci. U. S. A. 100 (2003) 13964.
[52] S. Thiel, H. Dahmen, A. Martens, G. Muller-Newen, F. Schaper, P.C. Heinrich, L. Graeve, FEBS Lett. 441 (1998) 231.

[53] Y. Zick, R. Sagi-Eisenberg, Biochemistry 29 (1990) 10240.
[54] S. Bourgoin, S. Grinstein, J. Biol. Chem. 267 (1992) 11908.
[55] H. Kim, H. Baumann, Mol. Cell. Biol. 19 (1999) 5326.
[56] P. Heneberg, P. Dráber, Curr. Med. Chem. 12 (2005) 1859.
[57] C. Bousquet, C. Susini, S. Melmed, J. Clin. Invest. 104 (1999) 1277.
[58] M.P. Myers, J.N. Andersen, A. Cheng, M.L. Tremblay, C.M. Horvath, J.P. Parisien, A. Salmeen, D. Barford, N.K. Tonks, J. Biol. Chem. 276 (2001) 47771.
[59] X. Zhang, A. Guo, J. Yu, A. Possemato, Y. Chen, W. Zheng, R.D. Polakiewicz, K.W. Kinzler, B. Vogelstein, V.E. Velculescu, Z.J. Wang, Proc. Natl. Acad. Sci. U. S. A. 104 (2007) 4060.
[60] M. Shah, K. Patel, S. Mukhopadhyay, F. Xu, G. Guo, P.B. Sehgal, J. Biol. Chem. 281 (2006) 7302.
[61] S. Hakomori, R. Kannagi, J. Natl. Cancer Inst. 71 (1983) 231.

**6.6**

**Lebduška, P.; Korb, J.; Tůmová, M.; Heneberg, P. & Dráber, P. (2007):**

**Topography of signaling molecules as detected by electron microscopy on plasma membrane sheets isolated from nonadherent mast cells.**

**Journal of Immunological Methods 328(1-2): 139-151.**

ELSEVIER

Journal of Immunological Methods 328 (2007) 139–151

JIM Journal of Immunological Methods

www.elsevier.com/locate/jim

Research paper

# Topography of signaling molecules as detected by electron microscopy on plasma membrane sheets isolated from non-adherent mast cells

Pavel Lebduška [a], Jan Korb [b], Magda Tůmová [a], Petr Heneberg [a], Petr Dráber [a,*]

[a] *Department of Signal Transduction, Institute of Molecular Genetics, Academy of Sciences of the Czech Republic, v.v.i., Vídeňská 1083, 142 20 Prague 4, Czech Republic*

[b] *Department of Micromorphology of Biopolymers, Institute of Molecular Genetics, Academy of Sciences of the Czech Republic, v.v.i., Vídeňská 1083, 142 20 Prague 4, Czech Republic*

Received 28 June 2007; received in revised form 16 August 2007; accepted 29 August 2007
Available online 18 September 2007

**Abstract**

Immunolabeling of isolated plasma membrane (PM) sheets combined with high-resolution electron microscopy is a powerful technique for understanding the topography of PM-bound signaling molecules. However, this technique has been mostly confined to analysis of membrane sheets from adherent cells. Here we present a rapid, simple and versatile method for isolation of PM sheets from non-adherent cells, and show its use for examination of the topography of Fcε receptor I (FcεRI) and transmembrane adaptors, LAT (linker for activation of T cells) and NTAL (non-T cell activation linker), in murine bone marrow-derived mast cells (BMMC). The data were compared with those obtained from widely used but tumor-derived rat basophilic leukemia (RBL) cells. In non-activated cells, FcεRI was distributed either individually or in small clusters of comparable size in both cell types. In multivalent antigen-activated BMMC as well as RBL cells, FcεRI was internalized to a similar extent, but, strikingly, internalization in BMMC was not preceded by formation of large (~200 nm) aggregates of FcεRI, described previously in activated RBL cells. On the other hand, downstream adaptor proteins, LAT and NTAL, were localized in independent domains in both BMMC and RBL cells before and after FcεRI triggering. The combined data demonstrate unexpected properties of FcεRI signaling assemblies in BMMC and emphasize the importance of studies of PM sheets isolated from non-tumor cells.


*Keywords:* Plasma membrane; Electron microscopy; Immunolabeling; Leukocytes; Mast cells

*Abbreviations:* BMMC, bone marrow-derived mast cells; BSA, bovine serum albumin; BSS, buffered salt solution; DNP, dinitrophenyl; EDTA, ethylenediaminetetraacetic acid; EM, electron microscopy; FcεRI, Fcε receptor I; FCS, fetal calf serum; FITC, fluorescein isothiocyanate; GPI, glycosylphosphatidylinositol; HEPES, *N*-(2-hydroxyethyl)piperazine-*N*′-(2-ethanesulfonic acid); HRP, horseradish peroxidase; IgE, immunoglobulin E; IL-3, interleukin 3; LAT, linker for activation of T cells; mAb, monoclonal antibody; NC, nitrocellulose; NTAL, non-T cell activation linker; PBS, phosphate buffered saline; PCCF, pair cross-correlation function; PCF, pair correlation function; PLC, phospholipase C; PLL, poly-L-lysine; PM, plasma membrane; RBL, rat basophilic leukemia; SCF, stem cell factor.

* Corresponding author. Tel.: +420 241062468; fax: +420 241062214.
*E-mail address:* draberpe@biomed.cas.cz (P. Dráber).

0022-1759/$ - see front matter © 2007 Elsevier B.V. All rights reserved.
doi:10.1016/j.jim.2007.08.015

## 1. Introduction

Plasma membrane (PM) is an important cellular compartment accommodating numerous proteins involved in various functions. Although it is known that immunoreceptors and other signaling molecules interact within the PM, their topographical changes in the course of cell activation are still poorly understood. Various methods, such as fluorescence energy transfer, immunofluorescence microscopy and electron microscopy (EM) have been used to locate PM-associated molecules (Lagerholm et al., 2005). Regarding resolution, EM represents a bridge between fluorescence resonance energy transfer, working at distances under 10 nm, and fluorescence microscopy with a 100-nm scale resolution. Transmission EM on ultrathin sections allows visualizing the PM components in the context of the whole cell. To provide a horizontal view, examination of PM sheets is the method of choice.

PM sheets from cells growing on glass coverslips have been isolated by attaching the dorsal side of the cells to poly-L-lysine (PLL)-coated film on EM grids, followed by separation of PM sheets connected to the EM grid from the rest of the cell. Components of the extracellular and intracellular leaflets of the PM can be labeled before or after membrane sheets isolation, respectively. As the cells must be attached to a glass coverslip prior to isolation of the PM sheets, the studies were confined mainly to adherent cells such as fibroblasts, cultured neurons, Chinese hamster ovary cells, rat basophilic leukemia (RBL) cells and baby hamster kidney cells (Sanan and Anderson, 1991; Wilson et al., 2000; Wyse et al., 2003; Choy et al., 2006). Non-adherent leukocytes have been either excluded from such studies or they had to be attached to a substrate by PLL or streptavidin in procedures taking about 45–60 min (Schade and Levine, 2002; Lillemeier et al., 2006), which itself could induce cell activation.

Mast cells, the effectors of allergic reactions, have been extensively used for studies of activation events induced by aggregation of the Fcε receptor I (FcεRI) (Metcalfe et al., 1997; Gilfillan and Tkaczyk, 2006). Although FcεRI and numerous other signaling molecules involved in antigen-mediated mast cell activation have been identified, sequenced and characterized, their topography in the PM at nanometer-scale resolution remained almost unknown until the experiments performed by Bridget Wilson's group on PM sheets isolated from adherent RBL cells (Lara et al., 2001; Wilson et al., 2000, 2002, 2004). These authors proposed a model of primary and secondary signaling domains formed in the PM after FcεRI triggering. The primary domains consist of FcεRI patches with a diameter of ~200 nm, rich in Syk kinase, phospholipase C (PLC)γ2, cytoplasmic adaptors Grb2, Gab2 and other signaling proteins. Interestingly, Lyn kinase, which phosphorylates FcεRI, was excluded from these domains. The primary signaling domains were proposed to pass the signal onto the secondary signaling domains represented by aggregates of the transmembrane adaptor LAT (linker for activation of T cells) and containing PLCγ1.

EM studies performed on PM sheets from RBL cells also contributed to understanding the topography of molecules thought to be localized predominantly in cholesterol- and sphingolipid-rich microdomains, called lipid rafts or membrane rafts (Simons and Toomre, 2000; Pike, 2006). Some molecules considered to be associated with lipid rafts, such as glycosylphosphatidylinositol (GPI)-anchored glycoprotein Thy-1 and glycosphingolipid GM1, turned out to be localized independently in the PM (Wilson et al., 2004). On the other hand, Thy-1 showed clear colocalization with palmitoylated adaptor proteins LAT and NTAL (non-T cell activation linker) (Wilson et al., 2004; Heneberg et al., 2006), even though these adaptors were found in different non-overlapping patches in both resting and activated RBL cells (Volná et al., 2004; Heneberg et al., 2006). However, RBL cells are of tumor origin, and it is therefore possible that the topography of signaling molecules in these cells differs from that found in non-tumor mast cells.

In this study we describe a new technique that is rapid, simple and versatile for isolation of PM sheets from non-adherent cells, and show its use for determination of topography of selected plasma membrane signaling molecules in murine bone marrow-derived mast cells (BMMC). Although these cells are more useful for analysis of signaling processes, compared to the widely used tumor-derived RBL cells, BMMC have been excluded from such studies because of their growth in suspension. Direct comparison of topography of several signaling molecules in BMMC and RBL cells revealed a substantial difference in the formation of FcεRI signaling spots, whereas the downstream signaling domains possessing adaptor proteins, LAT and NTAL, showed analogous distribution in both cell types.

## 2. Materials and methods

### 2.1. Antibodies and reagents

The following mouse monoclonal antibodies (mAb) were used: anti-FcεRI-β subunit (JRK, Rivera et al.,

1988), anti-NTAL (Brdička et al., 2002), anti-LAT (Tolar et al., 2001), anti-Lyn (Dráberová et al., 1996) and dinitrophenyl (DNP)-specific immunoglobulin E (IgE) (Liu et al., 1980). Horseradish peroxidase (HRP)-conjugated phosphotyrosine-specific mAb (PY20) was obtained from Becton Dickinson Biosciences (CA, USA). Rabbit polyclonal antibodies included anti-LAT (Upstate Biotechnology, NY, USA), anti-NTAL and anti-IgE (Volná et al., 2004). DNP conjugated to bovine serum albumin (BSA) was purchased from Molecular Probes (OR, USA), goat anti-mouse and anti-rabbit secondary antibodies conjugated to 5 nm or 10 nm gold particles (diluted 1/25 for intracellular and 1/5 for extracellular labeling) were from Amersham (UK), fluorescein isothiocyanate (FITC)-conjugated donkey anti-mouse Ig was from Jackson ImmunoResearch Laboratories (PA, USA), HRP-conjugated goat anti-mouse IgG was from Santa Cruz (CA, USA). Nickel EM grids (300 mesh), $OsO_4$ and pioloform were obtained from Christine Gröpl Elektronemikroskopie (Austria). Stem cell factor (SCF) and interleukin 3 (IL-3) were from PeproTech EC Ltd (UK). Poly-L-lysine (MW >300,000), fibronectin and other chemicals were purchased from Sigma (MO, USA). Water used for the preparation of solutions and cleaning of glass coverslips was deionized and further purified using a Milli-Q water purification system (Millipore S.A., France) and had a resistivity of ≥18 MΩ·cm.

### 2.2. Preparation of ultraclean glass coverslips

Round glass coverslips (#72196-15, 15-mm diameter, Electron Microscopy Sciences, PA, USA) were washed manually (using rubber gloves) one by one with a mix of ionic and non-ionic detergents, Jar (Procter & Gamble, Czech Republic). They were transferred to $H_2O$ (Millipore-purified, 500 ml) and washed several times to completely remove the detergent. Then the coverslips were washed briefly with 96% ethanol, dried and transferred one by one to 35% HCl and kept in HCl for 16–20 h. After repeated thorough washes with $H_2O$ the coverslips were kept in $H_2O$ for at least 30 min and again washed several times in $H_2O$ to remove all traces of HCl. After two brief washes with ethanol, the coverslips were stored in ethanol until use.

### 2.3. Cells

RBL-2H3 cells were cultured as described by Dráberová and Dráber (1991). Sixteen to eighteen hours before the experiment, the cells were transferred into fresh complete medium containing DNP-specific IgE (1 μg/ml) and allowed to settle on an ultraclean glass coverslip.

BMMC were isolated from murine femurs and tibias and cultivated in Iscove's medium containing 10% fetal calf serum (FCS), SCF (40 ng/ml) and IL-3 (20 ng/ml). Sixteen to eighteen hours before the experiment the cells were transferred into Iscove's medium without SCF, but with FCS, IL-3 and DNP-specific IgE (1 μg/ml), and incubated either in suspension, or on glass coverslips covered with fibronectin (50 μg/ml in phosphate buffered saline (PBS) for 1 h at 37 °C, followed by washing with PBS). Murine T cells were isolated from peripheral blood as described by Smrž et al. (2007).

### 2.4. Isolation and staining of PM sheets

#### 2.4.1. Preparation of EM grids

On the day of the experiment, EM grids covered with pioloform and coated with carbon were glow-discharged for 45–60 s by 300 V, then incubated with 1 mg/ml PLL in $H_2O$ for 30 min, washed once for 5 s in $H_2O$ and dried. Immediately before the PM sheet isolation, a round nitrocellulose (NC) membrane filter (Millipore; pores 0.45 μm) was placed onto a drop of *N*-(2-hydroxyethyl) piperazine-*N'*-(2-ethanesulfonic acid) (HEPES) buffer (25 mM HEPES, pH 7.0, 25 mM KCl, 2.5 mM magnesium acetate) on an ice-cold glass support. The filter had to be fully wetted, but no liquid should appear on its upper side. Two EM grids were placed with the PLL side up onto the filter (Fig. 1A and B).

#### 2.4.2. Cells

RBL cells cultured as adherent on glass coverslips, or BMMC bound to glass coverslips covered with fibronectin (as described above), were washed with PBS and, when indicated, activated by DNP-BSA in buffered salt solution (BSS; 20 mM HEPES, pH 7.4, 5 mM KCl, 135 mM NaCl, 1.8 mM $CaCl_2 \cdot 2H_2O$, 1 mM $MgCl_2$, 5.6 mM glucose) at 37 °C. In some experiments the cells were fixed for 7 min by 2% paraformaldehyde in PBS at room temperature, washed and incubated for 10–15 min with antibodies in PBS supplemented with 0.1% BSA (washing with PBS). Cells cultured in suspension were washed twice with BSS supplemented with 0.1% BSA and transferred to BSS without BSA. A 100-μl aliquot of the suspension (~$10^6$ cells/ml) was applied onto an ultraclean glass coverslip for 1 min and, when indicated, processed for activation (by DNP-BSA in BSS, 37 °C) and/or extracellular labeling (as described above). Alternatively, the cells were activated in suspension.

#### 2.4.3. Isolation of PM sheets

Coverslips with adherent RBL cells or fibronectin-bound BMMC (Fig. 1A, left) as well as with ultraclean

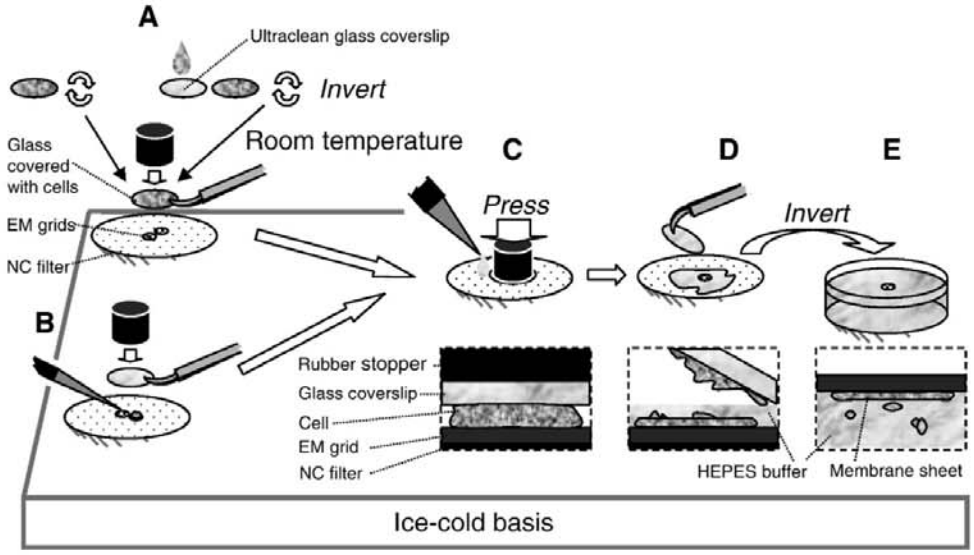


Fig. 1. Schematic drawing of the procedures used to isolate PM sheets. (A) Glass coverslip with cells growing as adherent or attached via fibronectin (left) or an ultraclean glass coverslip with cells adsorbed in protein-free buffer (right) was placed face-down onto PLL-coated EM grids laid on NC filter wetted with ice-cold HEPES buffer. (B) Alternatively, cells in suspension were dropped onto individual EM grids and covered with an ultraclean glass coverslip. (C) Immediately, a sandwich formed by the glass coverslip, cells and EM grid was pressed using an ice-cold rubber stopper. (D) The coverslip was quickly side-lifted, leaving the dorsal, Jar PM sheets bound to the EM grid. (E) The EM grid with the attached PM sheets was instantly transferred face-down onto ice-cold HEPES buffer surface for several seconds and further processed (fixation, immunolabeling and contrasting steps). Schematic transversal views of the PM sheet isolation procedure is shown at the bottom of (C)–(E) at high magnification.

glass-bound BMMC (Fig. 1A, right) were rinsed twice in PBS and once in ice-cold HEPES buffer and pressed face-down onto EM grids by firm finger pressure for 10 s using a rubber stopper (Fig. 1C); a drop of ice-cold HEPES buffer was applied to the edge of the coverslip to maintain moisture in the following step. The coverslip was quickly side-lifted, exposing the cells to shearing forces (Fig. 1D), and the grids with attached PM sheets were immediately placed face-down onto ice-cold HEPES buffer (Fig. 1E). After 5–10 s the grids were transferred onto ice-cold 2% paraformaldehyde in HEPES buffer for 10 min. The grids were then floated on PBS for 5–30 min. Alternatively, if the PM sheets were isolated from cells in suspension, 10-μl aliquots of cells suspended in BSS (without BSA) were loaded onto each EM grid, then covered with an ultraclean glass coverslip (Fig. 1B), pressed and processed as described above (Fig. 1C–E).

#### 2.4.4. Intracellular leaflet labeling and contrasting the specimen

Labeling of the intracellular leaflet was performed by incubation for 30 min on drops of PBS supplemented with 0.1% BSA and antibodies, followed by three 5-min washes with PBS. Samples were post-fixed with 2% glutaraldehyde in PBS for 10 min and then washed with PBS for 10 min. The specimens were further stained for 10 min with 1% $OsO_4$ in cacodylate buffer, washed three time for 5 min in $H_2O$, incubated for 10 min with 1% aqueous tannic acid, washed three times for 5 min in $H_2O$, and finally stained for 10 min with 1% aqueous uranyl acetate. After a 1-min wash in $H_2O$, the samples were air-dried and examined by electron microscope (JEOL JEM 1200EX operating at 60 kV).

### 2.5. Flow cytometry analysis

IgE-primed BMMC and RBL cells were fixed by 4% paraformaldehyde in PBS at various stages of their activation. Subsequently, they were washed with PBS and immuno-labeled with FITC-conjugated anti-mouse Ig. Samples were analyzed using FACSCalibur™ (Becton Dickinson, NJ, USA).

### 2.6. Degranulation assay

The extent of mast cell degranulation was assessed by measuring the relative content of β-glucuronidase released

into the supernatant. Twenty microliters of supernatant was mixed with 60 µl of 40 µM 4-methylumbelliferyl β-D-glucuronide and incubated for 60 min at 37 °C. The reaction was stopped by adding 200 µl of ice-cold 0.2 M glycine buffer (pH 10.5) and fluorescence was measured in a microtiter plate reader (Fluorostar, SLT Labinstruments, Austria) using 365 nm excitation and 460 nm emission filters. The total content of β-glucuronidase was evaluated in the supernatants from cells lysed by 0.1% Triton X-100.

To check for the effect of BMMC adsorption to ultraclean glass on degranulation, the cells ($10^5$ in 100 µl) were dropped onto ultraclean glass coverslips and incubated for 1, 5 or 10 min at room temperature. Then the supernatant and non-adsorbed cells were centrifuged, and amount of β-glucuronidase in the cell-free supernatant was determined as described above. As a control, degranulation of cells in suspension was measured at the respective time intervals. Three independent experiments were performed.

### 2.7. Immunoblotting

IgE-sensitized or non-sensitized BMMC were washed twice with BSS supplemented with 0.1% BSA and transferred to BSS without BSA. A 100-µl aliquot of the suspension ($10^6$ cells/ml) was applied onto an ultraclean glass coverslip for 1 min (approximately 50% of the cells adhered within this time period), rinsed in BSS and, when indicated, processed for activation by DNP-BSA in BSS at 37 °C. Then the cells were lyzed for 20 min in ice-cold lysis buffer (50 mM Tris–HCl, pH 7.5, 150 mM NaCl, 2 mM EDTA, 1 mM $Na_3VO_4$, 1 mM phenylmethylsulfonyl fluoride, 1 µg/ml aprotinin, 1 µg/ml leupeptin, 0.5% Triton X-100). Alternatively, the amount of BMMC corresponding approximately to those adherent to the glass was activated or not in suspension and lysed as described above. After lysis, cellular proteins were size-fractionated by sodium dodecylsulfate-polyacrylamide gel electrophoresis under reducing conditions and electrotransferred to NC membranes (BA85, Schleicher & Schuell, Germany). Tyrosine-phosphorylated proteins were detected by immunolabeling with HRP-conjugated PY20 mAb. To check for cell loading, the amount of Lyn kinase in the samples was detected by immunolabeling with mouse anti-Lyn mAb, followed by HRP-conjugated anti-mouse secondary antibody. The membrane-bound HRP was visualized with ECL Western blotting reagent (Amersham, UK) according to the manufacturer's instructions. Immunoblots were analyzed using a Luminescent Image Analyzer LAS-3000 (Fuji Photo Film Co., Japan) and AIDA image analyzer software (raytest Isotopenmeßgeräte GmbH, Germany).

### 2.8. Statistics

The GOLD computer program was used for statistical evaluation of clustering and colocalization of immunogold markers. It maps the distribution of gold particles by pair correlation function (PCF; analysis of clustering) or pair cross-correlation function (PCCF; analysis of colocalization). PCF is a ratio of the density of gold particles at a given distance from a typical particle to the average density of these particles. PCCF is a ratio of the density of particles of the first type at a given distance from a typical particle of the second type to the average density of the particles of the first type (Philimonenko et al., 2000). Data shown are means ± SD unless stated otherwise.

## 3. Results

### 3.1. New procedures for isolation of PM sheets from non-adherent cells

In pilot experiments we found that leukocytes, such as BMMC or T cells, which do not adhere to glass surfaces in media or buffers supplemented with serum, bound rapidly to ultraclean glass surfaces in protein-free buffer, and that this property can be used for isolation of PM sheets. The binding of cells to the ultraclean glass surface occurs rapidly (within ~1 min) at room temperature and is not dependent on the actin cytoskeleton, as PM sheets were isolated with comparable efficiency from BMMC pretreated with an inhibitor of actin polymerization latrunculin B (20 µM, 90 min, 37 °C) and from latrunculin B non-treated cells. Importantly, binding of BMMC to ultraclean glass for 1, 5 or 10 min at room temperature did not cause enhanced spontaneous degranulation when compared to cells kept in suspension for the indicated time intervals (not shown). Similarly, tyrosine phosphorylation of BMMC proteins was comparable between resting or DNP-activated cells incubated on glass or in suspension when normalized to the amount of Lyn protein (Fig. 2).

To elaborate the procedure for isolation of PM sheets by adsorption of cells to glass (Fig. 1A, right), we compared it with two other methods we developed for isolation of membrane sheets from BMMC. The first (Fig. 1A, left) makes use of the finding that BMMC under certain circumstances adhere to fibronectin, a component of the mast cell environment (Lam et al.,

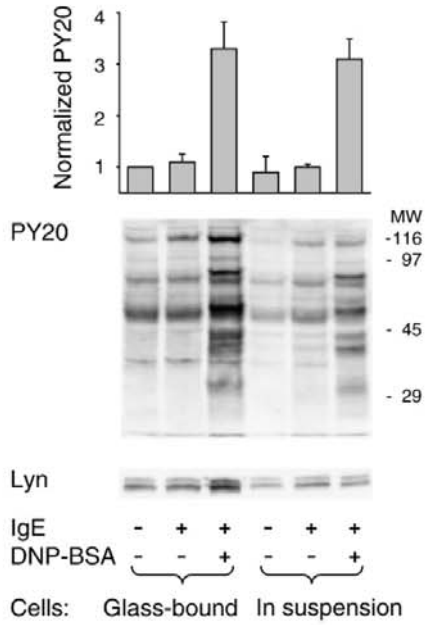


Fig. 2. Protein tyrosine phosphorylation profiles in cells bound to ultraclean glass and those incubated in suspension. The cells were cultured overnight in the presence (+) or absence (−) of DNP-specific IgE, transferred to protein-free BSS and then incubated for 1 min on ultraclean glass coverslips or in suspension. When indicated (+) they were activated with DNP-BSA (1 μg/ml) for 5 min at 37 °C and lysed directly on glass; cells in suspension were centrifuged before lysis. Tyrosine-phosphorylated proteins were detected using HRP-labeled PY20 mAb and the signal was normalized to Lyn protein detected by immunoblotting. Means±SD were calculated from three independent experiments.

2003), thus providing relatively physiological conditions for cell adhesion. The second method (Fig. 1B) is based on pressing the cells suspended in protein-free buffer to PLL-coated EM grids by ultraclean glass coverslip, thus reducing the length of attachment as much as possible. Further steps were identical in all isolation procedures used, and consisted of pressing the sandwich formed by the glass coverslip, cells and EM grid (Fig. 1C), followed by side-lifting the glass coverslip (Fig. 1D) and washing the membrane sheets attached to the EM grids by floating on ice-cold HEPES buffer (Fig. 1E).

PM sheets isolated from BMMC after binding to fibronectin (Fig. 3A), ultraclean glass (Fig. 3B) or pressing directly to PLL-covered EM grids (Fig. 3C) showed comparable distribution of the FcεRI-β subunit as detected by EM after intracellular leaflet double-step immunolabeling. Furthermore, no difference in the amount of receptor or in the PM structure was noticed. When PM sheets were isolated 2 min after exposure to antigen (DNP-BSA), a comparable decrease in the amount of FcεRI-β subunit in PM was observed for all three procedures (Fig. 3D). Therefore, we used only the method based on cell adsorption to ultraclean glass in subsequent studies.

As the density of FcεRI-β subunits on PM sheets was approximately twice as high for RBL cells (prepared by the technique of Sanan and Anderson, 1991) than for BMMC (Fig. 3E), we checked whether this difference was attributable to spreading of RBL cells on the glass surface, and thus possibly exposing the FcεRI on the dorsal membrane. PM sheets isolated from RBL cells in suspension using the same procedure as from BMMC (1 min adhesion to ultraclean glass coverslips, without spreading) showed an amount of detectable FcεRI-β (24.91±2.97 particles/μm$^2$, $n$=3, 60 μm$^2$) comparable to that detected on PM sheets of glass-grown RBL cells (23.96±2.66 particles/μm$^2$, $n$=3, 60 μm$^2$).

### 3.2. Topography of FcεRI in the course of IgE-dependent BMMC activation

Aggregation of FcεRI by IgE and multivalent antigen leads to FcεRI internalization by a dynamin-dependent mechanism in RBL cells (Fattakhova et al., 2006). We found that both RBL cells and BMMC show a similar decrease in detectable FcεRI on PM sheets when stimulated by DNP-BSA at concentrations optimal for degranulation (1 μg/ml for RBL, 0.1 μg/ml for BMMC). No obvious difference was observed in the amount of detectable FcεRI on BMMC stimulated by either 1 or 0.1 μg/ml DNP-BSA (Fig. 3E).

It has been reported that activation of RBL cells by multivalent antigen leads to formation of FcεRI patches several hundreds of nanometers in size (Wilson et al., 2000). To find out whether similar patches are also formed in BMMC, we analyzed the topography of FcεRI in resting and activated cells. To detect both FcεRI-α and FcεRI-β subunits on the same PM sheets, the IgE bound to FcεRI-α was detected by two-step immunolabeling from the extracellular side, PM sheets were isolated, and FcεRI-β was labeled from the intracellular side. As expected, in resting cells both immunogold markers colocalized in the PM and were distributed in small clusters (Fig. 4A and C). Surprisingly, in antigen (DNP-BSA)-activated BMMC, no dramatic changes in FcεRI topography were observed and no large patches of FcεRI in osmiophilic regions were formed. In fact, the number of FcεRI clusters in activated BMMC was lower than in resting cells; this

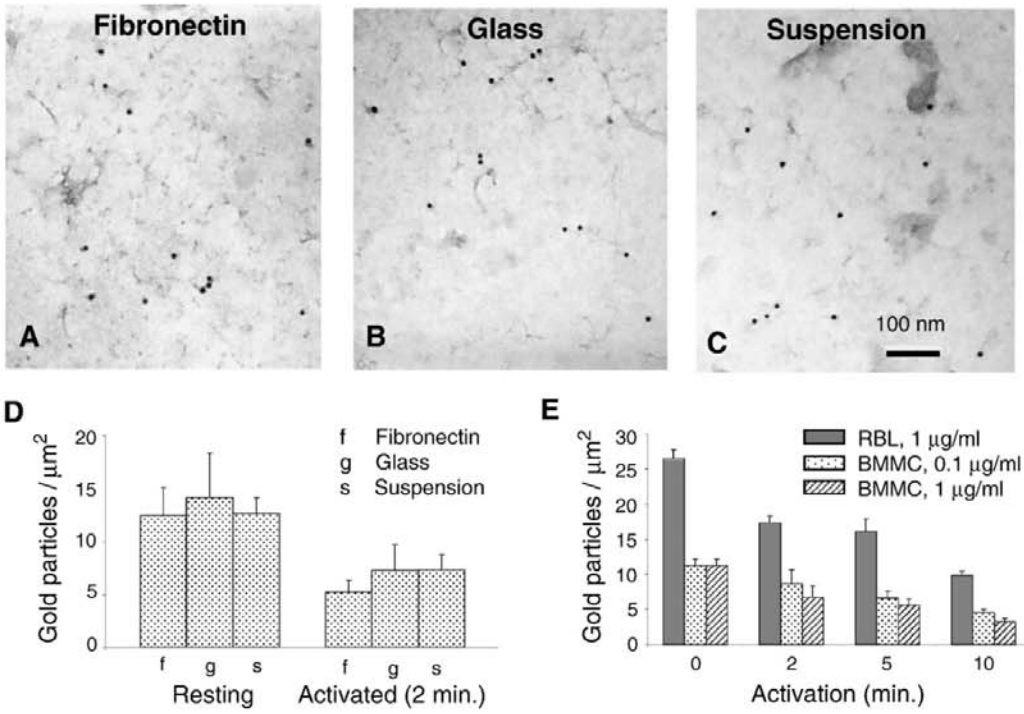


Fig. 3. Properties of PM sheets isolated by various procedures. (A)–(C) Examples of PM sheets isolated from resting BMMC by adhesion to fibronectin (A), adsorption to ultraclean glass coverslips (B), or direct pressing in suspension to EM grids (C). The FcεRI-β subunit was labeled on the cytoplasmic side with JRK mAb followed by goat anti-mouse IgG–10 nm gold conjugate. (D) The density of 10 nm gold immuno-labeled FcεRI-β on plasma membrane sheets isolated from resting or activated (2 min, 37 °C, 0.1 µg/ml DNP-BSA) BMMC by adhesion to fibronectin (f), adsorption to ultraclean glass coverslips (g), or pressing in suspension to EM grids (s). (E) The density of 10 nm gold immuno-labeled FcεRI-β on PM sheets isolated from adherent RBL cells or ultraclean glass-adsorbed BMMC in the course of their activation with DNP-BSA at 37 °C. Means and SD from three independent experiments are shown; each experiment covers approximately 30 µm$^2$ of the PM.

was probably caused by internalization of aggregated FcεRI. The clusters that remained on PM after BMMC activation were slightly smaller than those before activation (Fig. 4A–D). As expected, analogous treatment of RBL cells led to formation of large (~200 nm) FcεRI aggregates (Fig. 4E–H). FcεRI clusters were of comparable size on resting BMMC and RBL cells, but they were more numerous in RBL cells. Thus the difference in FcεRI content of BMMC and RBL cell PM reflects differences in the number of FcεRI domains, but not in the FcεRI content of the individual domains.

Further experiments showed that no large FcεRI patches were formed at any time interval after BMMC triggering, either with low (0.1 µg/ml; Fig. 5A) or high (1 µg/ml; Fig. 5B) concentrations of antigen. When RBL cells were analyzed under comparable conditions, the formation of large FcεRI aggregates was clearly observed 2 min after triggering (Fig. 5C). Thus, although FcεRI aggregates in BMMC are internalized to the same extent as in RBL cells (Fig. 3E), large patches of aggregated FcεRI are observed only in RBL cells.

Quantitative changes in the total amount of PM FcεRI in the course of activation were detected by flow cytometry. Data in Fig. 6 show that both BMMC and RBL cells rapidly internalized FcεRI during DNP-mediated stimulation (approximately 40% internalized within 2 min) and to a comparable extent, and that there was no significant difference between BMMC activated by 0.1 and 1 µg/ml DNP-BSA. These results are in agreement with data obtained by EM on PM sheets.

In all previous experiments cells were activated at 37 °C. It has been shown that decreasing the temperature to 4 °C delays all signaling events including

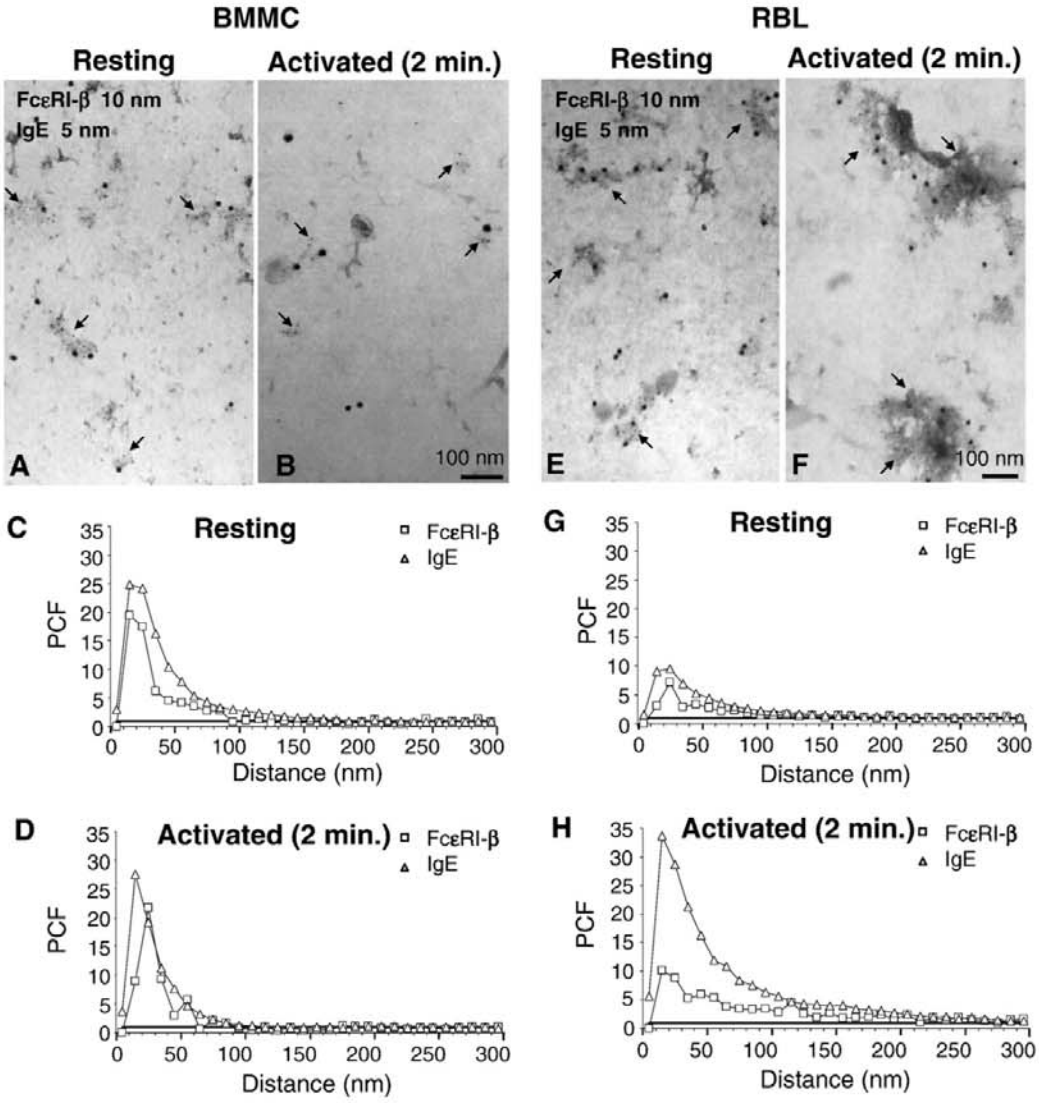


Fig. 4. Different topography of FcεRI in activated BMMC and RBL cells. (A, B) Topography of intracellularly labeled FcεRI-β subunit (10 nm gold particles) and FcεRI-α subunit-associated extracellular IgE (5 nm gold particles, indicated by arrows) in PM sheets isolated from resting (A) or activated (B; 2 min; 37 °C; 0.1 μg/ml DNP-BSA) BMMC. (C, D) Clustering of IgE (triangles) and FcεRI-β (squares) in resting (C) and activated (D) BMMC. Clustering is indicated at respective distance from a typical particle, when the pair correlation function (PCF) exceeds 1. Ideal random distribution of gold markers (PCF = 1) is indicated by a solid line. The distance at which the peak of the PCF value falls to 1 indicates the size of the immuno-labeled aggregates of the respective membrane antigen (the real aggregates are, however, smaller, as the size of antibody sandwiches must be taken into consideration). The height of the peak indirectly reflects the density of these aggregates in PM (the higher the number of distinct aggregates within a certain area, the lower is the PCF peak) but it also reflects saturation of labeling within the aggregates (5 nm immunogold label provides a more intense signal than 10 nm immunogold label). Each graph represents data from two independent experiments covering approximately 60 $\mu m^2$. (E, F) As a control, topography of the FcεRI-β subunit and FcεRI-α subunit-associated extracellular IgE in resting (E) and activated (F) RBL cells is shown. (G, H) Clustering of IgE (triangles) and FcεRI-β (squares) in resting (G) and activated (H) RBL cells was calculated as above.

internalization, and preserves the formation of larger signaling assemblies (Holowka et al., 2000). We therefore assessed the formation of FcεRI patches in cells activated at 4 °C. Under these conditions, enhanced FcεRI clustering in a time-dependent manner was found in both RBL cells and BMMC (Fig. 7).

### 3.3. Independent distribution of LAT and NTAL in BMMC

We have reported previously that the transmembrane adaptor proteins, LAT and NTAL, are localized in independent regions of the PM sheets isolated from resting RBL cells as well as after activation via FcεRI or Thy-1 (Volná et al., 2004; Heneberg et al., 2006). This was an unexpected finding because LAT and NTAL exhibit structural similarities, including submembrane localization of their palmitoylation sites and association with detergent-resistant membranes. To exclude the possibility that the observed independent distribution of the adaptors is connected with the tumor origin of RBL cells or their adhesive properties, we analyzed the topography of LAT and NTAL in PM sheets isolated from BMMC. In initial control experiments, LAT (Fig. 8A and D) or NTAL (Fig. 8B and E) were labeled with two different antibodies directed against the same target antigen. As anticipated, this resulted in colocalization of the immunogold markers on PM in both BMMC and RBL cells, and was reflected in enhanced values of the pair cross-correlation function (PCCF; Fig. 9A and B, black squares and black diamonds). This is an important control, excluding the possibility that localization of various proteins in different domains is caused by segregating activity of the antibodies. In contrast, when LAT and NTAL were labeled on the same membrane, both proteins were accumulated in separate domains not only in RBL cells but also in BMMC (Fig. 8C and F). Analysis of colocalization confirmed the topographical independence of LAT and NTAL in the PM sheets isolated from resting or activated BMMC (Fig. 9A) and RBL cells (Fig. 9B). These data prove that LAT and NTAL are clustered in different domains in non-tumor mast cells.

## 4. Discussion

Examination of isolated PM sheets by high-resolution EM is an established and powerful method for topographical analyses of various PM molecules. Originally, this method was developed for studies of cells growing adherent to a glass surface in the presence of culture media (Sanan and Anderson, 1991); however, such cells are rare among non-transformed leukocytes. Later, the method was modified to allow isolation of PM sheets from non-adherent T cells (Schade and Levine, 2002; Lillemeier et al., 2006). The cells were attached to the glass surface by interaction with immobilized immuno-ligands or by binding to PLL at 37 °C or 4 °C. Alternatively, biotinylated T cells were bound to glass coverslips covered with streptavidin. In these methods, the immobilization step itself was lengthy (45–60 min). Here we report a new procedure for isolation of PM sheets from non-adherent leukocytes that is based on non-specific adhesion of cells to ultraclean glass in protein-free buffer. Compared to previous methods for isolation of membrane sheets from non-adherent cells, this new method has several advantages. First, it is very rapid, requiring only ~1 min for settling the cells onto ultraclean glass coverslips. This reduces the risk of artificial rearrangement of PM components during interaction of the cell with the substrate. Second, it is independent of binding of the cells to PLL, which has been reported to cause mast cell activation (Benyon et al., 1987). It should be noted that the mere binding of BMMC to ultraclean glass did not cause their degranulation or enhanced tyrosine phosphorylation of cellular proteins. Third, this method does not require preincubation of the cells at low temperature, which causes changes in organization of the PM (Magee et al., 2005). The only step required to be done at 4 °C before paraformaldehyde fixation, i.e. the plasma membrane ripping off procedure, takes no more than several seconds and is almost identical with the well-established procedure of isolation of plasma membrane sheets from adherent cells (Sanan and Anderson, 1991; Wilson et al., 2000). Fourth, the method can be performed in the presence of actin polymerization inhibitors such as latrunculin B, because it does not require active cytoskeleton-driven adsorption. This will facilitate future studies on the role of cytoskeletal components in the topography of various PM molecules.

In control experiments, we analyzed PM sheets prepared from BMMC bound to fibronectin-coated surfaces, a process dependent on cell sensitization. Alternatively, PM sheets were isolated from suspended cells pressed directly onto PLL-covered EM grids. As the topography of FcεRI and the quality of the isolated PM sheets did not differ among these two controls and the cells adsorbed to ultraclean glass, the technique based on adsorption to glass was used in subsequent studies. It is fast, can be used universally, and enables high effectivity even of extracellular leaflet labeling.

Changes in the topography of PM signaling molecules in the course of FcεRI-mediated activation have previously been examined by high-resolution EM almost exclusively in RBL cells (Lara et al., 2001; Wilson et al., 2000, 2002, 2004; Dráberová et al., 2004; Heneberg et al., 2006). Wilson et al. (2002) proposed the existence of primary signaling domains, possessing aggregated FcεRI in ~200 nm patches, and secondary signaling domains, enriched with the transmembrane adaptor protein LAT. Here we present for the first time

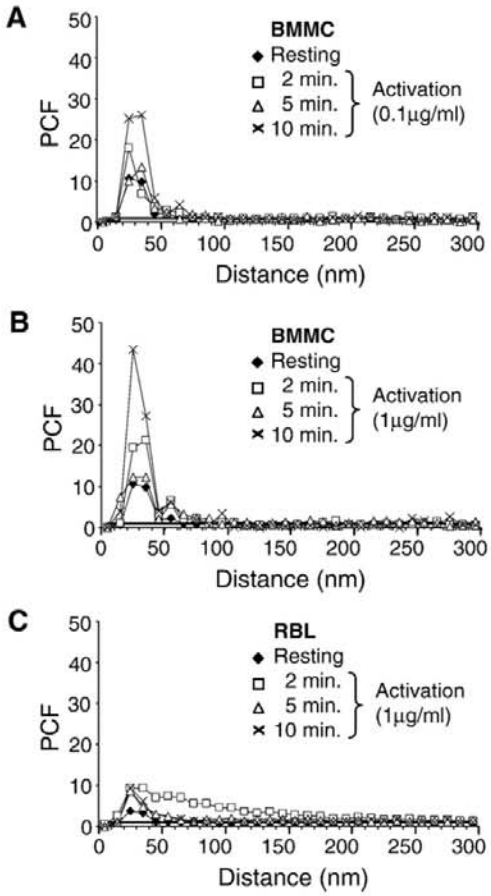


Fig. 5. Clustering of 10 nm immunogold-labeled FcεRI-β in the course of BMMC and RBL cell activation. BMMC were stimulated with 0.1 μg/ml (A) or 1 μg/ml (B), RBL cells with 1 μg/ml (C) DNP-BSA at 37 °C. Clustering is plotted as described in Fig. 4. Each graph represents data from two independent experiments covering approximately 60 $\mu m^2$.

the topography of FcεRI and downstream adaptors in PM sheets isolated from BMMC. In resting BMMC, the FcεRI was distributed in small clusters of comparable size to those observed in RBL cells, but the clusters were less numerous than in RBL cells. The overall amount of FcεRI-β subunits per $\mu m^1$ was reduced almost to half in BMMC compared to RBL cells. The possibility that the enhanced amount of FcεRI-β in RBL cells is caused by transfer of the receptor from the ventral to the dorsal side during adhesive growth of the cells was excluded by experiments in which the membrane sheets from RBL cells were isolated in the same way as from BMMC and the difference still remained.

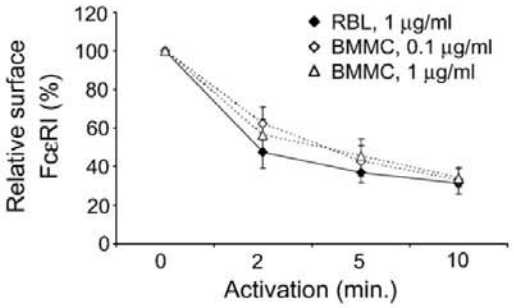


Fig. 6. Relative concentration of surface FcεRI on BMMC and RBL cells in the course of their activation by DNP-BSA as detected by flow cytometry. FcεRI-bound IgE was labeled by FITC-conjugated donkey anti-mouse Ig on fixed resting or activated cells. Means±SD from three independent experiments are shown.

Unexpectedly, activation of IgE-sensitized BMMC with DNP-BSA at concentrations which are either optimal (0.1 μg/ml) or supraoptimal (1 μg/ml) for degranulation did not lead to formation of large FcεRI signaling domains. However, this treatment caused a decrease in the amount of detectable FcεRI-β on the

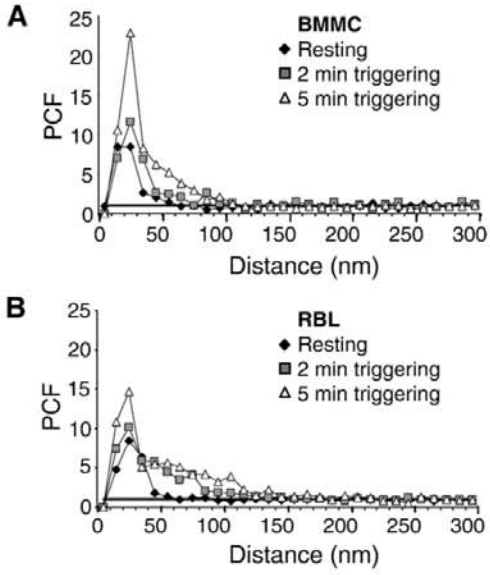


Fig. 7. Enhanced FcεRI clustering in BMMC stimulated at low temperature. IgE-sensitized BMMC (A) or RBL cells (B) were incubated for 10 min on ice and FcεRI was then triggered for 2 or 5 min with DNP-BSA on ice. PM sheets were isolated and FcεRI-β was labeled with JRK mAb followed by goat anti-mouse IgG–10 nm gold conjugate. Clustering is plotted as described in Fig. 4. Each graph represents data from two independent experiments covering approximately 60 $\mu m^2$.

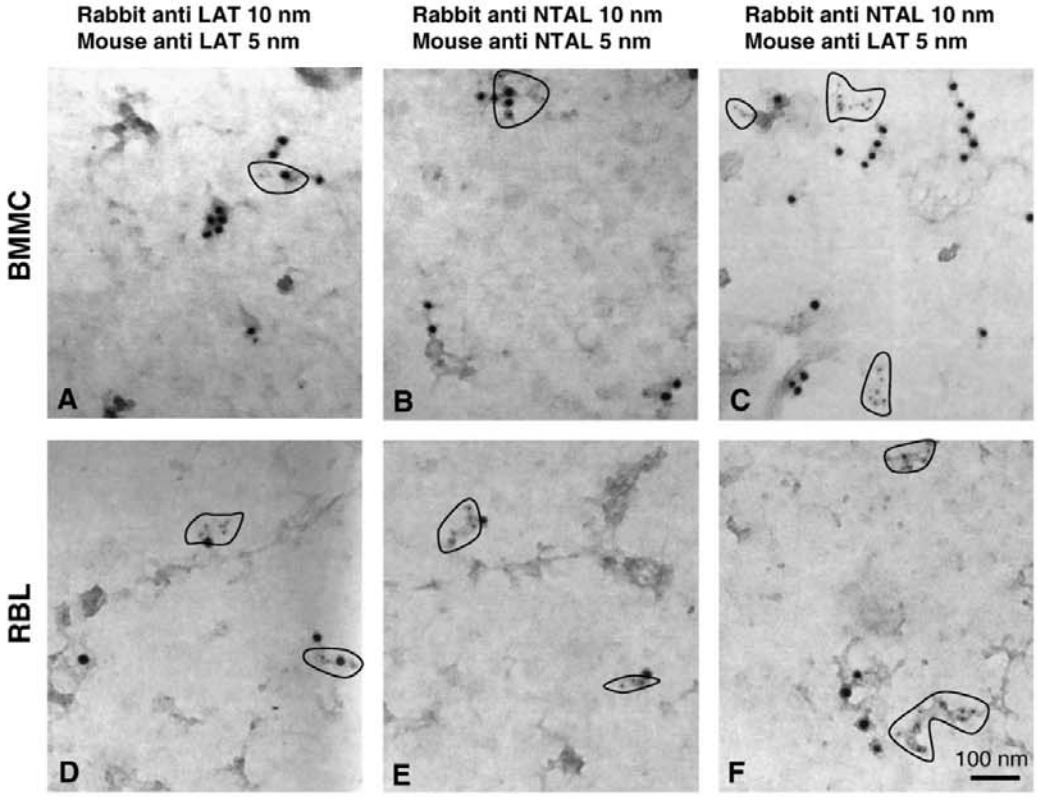


Fig. 8. Topography of LAT and NTAL on the PM sheets from resting cells. PM sheets were isolated from BMMC (A–C) or RBL cells (D–F). LAT (A, D) or NTAL (B, E) were labeled by two different antibodies or they were labeled together on the same membrane (C, F). Clusters of 5 nm gold are circled.

cytoplasmic side of the membrane sheets isolated from both BMMC and RBL cells. The observed decrease was probably caused by receptor internalization as shown using flow cytometry, which demonstrated an activation-dependent loss of cell surface FcεRI. The combined data indicate that activation of BMMC by multivalent antigen-IgE complexes leads to a rapid FcεRI internalization from multiple small patches of FcεRI aggregates. Thus, formation of large receptor aggregates, comparable in size to those formed in RBL cells activated under similar conditions, are not required for initiation of BMMC signaling events. The observed difference in size of the antigen-induced FcεRI patches between both mast cell types is likely to reflect different local dynamics, favoring formation of more numerous but smaller signaling domains in BMMC compared to RBL cells. When FcεRI triggering occurred at 4 °C, the differences between the two cell types disappeared. These data, together with our previous results that RBL cells can be activated by mAb-mediated dimerization of the FcεRI without formation of detectable receptor clusters (Dráberová et al., 2004), suggest that primary signaling domains are much smaller than previously thought; their size in BMMC is comparable to that of FcεRI clusters observed in the PM isolated from resting cells. This calls for reconsideration of the view of initiation of mast cell signaling, thereby stressing subtle and dynamic processes, as well as the importance of further studies on other mast cell types.

FcεRI-mediated activation leads to rapid phosphorylation of the transmembrane adaptor proteins, LAT and NTAL, which serve as scaffolds for downstream signaling. Both adaptors are very similar in structure, including two acylation sites which are likely to cause enhanced resistance to solubilization in non-ionic detergents. Our previous EM studies on isolated PM sheets revealed that LAT and NTAL were localized in separate non-overlapping domains from both non-activated and FcεRI-activated RBL cells. When the GPI-anchored protein Thy-1 (whose aggregation causes

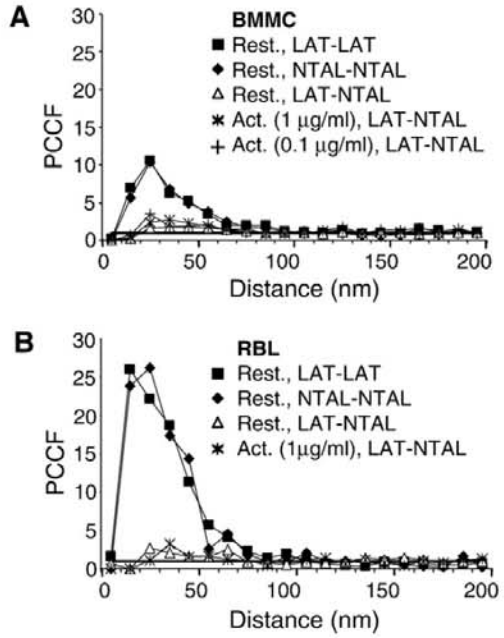


Fig. 9. Quantitative analysis of the topographical relationship between LAT and NTAL. The distribution of gold particles on PM sheets isolated from BMMC (A) or RBL cells (B) was mapped by pair cross-correlation function (PCCF). Co-localization is indicated at the respective distance from a typical particle when the PCCF exceeds 1. The ideal independent distribution of both gold markers (PCCF=1) is indicated by a solid line. The maximal width of the peak above value 1 reflects the distance at which both antigens are selectively closer to each other than would be in the case of random distribution. The height of the peak corresponds to the tendency of both antigens to co-localize and it is reduced when the overall label density is higher. The black squares and black diamonds show LAT or NTAL simultaneously labeled with rabbit and mouse antibodies against the same adaptor (positive controls). Other markers show PCCF for LAT and NTAL labeled together on resting or DNP-BSA-activated cells as indicated. Each graph represents data from two independent experiments covering approximately 60 $\mu m^2$.

mast cell degranulation (Dráberová, 1989)) were labeled in fixed state or aggregated by mAb, both adaptors colocalized with the clustered Thy-1, but again, no mixed adaptor clusters were formed (Volná et al., 2004; Heneberg et al., 2006). Experiments with BMMC from knock-out mice revealed that LAT and NTAL had different functions (Volná et al., 2004; Zhu et al., 2004). Because the topography of these adaptors in BMMC has not yet been studied, we made use of the method of isolation of PM sheets described above to address this issue. To exclude the objection that separation of both adaptors may be induced secondarily by the antibodies used for detection, each of the adaptor proteins was labeled with different (rabbit and mouse) antibodies together. This resulted in strong colocalization of both markers, indicating that the antibodies are not by themselves responsible for separation of the proteins. However, when the same antibodies were used for simultaneous detection of LAT and NTAL, they clearly showed different domains for both adaptors not only in RBL cells, but also in BMMC. Thus, sequestration of LAT and NTAL does not seem to be an artifact observed only in the immortalized RBL cell line, and does not reflect the experimental procedures.

Why should these two structurally similar proteins form separate domains in the PM? Perhaps differences in the amino acid sequence of their transmembrane domains could cause association with different lipids within the membrane rafts. Alternatively, cytoplasmic domains may interact with different proteins leading to formation of variant signalosomes. The latter possibility is supported by findings that in T cells, LAT associates with CD2 coreceptor and tyrosine kinase Lck in discrete PM regions, which depend on protein–protein interactions mediated through LAT phosphorylation sites but not on interactions with lipid rafts (Douglass and Vale, 2005). As the repertoire of LAT and NTAL cytoplasmic docking sites is not identical (Brdička et al., 2002), the specific protein–protein network might result in separation of both adaptors. However, the finding that NTAL and LAT are sequestered into discrete domains even before cell triggering and therefore in the absence of their tyrosine phosphorylation, suggests that other mechanisms are also involved.

Although restricted to fixed specimens, high-resolution EM combined with immunogold labeling is a powerful technique that has brought about important findings on PM organization (Wilson et al., 2002, 2004; Prior et al., 2003; Heneberg et al., 2006; Lillemeier et al., 2006). Extension of the method to rapid and simple isolation of PM sheets from non-adherent cells will contribute to its wider use and thus to better understanding of signaling events in various immune system cells which are mostly non-adherent.

## Acknowledgments

We thank D. Lorenčíková, H. Mrázová, I. Lišková and J. Musilová for technical assistance. This work was supported by project 1M0506 (Center of Molecular and Cellular Immunology) from the Ministry of Education, Youth and Sports of the Czech Republic, grants 204/05/H023 and 301/06/0361 from the Grant Agency of the Czech Republic, and Institutional project AVOZ50520514. Petr Heneberg's research was supported in part by research

goal MSM0021620814 from the 3rd Faculty of Medicine, Charles University, Prague.

## References


Benyon, R.C., Lowman, M.A., Church, M.K., 1987. Human skin mast cells: their dispersion, purification, and secretory characterization. J. Immunol. 138, 861.

Brdička, T., Imrich, M., Angelisová, P., Brdičková, N., Horváth, O., Špička, J., Hilgert, I., Lusková, P., Dráber, P., Novák, P., Engels, N., Wienands, J., Simeoni, L., Österreicher, J., Aguado, E., Malissen, M., Schraven, B., Hořejší, V., 2002. Non-T cell activation linker (NTAL): a transmembrane adaptor protein involved in immunoreceptor signaling. J. Exp. Med. 196, 1617.

Choy, M.S., Bay, B.H., Cheng, H.C., Cheung, N.S., 2006. PTEN is recruited to specific microdomains of the plasma membrane during lactacystin-induced neuronal apoptosis. Neurosci. Lett. 405, 120.

Douglass, A.D., Vale, R.D., 2005. Single-molecule microscopy reveals plasma membrane microdomains created by protein–protein networks that exclude or trap signaling molecules in T cells. Cell 121, 937.

Dráberová, L., 1989. The involvement of Thy-1 antigen in the activation of rat mast cells. Eur. J. Immunol. 19, 1715.

Dráberová, L., Dráber, P., 1991. Functional expression of the endogenous Thy-1 gene and the transfected murine Thy-1.2 gene in rat basophilic leukemia cells. Eur. J. Immunol. 21, 1583.

Dráberová, L., Amoui, M., Dráber, P., 1996. Thy-1-mediated activation of rat mast cells: the role of Thy-1 membrane microdomains. Immunology 87, 141.

Dráberová, L., Lebduška, P., Hálová, I., Tolar, P., Štokrová, J., Tolarová, H., Korb, J., Dráber, P., 2004. Signaling assemblies formed in mast cells activated via Fcε receptor I dimers. Eur. J. Immunol. 34, 2209.

Fattakhova, G., Masilamani, M., Borrego, F., Gilfillan, A.M., Metcalfe, D.D., Coligan, J.E., 2006. The high-affinity immunoglobulin-E receptor (FcεRI) is endocytosed by an AP-2/clathrin-independent, dynamin-dependent mechanism. Traffic 7, 673.

Gilfillan, A.M., Tkaczyk, C., 2006. Integrated signalling pathways for mast-cell activation. Nat. Rev. Immunol. 6, 218.

Heneberg, P., Lebduška, P., Dráberová, L., Korb, J., Dráber, P., 2006. Topography of plasma membrane microdomains and its consequences for mast cell signaling. Eur. J. Immunol. 36, 2795.

Holowka, D., Sheets, E.D., Baird, B., 2000. Interactions between FcεRI and lipid raft components are regulated by the actin cytoskeleton. J. Cell Sci. 113, 1009.

Lagerholm, B.C., Weinreb, G.E., Jacobson, K., Thompson, N.L., 2005. Detecting microdomains in intact cell membranes. Annu. Rev. Phys. Chem. 56, 309.

Lam, V., Kalesnikoff, J., Lee, C.W., Hernandez-Hansen, V., Wilson, B.S., Oliver, J.M., Krystal, G., 2003. IgE alone stimulates mast cell adhesion to fibronectin via pathways similar to those used by IgE + antigen but distinct from those used by Steel factor. Blood 102, 1405.

Lara, M., Ortega, E., Pecht, I., Pfeiffer, J.R., Martinez, A.M., Lee, R.J., Surviladze, Z., Wilson, B.S., Oliver, J.M., 2001. Overcoming the signaling defect of Lyn-sequestering, signal-curtailing FcεRI dimers: aggregated dimers can dissociate from Lyn and form signaling complexes with Syk. J. Immunol. 167, 4329.

Lillemeier, B.F., Pfeiffer, J.R., Surviladze, Z., Wilson, B.S., Davis, M.M., 2006. Plasma membrane-associated proteins are clustered into islands attached to the cytoskeleton. Proc. Natl. Acad. Sci. U.S.A. 103, 18992.

Liu, F.-T., Bohn, J.W., Ferry, E.L., Yamamoto, H., Molinaro, C.A., Sherman, L.A., Klinman, N.R., Katz, D.H., 1980. Monoclonal dinitrophenyl-specific murine IgE antibody: preparation, isolation, and characterization. J. Immunol. 124, 2728.

Magee, A.I., Adler, J., Parmryd, I., 2005. Cold-induced coalescence of T-cell plasma membrane microdomains activates signalling pathways. J. Cell Sci. 118, 3141.

Metcalfe, D.D., Baram, D., Mekori, Y.A., 1997. Mast cells. Physiol. Rev. 77, 1033.

Philimonenko, A.A., Janáček, J., Hozák, P., 2000. Statistical evaluation of colocalization patterns in immunogold labeling experiments. J. Struct. Biol. 132, 201.

Pike, L.J., 2006. Rafts defined: a report on the Keystone Symposium on Lipid Rafts and Cell Function. J. Lipid Res. 47, 1597.

Prior, I.A., Muncke, C., Parton, R.G., Hancock, J.F., 2003. Direct visualization of Ras proteins in spatially distinct cell surface microdomains. J. Cell Biol. 160, 165.

Rivera, J., Kinet, J.-P., Kim, J., Pucillo, C., Metzger, H., 1988. Studies with a monoclonal antibody to the beta subunit of the receptor with high affinity for immunoglobulin E. Mol. Immunol. 25, 647.

Sanan, D.A., Anderson, R.G., 1991. Simultaneous visualization of LDL receptor distribution and clathrin lattices on membranes torn from the upper surface of cultured cells. J. Histochem. Cytochem. 39, 1017.

Schade, A.E., Levine, A.D., 2002. Lipid raft heterogeneity in human peripheral blood T lymphoblasts: a mechanism for regulating the initiation of TCR signal transduction. J. Immunol. 168, 2233.

Simons, K., Toomre, D., 2000. Lipid rafts and signal transduction. Nat. Rev. Mol. Cell Biol. 1, 31.

Smrž, D., Dráberová, L., Dráber, P., 2007. Non-apoptotic phosphatidylserine externalization induced by engagement of glycosylphosphatidylinositol-anchored proteins. J. Biol. Chem. 282, 10487.

Tolar, P., Tůmová, M., Dráber, P., 2001. New monoclonal antibodies recognizing the adaptor protein LAT. Folia Biol. (Prague) 47, 215.

Volná, P., Lebduška, P., Dráberová, L., Šímová, S., Heneberg, P., Boubelík, M., Bugajev, V., Malissen, B., Wilson, B.S., Hořejší, V., Malissen, M., Dráber, P., 2004. Negative regulation of mast cell signaling and function by the adaptor LAB/NTAL. J. Exp. Med. 200, 1001.

Wilson, B.S., Pfeiffer, J.R., Oliver, J.M., 2000. Observing FcεRI signaling from the inside of the mast cell membrane. J. Cell Biol. 149, 1131.

Wilson, B.S., Pfeiffer, J.R., Oliver, J.M., 2002. FcεRI signaling observed from the inside of the mast cell membrane. Mol. Immunol. 38, 1259.

Wilson, B.S., Steinberg, S.L., Liederman, K., Pfeiffer, J.R., Surviladze, Z., Zhang, J., Samelson, L.E., Yang, L.H., Kotula, P.G., Oliver, J.M., 2004. Markers for detergent-resistant lipid rafts occupy distinct and dynamic domains in native membranes. Mol. Biol. Cell 15, 2580.

Wyse, B.D., Prior, I.A., Qian, H., Morrow, I.C., Nixon, S., Muncke, C., Kurzchalia, T.V., Thomas, W.G., Parton, R.G., Hancock, J.F., 2003. Caveolin interacts with the angiotensin II type 1 receptor during exocytic transport but not at the plasma membrane. J. Biol. Chem. 278, 23738.

Zhu, M., Liu, Y., Koonpaew, S., Granillo, O., Zhang, W., 2004. Positive and negative regulation of FcεRI-mediated signaling by adaptor protein LAB/NTAL. J. Exp. Med. 200, 991.

**6.7**

**Dráberová, L.; Shaik, G.M.; Volná, P.; Heneberg, P.; Tůmová, M.; Lebduška, P.; Korb, J. & Dráber, P. (2007):**

**Regulation of $Ca^{2+}$ signaling in mast cells by tyrosine-phosphorylated and unphosphorylated non-T cell activation linker, NTAL.**

**Journal of Immunology 179(8): 5169-5180.**

# Regulation of $Ca^{2+}$ Signaling in Mast Cells by Tyrosine-Phosphorylated and Unphosphorylated Non-T Cell Activation Linker[1]

**Lubica Dráberová,* Gouse Mohiddin Shaik,* Petra Volná,* Petr Heneberg,*‡ Magda Tůmová,* Pavel Lebduška,* Jan Korb,† and Petr Dráber[2]***

**Engagement of the FcεRI in mast cells and basophils leads to a rapid tyrosine phosphorylation of the transmembrane adaptors LAT (linker for activation of T cells) and NTAL (non-T cell activation linker, also called LAB or LAT2). NTAL regulates activation of mast cells by a mechanism, which is incompletely understood. Here we report properties of rat basophilic leukemia cells with enhanced or reduced NTAL expression. Overexpression of NTAL led to changes in cell morphology, enhanced formation of actin filaments and inhibition of the FcεRI-induced tyrosine phosphorylation of the FcεRI subunits, Syk kinase and LAT and all downstream activation events, including calcium and secretory responses. In contrast, reduced expression of NTAL had little effect on early FcεRI-induced signaling events but inhibited calcium mobilization and secretory response. Calcium response was also repressed in Ag-activated cells defective in Grb2, a major target of phosphorylated NTAL. Unexpectedly, in cells stimulated with thapsigargin, an inhibitor of the endoplasmic reticulum $Ca^{2+}$ ATPase, the amount of cellular NTAL directly correlated with the uptake of extracellular calcium even though no enhanced tyrosine phosphorylation of NTAL was observed. The combined data indicate that NTAL regulates FcεRI-mediated signaling at multiple steps and by different mechanisms. At early stages NTAL interferes with tyrosine phosphorylation of several substrates and formation of signaling assemblies, whereas at later stages it regulates the activity of store-operated calcium channels through a distinct mechanism independent of enhanced NTAL tyrosine phosphorylation. *The Journal of Immunology*, 2007, 179: 5169–5180.**

Aggregation of FcεRI in mast cells and basophils triggers numerous signaling steps, which eventually lead to degranulation and cytokine production. Early signaling events involve sequential activation of Src family protein tyrosine kinases Lyn and Fyn, and Syk/Zap family kinase Syk (1–4). The kinases phosphorylate several substrates, including $\beta$ and $\gamma$ subunits of the FcεRI and transmembrane adaptor protein linker for activation of T cells (LAT).[3] Phosphorylated LAT becomes a docking site for phospholipase C (PLC)$\gamma$1 and PLC$\gamma$2 and some other Src homology 2 (SH2) domain containing signaling proteins, namely Grb2 adaptor (5, 6). Recently two groups have identified in mast cells another transmembrane adaptor protein called NTAL (non-T cell activation linker) or LAB (linker for activation of B cells) (7, 8), a product of the Williams-Beuren syndrome gene, *Wbscr5*. This protein, also expressed in B cells and NK cells but not in resting T cells, resembles LAT in possessing a short extracellular domain, a single transmembrane region, and a cytoplasmic tail with two palmitoylation cysteine residues and evolutionary conserved motifs containing tyrosine residues. Five of these motifs are of the YXN type (where X is any amino acid), and thus are potential binding sites for the SH2 domain of the cytosolic adaptor protein Grb2. However, unlike LAT, NTAL does not possess a consensus binding motif for PLC$\gamma$1 and PLC$\gamma$2 (7–9).

An important role of NTAL in immunoreceptor signaling was inferred from experiments in which diminution of NTAL expression by silencing RNA oligonucleotides resulted in reduced BCR-mediated activation of MAPK in A20 cell line (8), as well as impaired degranulation in FcεRI-activated human mast cells (9). Unexpectedly, bone marrow-derived mast cells (BMMCs) isolated from NTAL-deficient mice were hyperresponsive to stimulation via the FcεRI, as evidenced by enhanced tyrosine phosphorylation of several substrates, calcium response, degranulation, and cytokine production. However, BMMCs obtained from mice lacking both LAT and NTAL had a more severe block in FcεRI-mediated signaling than BMMCs deficient in LAT alone (10, 11), suggesting

*Department of Signal Transduction, †Department of Micromorphology of Biopolymers, Institute of Molecular Genetics, Academy of Sciences of the Czech Republic, and ‡Center for Research in Diabetes, Metabolism and Nutrition, 3rd Medical Faculty, Charles University, Prague, Czech Republic

Received for publication March 23, 2007. Accepted for publication August 7, 2007.

The costs of publication of this article were defrayed in part by the payment of page charges. This article must therefore be hereby marked *advertisement* in accordance with 18 U.S.C. Section 1734 solely to indicate this fact.

[1] This work was supported by projects 1M6837805001 (Center of Molecular and Cellular Immunology) and LC-545 from Ministry of Education, Youth and Sports of the Czech Republic; Grants 204/05/H023 and 301/06/0361 from the Grant Agency of the Czech Republic; Grants A5052310 and 1QS500520551 from the Grant Agency of the Academy of Sciences of the Czech Republic; and Institutional project AVOZ50520514. The research of P.D. and P.H. was supported, respectively, by an International Research Scholar's award from Howard Hughes Medical Institute and Research goal MSM0021620814 from the 3rd Faculty of Medicine, Charles University, Prague.

[2] Address correspondence and reprint requests to Dr. Petr Dráber, Department of Signal Transduction, Institute of Molecular Genetics, Academy of Sciences of the Czech Republic, Videňská 1083, Prague, Czech Republic. E-mail address: draberpe@biomed.cas.cz

[3] Abbreviations used in this paper: LAT, linker for activation of T cells; PLC, phospholipase C; SH2, Src homology 2; NTAL, non-T cell activation linker; BMMC, bone marrow-derived mast cell; RBL, rat basophilic leukemia; SOC, store-operated $Ca^{2+}$; BSS, buffered saline solution; NP-40, Nonidet P-40; $PIP_2$, phosphatidylinositol 4,5-bisphosphate; $IP_3$, inositol 1,4,5-trisphosphate; $[Ca^{2+}]_i$, concentration of free intracellular $Ca^{2+}$; PIP3, phosphatidylinositol 3,4,5-trisphosphate; TNP, trinitrophenyl.

that under certain circumstances NTAL may exert a positive signaling role even in BMMC.

Positive regulatory role of NTAL in immunoreceptor signaling was also observed in studies with immature chicken B cell line, DT40 (12). In these cells, Grb2 negatively regulates the $Ca^{2+}$ response through its binding to so far unidentified suppressor. It has been shown that SH2-mediated binding of Grb2 to tyrosine phosphorylated NTAL resulted in sequestering of the Grb2 inhibitory complex away from the cytosol, enhancing thus the calcium response. However, the role of NTAL in $Ca^{2+}$ signaling is more complex as indicated by previous studies describing enhanced calcium responses in NTAL-deficient BMMCs (10, 11).

To enlighten the role of NTAL in FcεRI signaling, we investigated by genetic and biochemical approaches the properties of rat basophilic leukemia (RBL) cells with enhanced or reduced expression of NTAL, and cells defective in Grb2 alone or in combination with NTAL. Our data indicate multiple regulatory roles of NTAL in FcεRI signaling in mast cells and document for the first time that activity of the store-operated $Ca^{2+}$ (SOC) channels could be regulated by NTAL even in the absence of its enhanced tyrosine phosphorylation.

## Materials and Methods

### *Abs, reagents, and cell cultures*

The following mAbs were used: anti-Syk (13), anti-Lyn (14), anti-LAT (15), anti-FcεRI β subunit (JRK) (16), trinitrophenyl (TNP)-specific IgE mAb (IGEL b4 1) (17), DNP-specific IgE (18), and anti-NTAL (NAP-07; Exbio). Phospho-Tyr-specific mAb (PY-20), conjugated to HRP, was purchased from Transduction Laboratories. Rabbit polyclonal Abs specific for Syk, Lyn, LAT, and NTAL were prepared by immunization with recombinant fragments of Syk (13), Lyn (14), LAT (15) or rat NTAL (aa 30–196; GenBank accession no. Q8CGL2), respectively. Rabbit anti-IgE was prepared by immunization with whole IGEL b4 1. Polyclonal Abs specific for PLCγ1, PLCγ2, Erk1, phospho-Erk (specific for phosphorylated $Tyr^{204}$), Grb2, Akt1, phospho-Akt1 (specific for phosphorylated $Ser^{473}$), and HRP-conjugated donkey anti-goat IgG, goat anti-mouse IgG and goat anti-rabbit IgG, were obtained from Santa Cruz Biotechnology. Rabbit anti-PI3K p85 subunit Ab (a mixture of equal amounts of antisera against the intact p85 subunit and the N-SH2 region of PI3K) was obtained from Upstate Biotechnology. Goat anti-mouse IgG and anti-rabbit IgG conjugated to colloidal gold particles of 10- or 5-nm were obtained from Amersham Biosciences. Fura-2/AM and $^{45}Ca$ (sp. act. 566 MBq/mg $Ca^{2+}$) were purchased, respectively, from Molecular Probes and MP Biomedicals. Origin of RBL cells (clone 2H3) and their culture conditions have been described (19).

### *Cloning of rat NTAL cDNA and its sequencing*

Based on the nucleotide sequence of human *Wbscr5* (GenBank accession no. AF045555) and mouse *Wbscr5* (AF139987) we used 5′ primer 5′-AAAGAATTCGTCAGTGGTGTTGGCATCAGC-3′ (*Eco*RI site underlined) and 3′ primer 5′-AAAAAGCTTGGGCTTCCAGTCAGCACAG TC-3′ (*Hind*III site underlined) to amplify the *NTAL* cDNA from RBL cells by RT-PCR as described (20). The PCR product was digested with *Eco*RI and *Hind*III and ligated into pGEM3Z vector (Promega). The plasmid was amplified and the sequence of the insert was verified by DNA sequencing. All primers used in this study were obtained from Generi Biotech.

### *Construction of plasmid vectors and isolation of cell lines with changes in expression of NTAL and/or Grb2*

Mouse *NTAL* cDNA was obtained from V. Hořejší and cloned into *Eco*RI site of pcDNA3.1/Zeo vector (Invitrogen). The plasmid, pZeo-NTAL-1, was isolated and its sequence confirmed by sequencing. The plasmid or empty pcDNA3.1/Zeo vector (negative control) were transfected into RBL cells by electroporation (250 V and 750 μF) using Gene Pulser (Bio-Rad). Colonies resistant to zeocin (300 μg/ml) were then isolated, and clones with enhanced expression of NTAL were selected.

For production of NTAL− and Grb2-specific RNA silencing vectors, two sets of oligonucleotides, 5′-TTTGAACTCCTACGAGAATGTGCTC GGAAGCTTGCGAGCACATTCTCGTAGGAGTTTTTTT-3′ and 5′-CT AGAAAAAAACTCCTACGAGAATGTGCTCGCAAGCTTCCGAGCA CATTCTCGTAGGAGTT-3′ (for NTAL), and 5′-TTTGAATAGATTAC CACAGATCAACATAAGCTTTTGTTGATCTGTGGTAATCTATTTTT TT-3′ and 5′-CTAGAAAAAAATAGATTACCACAGATCAACAAAAG CTTATGTTGATCTGTGGTAATCTATT-3′ (for Grb2) were annealed and cloned into mU6pro vector as described (21). These sequences upon expression form hairpins using the loops in the middle of the sequences (underlined). The plasmids, pU6/siNTAL and pU6/siGrb2 were amplified, the sequences of the inserts were verified by DNA sequencing, and co-transfected at a ratio 10:1 with pstNeoB vector (22) into RBL cells by electroporation. In some experiments RBL cells were transfected with a mix of plasmids, pU6/siGrb2, pU6/siNTAL and pSTneoB at a ratio 5:5:1. Negative controls included empty mU6pro vector or mU6pro vector with the annealed NTAL insert as above except that two mismatches were introduced at positions 30 and 50 (pU6/NTAL-30/50). Clones resistant to antibiotic G418 (0.4 mg/ml) were isolated and analyzed by immunoblotting for NTAL and/or Grb2 expression.

### *Cell activation, immunoprecipitation, and immunoblotting*

Cells were harvested, resuspended in culture medium at a concentration $10 \times 10^5$ cells/ml and sensitized with IgE (IGEL b4 1; ascites diluted 1/1000). After 30 min at 37°C the cells were washed in buffered saline solution (BSS) containing 20 mM HEPES (pH 7.4), 135 mM NaCl, 5 mM KCl, 1.8 mM $CaCl_2$, 1 mM $MgCl_2$, 5.6 mM glucose, and 0.1% BSA, and challenged with Ag (TNP-BSA) for different time intervals. When the cells were activated with thapsigargin, the sensitization step was omitted. Toward the end of the activation period the cells were briefly centrifuged, and β-glucuronidase released into supernatant was determined as described (23) using 4-methylumbelliferyl β-D-glucuronide (Sigma-Aldrich) as a substrate. The cell pellets were lysed in an ice-cold lysis buffer containing 50 mM Tris-HCl (pH 7.4), 150 mM NaCl, 2 mM EDTA, 10 mM β-glycerophosphate, 1 mM $Na_3VO_4$, 1 mM PMSF, 1 μg/ml aprotinin, 1 μg/ml leupeptin, and supplemented with 1% Nonidet P-40 (NP-40) (for Lyn, Syk, Erk), 0.2% Brij 96 (for FcεRI) or 1% NP40 plus 1% *n*-dodecyl β-D-maltoside (for NTAL and LAT). In experiments analyzing the association of proteins with large signaling assemblies, the activated or nonactivated cells were resuspended in ice-cold PBS supplemented with 0.1% saponin, 5 mM $MgCl_2$ and 1 mM $Na_3VO_4$ (permeabilization buffer). After 5 min of incubation on ice, the cells were spun down and extracted for 15 min in a lysis buffer containing 1% Triton X-100. Postnuclear supernatants were immunoprecipitated with corresponding Abs prebound to UltraLink-immobilized protein A or G (Pierce), size fractionated by SDS-PAGE and immunoblotted with PY-20-HRP conjugate or with protein-specific Abs followed by an appropriate second stage HRP-conjugated anti-mouse or anti-rabbit IgG. HRP signal was detected by the ECL reagent (Amersham Biosciences). Tyrosine-phosphorylated Erk and Akt were determined by direct immunoblotting with phosphospecific Abs. Immunoblots were quantified by Luminescent Image Analyzer LAS 3000 (Fuji Photo Film) and further analyzed by AIDA image analyzer software (Raytest). The amount of tyrosine-phosphorylated proteins was corrected for the amount of proteins immunoprecipitated as determined by densitometry of immunoblots after stripping of the membranes, followed by development with the corresponding Abs.

### *Flow cytofluorometry analysis of FcεRI and F-actin*

To determine the surface FcεRI, cells were exposed to 1 μg/ml anti-TNP IgE followed by FITC-conjugated anti-mouse IgG cross-reacting with mouse IgE, and probed by flow cytofluorometry using a FACSCalibur (BD Biosciences). The total amount of polymeric actin was measured as previously described (24, 25). In brief, $10^5$ cells in 200 μl of BSS-BSA were sensitized with IgE and stimulated or not with Ag for various time intervals. The reaction was terminated by adding 300 μl of PBS containing 50 μg of lysophosphatidylcholine, 6% formaldehyde, and 0.125 μg/ml FITC-phalloidin (Sigma-Aldrich). After 10 min of incubation at 37°C, the cells were centrifuged and resuspended in 1 ml of PBS before flow cytofluorometry analysis. The geometric mean fluorescence intensity was determined for each sample, and data points were plotted relative to the mean fluorescence intensity of nonactivated control cells.

### *Cytokine detection*

Quantitative measurements of rat TNF-α was performed using murine TNF-α ELISA development kit (cross-reacting with rat TNF-α; PeproTech) according to the manufacturer's instructions.

### *Lyn kinase assay*

In vitro Lyn kinase assay was performed as previously described (26). In brief, Lyn was immunoprecipitated from cells lysed by sequential

treatment with 0.1% saponin and 1% Triton X-100. Saponin/Triton X-100-extracted material was incubated with rabbit anti-Lyn Ab and the immunocomplexes were collected on protein A beads. The kinase reaction was conducted for 30 min at 37°C in kinase buffer (25 mM HEPES (pH 7.2) 3 mM $MnCl_2$, 0.1% NP-40, 100 mM $Na_3VO_4$, 20 mM $MgCl_2$) containing 1 $\mu$Ci [$\gamma$-$^{32}$P]ATP (Amersham Biosciences), 100 $\mu$M cold ATP, and 0.5 $\mu$g/$\mu$l denatured enolase as exogenous substrate. The kinase reaction products were resolved by SDS-PAGE, transferred to nitrocellulose, visualized by autoradiography, and quantified by Fuji Bio-Imaging Analyzer Bas 5000.

### *Electron microscopy*

Plasma membrane sheets were prepared from nonactivated or activated cells and examined by electron microscopy as described (27) with some modifications (28).

### *Immune complex PI3K and PLC$\gamma$ assay*

PI3K and PLC$\gamma$ enzymatic activity was measured as previously described (25). In brief, Fc$\varepsilon$RI-activated or control cells ($2 \times 10^6$) were solubilized in lysis buffer supplemented with 1% Triton X-100. PI3K in postnuclear supernatant was immunoprecipitated with anti-PI3K p85 subunit Ab and immunocomplexes were collected on UltraLink-immobilized protein A. PI3K assay was initiated by addition of 25 $\mu$l of kinase buffer (20 mM HEPES (pH 7.4), 20 mM $MgCl_2$, and 0.25 mM EGTA) containing 10 $\mu$g of sonicated phosphatidylinositol (Sigma-Aldrich) and 37 kBq [$\gamma$-$^{32}$P]ATP. After 30 min at 25°C, the reaction was terminated and lipids were separated on TLC Silica gel-60 plate (Merck) in a mixture of chloroform/methanol/4 M ammonium hydroxide (9:7:2, v/v/v) for 1 h. $^{32}$P-labeled materials were visualized by autoradiography and quantified by Fuji Bio-Imaging analyzer Bas 5000.

To determine the PLC$\gamma$ enzymatic activity, postnuclear supernatants from nonactivated or activated cells were immunoprecipitated with anti-PLC$\gamma$1 and immunocomplexes were collected on beads of UltraLink-immobilized protein A. The beads were washed and resuspended in 25 $\mu$l of reaction buffer followed by addition of 10 $\mu$l substrate solution (25 mM sodium phosphate (pH 6.8), 50 mM KCl, 2.5% Triton X-100, 6 $\mu$g of phosphatidylinositol 4,5-bisphosphate ($PIP_2$)) supplemented with 1.1 kBq of P[$^3$H]$IP_2$ (PerkinElmer Life Sciences). After 30 min at 37°C, the reaction was stopped by adding 300 $\mu$l of ice-cold 0.5% BSA in PBS. The samples were centrifuged and 300-$\mu$l aliquots of the supernatant were mixed with 100 $\mu$l of ice-cold 25% (w/v) TCA. Precipitates were removed by centrifugation, and supernatants were collected for quantification of released [$^3$H]inositol 1,4,5-trisphosphate ($IP_3$) by liquid scintillation counting.

### *$IP_3$ determination*

The procedure used a commercially available [$^3$H]$IP_3$ radioreceptor assay kit and followed the manufacturer's protocol (PerkinElmer Life Sciences). In brief, IgE-sensitized cells ($6 \times 10^6$) were stimulated or not with TNP-BSA (500 ng/ml) in 500 $\mu$l BSS-BSA. At various time intervals the reactions were terminated by adding 100 $\mu$l of ice-cold 100% TCA and the tubes were incubated on ice for 15 min. After centrifugation, supernatants were incubated for 15 min at room temperature and then mixed with a mixture of 1,1,2-trichloro-1,2,2,-trifluoroethane-trioctylamin (3:1). The tubes were vortexed, centrifuged, and water phase was used for determination the radioactivity bound to $IP_3$-binding protein.

### *Measurement of intracellular $Ca^{2+}$ concentrations*

Changes in the concentration of free intracellular $Ca^{2+}$ [$Ca^{2+}$]$_i$ were determined using fura-2/AM as a probe as previously described (23). IgE-sensitized and control cells were resuspended in BSS-BSA supplemented with 2.5 mM probenecid and 2 $\mu$M fura-2/AM. After 40 min at 37°C, the cells were washed with BSS-BSA-probenecid and immediately before measurement briefly centrifuged and resuspended in BSS-BSA. The levels of [$Ca^{2+}$]$_i$ were monitored using luminescence spectrometer LS-50B (PerkinElmer Life Sciences) with excitation wavelengths 340 and 380 nm, and with constant emission at 510 nm. The values were calculated using ICBC Calibration PerkinElmer Fluorescence WinLab software (PerkinElmer Life Sciences).

### *Uptake of extracellular calcium*

Calcium uptake was determined by a modified previously described procedure (29). Briefly, the cells ($2 \times 10^6$) were resuspended in 100 $\mu$l of BSS-BSA with 1 mM $Ca^{2+}$, mixed with 100 $\mu$l of BSS-BSA supplemented with $^{45}Ca^{2+}$ and various concentrations of thapsigargin, and incubated for 5 min at 37°C. The reaction was terminated by placing the tubes on ice followed by suspending 100-$\mu$l aliquots on the wall of the microtest tube separated by air space from the 12% BSA in PBS (300 $\mu$l) at the bottom. Cells with bound $^{45}Ca$ were separated from free $^{45}Ca^{2+}$ by centrifugation at $1200 \times g$ for 15 min at 4°C through 12% BSA. The cell pellets were recovered by freezing the tubes, slicing off the tube bottom, and solubilized with 1 ml of 1% Triton X-100. The radioactivity was measured in 10 ml of scintillation liquid (EcoLite; ICN Biomedicals) in a scintillation counter with QuantaSmart software (PerkinElmer). The efflux of calcium was determined in cells loaded with $^{45}Ca^{2+}$ after 2 $\mu$M thapsigargin-induced $^{45}Ca^{2+}$ influx for 15 min at 37°C. The cells were then washed and incubated in BSS-BSA containing 1 mM $Ca^{2+}$ for different time intervals. The amount of cell-associated $^{45}Ca^{2+}$ was determined after removing free extracellular $^{45}Ca^{2+}$ as described above.

## Results

### *Generation and initial characterization of mast cell lines with enhanced or reduced expression of NTAL*

To prepare RNA silencing probes specific for rat NTAL, we first cloned rat NTAL (*Wbscr5*) cDNA (GenBank accession no. AY170849). As shown in Fig. 1*A*, the predicted amino acid sequence of rat NTAL (204 aa) is one amino acid longer than its mouse ortholog (GenBank accession no. NM_020044). All tyrosine motifs as well as a potential palmitoylation site (CxxC motif) are conserved in rat and mouse NTAL sequence, suggesting identical functions.

Next, we transfected RBL cells with pZeo-NTAL-1 vector containing mouse NTAL cDNA or empty pcDNA3.1/Zeo vector, and isolated stable cell lines resistant to zeocin. We also isolated RBL cells transfected with pU6/siNTAL-1, encoding rat NTAL-specific hairpin small interferring RNA (siRNA), and pstNeoB, and isolated G418-resistant stable cell lines. As controls, G418-resistant cells after transfection with pU6/NTAL-30/50 and pstNeoB were also isolated. The expression levels of NTAL in individual clones are shown in Fig. 1*B*. Compared with control RBL cells, there was an up to 7.4-fold increase in the expression of NTAL in cells after transfection with pZeo-NTAL-1, and almost no detectable endogenous NTAL in cells transfected with pU6/siNTAL-1 (>95% inhibition). Lyn (Fig. 1*B*) and several other signaling proteins (see below) were not affected by the transfection and knock-down procedure. Cells transfected with empty pcDNA3.1/Zeo, pU6/NTAL-30/50 or pstNeoB vector did not differ in NTAL expression and their secretory response from untransfected RBL cells; only control RBL cells are therefore presented in Fig. 1*B* and other figures.

After stimulation of RBL cells with Ag, NTAL was phosphorylated on tyrosine residues as detected by immunoblotting with PY-20-HRP conjugate (Fig. 1*C*, *top*). We confirmed previous data (7, 8, 10–12) that phosphorylated NTAL bound the Grb2 adaptor (Fig. 1*C*, *middle*); the amount of bound Grb2 correlated with that of phosphorylated NTAL present.

The relationship between the amount of NTAL and Fc$\varepsilon$RI-mediated degranulation was estimated by the production of $\beta$-glucuronidase in individual cell lines at various time intervals after triggering with Ag (Fig. 1, *D* and *E*). In cells expressing high levels of NTAL (3B/18, 3B/17 and 2A/4), the secretory response was reduced to ~50% of that found in control RBL cells or cells transfected with empty vector (not shown). In the cell line with lower level of exogenous NTAL expression (1A/1), the secretory response was inhibited less, indicating a correlation between the inhibitory effect and the extent of NTAL overexpression. The secretory response of 2A/4 cells was reduced at all concentrations of Ag used; two other clones with high NTAL levels (3B/18 and 3B/17) exhibited similar properties. To simplify the presentation, only data from clone 2A/4 (NTAL+) are included in Fig. 1*F* and other figures. The secretory response was also inhibited in all cell lines with decreased amount of NTAL (Fig. 1*E*) at all concentrations of Ag used; only

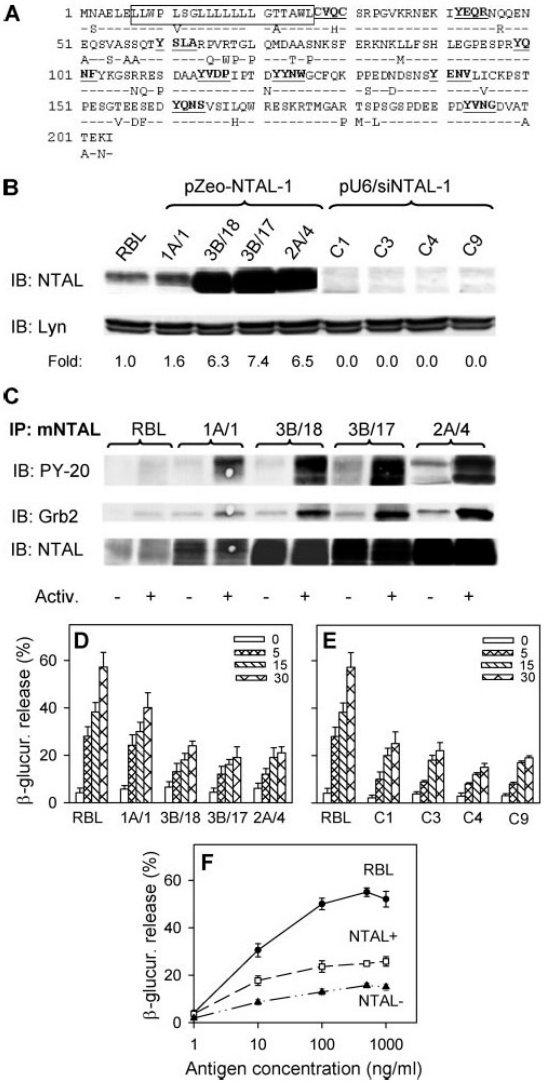


**FIGURE 1.** Rat NTAL cDNA sequence and initial characterization of RBL-derived cell lines with either enhanced or reduced NTAL expression. *A*, Comparison of predicted amino acid sequence of rat NTAL (*top line*) and mouse NTAL (*bottom line*; only the different amino acids are shown). In rat NTAL, the putative transmembrane region is boxed, and potential palmitoylation sequence (CVQC) and tyrosine-containing motifs are underlined and in bold. *B*, RBL cells were transfected with vector pZeo-NTAL-1 or pU6/siNTAL-1, and stable clones with, respectively, enhanced or reduced NTAL expression were selected. Total cell lysates were analyzed by immunoblotting (IB) with anti-NTAL or anti-Lyn mAbs and amounts of the corresponding proteins were quantified by densitometry. NTAL expression was normalized to control RBL cells and to the amount of Lyn in individual samples (Fold). *C*, IgE-sensitized control RBL cells or individual transfectants with enhanced expression of NTAL were activated for 5 min by Ag (TNP-BSA, 100 ng/ml; +) or incubated with BSS-BSA alone (−). Lysates from $10^7$ cells were immunoprecipitated (IP) with anti-NTAL mAb, and analyzed by immunoblotting with anti-pTyr-HRP conjugate (PY-20), anti-Grb2 and anti-NTAL Abs. *D* and *E*, IgE-sensitized control RBL cells or cells with enhanced (*D*) or decreased (*E*) expression of NTAL were stimulated for the indicated time intervals (0–30 min) with Ag (100 ng/ml) and release of β-glucuronidase was determined in individual clones. *F*, IgE-sensitized control RBL cells, or cells with enhanced [clone 2A/4 (NTAL+)] or decreased [clone C4 cells (NTAL−)] expression of NTAL were stimulated for 30 min with different concentrations of Ag and release of β-glucuronidase was determined. Data in *D–F* represent the average of three to four separate experiments, and are expressed as the mean ± SD.

data from clone C4 (NTAL−) are shown in Fig. 1*F* and other figures. The finding that FcεRI-mediated secretory response was inhibited in both NTAL+ and NTAL− cells was unexpected and induced additional experiments.

Using IgE-sensitized cells and fluorescently labeled anti-IgE we found that all cell lines differing in NTAL expression exhibited comparable amount of FcεRI as detected by flow cytometry (Fig. 2*A*). Light microscopy of cultured NTAL+ cells (Fig. 2*B*) and other NTAL overexpressors (not shown) revealed their decreased adhesion to tissue culture plastic surface, a more rounded morphology and less developed processes when compared with RBL cells. In contrast, NTAL− cells had fewer but more developed processes (Fig. 2*B*). The observed changes in morphology in NTAL− cells were probably related to an enhanced amount of F-actin observed in nonactivated cells (Fig. 2*C*). After FcεRI-triggering, the amount of F-actin rose as described before (30, 31) and remained higher in NTAL− cells than RBL cells. In contrast, in NTAL+ cells activation-induced increase in F-actin was less pronounced (Fig. 2*C*).

Electron microscopy on membrane sheets isolated from nonactivated NTAL+ cells showed NTAL distributed in clusters, which resembled NTAL clusters present in RBL cells (Fig. 2*D*, *a* and *b*; 5-nm gold particles). However, the average cluster size was higher in NTAL+ cells (94.0 ± 24.8 nm; mean ± SD, $n = 3$) than in RBL cells (48.0 ± 8.1 nm, $n = 3$). As expected, the density of NTAL-bound gold particles was elevated in NTAL+ cells (68.7 ± 23.4/$\mu m^2$) compared with RBL cells (35.9 ± 13.0/$\mu m^2$). For control we also assessed the distribution of gold particles in NTAL− cells, where only background levels were found (Fig. 2*Dc*); the numbers of FcεRI β subunit were comparable in RBL, NTAL+ and NTAL− cells (Fig. 2*D*, *a–c*; 10-nm gold particles). In Ag-activated cells, FcεRI formed clusters within osmiophilic regions, which were often associated, but not intermixed, with NTAL clusters; the NTAL average cluster sizes and label densities were analogous to those in nonactivated cells. Ag-induced formation of FcεRI clusters in osmiophilic regions of the plasma membrane was not affected by enhanced or reduced NTAL expression (Fig. 2*D*, *d–f*), suggesting that the expression of NTAL does not interfere with receptor aggregation.

### *NTAL overexpression inhibits the FcεRI-induced tyrosine phosphorylation of FcεRI subunits, Syk, and LAT*

Next we assessed the tyrosine phosphorylation of several proteins known to be pivotal for initial phases of FcεRI signaling. When total cell lysates from nonactivated or Ag-activated cells were analyzed by SDS-PAGE and immunoblotting with phosphotyrosine-specific mAb, NTAL+ cells, compared with the control RBL cells, exhibited significantly reduced tyrosine phosphorylation of several proteins (~38, 55, 70, 97, and 115 kDa) and enhanced phosphorylation of some other proteins, including a protein of ~30 kDa, presumably NTAL (Fig. 3*A*). In contrast, NTAL− cells showed a phosphorylation pattern more similar to that in control RBL cells; some proteins (e.g., ~40 and 50 kDa) showed an increase, other (~30 kDa (presumably NTAL) and ~70 kDa) a decrease in phosphorylation.

To analyze individual molecules, we first immunoprecipitated FcεRI, Syk, or LAT from control and Ag-activated cells and found

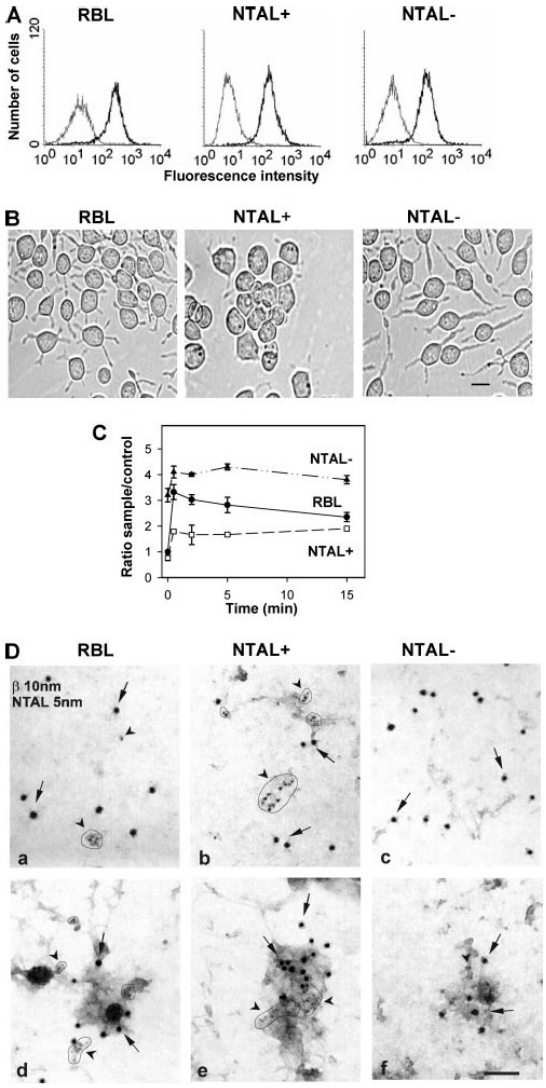


**FIGURE 2.** Expression of FcεRI, cell morphology, actin polymerization, and topography of NTAL on plasma membrane sheets. *A*, The cells were stained for surface FcεRI by sequential exposure to TNP-specific IgE (thick line; 1 μg/ml) or PBS alone (negative control; thin line) followed by anti-mouse IgE-FITC conjugate. The samples were analyzed by flow cytometry. *B*, Phase contrast images of cells cultured for 48 h under standard conditions. Bar, 10 μm. *C*, Actin polymerization in nonactivated or Ag-activated cells. The cells were sensitized with TNP-specific IgE (1 μg/ml) and then activated by Ag (TNP-BSA; 100 ng/ml) for the indicated time intervals. The amount of F-actin was determined by flow cytometry. Means ± SD were calculated from three independent experiments. *D*, Membrane sheets were prepared from resting cells (*a–c*) or from Ag-activated cells (DNP-BSA, 1 μg/ml, 2 min; *d–f*), and double-labeled from the cytoplasmic side of the plasma membrane for FcεRI β subunit (10-nm gold particles, arrows) and NTAL (5-nm gold particles, arrowheads). Bar, 100 nm.

decreased tyrosine phosphorylation of all of those proteins during activation of NTAL+ cells, compared with RBL cells (Fig. 3, *B–G*). In NTAL− cells, phosphorylation of FcεRI β and γ subunit, Syk and LAT was comparable to that in RBL cells. Phosphorylation of these proteins depends on Lyn kinase activity (3); we therefore also examined the binding of Lyn to FcεRI, the first well defined intermolecular interaction step in FcεRI signaling (32), and the enzymatic activity of Lyn. Immunoprecipitation studies showed a clear activation-dependent association of Lyn with FcεRI in both control RBL and NTAL− cells (Fig. 3*B*, *bottom*). In contrast, no Lyn was coprecipitated with FcεRI in NTAL+ cells. To elucidate the molecular basis of this difference we assessed Lyn kinase enzymatic activity in immunocomplex kinase assay in vitro (Fig. 3*H*). Surprisingly, Lyn kinase autophosphorylation and phosphorylation of the Lyn substrate, enolase, was higher in NTAL+ cells than in control RBL or NTAL− cells. Thus, the observed inhibition of phosphorylation of FcεRI and several other proteins is not caused by suppressed Lyn kinase activity.

### *Properties of signaling assemblies depend on NTAL expression levels*

To examine signaling assemblies during FcεRI-induced activation, the cells were first permeabilized with cholesterol-sequestering reagent saponin to release free cytoplasmic components. All membrane components, including those residing in lipid rafts and otherwise insoluble in nonionic detergents, were then efficiently solubilized with Triton X-100. In our previous study, we have found that this two-step solubilization procedure allows better estimation of formation of signaling assemblies in the course of cell activation (25). Using this two-step solubilization procedure we compared the signaling assemblies formed by Grb2, which is the major adaptor protein bound to tyrosine phosphorylated NTAL (7, 8). Immunoblotting analyses of Grb2 immunoprecipitates with PY-20 mAb showed that the amount of Grb2-associated and tyrosine phosphorylated proteins increased during Ag-mediated activation (Fig. 4*A*). One of the participating tyrosine phosphorylated proteins was LAT, as determined by its molecular mass (~38 kDa) and immunoblotting with LAT-specific Abs (Fig. 4, *A*, *B*, and *D*). Consistent with previous data (Fig. 3), the amount of phosphorylated LAT bound to Grb2 was reduced in NTAL+ cells and enhanced in NTAL− cells. There was only an insignificant decrease in the amount of LAT in Grb2 immunocomplexes from NTAL+ cells, compared with RBL cells (Fig. 4*D*), suggesting that reduced LAT phosphorylation did not remove all Grb2 binding sites. Another of the tyrosine phosphorylated proteins was NTAL, as determined by its molecular mass (~30 kDa) and immunoblotting with NTAL-specific Abs (Fig. 4, *A*, *C*, and *E*). As expected, the amount of Grb2-associated NTAL was enhanced in NTAL+ cells and undetectable in NTAL− cells.

Recently we and others have found that Grb2 immunocomplexes from Ag-activated RBL cells possess PI3K activity (28, 33, 34). To determine whether NTAL has any effect on the formation of these complexes, we measured PI3K activity in Grb2 immunoprecipitates. Data in Fig. 4*F* indicate that in resting cells the activity of PI3K in Grb2 immunoprecipitates was higher in NTAL− cells than in RBL and NTAL+ cells. After FcεRI triggering, higher activity of PI3K in Grb2 immunocomplexes was observed at all time intervals analyzed in RBL cells and even more in NTAL− cells, whereas in NTAL+ cells only a transient increase (2.1-fold after 0.5 min) was seen. When PI3K was directly immunoprecipitated and the immunocomplexes were tested for PI3K activity, all cell lines showed enhanced activity in response to FcεRI-mediated activation, and the dramatic differences between NTAL+ and NTAL− cells were less pronounced (Fig. 4*G*). Nevertheless, even under these conditions, PI3K activity associated with large signaling assemblies was higher in NTAL− cells than in RBL or NTAL+ cells. When NTAL was immunoprecipitated from RBL or NTAL+ cells, no PI3K activity was detected in

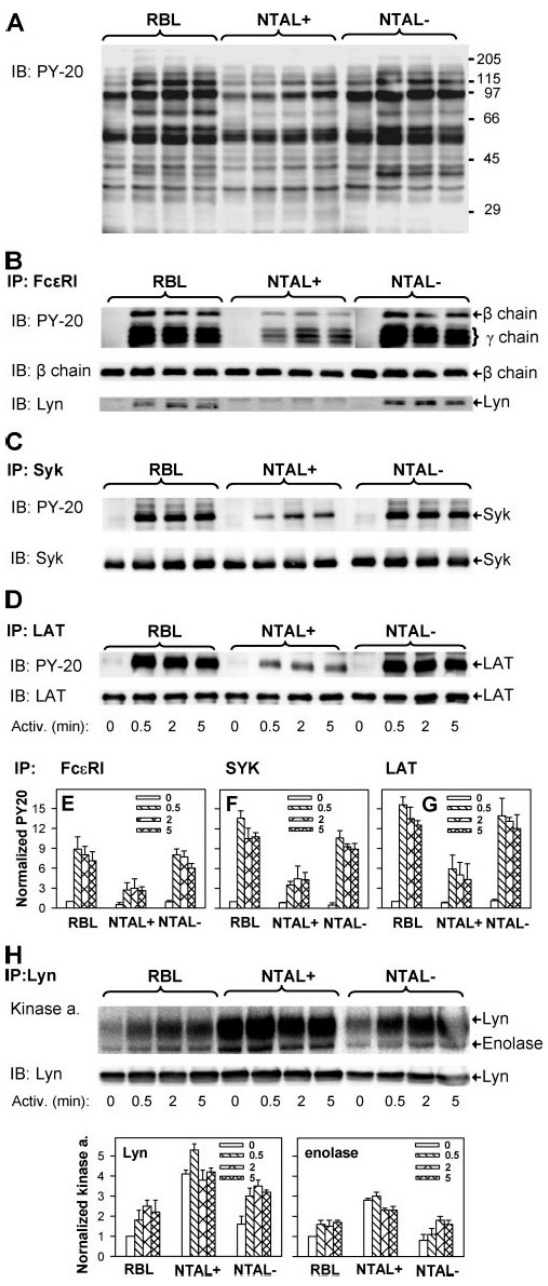


**FIGURE 3.** Overexpression of NTAL inhibits tyrosine phosphorylation of FcεRI, Syk, and LAT but enhances enzymatic activity of Lyn kinase. IgE-sensitized cells were stimulated with Ag (TNP-BSA, 500 ng/ml) for the indicated time intervals. *A*, Cells were lysed in 1% NP-40-containing lysis buffer and total cell lysates were analyzed for protein tyrosine phosphorylation by immunoblotting with PY-20-HRP conjugate. Numbers on the right indicate positions of molecular mass standards (in kDa). *B–D*, Cells were solubilized in 0.2% Brij 96 (*B*), 1% NP-40 (*C*) or a mix of 1% NP-40 and 1% *n*-dodecyl β-D-maltoside (*D*) and the target proteins were immunoprecipitated with Abs specific for IgE (*B*), Syk (*C*), or LAT (*D*) and analyzed by immunoblotting with PY-20-HRP conjugate. After stripping, the membranes were reblotted with protein-specific Abs as indicated. *E–G*, Densitometry analysis of phosphotyrosine immunoblots (as in *B–D*) normalized to the amount of the proteins immunoprecipitated and to their phosphorylation in nonactivated RBL cells. *H*, Lyn was immunoprecipitated and its enzymatic activity was determined by in vitro kinase assay using $^{32}$P-γATP and enolase as a substrate. The kinase reaction products were quantified by autoradiography and after stripping off the membranes the amount of Lyn was determined by immunoblotting. Kinase activity of Lyn, as determined by autoradiography of $^{32}$P-labeled Lyn and enolase, normalized to the parameters in nonactivated RBL cells and corrected for the amount of Lyn in each immunoprecipitate is also indicated. Means ± SD in *E–H* were calculated from three experiments.

immunoprecipitates from either nonactivated or FcεRI-activated cells (not shown). Thus, NTAL does not form complexes possessing PI3K activity, but inhibits the formation of functional PI3K-Grb2 complexes.

Enzymatic activity of PI3K results in the production of phosphatidylinositol 3,4,5-trisphosphate (PIP3). PIP3 and phosphatidylinositol 3,4-bisphosphate recruit Akt to the plasma membrane, where it is phosphorylated and activated. Phosphorylation of Akt was enhanced after FcεRI triggering in RBL cells (Fig. 4*H*). In nonactivated NTAL+ cells the amount of Akt and phospho-Akt associated with saponin-permeabilized cells was higher, but the changes faded out 2 and 5 min after FcεRI triggering. In accordance with the enhanced activity of PI3K in NTAL− cells (Fig. 4*G*), the amount of membrane-bound Akt and its phosphorylation was also enhanced. These data support the concept that NTAL regulates the formation of signaling assemblies containing PI3K and Akt.

### *Cytokine TNF-α production in NTAL$^+$ and NTAL$^-$ cells*

Previous experiments showed that production of several inflammatory mediators, including TNF-α, is enhanced in FcεRI-activated BMMC from NTAL-deficient mice (11). Central to regulation of cytokine gene transcription is Ras/Raf/MEK/Erk signaling pathway (35–37). As expected, enhanced tyrosine phosphorylation of Erk was indeed observed in NTAL$^{-/-}$ BBMC (10). In additional experiments we therefore examined phosphorylation of Erk and secretion of TNF-α in NTAL+ and NTAL− RBL cells. Immunoblotting experiments showed that the amount of tyrosine phosphorylated Erk in Ag-activated RBL cells was increased, reaching the peak 2 min after triggering (Fig. 5*A*). NTAL overexpression resulted in an impaired phosphorylation of Erk. In contrast, the onset of Erk phosphorylation in NTAL− cells was faster and remained higher at all time intervals tested. Inhibition of Erk phosphorylation in NTAL+ cells correlated with an inhibition of TNF-α secretion from the cells activated by two different doses of Ag (Fig. 5*B*). In NTAL− cells, Ag-induced secretion of TNF-α was, surprisingly, also reduced, but less dramatically than in NTAL+ cells and only at lower Ag concentration (100 ng/ml); no inhibition was observed at 500 ng/ml. These data suggest that NTAL in NTAL+ cells negatively regulates cytokine production through inhibition of Ras/Raf/MEK/Erk signaling pathway. In NTAL− cells this pathway is potentiated; the observed inhibition of TNF-α production in NTAL− cells seems therefore to reflect some positive effects of NTAL on later stages of mast cell signaling (see below).

### *Expression levels of NTAL modulate activity of PLCγ*

Immunoblotting analyses of PLCγ1 and PLCγ2 immunoprecipitates from saponin/Triton X-100 solubilized cells showed that the amount of tyrosine phosphorylated PLCγ1 associated with signaling assemblies decreased in both NTAL+ cells and NTAL− activated cells (Fig. 6*A*). Recruitment of PLCγ2 and

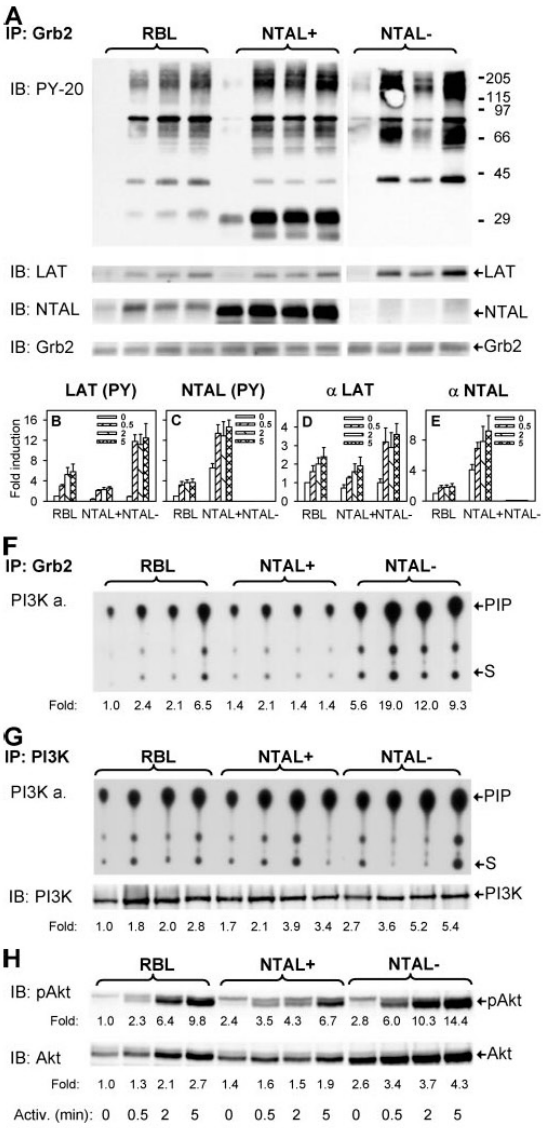


**FIGURE 4.** Changes in Grb2 signaling assemblies, PI3K activity and tyrosine phosphorylation of Akt. Cells were activated as in Fig. 3, solubilized with saponin/Triton X-100 procedure, and Grb2 immunocomplexes were isolated by precipitation with anti-Grb2 Ab. *A*, Grb2 immunocomplexes were analyzed by immunoblotting for the presence of total tyrosine-phosphorylated proteins (PY-20), LAT, NTAL and Grb2. *B–E*, Densitometry analysis of tyrosine-phosphorylated (PY) LAT (*B*) and NTAL (*C*), and total amount of LAT (*D*) and NTAL (*E*) in Grb2 immunocomplexes. Means ± SD in *B–E* were calculated from three to four experiments. *F*, PI3K activity associated with Grb2 immunocomplexes was estimated using [$^{32}$P-γ]ATP and phosphatidylinositol as a substrate in PI3K assay (PI3K a.). Positions of [$^{32}$P]PI (PIP) and start (S) are indicated by arrows. *G*, PI3K immunoprecipitates were analyzed in parallel for PI3K enzymatic activity by PI3K assay and for the amount of immunoprecipitated PI3K by immunoblotting with anti-p85 subunit of PI3K. Enzymatic activity of PI3K normalized to its levels in nonactivated RBL cells and corrected for the amount of PI3K-p85 subunit precipitated is also indicated. *H*, The cells were solubilized with the saponin/Triton X-100 procedure and postnuclear supernatants were analyzed by immunoblotting with anti-phospho-Akt, followed by stripping and immunoblotting with Akt-specific Ab. Relative amounts of the proteins were normalized to nonactivated RBL cells. Representative data from three experiments performed are shown.

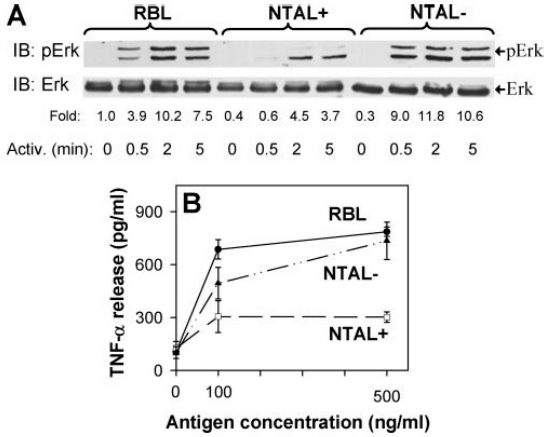


**FIGURE 5.** Changes in tyrosine phosphorylation of Erk and TNF-α production. *A*, Cells were activated as in Fig. 3 and then solubilized with 1% Triton X-100. Postnuclear supernatants were analyzed by immunoblotting with anti-phospho-Erk, followed by stripping and immunoblotting with Erk-specific Ab. Relative amounts of the proteins were normalized to nonactivated RBL cells. A typical result from three experiments is shown. *B*, IgE-sensitized cells were activated with different concentrations of Ag for 3 h and the amount of TNF-α released into supernatant was determined by ELISA. Data represent means ± SD from three experiments performed in triplicates.

degree of its phosphorylation were comparable in all cell lines (Fig. 6*B*). Enzymatic activity of PLCγ was detected by immunocomplex PLCγ assay, determining the production of [$^3$H]$IP_3$ from P[$^3$H]$IP_2$ substrate. In nonstimulated cells the activity of PLCγ was comparable in RBL, NTAL+ and NTAL− cells (Fig. 6*C*). After FcεRI triggering, PLCγ activity rapidly increased in all cell lines; however, in NTAL− cells, and especially in NTAL+ cells the increase was lower than in RBL cells. These findings were corroborated by direct measurements of $IP_3$ levels (Fig. 6*D*). In nonactivated cells $IP_3$ concentrations were similar in all cell lines under study, but in FcεRI-activated cells $IP_3$ reached higher levels in RBL cells compared with NTAL− cells, and especially to NTAL+ cells.

*Intracellular $Ca^{2+}$ mobilization and uptake of extracellular $Ca^{2+}$ are affected by NTAL expression levels*

Enhanced levels of IP3 induce a release of calcium from intracellular stores, followed by calcium influx through SOC channels in the plasma membrane (38). To determine the role of NTAL in both these steps we followed the calcium response in cells under different conditions. NTAL− cells activated with Ag in the presence of extracellular $Ca^{2+}$showed a lower calcium response than control cells, but identical initial kinetics. In contrast, NTAL+ cells exhibited a delay in calcium response and a slower decline to baseline levels (Fig. 7*A*). Activation of the cells by Ag in the absence of extracellular calcium resulted in ~30% inhibition of the calcium response in NTAL− cells relative to RBL cells, whereas in NTAL+ cells this response was dramatically inhibited and delayed (Fig. 7*B*). After increasing the concentration of extracellular $Ca^{2+}$, both RBL and NTAL− cells showed rapid increase in

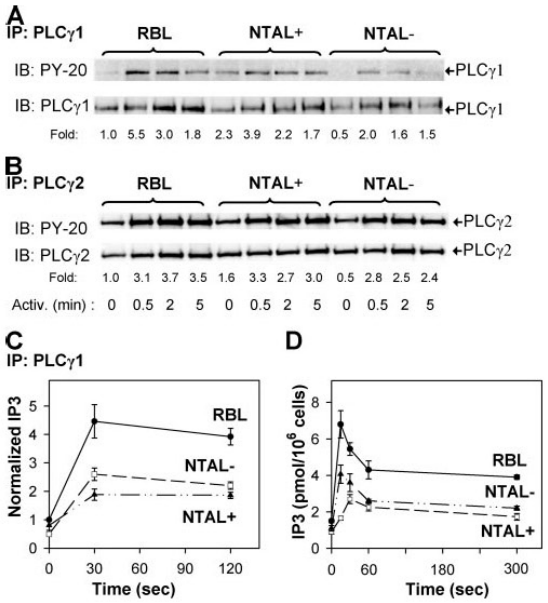


**FIGURE 6.** Changes in the properties of PLCγ1 and PLCγ2. *A* and *B*, Cells were activated as in Fig. 3, solubilized with saponin/Triton X-100 procedure, and PLCγ1 (*A*) and PLCγ2 (*B*) were immunoprecipitated and analyzed by immunoblotting with PY-20-HRP conjugate. After stripping the same membrane was reblotted with protein-specific Abs. Relative amounts of proteins were normalized to nonactivated cells. Data from representative experiments from at least three performed are shown. *C*, Cells were lysed in 1% Triton X-100, and enzymatic activity of the immunoprecipitated PLCγ1 was measured by immune complex PLCγ assay. *D*, Cellular $IP_3$ levels were determined by $^3$H-labeled radioreceptor assay kit. Data in *C and D* represent means ± SD from three to four experiments.

$[Ca^{2+}]_i$, with faster return to initial levels in NTAL− cells, whereas NTAL+ cells showed only a week response (Fig. 7*B*).

The observed dramatic decrease in calcium response in Ag-activated NTAL+ cells could be related to decreased activity of PLCγ and impaired production of IP3 (Fig. 6, *C* and *D*), and/or to negative regulatory role of NTAL in $Ca^{2+}$ mobilization at later stages. To explore the role of NTAL on $Ca^{2+}$ mobilization independently of its effect on activity of PLCγ, cells were activated by thapsigargin, an agent that induces the release of $Ca^{2+}$ from intracellular stores by inhibiting the endoplasmic reticulum ATPase (39). In the absence of extracellular $Ca^{2+}$, thapsigargin induced a small increase in $[Ca^{2+}]_i$ in all cell lines, suggesting that NTAL does not interfere with the transport of thapsigargin to its target and release of $Ca^{2+}$ from cytoplasmic stores. Interestingly, when the extracellular $Ca^{2+}$ level was restored, 5 independent experiments showed that the maximum $[Ca^{2+}]_i$ in NTAL+ cells was higher (750 ± 80 nM; mean ± SD) than in RBL cells (620 ± 54 nM) and NTAL− cells (580 ± 37). Furthermore, $[Ca^{2+}]_i$ reverted to baseline level more rapidly in NTAL− cells than in RBL and NTAL+ cells (Fig. 7*C*).

These data suggested that NTAL could regulate the transport of extracellular $Ca^{2+}$ through the plasma membrane. To test this we measured the $^{45}Ca$ uptake in thapsigargin-stimulated cells. A direct correlation was found between the amount of NTAL expressed and calcium uptake; it was high in NTAL+ cells, medium in RBL cells and low in NTAL− cells (Fig. 7*D*). The observed correlation could imply not just an important role of NTAL in regulating $Ca^{2+}$ uptake but also an inhibitory effect of NTAL on the release of $Ca^{2+}$ from the cells. Next we therefore labeled the cells with $^{45}Ca^{2+}$, washed them and measured the radioactivity retained within the cells at different time intervals. Results presented in Fig. 7*E* show that all cell lines exhibited the same kinetics of $^{45}Ca^{2+}$ efflux. Together with previous findings on $Ca^{2+}$ uptake, these data

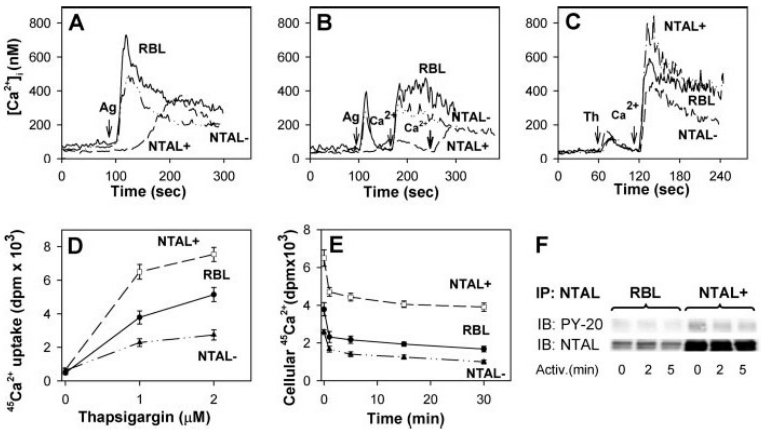


**FIGURE 7.** Intracellular $Ca^{2+}$ mobilization, extracellular $^{45}Ca$ uptake and calcium release from the cells. *A–C*, Calcium responses in fura-2 loaded RBL, NTAL+, and NTAL− cells. *A*, The cells were sensitized with IgE and stimulated in the presence of 1 mM extracellular calcium with TNP-BSA (500 ng/ml; arrow, Ag). Calcium levels were determined by spectrophotometry. *B*, Cells were stimulated with Ag in the absence of extracellular calcium (arrow, Ag) and 1 mM $Ca^{2+}$ was added after $Ca^{2+}$ calcium levels returned to original values (arrow, $Ca^{2+}$). *C*, Cells were exposed to thapsigargin (1 μM; arrow, Th) in the absence of extracellular calcium and 1 mM $Ca^{2+}$ was added later on (arrow, $Ca^{2+}$). *D*, The cells were activated with various concentrations of thapsigargin in the presence of extracellular $^{45}Ca^{2+}$ (1 mM). After 5 min at 37°C, the reaction was terminated and the cells were centrifuged through 12% BSA in BSS and cell-bound radioactivity was determined. *E*, The cells were loaded with $^{45}Ca^{2+}$ during 15-min activation with thapsigargin, unbound $^{45}Ca^{2+}$ was washed out and calcium efflux was determined at different time intervals. *F*, The cells were activated with thapsigargin (2 μM) for different time intervals and solubilized in lysis buffer containing 1% NP-40 plus 1% *n*-dodecyl β-D-maltoside. NTAL was immunoprecipitated from postnuclear supernatant and analyzed by immunoblotting with PY-20-HRP conjugate. After stripping, the membrane was reblotted with NTAL-specific Ab. Data in *A–C* and *F* are representative experiments from, respectively, three and two performed. Data in *D* and *E represent* means ± SD from four experiments performed in duplicates or triplicates.

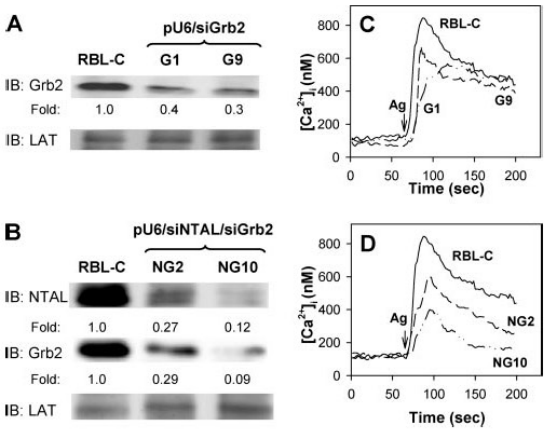


**FIGURE 8.** Positive regulatory role of Grb2 in Ag-induced $Ca^{2+}$ signaling. *A* and *B*, Immunoblotting analysis of Grb2- or Grb2/NTAL-deficient cells. RBL cells transfected with empty vector (RBL-C), pU6/siGrb2 vector (clones G1 and G9) or both pU6/siNTAL-1 and pU6/siGrb2 (clones NG2 and NG10) were lysed and postnuclear supernatants were analyzed by immunoblotting for the presence of Grb2, LAT, and NTAL. Relative amounts of Grb2 and NTAL were normalized to the amount of LAT in each sample. *C* and *D*, Calcium response in fura-2-loaded control and transfected cells. The cells were sensitized with IgE and stimulated in the presence of 1 mM extracellular $Ca^{2+}$ with TNP-BSA (500 ng/ml, arrow, Ag). Calcium levels were determined by spectrophotometry. Data are representative of at least two experiments performed.

indicate that NTAL positively regulates $Ca^{2+}$ uptake rather than $Ca^{2+}$ efflux.

Experiments with DT40 chicken B cells suggested that phosphorylated NTAL could regulate the $Ca^{2+}$ uptake by a mechanism involving its binding with Grb2, a negative regulator of $Ca^{2+}$ signaling (12). We therefore attempted to find out whether or not NTAL is phosphorylated in thapsigargin-activated cells. NTAL was immunoprecipitated from nonactivated or thapsigargin-activated RBL or NTAL+ cells and its phosphorylation was assessed by immunoblotting with PY-20-HRP. Data presented in Fig. 7*F* indicate that thapsigargin had no effect on NTAL tyrosine phosphorylation in either RBL or NTAL+ cells. To determine whether Grb2 could function as a negative regulator of $Ca^{2+}$ response in RBL cells, we transfected the cells with pU6/siGrb2 plus pSTneoB and selected G418-resistant clones, G1 and G9, with decreased amount of Grb2 (Fig. 8*A*). We also isolated RBL-derived cells with decreased amounts of both NTAL and Grb2 after simultaneous transfection with pU6/siNTAL, pU6/siGrb2 and pSTneoB (Fig. 8*B*, clones NG2 and NG10). It should be noted that the amount of LAT was not affected in any transfectant (Fig. 8, *A* and *B*), confirming the specificity of the knock-down procedure. Detailed analysis showed that Ag-activated RBL cells with decreased amount of Grb2 exhibited lower increase in $[Ca^{2+}]_i$ than RBL cells transfected with empty vector (Fig. 8*C*). When the expression of both NTAL and Grb2 was reduced, an even deeper decrease in $[Ca^{2+}]_i$ was observed (Fig. 8*D*). These data indicate that Grb2 functions as a positive regulator of $Ca^{2+}$ response in RBL cells.

## Discussion

Variation of NTAL expression levels is shown to have multiple effects on FcεRI-mediated activation events in RBL cells. Permanent cell lines with low expression were isolated after transfection with U6-based expression vector producing NTAL siRNA. In contrast to previous studies in which the transfected RNA reduced the expression levels by ~70% (9), hairpin siRNA strategy lowered it by >95%. Stable cell lines with enhanced NTAL expression were obtained after transfection of mouse NTAL cDNA under cytomegalovirus promoter. We expected that NTAL overexpression would uncover additional signaling pathways undetectable in NTAL-deficient cells if they acted downstream of the early regulatory effects of NTAL.

Initial characterization revealed that cells with increased or decreased amount of NTAL exhibited restricted secretory response after FcεRI triggering, unrelated to differences in surface expression of FcεRI and evident at all concentrations of Ag used. NTAL levels also affected morphology of the cells; NTAL+ cells being less adherent to tissue culture plastic surface and NTAL− cells having longer processes. The observed changes in cell morphology could be related to the amount of F-actin and its formation during FcεRI signaling. Thus, NTAL− cells had more F-actin than parental RBL or NTAL+ cells, and only a weak increase in F-actin formation was induced by activation of both NTAL+ and NTAL− cells.

Previously we have examined the distribution of NTAL and LAT by electron microscopy of membrane sheets. NTAL in resting RBL cells was localized in small clusters, topographically separated from clusters of LAT and FcεRI (10), but not Thy-1 (40). When membrane sheets were isolated from NTAL overexpressors, no difference in the distribution of FcεRI and NTAL was observed except that the average cluster size and density of NTAL-bound gold particles was higher in NTAL+ than control cells. Importantly, the absence of NTAL from the FcεRI aggregates is not confined just to control RBL cells, as reported previously (10), but applies also to NTAL+ cells (this study). Together with our finding of normal redistribution of aggregated FcεRI into osmiophilic regions in NTAL+ cells, these data suggest that the initial FcεRI aggregation step induced by multivalent Ag is not changed in NTAL overexpressors.

Immunochemical studies showed that overexpression of NTAL inhibited the tyrosine phosphorylation of FcεRI $\beta$ and $\gamma$ subunits, Syk and LAT in Ag-activated cells. Consequently, recruitment of PLC$\gamma$ to signaling assemblies and its tyrosine phosphorylation and activation were inhibited. Reduced production of PLC$\gamma$ metabolite IP3 led to a reduction in both the release of $Ca^{2+}$ from intracellular stores and the uptake of extracellular $Ca^{2+}$ through SOC channels. This could explain the inhibition of the secretory response in Ag-activated cells. The MAP kinase signaling pathway was also inhibited in NTAL+ cells as reflected in the impaired tyrosine phosphorylation of Erk and subsequent low secretion of TNF-$\alpha$.

Decreased tyrosine phosphorylation of FcεRI subunits in NTAL+ cells suggested that the activity of Lyn kinase is inhibited. However, immunocomplex kinase assays showed Lyn kinase activity in NTAL+ cells is undiminished, implying that NTAL interferes with the accessibility of Lyn to FcεRI. This possibility is strengthened by data indicating that the amount of Lyn coprecipitated with FcεRI was higher in activated RBL cells than in NTAL+ cells. Because Lyn, like NTAL, seems to be localized in lipid rafts (7, 41), it is possible that direct or indirect interactions of Lyn with NTAL preclude the interaction between Lyn and FcεRI subunits. Although immunoprecipitation and immunocomplex kinase assays failed to show NTAL-Lyn interactions (L. Dráberová, unpublished data), it is possible that procedures used to isolate NTAL immunocomplexes destroyed these interactions.

Our results indicate that the signaling assemblies formed in NTAL+ cells are different from those formed in control or NTAL− cells. Indeed, in Ag-activated NTAL+ cells, more NTAL

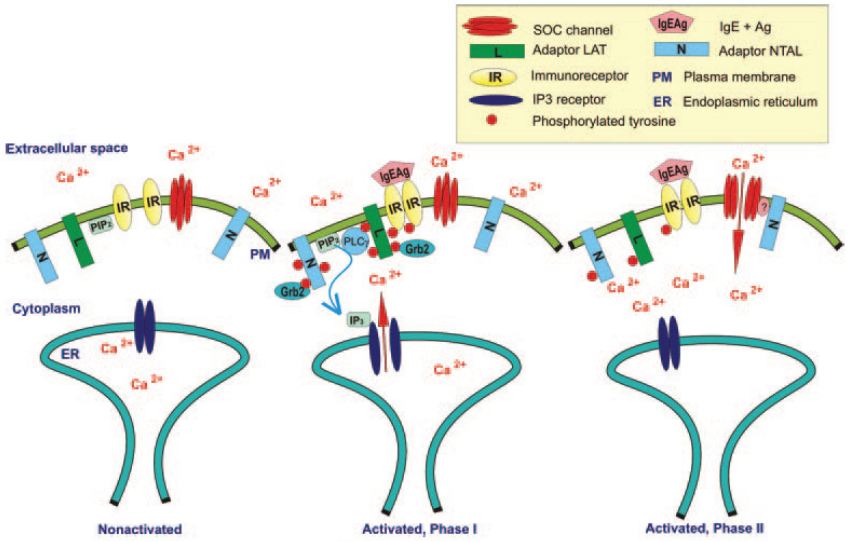


**FIGURE 9.** A model of NTAL function in FcεRI-mediated $Ca^{2+}$ signaling. At early stages after FcεRI aggregation (phase I), NTAL is rapidly tyrosine phosphorylated, competing with phosphorylation of FcεRI and LAT. Phosphorylated NTAL binds Grb2 complexes and interferes with the activity of PI3K and several other signaling molecules. NTAL affects activity of PLCγ and in this way the generation of $IP_3$ followed by release of $Ca^{2+}$ from internal stores. At later stages of activation (phase II), extracellular $Ca^{2+}$ flows into the cytoplasm through SOC channels. Activity of these channels could be modulated by direct or indirect interaction of NTAL with SOC channel proteins and/or regulators of their activity. However, this effect is independent of enhanced NTAL tyrosine phosphorylation.

and less LAT is bound to Grb2, supporting the concept of competition between NTAL and LAT for Grb2 as a substrate (10). In contrast, in activated NTAL− cells phosphorylation of FcεRI subunits, Syk and LAT was not inhibited. However, association of PLCγ with insoluble complexes, its phosphorylation and its enzymatic activity were less efficient and resulted in a partial inhibition of downstream events. The impaired function of PLCγ could reflect involvement of NTAL in the formation of signaling assemblies required for PLCγ enzymatic activity (42–44). As previously shown (10, 45), Grb2 forms complexes with SHP-2 phosphatase, and these complexes could bind to NTAL to regulate early signaling events. Alternatively, if PLCγ somehow interacts with NTAL, its enzymatic activity would be inhibited in NTAL− cells even though the early FcεRI-activation events proceed normally. Although we were unable to coprecipitate PLCγ with NTAL (L. Dráberová, unpublished data), it remains possible that these interaction are sensitive to the solubilization and immunoprecipitation procedures.

If IP3 signal generated by FcεRI aggregation is bypassed by thapsigargin, NTAL+ cells show a higher uptake of extracellular $Ca^{2+}$ than control RBL cells. This suggests that NTAL could have a positive regulatory role in $Ca^{2+}$ uptake. This is corroborated by complementary studies in which thapsigargin-activated NTAL− cells showed a lower $Ca^{2+}$ uptake. The role of NTAL in uptake of extracellular $Ca^{2+}$ is unclear but could be related to NTAL-dependent $Ca^{2+}$-regulating signal circuit recently described in DT40 B lymphocytes (12). In these cells, Grb2 plays a negative regulatory role in $Ca^{2+}$ uptake, which appears to be eliminated upon binding to NTAL. However, several pieces of evidence indicate that in rodent mast cells NTAL plays a different role in $Ca^{2+}$ response. First, no inhibition in $[Ca^{2+}]_i$ was observed in Ag-activated BMMC from $NTAL^{-/-}$ mice; rather, there was an enhancement of the $Ca^{2+}$ response (10, 11). Second, Ag-activated $NTAL^{-/-}$ BMMC showed no decrease, but rather an increase in the uptake of extracellular $^{45}Ca^{2+}$; this could be related to enhanced activity of PLCγ (10, 11). Third, there was a higher $Ca^{2+}$ response to FcεRI triggering in NTAL− cells than in NTAL+ cells. It should be emphasized that the highest $Ca^{2+}$ response was observed in control RBL cells, suggesting that an optimal concentration and/or topography of NTAL is required for maximum $Ca^{2+}$ response. Fourth, after activation by Ag in the absence of extracellular $Ca^{2+}$ and restoration of $Ca^{2+}$ level later on, there was no dramatic difference between control and NTAL− cells in initial $Ca^{2+}$ uptake. In contrast, the response in NTAL+ was markedly inhibited. This inhibition reflected low levels of $Ca^{2+}$ released from intracellular stores and consequently low $Ca^{2+}$ influx through the SOC channels. Finally, $[Ca^{2+}]_i$ in cells activated with thapsigargin in the absence of extracellular $Ca^{2+}$ was not dependent on NTAL. However, when $Ca^{2+}$ was replenished, a significant increase in $[Ca^{2+}]_i$ occurred in the following sequence: NTAL+ cells > control RBL cells > NTAL− cells. These data suggest that NTAL could play a positive role in regulating the $Ca^{2+}$ uptake at the level of SOC channels. Our finding of correlation between $^{45}Ca^{2+}$ uptake and the amount of NTAL in thapsigargin-activated cells supports the notion. The possibility that NTAL modulated $Ca^{2+}$ efflux rather then its influx was excluded by experiments measuring the kinetics of calcium release from activated $^{45}Ca^{2+}$-labeled cells. Interestingly, no increase in tyrosine phosphorylation of NTAL was observed in thapsigargin-triggered cells. Thus, our data indicate that NTAL could have a novel regulatory role in $Ca^{2+}$ uptake independent of de novo NTAL tyrosine phosphorylation.

Possible regulatory functions of NTAL at different phases of FcεRI-mediated $Ca^{2+}$ signaling are shown in Fig. 9. At early stages of activation (phase I) NTAL serves as a substrate for protein tyrosine kinases and thus could interfere with phosphorylation of FcεRI and LAT by a competitive mechanism. Furthermore, phosphorylated NTAL binds Grb2 and other signaling molecules,

which could modulate the activity of various enzymes, including PI3K and PLCγ. Enhanced activity of PLCγ leads to increased production of IP3 and consequently to elevated levels of cytoplasmic $Ca^{2+}$. At later stages of activation (phase II), NTAL could affect the function of SOC channels, reflecting its direct or indirect interactions with channel-forming proteins and/or their regulators such as Orai1 and/or Stim1 (46–49). This function of NTAL is not dependent on its enhanced tyrosine phosphorylation.

This model is based on functional analysis of cells with increased or decreased levels of NTAL. Although useful, this genetic approach has, however, its limitations. Knockdown or knockout approaches may not disclose all functions of the proteins, due to compensatory activities of other proteins. Overexpression approach, which is complementary to down-regulation approach and could reveal otherwise undetectable activities of the proteins under study, could impose indirect effects by sequestering proteins to which they bind or by targeting proteins that are not their natural targets. It is very likely that NTAL is a natural target of Lyn kinase and therefore enhanced expression of NTAL could compromise the ability of Lyn to interact with the FcεRI; this could explain the inhibition of phosphorylation of FcεRI β and γ subunits and all downstream targets in FcεRI-activated NTAL+ cells. Provided that NTAL, through its interaction with Lyn, negatively regulates phosphorylation of the FcεRI under physiological conditions, this phosphorylation should be enhanced in activated NTAL-deficient cells. Although the results of this and our previous study (10) show no clear increase in phosphorylation of the receptor in such cells, it still remains possible that enhanced Lyn-mediated phosphorylation of the FcεRI subunits in NTAL-deficient cells is compromised by enhanced activity of phosphatases. In fact, our unpublished data, showing indirect correlation between activity of the membrane-associated tyrosine phosphatases and amount of cellular NTAL, support this notion. Thus, although activities of the relevant kinases and phosphatases toward the FcεRI could be higher in NTAL-deficient than in wild-type cells, their functional equilibrium could be comparable in both cell types. When this equilibrium is shifted, e.g., by exposure of the cells to a phosphatase inhibitor, such as pervanadate, NTAL is tyrosine phosphorylated even in the absence of FcεRI aggregation (L. Dráberová, unpublished data). The combined data suggest that NTAL, through its interaction with Lyn and other signaling molecules, could contribute to setting a threshold for FcεRI-induced degranulation and cytokine response. This concept is corroborated by our findings of enhanced activity of PI3K (Fig. 4*G*) and enhanced association of Akt and pAkt with signaling assemblies (Fig. 4*H*) even in nonactivated NTAL-deficient cells.

In summary, NTAL overexpression suppresses early FcεRI-induced activation events, but has a positive effect on the uptake of extracellular $Ca^{2+}$ in thapsigargin-stimulated cells. Accordingly, inhibition of NTAL expression has no inhibitory effect on early signaling pathways but does suppress the late ones, including the uptake of extracellular $Ca^{2+}$. Expression levels of NTAL may thus regulate mast cells activation at multiple steps. Differences in interaction of NTAL with various regulatory proteins and signaling pathways (50) could explain why down-regulation of NTAL expression either inhibited (9) or enhanced (10, 11) FcεRI-induced secretory response in different mast cell types.

## Acknowledgments

We thank H. Mrázová, R. Budovičová, D. Lorenčíková, M. Dráber, I. Lišková, and J. Musilová for technical assistance; and A. Koffer for critical reading of the manuscript.

## Disclosure

The authors have no financial conflict of interest.

## References

1. Eiseman, E., and J. B. Bolen. 1992. Engagement of the high-affinity IgE receptor activates src protein-related tyrosine kinases. *Nature* 355: 78–80.
2. Minoguchi, K., W. D. Swaim, E. H. Berenstein, and R. P. Siraganian. 1994. Src family tyrosine kinase p53/56$^{lyn}$, a serine kinase and FcεRI associate with α-galactosyl derivatives of ganglioside $GD_{1b}$ in rat basophilic leukemia RBL-2H3 cells. *J. Biol. Chem.* 269: 5249–5254.
3. Parravicini, V., M. Gadina, M. Kovarova, S. Odom, C. Gonzalez-Espinosa, Y. Furumoto, S. Saitoh, L. E. Samelson, J. J. O'Shea, and J. Rivera. 2002. Fyn kinase initiates complementary signals required for IgE-dependent mast cell degranulation. *Nat. Immunol.* 3: 741–748.
4. Daëron, M., and R. Lesourne. 2006. Negative signaling in Fc receptor complexes. *Adv. Immunol.* 89: 39–86.
5. Zhang, W., J. Sloan-Lancaster, J. Kitchen, R. P. Trible, and L. E. Samelson. 1998. LAT: the ZAP-70 tyrosine kinase substrate that links T cell receptor to cellular activation. *Cell* 92: 83–92.
6. Saitoh, S., R. Arudchandran, T. S. Manetz, W. Zhang, C. L. Sommers, P. E. Love, J. Rivera, and L. E. Samelson. 2000. LAT is essential for FcεRI-mediated mast cell activation. *Immunity* 12: 525–535.
7. Brdička, T., M. Imrich, P. Angelisová, N. Brdičková, O. Horváth, J. Špička, I. Hilgert, P. Lusková, P. Dráber, P. Novák, et al. 2002. Non-T cell activation linker (NTAL): a transmembrane adaptor protein involved in immunoreceptor signaling. *J. Exp. Med.* 196: 1617–1626.
8. Janssen, E., M. Zhu, W. Zhang, S. Koonpaew, and W. Zhang. 2003. LAB: a new membrane-associated adaptor molecule in B cell activation. *Nat. Immunol.* 4: 117–123.
9. Tkaczyk, C., V. Horejsi, I. Shoko, P. Draber, L. E. Samelson, A. B. Satterthwaite, D. H. Nahm, D. D. Metcalfe, and A. M. Gilfillan. 2004. NTAL phosphorylation is a pivotal link between the signaling cascades leading to human mast cell degranulation following kit activation and FcεRI aggregation. *Blood* 104: 207–214.
10. Volná, P., P. Lebduška, L. Dráberová, Š. Šimová, P. Heneberg, M. Boubelík, V. Bugajev, B. Malissen, B. S. Wilson, V. Hořejší, et al. 2004. Negative regulation of mast cell signaling and function by the adaptor LAB/NTAL. *J. Exp. Med.* 200: 1001–1013.
11. Zhu, M., Y. Liu, S. Koonpaew, O. Granillo, and W. Zhang. 2004. Positive and negative regulation of FcεRI-mediated signaling by adaptor protein LAB/NTAL. *J. Exp. Med.* 200: 991–1000.
12. Stork, B., M. Engelke, J. Frey, V. Horejsi, A. Hamm-Baarke, B. Schraven, T. Kurosaki, and J. Wienands. 2004. Grb2 and the non-T cell activation linker NTAL constitute a $Ca^{2+}$-regulating signal circuit in B lymphocytes. *Immunity* 21: 681–691.
13. Tolar, P., L. Dráberová, and P. Dráber. 1997. Protein tyrosine kinase Syk is involved in Thy-1 signaling in rat basophilic leukemia cells. *Eur. J. Immunol.* 27: 3389–3397.
14. Dráberová, L., M. Amoui, and P. Dráber. 1996. Thy-1-mediated activation of rat mast cells: the role of Thy-1 membrane microdomains. *Immunology* 87: 141–148.
15. Tolar, P., M. Tůmová, and P. Dráber. 2001. New monoclonal antibodies recognizing the adaptor protein LAT. *Folia Biol.* 47: 215–217.
16. Rivera, J., J.-P. Kinet, J. Kim, C. Pucillo, and H. Metzger. 1988. Studies with a monoclonal antibody to the β subunit of the receptor with high affinity for immunoglobulin E. *Mol. Immunol.* 25: 647–661.
17. Rudolph, A. K., P. D. Burrows, and M. R. Wabl. 1981. Thirteen hybridomas secreting hapten-specific immunoglobulin E from mice with $Ig^a$ or $Ig^b$ heavy chain haplotype. *Eur. J. Immunol.* 11: 527–529.
18. Liu, F.-T., J. W. Bohn, E. L. Ferry, H. Yamanoto, C. A. Molinaro, L. A. Sherman, N. R. Klinman, and D. H. Katz. 1980. Monoclonal dinitrophenyl-specific murine IgE antibody: preparation, isolation, and characterization. *J. Immunol.* 124: 2728–2737.
19. Dráberová, L., and P. Dráber. 1991. Functional expression of the endogenous Thy-1 gene and the transfected murine Thy-1.2 gene in rat basophilic leukemia cells. *Eur. J. Immunol.* 21: 1583–1590.
20. Hálová, I., L. Dráberová, and P. Dráber. 2002. A novel lipid raft-associated glycoprotein, TEC-21, activates rat basophilic leukemia cells independently of the type 1 Fcε receptor. *Int. Immunol.* 14: 213–223.
21. Yu, J. Y., S. L. DeRuiter, and D. L. Turner. 2002. RNA interference by expression of short-interfering RNAs and hairpin RNAs in mammalian cells. *Proc. Natl. Acad. Sci. USA* 99: 6047–6052.
22. Katoh, K., Y. Takahashi, S. Hayashi, and H. Kondoh. 1987. Improved mammalian vectors for high expression of G418 resistance. *Cell Struct. Funct.* 12: 575–580.
23. Surviladze, Z., L. Dráberová, M. Kovářová, M. Boubelík, and P. Dráber. 2001. Differential sensitivity to acute cholesterol lowering of activation mediated via the high-affinity IgE receptor and Thy-1 glycoprotein. *Eur. J. Immunol.* 31: 1–10.
24. Howard, T. H., and W. H. Meyer. 1984. Chemotactic peptide modulation of actin assembly and locomotion in neutrophils. *J. Cell Biol.* 98: 1265–1271.
25. Dráberová, L., L. Dudková, M. Boubelík, H. Tolarová, F. Šmíd, and P. Dráber. 2003. Exogenous administration of gangliosides inhibits FcεRI-mediated mast cell degranulation by decreasing the activity of phospholipase Cγ. *J. Immunol.* 171: 3585–3593.
26. Amoui, M., P. Dráber, and L. Dráberová. 1997. Src family-selective tyrosine kinase inhibitor, PP1, inhibits both FcεRI- and Thy-1-mediated activation of rat basophilic leukemia cells. *Eur. J. Immunol.* 27: 1881–1886.

27. Wilson, B. S., J. R. Pfeiffer, and J. M. Oliver. 2000. Observing FcεRI signaling from the inside of the mast cell membrane. *J. Cell Biol.* 149: 1131–1142.
28. Dráberová, L., P. Lebduška, I. Hálová, P. Tolar, J. Štokrová, H. Tolarová, J. Korb, and P. Dráber. 2004. Signaling assemblies formed in mast cells activated via Fcε receptor I dimers. *Eur. J. Immunol.* 34: 2209–2219.
29. Dráberová, L. 1990. Cyclosporin A inhibits rat mast cell activation. *Eur. J. Immunol.* 20: 1469–1473.
30. Frigeri, L., and J. R. Apgar. 1999. The role of actin microfilaments in the down-regulation of the degranulation response in RBL-2H3 cells. *J. Immunol.* 162: 2243–2250.
31. Tolarová, H., L. Dráberová, P. Heneberg, and P. Dráber. 2004. Involvement of filamentous actin in setting the threshold for degranulation in mast cells. *Eur. J. Immunol.* 34: 1627–1636.
32. Yamashita, T., S.-Y. Mao, and H. Metzger. 1994. Aggregation of the high-affinity IgE receptor and enhanced activity of $p53/p56^{lyn}$ protein-tyrosine kinase. *Proc. Natl. Acad. Sci. USA* 91: 11251–11255.
33. Nishida, K., Y. Yoshida, M. Itoh, T. Fukada, T. Ohtani, T. Shirogane, T. Atsumi, M. Takahashi-Tezuka, K. Ishihara, M. Hibi, and T. Hirano. 1999. Gab-family adapter proteins act downstream of cytokine and growth factor receptors and T- and B-cell antigen receptors. *Blood* 93: 1809–1816.
34. Wilson, B. S., J. R. Pfeiffer, Z. Surviladze, E. A. Gaudet, and J. M. Oliver. 2001. High resolution mapping of mast cell membranes reveals primary and secondary domains of FcεRI and LAT. *J. Cell Biol.* 154: 645–658.
35. Hirasawa, N., A. Scharenberg, H. Yamamura, M. A. Beaven, and J. P. Kinet. 1995. A requirement for Syk in the activation of the microtubule-associated protein kinase/phospholipase A2 pathway by FcεR1 is not shared by a G protein-coupled receptor. *J. Biol. Chem.* 270: 10960–10967.
36. Jabril-Cuenod, B., C. Zhang, A. M. Scharenberg, R. Paolini, R. Numerof, M. A. Beaven, and J. P. Kinet. 1996. Syk-dependent phosphorylation of Shc: a potential link between FcεRI and the Ras/mitogen-activated protein kinase signaling pathway through SOS and Grb2. *J. Biol. Chem.* 271: 16268–16272.
37. Kawakami, Y., J. Kitaura, L. Yao, R. W. McHenry, Y. Kawakami, A. C. Newton, S. Kang, R. M. Kato, M. Leitges, D. J. Rawlings, and T. Kawakami. 2003. A Ras activation pathway dependent on Syk phosphorylation of protein kinase C. *Proc. Natl. Acad. Sci. USA* 100: 9470–9475.
38. Putney, J. W., Jr., L. M. Broad, F. J. Braun, J. P. Lievremont, and G. S. Bird. 2001. Mechanisms of capacitative calcium entry. *J. Cell Sci.* 114: 2223–2229.
39. Thastrup, O., A. P. Dawson, O. Scharff, B. Foder, P. J. Cullen, B. K. Drobak, P. J. Bjerrum, S. B. Christensen, and M. R. Hanley. 1989. Thapsigargin, a novel molecular probe for studying intracellular calcium release and storage. *Agents Actions* 27: 17–23.
40. Heneberg, P., P. Lebduška, L. Dráberová, J. Korb, and P. Dráber. 2006. Topography of plasma membrane microdomains and its consequences for mast cell signaling. *Eur. J. Immunol.* 36: 2795–2806.
41. Dráberová, L., and P. Dráber. 1993. Thy-1 glycoprotein and src-like protein-tyrosine kinase $p53/p56^{lyn}$ are associated in large detergent-resistant complexes in rat basophilic leukemia cells. *Proc. Natl. Acad. Sci. USA* 90: 3611–3615.
42. Zhao, C., D. H. Yu, R. Shen, and G. S. Feng. 1999. Gab2, a new pleckstrin homology domain-containing adapter protein, acts to uncouple signaling from ERK kinase to Elk-1. *J. Biol. Chem.* 274: 19649–19654.
43. Gu, H., K. Saito, L. D. Klaman, J. Shen, T. Fleming, Y. Wang, J. C. Pratt, G. Lin, B. Lim, J.-P. Kinet, and B. G. Neel. 2001. Essential role for Gab2 in the allergic response. *Nature* 412: 186–190.
44. Xie, Z. H., I. Ambudkar, and R. P. Siraganian. 2002. The adapter molecule Gab2 regulates FcεRI-mediated signal transduction in mast cells. *J. Immunol.* 168: 4682–4691.
45. Tailor, P., T. Jascur, S. Williams, M. von Willebrand, C. Couture, and T. Mustelin. 1996. Involvement of Src-homology-2-domain-containing protein-tyrosine phosphatase 2 in T cell activation. *Eur. J. Biochem.* 237: 736–742.
46. Liou, J., M. L. Kim, H. W. Do, J. T. Jones, J. W. Myers, J. E. Ferrell, Jr., and T. Meyer. 2005. STIM is a $Ca^{2+}$ sensor essential for $Ca^{2+}$-store-depletion-triggered $Ca^{2+}$ influx. *Curr. Biol.* 15: 1235–1241.
47. Roos, J., P. J. DiGregorio, A. V. Yeromin, K. Ohlsen, M. Lioudyno, S. Zhang, O. Safrina, J. A. Kozak, S. L. Wagner, M. D. Cahalan, et al. 2005. STIM1, an essential and conserved component of store-operated $Ca^{2+}$ channel function. *J. Cell Biol.* 169: 435–445.
48. Feske, S., Y. Gwack, M. Prakriya, S. Srikanth, S. H. Puppel, B. Tanasa, P. G. Hogan, R. S. Lewis, M. Daly, and A. Rao. 2006. A mutation in Orai1 causes immune deficiency by abrogating CRAC channel function. *Nature* 441: 179–185.
49. Putney, J. W., Jr. 2007. Recent breakthroughs in the molecular mechanism of capacitative calcium entry (with thoughts on how we got here). *Cell Calcium* 42: 103–110.
50. Gilfillan, A. M., and C. Tkaczyk. 2006. Integrated signalling pathways for mast-cell activation. *Nat. Rev. Immunol.* 6: 218–230.

**6.8**

**Heneberg, P.; Dráberová, L. & Dráber, P. (2007):**

**Spatiotemporal distribution of PTP20 in signaling of mast cells and basophils.**

**submitted to European Journal of Immunology**

# Spatiotemporal distribution and signaling assemblies of protein tyrosine phosphatase PTP20 in mast cells

Petr Heneberg[1,2], Ľubica Dráberová[1] & Petr Dráber[1]

[1] Institute of Molecular Genetics, Academy of Sciences of the Czech Republic, Prague, Czech Republic

[2] 3rd Faculty of Medicine, Charles University, Prague, Czech Republic

**Key words:** protein tyrosine phosphatase, mast cells, PTP20/HSCF, Cbp/PAG, Csk

**Correspondence:** Dr. Petr Dráber, Department of Signal Transduction, Institute of Molecular Genetics AS CR, v.v.i., Vídeňská 1083, CZ-142 20 Prague 4, Czech Republic.

Tel.: +420-241062468; Fax: +420-241470339; e-mail: draberpe@img.cas.cz

**Abbreviations:** BDP: brain-derived phosphatase · BMMC: bone-marrow-derived mast cell · Csk: c-Src tyrosine kinase · FcεRI: type I Fcε receptor · FLP: fetal liver phosphatase · Grb2: growth factor receptor-bound protein 2 · HePTP: hematopoietic PTP · LAT: linker for activation of T cells · NTAL: non–T cell activation linker · PAG: phosphoprotein associated with GEMs · PEP: PEST domain phosphatase · PEST: Pro, Glu, Ser and Thr-rich · PSTPIP: proline-serine-threonine phosphatase interacting protein · PTK: protein tyrosine kinases · PTP: protein tyrosine phosphatase · RBL: rat basophilic leukemia · SHP: Src homology phosphatase · STAT3: signal transducer and activator of transcription 3

**Note:** Nucleotide sequence data reported are available in the GenBank database under the accession numbers AF468653, AF502572, AF502573, AF520784, AF543484, AY062269, and BK001033-BK001040.

**Abstract**

Although protein tyrosine phosphatases are required for proper activation and deactivation of mammalian cells, their repertoir and molecular mechanisms of action are poorly understood. In this study we have identified mRNA for seven new mast cell protein tyrosine phoshatases - PTP-MEG1, TC-PTP, FAP-1, PTP36, PTP20, PRL1 and PRL2. One of them, PTP20, was analyzed in detail. Confocal microscopy showed that a large pool of PTP20 interacts with nuclear membrane in quiescent cells and deassociate from it following the high affinity IgE receptor (FcεRI) or GPI-anchored proteins triggering. PTP20 formed complexes with c-src tyrosine kinase (Csk) in mouse bone-marrow-derived mast cells (BMMC) but not in rat basophilic leukemia (RBL) cells. FcεRI-mediated activation of BMMC resulted in decreased activity of PTP20 in Csk immunoprecipitates. In RBL cells, Csk formed complexes with another PEST-type phosphatase, PTP-PEST. Neither of these phosphatase was, however, found in immunoprecipitates of the adaptor protein PAG, previously described to be an important Csk binding partner. Interestingly, Csk-PAG immunocomplexes were found in RBL cells but not in BMMC. Different association of PTP20 with Csk immunocomplexes in BMMC and RBL cells, may be related to recently reported role of PTP20 as a tumor suppressor.

## Introduction

Mast cells have been recognized as an important defence component connecting innate and adaptive immune responses, as well as linking the immune and nervous systems [1]. Their activation via the high-affinity IgE receptor (FcεRI) and some other surface receptors leads to enhanced activity of numerous protein tyrosine kinases, changes in phosphorylation pattern and activity of various signaling molecules, and release of cytokines and other secretory mediators. Although the involvement of phosphatases in early events of mast cell signaling is known for years [2], mechanisms of their action are in general poorly understood [3;4].

Till now, only five nonreceptor protein tyrosine phosphatases (PTP) are known to change their activity following the FcεRI triggering. These involve Src homology phosphatase (SHP)-1, which is recruited by the phosphorylated tyrosine residues in immunoreceptor tyrosine-based inhibitory motifs of the inhibitory receptors [5]. SHP-1 is then activated and dephosphorylates its C-terminal regulatory domain [6], followed by inhibiting MAPK activation and cytokine responses [6;7]. Another nonreceptor PTP involved in FcεRI-driven cell activation is SHP-2, which associates with growth factor receptor-bound protein 2 (Grb2), Dos/Gab protein family members and with FcεRI [8]. Third, PTP-MEG2 was reported to be involved in the vesicle formation in rat basophilic leukemia (RBL) cells [9]. Fourth, PTP-PEST, which is broadly expressed in haemopoietic cells, including bone-marrow-derived mast cells (BMMC), is constitutively associated with several signaling molecules (Shc, paxillin, Csk and Cas) and serves a negative regulator of lymphocyte activation [10]. Finally, hematopoietic PTP (HePTP) is known to be phosphorylated following FcεRI-aggregation [8].

Compared to the number of protein tyrosine kinases (PTK) described in mast cells, the number of known PTP is relatively low and, therefore, we expected that other PTP could be present in mast cells and involved in regulation of mast cell signaling. In an attempt to contribute to elucidation of the mast cell phosphatom, we tested in RBL cells and BMMC the presence of mRNA for all 18 nonreceptor PTP known at the beginning of the project to be expressed in mammals. Out of seven nonreceptor PTPs found to be new for mast cells we selected for further studies PTP20, which was previously found to associate with the c-Src tyrosine kinase (Csk), and to inactivate Src-family PTKs by dephosphorylation of the regulatory tyrosine in their kinase domain [11]. Here we report topography of PTP20 as determined by confocal microscopy, and properties of PTP complexes in RBL cells and BMMC.

## Results

### Expression profile of nonreceptor PTPs in mast cells

To detect expression profile of genes for nonreceptor PTPs in BMMC and RBL cells we designed a set of 18 primer pairs covering all nonreceptor PTPs known to be expressed in mammals at the beginning of the project (Table 1). When possible, the primers were designed to bind to regions of homology between hitherto known orthologs.

Using RT-PCR, we detected mRNA for 12 nonreceptor PTPs in BMMC and RBL cells: TC-PTP, PTP-MEG1, SHP-1, HePTP, PTP-MEG2, SHP-2, PTP-PEST, FAP-1, PTP20, PRL1, and PRL2. Expression of PTP36 was detected in BMMC only (Table 1). Furthermore, we sequenced and identified three new rat cDNAs of potentially important phosphatase molecules: rat ortholog of PTP-

MEG1 (PTPN4; GenBank accession number AF502572), known to participate in Src/Fyn signaling [8]; rat ortholog of FAP-1 (PTPN13; AF543484) known to play role in apoptosis, oxidative stress and cell migration [8]; and rat PTP-MEG2 (AF520784), which has been previously reported in mast cells by immunoblotting [9], but isolation of a clone AF520784 reported here is the first sequential confirmation of its presence in rat cells. The sequences of the three newly identified molecules were also confirmed from EST clones of other vertebrate species and submitted to the GenBank under accession numbers BK001033-BK001040.

We also detected three alternative splicing forms of previously known rat PTPs. Among them was a rat ortholog of mouse TC-PTP (PTPN2; NM_008977), newly called PTPN2A (AF502573). It contains an insertion of several tens of bp known previously from mice only. The next was rat isoform of SHP-1 (AF468653) differing by insertion of 32 basepairs known previously from mice (NM_013545) only, and causing an abortive termination of translation (see partial protein sequence AAL77056). Finally, we identified a mutation in PRL1, C170W, localized out of the phosphatase domain (AY062269), which is an ortholog of mouse NM_011200.

Among the molecules new for mast cells were PTP-MEG1, TC-PTP, FAP-1, PTP36, PTP20, PRL1 and PRL2, out of which we selected PTP20 for further studies.

**Spatiotemporal distribution of PTP20**

As PTP20 was reported to interact with Csk in early myeloid cells [11], with cytoskeleton-associated proteins in CHO, Baf3, and rat ovarian granulosa cells, and even with nuclei in Baf3 murine cells [12-14], we were interested in its

subcellular localization and its changes during activation of mast cells. In initial experiments, we investigated the spatial distribution of PTP20 in cells sequentially solubilized with detergents. This method is based on a gentle release of free cytoplasmic components after permeabilization of the cells with the cholesterol sequestering reagent saponin, followed by complete solubilization of all membrane components, including lipid rafts, by NP-40 detergent [15]. Using this method we found that ~75% of total PTP20 in resting cells (time = 0 min; Fig. 1A) was located as free molecules or small complexes, which could be released from the cells after saponin-induced cell permeabilization (saponin supernatant fraction); the rest of PTP20 bound to membranes and/or other cytoplasmic structures was solubilized from saponin-permeabilized cells by NP-40 (NP-40 supernatant fraction). There was just a barely detectable amount of PTP20 in saponin/NP-40 sediments composed mostly of nuclei and cytoskeleton remnants (data not shown). After FcεRI dimerization with 5.14 mAb, amount of cytoplasmic PTP20 in saponin supernatants sligthly increased, reaching its peak at 5 min after triggering (Fig. 1A). It should be noted that in the same detergent extracts, there were no changes in amount of adaptor protein LAT, which was localized mostly in saponin/NP-40 supernatant, as expected. When the cells were sensitized with IgE, followed by extensive aggregation of the FcεRI-IgE complexes by TNP-BSA, amount of cytoplasmic PTP20 in saponin supernatant was increased more, reaching its peak at 15 min after triggering; amount of PTP20 in saponin/NP40 supernatant was therefore decreased (Fig. 1B).

Next we attempted to determine whether PTP20 is located submembranously as one could infer from its changes following FcεRI triggering (see below), or subnuclearly where it should associate with Tec-family kinases [16]. Confocal microscopy on resting RBL cells showed that PTP20 is located

prevalently in distinct spots in a subnuclear area. Fraction of PTP20 colocalized with a nuclear membrane and a small fraction of it was irregularly associated with the plasma membrane (Fig. 2A). After FcεRI triggering, there was a decrease in amount of PTP20 associated with nuclear membrane and enhanced amount in cytoplasmic spots (Fig. 2B). To quantify changes in distribution of PTP-20 in the course of cell activation, histograms of the relative fluorescence profiles intensities were created (Fig. 2C-H). These histograms confirmed, that PTP20 was found mainly to be associated with nuclear membrane, plasma membrane, cytoplasmic granules and was absent in nucleus. After activation of the cells with 5.14 mAb, which induces dimerization of FcεRI, rapid decrease of PTP20 associated with the nuclear membrane was noticed, peaking at 5 min (Fig. 2E). Extensive aggregation of the FcεRI through aggregation of FcεRI-IgE complexes by multivalent antigen, TNP-BSA resulted in more rapid release of PTP20 from nuclear membrane (Fig. 4F). We also measured changes in PTP20 topography after aggregation of GPI-anchored glycoproteins Thy-1 and TEC-21, which have been previosuly shown to induce activation events which are distinct from those induced by aggregation of FcεRI [17;18]. Aggregation of Thy-1.1 with biotinylated OX-7 mAb, followed by streptavidin (Fig. 2G) or dimerization of TEC-21 glycoprotein with the anti-TEC-21 mAb (Fig. 2H), also resulted in release of PTP20 from the nuclear membrane, peaking at 15 min after triggering.

**Is PTP20 in RBL cells present in complexes with Csk and PAG?**

PTP20, as well as other members of the PEST family phosphatases, PTP-PEST and PEP, were reported to interact with Csk [11;19;20]. Csk and PTP20 were found to synergize in inhibition of enzymatic activity of Src family kinases in transfected COS cells [11]. Next we therefore analyzed formation of functional

assemblies of PTP-20 with Csk, and interaction of PTP20-Csk complexes with adaptor protein PAG, which has been previously described to be an important Csk binding partner in RBL cells [21]. Immunoprecipitation of PAG from nonactivated and saponin/NP-40 solubilized RBL cells, followed by immunoblotting with PY-20-HRP mAb conjugates showed that PAG itself was strongly tyrosine phosphorylated and associated with several tyrosine phopshorylated proteins. PAG immunoprecipitates possessed Csk, as determined by immunoblotting with Csk-specific Ab, and SHP-2, as determined by in-gel phopshatase assay. However, no PTP20 was determined in PAG immunoprecipitates as determined by both enzymatic assay (Fig. 3A) or immunoblotting (not shown). In cells activated through FcεRI, a small increase in tyrosine phosphorylation of PAG was detected, peaking at 0.5 min after triggering. This corresponded to enhanced association of Csk with PAG (Fig. 3A,B). Interestingly, there were no dramatic changes in activity of PAG-associated SHP-2 in the course of mast cell activation, although total activity of SHP-2 immunoprecipitated from saponin/NP-40 lysates was dramatically enhanced (Fig. 3C).

After we failed to show any association of PTP20 with PAG immunocomplexes, we analyzed properties of Csk immunoprecipitates (Fig. 3B). Immunoblotting studies showed only small increase in amount of Csk in saponin/NP-40 lysates in the course of mast cell triggering. Interestingly, PTK assays showed that enzymatic activity of Csk associated with large signaling assemblies was decreased after FcεRI triggering. Moreover, when Csk immunoprecipitates were tested for PTP20 enzymatic activity by in-gel assay, none was found (Fig. 5B, bottom); instead, Csk-associated phosphatase activity was found molecular weight of PTP-PEST, which we found previously found to

be associated with Csk in RBL cells [20]. Under the same conditions, PTP20 immunoprecipitates shown moderate increase of phosphatase activity (Fig. 4) visible as a single band on the PTP in-gel assay gel. Phosphatase activity of PTP20 was slightly enhanced after FcεRI or OX7 aggregation (Fig. 4), but this entirely did not have any effect on the Csk- or PAG-associated PTP20 activity in RBL cells (Fig. 3A,B), which remained below the detection level.

Absence of PTP20 in large signaling assemblies in detergent solubilized RBL cells was also supported by studies of elution profile of PTP20 on a column of Sepharose 4B. It allowed us to detect activation-induced changes in size of signaling complexes. PTP20 was eluted in the fraction of nonaggregated molecules compared to e.g. Lyn kinase eluted in the fraction of large signaling complexes (Fig. 5). Furthermore, no changes in size of PTP20 complexes were recorded in activated cells (Fig. 5C). When Triton solubilized cells were analyzed by sucrose density gradient ultracentrifugation, small amount of PTP20 (15.8 ± 4.2%, mean ± S.D.; n = 6) was associated with low density fractions (fractions 1-4). In contrast, more Csk (37.6 ± 12.2), Lyn (77.6 ± 8.5) and PAG (68.5 ± 12.9), but not STAT3 (0.5 ± 0.4,) was found in low density fractions. In agreement with these data, we didn`t find PTP20 coprecipitating with Csk, Lyn, LAT, NTAL, PAG, Syk, Src, or p38 in resting as well as in FcεRI-activated RBLs cells (data not shown). These data indicate that in RBL cells PTP20 does not form complexes with Csk and other signaling molecules involved in early stages of FcεRI activation.

**Is PTP20 in BMMC present in complexes with Csk and PAG?**

The unexpected finding that PAG and Csk immunoprecipitates did not contain PTP20 could be somehow related to unusual signaling assemblies in RBL cells,

which are of tumor origin. In further experiments we therefore analyzed properties of PAG and Csk immunocomplexes isolated from BMMC obtained after cultivation of mouse bone marrow cells in the presence of IL-3 and SCF. Immunoblotting analysis of PAG immunoprecipitates showed slight increase of tyrosine phosphorylation of PAG during mast cells activation, but not PTP20 enzymatic activity, and, surprisingly, no Csk (Fig. 3D). When Csk immunoprecipitates were analyzed, no changes in amount of Csk associated with large signaling assemblies were found. In accordance with previous data, no PAG was found in Csk immunoprecipitates (not shown). In-gel kinase assays showed that Csk immunoprecipitates from resting BMMC possessed strong enzymatic activity corresponding to PTP20 (Fig. 3D). This activity rapidly disappeared 30 sec after FcεRI triggering and remained low for at least 15 min. Alternatively, when PTP20 immunoprecipitates were analyzed in kinase assay, a band corresponding to enzymatically active Csk was strong in resting cells, and weak in FcεRI-activated cells (data not shown).

Different properties of signaling assemblies between BMMC and RBL cells, were also detected by immunoblotting analysis of sucrose density gradient fractions. In contrast to RBL cells (Fig. 5A), low density fractions of BMMC (fig. 5B) possessed no PTP20 and Csk and less Lyn and PAG. The observed differences in association of Csk with lipid rafts could be related to the absence of PAG-Csk interactions.

## Discussion

The recent boom in identification of PTPs proves that their heterogeneity matches that of protein tyrosine kinases, and that both play more complex roles in intracellular signalling than previously thought. Despite the progress within last years, mRNA for only seven nonreceptor PTPs was known from mast cells and basophils [8;22], which did not suffice the needs for explanation of changes in protein tyrosine phosphorylation in mast cells. In attempt to identify PTP present in mast cells we used RT-PCR for analysis of cDNA from RBL cells and BMMC. We have found seven new PTP expressed in rodent mast cells, PTP-MEG1, TC-PTP, FAP-1, PTP36, PTP20, PRL1 and PRL2. PTP36 was found only in BMMC. Furthermore, we have sequenced number of these and other phosphatase and and deposited the sequences in GenBank. One of them, PTP-20 has been reported to be expressed in brain, colon, in primitive hematopoietic cells and in several tumor-derived cell lines [23-25]. As PTP20 was known to interact with Csk kinase [11], with actin through proline-serine-threonine phosphatase interacting protein (PSTPIP)-family adaptors [13], to inhibit the phosphorylation of Gab1 adaptor and MAPK activation [26], and even to be upregulated by the c-kit tyrosine kinase activation [27], we selected this molecule as a potential candidate molecule important for mast cell signaling.

In initial experiments we analysed topography of PTP20 in noactivated and activated cells. Using saponin/NP-40 solubilization procedure, we found that most of PTP20 is found as free molecules or small cytoplasmic complexes which could be released from the cells after their permeabilization with saponin. Amount of PTP20 bound to large signaling assemblies was enhanced after FcεRI dimerization by anti-FcεRI mAb 5.14 and even more after extensive FcεRI

aggregation. Unexpected finding was that significant fraction of PTP20 was bound to plasma membrane and that activation through FcεRI or GPI-anchored proteins (Thy-1 or TEC-21) was accompanied by release of PTP20 from nuclear membrane into cytoplasm.

Previous studies showed that PTP20 interacts with Csk in early myeloid cells [11], with cytoskeleton in CHO cells [13] and even with nuclei in Baf3 murine cells [12], and that PTP20 could serves together with Csk as negative regulators of Src family tyrosine kinases. Csk is known to bind to PAG which is located in lipid rafts and through these interactions Csk and PTP20 could regulate enzymatic activity of the relevant PTK. Several lines of evidence, however, suggest that PTP20 in mast cells has different roles compared to systems so far studied. PTP20 is a new mast cell signaling molecule, the activity of which is slightly increased following FcεRI- or Thy-1-mediated activation. PTP20 was reported to coprecipitate with Csk in transfected COS cells [11], but we corroborated this interaction in BMMC only, not in RBL cells (Fig. 3). In Csk immunoprecipitates from RBL cells, PTP20 is replaced by another PEST-type phosphatase, PTP-PEST (Fig. 3B) and is not present in large macromolecular aggregates (Fig. 5C), and only in trace amounts in detergent-resistant membrane fractions of RBL cells (Fig. 5A). It is the first evidence that PAG doesn`t bind Csk in BMMC, whereas Csk is a main interaction partner of PAG in RBL cells [28] and T-cells [29;30], even though BMMC express both these molecules in large quantities.

Interestingly, absence of Csk association with PAG led to the absence of Csk in light fractions of the sucrose density gradients (Fig. 5). Among the sucrose density gradient findings, first, PTP20 is not associated with light-density fractions in BMMC, and only to limited amount in RBL cells (Fig. 5, first row). Second, Csk

is not associated with light-density fractions in BMMC, but is associated with them in RBL cells (Fig. 5, second row). Third, part of the total PAG and Lyn is associated with light-density fractions in both, RBL and BMMC. Fourth, signal transducer and activator of transcription 3 (STAT3) is not associated with light-density fractions in both RBL and BMMC, which is in contrary to data published previously [31;32], but is in-line with our current observations from some other cell types [33]. As STAT3 was reported to form signaling clusters with PAG and Src-family kinases [34-36] and as membrane microdomains had been reported as crucial for its action [31;32], it was expected to be present in light-density fractions. Similarly, Csk was frequently reported to be associated with PAG and light-density fractions [29;37-39], but here we report that it is not associated with PAG neither with light density fractions in BMMC (Fig. 5, second row). Thus the composition of light-density fractions in RBL cells, BMMC, and some other immune cells differ significantly, and these differences affect to a large extent the proposed signaling pathway involving PTP20, Csk, PAG, Lyn, and STAT3.

As PTP20 was recently described as a possible tumor supressor [25;26;40;41], it is possible that dissimilar properties of PTP20 in RBL cells, which are of the tumorigenic origin, compared to BMMC cultivated from freshly isolated bone marrows may reflect its tumor-suppresor activity. Importance of its role in the immune cell system is supported by the group of J.M.Cerutti [41], who found that alternative splicings of PTP20 occured with the high frequency in some thyroid cancers, especially in follicular thyroid carcinoma cells, follicular variant of papillary thyroid carcinoma, and in follicular thyroid adenoma. This suggests that most of the tumor-specific splice forms of PTP20 are not associated with thyroid tumor progression, but instead with events occuring early in the tumor development. The upregulation of PTP20 activity by c-kit [27],

negative regulation of erbB2 phosphorylation correlating with the dephosphorylation of the Gab1 adaptor and reduction of the Erk2 activity [24], and finally frequent irregularities in PTP20-Csk and Csk-PAG complexes suggest importance of PTP20 as one of major phosphatase molecules controlling the tumor occurence in immune tissues.

## Material and methods

### Cells, antibodies, and reagents

The origin and culture conditions for BMMC had been described [42]. The HepG2 cells were cultured in RPMI-1640 medium. The RBL, COS and CHO cells were cultured in the mix of RPMI-1640 medium with H-MEM 1:1 under the same conditions.

The following mAbs were used: MRC OX7 (OX7; IgG1) recognizing Thy-1.1, 5.14 directed to FcεRI β-subunit, IGEL b4 1(IgE) recognizing TNP, and antibodies against NTAL, LAT, TEC-21 and Syk described described in [15;42;43]. HRP-conjugated antiphosphotyrosine antibody PY20, RαM IgG, and Cy3-conjugated RαM IgG were purchased from Sigma (St. Louis, MO). RαSHP-2, Rαp38 and RαCsk were from Santa Cruz Biotechnology, Inc. RαPAG was from Exbio (Prague, Czech Republic). Some antibodies were biotinylated with ImmunoPure NHSLC-biotin (Pierce, Rockford, IL) according to the manufacturer's instructions. All other reagents used were from Sigma.

To prepare a mAb specific for PTP20, BALB/c mice were immunized with a peptide CMSRQSDLVRSFLEQQEARDH (PolyPeptide Laboratories, Prague, Czech Republic) conjugated with the keyhole limpet hemocyanin (Pierce, Rockford, IL). Hybridomas were obtained as described [44] and screened for ELISA reactivity with the ovalbumin-conjugated CMSRQSDLVRSFLEQQEARDH peptide. Another ELISA was performed with the recombinant PTP20 produced by the NruI.-digested pAxCAwt cosmid containing rat cDNA for PTP20 (gift of H.Miyazaki, Tsukuba, Japan) [14]. One of the hybridoma cell lines, PTP20/35 (of the IgM isotype), produced antibodies reacting with with the recombinant PTP 20 but not other recombinant proteins. Furthermore, immunoblotting analysis with

lysates from RBL cells showed that the mAb reacted with a band of ~50 kDa, which is expected MW for PTP50. No reactivity was observed with lysates from BMMC cells. Rabbit polyclonal antibodies directed against PTP20 were prepared, analyzed and purified using the same peptide conjugates as described above.

**Detection of PTP mRNA by RT-PCR**

Total RNA isolated from RBL-2H3 cells employing acidic phenol extraction reagent (Tri Reagent; Sigma) was reverse transcribed using mouse Moloney virus reverse transcriptase (Gibco/BRL, Gaithersburg, MD). We used primers designed according to all rat, mouse, and human nonreceptor PTP sequences accessible in the PubMed database up to the end of year 2001 (sequences available on-line as a supporting information). The cDNA obtained was used in PCR. The PCR-generated DNA fragments were cloned into the vector pcDNA3 (Invitrogen, Groningen, Netherlands) or pGEM-3Z (Promega, Madison, WI). Four independent clones were sequenced bidirectionally on ABI Prism 3100 (Applied Biosystems, Foster City, CA), and analyzed using DNASTAR software (DNASTAR, Madison, WI). Database searches were performed using the BLAST algorithm.

**Immunoprecipitation immunoblotting, and enzymatic assays**

Cells were solubilized in lysis buffer containing 25 mM Tris, pH 8.0; 140 mM NaCl; 2 mM EDTA; 1 mM $NaVO_3$; protease inhibitor cocktail and 0.2% Triton X-100 and analyzed by SDS PAGE. In some experiments the cells were incubated for 5 min on ice in PBS containing 0.1% saponin, 5 mM $MgCl_2$, and 1 mM $Na_3VO_4$, and then extracted for 15 min on ice in lysis buffer supplemented with 1% NP-40 or 1% Triton X-100 [15;43]. Immunoblots were quantified by

Luminescent Image Analyzer LAS-3000 (Fuji Photo Film Co., Tokyo, Japan). To detect the enzymatic activity of nonreceptor PTPs, a phosphatase in-gel assay was used as described [15]. To detect the enzymatic activity of kinases, a tyrosine kinase assay was used as described [45].

**Confocal microscopy and flow cytometry analyses**

RBL cells were fixed with 4% paraformaldehyde, permeabilized with 0.1% Triton X-100, and labeled with PTP20/35 (20 µg/ml). As a secondary Ab we used Cy3-conjugated RαM IgG. Cell fluorescence was analysed on the FACSCalibur (BD Biosciences, San Jose, CA). For microscopical experiments was alternatively used PTP20/35 labeled directly with TRITC, or rabbit rabbit polyclonal antibodies against PTP20 followed by the incubation with secondary Cy3-conjugated anti rabbit IgG. All three types of labeling resulted into the similar distribution pattern. Deassociation from the nuclear membrane was measured using program AIDA (Raytest Isotopen-Messgeräte GmbH). First, a strip having 0.5 µm width was created randomly across the cell (Fig. 4A). Histogram of the relative fluorescence profile was created using AIDA software and 1 µm area around the nuclear membrane (peak) was selected (Fig. 4B) and its total fluorescence measured densitometrically. Figs. 4C-F show the relative fluorescence values of those nuclear membrane peaks compared to the total fluorescence of the whole strip.

**Acknowledgements**

We thank H.Mrázová and D.Lorenčíková for technical assistance. This work was supported by projects 1M6837805001 (Center of Molecular and Cellular Immunology) and LC-545 from Ministry of Education, Youth and Sports of the Czech Republic; Grants 204/05/H023 and 301/06/0361 from the Grant Agency of the Czech Republic; Grants A5052310 and 1QS500520551 from the Grant Agency of the Academy of Sciences of the Czech Republic; and Institutional project AVOZ50520514. The research of P.H. was supported by Research goal MSM0021620814 from the 3rd Faculty of Medicine, Charles University, Prague.

**References**


1. **Bischoff,S.C.**, Role of mast cells in allergic and non-allergic immune responses: comparison of human and murine data. *Nature Reviews Immunology* 2007. **7**: 93-104.

2. **Paolini,R., Jouvin,M.H., and Kinet,J.P.**, Phosphorylation and dephosphorylation of the high-affinity receptor for immunoglobulin-E immediately after receptor engagement and disengagement. *Nature* 1991. **353**: 855-858.

3. **Mustelin,T., Vang,T., and Bottini,N.**, Protein tyrosine phosphatases and the immune response. *Nature Reviews Immunology* 2005. **5**: 43-57.

4. **Pao,L.I., Badour,K., Siminovitch,K.A., and Neel,B.G.**, Nonreceptor protein-tyrosine phosphatases in immune cell signaling. *Annual Review of Immunology* 2007. **25**: 473-523.

5. **Yamashita,Y., Ono,M., and Takai,T.**, Inhibitory and stimulatory functions of paired Ig-like receptor (PIR) family in RBL-2H3 cells. *Journal of Immunology* 1998. **161**: 4042-4047.

6. **Ozawa,T., Nakata,K., Mizuno,K., and Yakura,H.**, Negative autoregulation of Src homology region 2-domain-containing phosphatase-1 in rat basophilic leukemia-2H3 cells. *International Immunology* 2007. **19**: 1049-1061.

7. **Xie,Z.H., Zhang,J., and Siraganian,R.P.**, Positive regulation of c-Jun N-terminal kinase and TNF-a production but not histamine release by SHP-1 in RBL-2H3 mast cells. *Journal of Immunology* 2000. **164**: 1521-1528.

8. **Heneberg,P. and Dráber,P.**, Nonreceptor protein tyrosine and lipid phosphatases in type I Fce receptor-mediated activation of mast cells and basophils. *International Archives of Allergy and Immunology* 2002. **128**: 253-263.

9. **Huynh,H., Bottini,N., Williams,S., Cherepanov,V., Musumeci,L., Saito,K., Bruckner,S., Vachon,E., Wang,X.D., Kruger,J., Chow,C.W., Pellecchia,M., Monosov,E., Greer,P.A., Trimble,W., Downey,G.P., and Mustelin,T.**, Control of vesicle fusion by a tyrosine phosphatase. *Nature Cell Biology* 2004. **6**: 831-839.

10. **Davidson,D. and Veillette,A.**, PTP-PEST, a scaffold protein tyrosine phosphatase, negatively regulates lymphocyte activation by targeting a unique set of substrates. *Embo Journal* 2001. **20**: 3414-3426.

11. **Wang,B., Lemay,S., Tsai,S., and Veillette,A.**, SH2 domain-mediated interaction of inhibitory protein tyrosine kinase Csk with protein tyrosine phosphatase-HSCF. *Molecular and Cellular Biology* 2001. **21**: 1077-1088.

12. **Dosil,M., Leibman,N., and Lemischka,I.R.**, Cloning and characterization of fetal liver phosphatase 1, a nuclear protein tyrosine phosphatase isolated from hematopoietic stem cells. *Blood* 1996. **88**: 4510-4525.

13. **Wu,Y., Dowbenko,D., and Lasky,L.K.,** PSTPIP 2, a second tyrosine phosphorylated, cytoskeletal-associated protein that binds a PEST-type protein-tyrosine phosphatase. *Journal of Biological Chemistry* 1998. **273**: 30487-30496.

14. **Shiota,M., Tanihiro,T., Nakagawa,Y., Aoki,N., Ishida,N., Miyazaki,K., Ullrich,A., and Miyazaki,H.,** Protein tyrosine phosphatase PTP20 induces actin cytoskeleton reorganization by dephosphorylating p190 RhoGAP in rat ovarian granulosa cells stimulated with follicle-stimulating hormone. *Molecular Endocrinology* 2003. **17**: 534-549.

15. **Tolarová,H., Dráberová,L., Heneberg,P., and Dráber,P.,** Involvement of filamentous actin in setting the threshold for degranulation in mast cells. *European Journal of Immunology* 2004. **34**: 1627-1636.

16. **Aoki,N., Ueno,S., Mano,H., Yamasaki,S., Shiota,M., Miyazaki,H., Yamaguchi-Aoki,Y., Matsuda,T., and Ullrich,A.,** Mutual regulation of protein-tyrosine phosphatase 20 and protein-tyrosine kinase Tec activities by tyrosine phosphorylation and dephosphorylation. *Journal of Biological Chemistry* 2004. **279**: 10765-10775.

17. **Hálová,I., Dráberová,L., and Dráber,P.,** A novel lipid raft-associated glycoprotein, TEC-21, activates rat basophilic leukemia cells independently of the type 1 Fce receptor. *International Immunology* 2002. **14**: 213-223.

18. **Dráberová,L. and Dráber,P.**, Thy-1-Mediated Activation of Rat Basophilic Leukemia-Cells Does Not Require Coexpression of the High-Affinity Ige Receptor. *European Journal of Immunology* 1995. **25**: 2428-2432.

19. **Ghose,R., Shekhtman,A., Goger,M.J., Ji,H., and Cowburn,D.**, A novel, specific interaction involving the Csk SH3 domain and its natural ligand. *Nature Structural Biology* 2001. **8**: 998-1004.

20. **Davidson,D., Cloutier,J.F., Gregorieff,A., and Veillette,A.**, Inhibitory tyrosine protein kinase p50(csk) is associated with protein-tyrosine phosphatase PTP-PEST in hemopoietic and non-hemopoietic cells. *Journal of Biological Chemistry* 1997. **272**: 23455-23462.

21. **Ohtake,H., Ichikawa,N., Okada,M., and Yamashita,T.**, Cutting edge: Transmembrane phosphoprotein Csk-binding protein/phosphoprotein associated with glzcosphingolipid-enriched microdomains as a negative feedback regulator of mast cell signaling through the FceRI. *Journal of Immunology* 2002. **168**: 2087-2090.

22. **Heneberg,P. and Dráber,P.**, Regulation of Cys-based protein tyrosine phosphatases via reactive oxygen and nitrogen species in mast cells and basophils. *Current Medicinal Chemistry* 2005. **12**: 1859-1871.

23. **Cong,F., Spencer,S., Cote,J.F., Wu,Y., Tremblay,M.L., Lasky,L.A., and Goff,S.P.**, Cytoskeletal protein PSTPIP1 directs the PEST-type protein

tyrosine phosphatase to the c-Abl kinase to mediate Abl dephosphorylation. *Molecular Cell* 2000. **6**: 1413-1423.

24. **Kim,Y.W., Wang,H.Y., Sures,I., Lammers,R., Martell,K.J., and Ullrich,A.,** Characterization of the PEST family protein tyrosine phosphatase BDP1. *Oncogene* 1996. **13**: 2275-2279.

25. **Chen,Y., Yee,C.L., Lin,Q., Philp,R., Hong,W.C., Keong,A.B., Ling,T.Y., Chiew Shia,L.M., Leong,H.C., Shah,N., Druker,B.J., Kuan,C.P., and Pin,L.Y.,** Differential expression of novel tyrosine kinase substrates during breast cancer development. *Mol.Cell Proteomics* 2007.

26. **Gensler,M., Buschbeck,M., and Ullrich,A.,** Negative regulation of HER2 signaling by the PEST-type protein-tyrosine phosphatase BDP1. *Journal of Biological Chemistry* 2004. **279**: 12110-12116.

27. **Petti,F., Thelemann,A., Kahler,J., McCormack,S., Castaldo,L., Hunt,T., Nuwaysir,L., Zeiske,L., Haack,H., Sullivan,L., Garton,A., and Haley,J.D.,** Temporal quantitation of mutant Kit tyrosine kinase signaling attenuated by a novel thiophene kinase inhibitor OSI-930. *Molecular Cancer Therapeutics* 2005. **4**: 1186-1197.

28. **Ohtake,H., Ichikawa,N., Okada,M., and Yamashita,T.,** Cutting edge: Transmembrane phosphoprotein Csk-binding protein/phosphoprotein associated with glycosphingolipid-enriched microdomains as a negative

feedback regulator of mast cell signaling through the FceRI. *Journal of Immunology* 2002. **168**: 2087-2090.

29. **Brdička,T., Pavlištová,D., Leo,A., Bruyns,E., Kořínek,V., Angelisová,P., Scherer,J., Shevchenko,A., Shevchenko,A., Hilgert,I., Černý,J., Drbal,K., Kuramitsu,Y., Kornacker,B., Hořejší,V., and Schraven,B.,** Phosphoprotein associated with glycosphingolipid-enriched microdomains (PAG), a novel ubiquitously expressed transmembrane adaptor protein, binds the protein tyrosine kinase Csk and is involved in regulation of T cell activation. *Journal of Experimental Medicine* 2000. **191**: 1591-1604.

30. **Takeuchi,S., Takayama,Y., Ogawa,A., Tamura,K., and Okada,M.,** Transmembrane phosphoprotein Cbp positively regulates the activity of the carboxyl-terminal Src kinase, Csk. *Journal of Biological Chemistry* 2000. **275**: 29183-29186.

31. **Sehgal,P.B., Guo,G.G., Shah,M., Kumar,V., and Patel,K.,** Cytokine signaling - STATs in plasma membrane rafts. *Journal of Biological Chemistry* 2002. **277**: 12067-12074.

32. **Shah,M., Patel,K., Fried,V.A., and Sehgal,P.B.,** Interactions of STAT3 with caveolin-1 and heat shock protein 90 in plasma membrane raft and cytosolic complexes - Preservation of cytokine signaling during fever. *Journal of Biological Chemistry* 2002. **277**: 45662-45669.

33. **Dráber,P., Dráberová,L., Heneberg,P., Šmíd,F., Farghali,H., and Dráber,P.**, Preformed STAT3 transducer complexes in human HepG2 cells and rat hepatocytes. *Cellular Signalling* 2007. **19**: 2400-2412.

34. **Read,R.D., Bach,E.A., and Cagan,R.L.**, Drosophila C-terminal Src kinase negatively regulates organ growth and cell proliferation through inhibition of the Src, Jun N-terminal kinase, and STAT pathways. *Molecular and Cellular Biology* 2004. **24**: 6676-6689.

35. **Wang,Y.P., Ripperger,J., Fey,G.H., Samols,D., Kordula,T., Wetzler,M., Van Etten,R.A., and Baumann,H.**, Modulation of hepatic acute phase gene expression by epidermal growth factor and Src protein tyrosine kinases in murine and human hepatic cells. *Hepatology* 1999. **30**: 682-697.

36. **Lo,R.K., Cheung,H., and Wong,Y.H.**, Constitutively active Ga16 stimulates STAT3 via a c-Src/JAK- and ERK-dependent mechanism. *Journal of Biological Chemistry* 2003. **278**: 52154-52165.

37. **Khanna,S., Roy,S., Park,H.A., and Sen,C.K.**, Regulation of c-Src activity in glutamate-induced neurodegeneration. *Journal of Biological Chemistry* 2007. **282**: 23482-23490.

38. **Ohtake,H., Ichikawa,N., Okada,M., and Yamashita,T.**, Cutting edge: Transmembrane phosphoprotein Csk-binding protein/phosphoprotein associated with glycosphingolipid-enriched microdomains as a negative

feedback regulator of mast cell signaling through the FceRI. *Journal of Immunology* 2002. **168**: 2087-2090.

39. **Ingley,E., Schneider,J.R., Payne,C.J., McCarthy,D.J., Harder,K.W., Hibbs,M.L., and Klinken,S.P.**, Csk-binding protein mediates sequential enzymatic down-regulation and degradation of Lyn in erythropoietin-stimulated cells. *Journal of Biological Chemistry* 2006. **281**: 31920-31929.

40. **Gandhi,T.K.B., Chandran,S., Peri,S., Saravana,R., Amanchy,R., Prasad,T.S.K., and Pandey,A.**, A bioinformatics analysis of protein tyrosine phosphatases in humans. *DNA Research* 2005. **12**: 79-89.

41. **Guimaraes,G.S., Latini,F.R.M., Camacho,C.P., Maciel,R.M.B., Dias-Neto,E., and Cerutti,J.M.**, Identification of candidates for tumor-specific alternative splicing in the thyroid. *Genes Chromosomes & Cancer* 2006. **45**: 540-553.

42. **Volná,P., Lebduška,P., Dráberová,L., Šímová,Š., Heneberg,P., Boubelík,M., Bugajev,V., Malissen,B., Wilson,B.S., Hořejší,V., Malissen,M., and Dráber,P.**, Negative regulation of mast cell signaling and function by the adaptor LAB/NTAL. *Journal of Experimental Medicine* 2004. **200**: 1001-1013.

43. **Dráberová,L., Dudková,L., Boubelík,M., Tolarová,H., Šmíd,F., and Dráber,P.**, Exogenous administration of gangliosides inhibits FceRI-

mediated mast cell degranulation by decreasing the activity of phospholipase C g. *Journal of Immunology* 2003. **171**: 3585-3593.

44. **Dráber,P., Zikán,J., and Vojtíšková,M.,** Establishment and characterization of permanent murine hybridomas secreting monoclonal anti-Thy-1 antibodies. *Journal of Immunogenetics* 1980. **7**: 455-474.

45. **Surviladze,Z., Dráberová,L., Kubínová,L., and Dráber,P.,** Functional heterogeneity of Thy-1 membrane microdomains in rat basophilic leukemia cells. *European Journal of Immunology* 1998. **28**: 1847-1858.

**Figure legend**

**Fig. 1. Subcellular localization of PTP20.** (A) 5.14-activated, and (B) IgE-sensitized and TNP/BSA-activated RBL cells were activated for the indicated time intervals, and lysed in saponin/NP-40. The samples were size-fractionated by SDS-PAGE followed by immunoblotting with PTP20/35, RαLAT, and RαCsk. Quantitative analysis of protein amount was corrected for the cell volume (Fold). Three experiments with similar results were performed.

**Fig. 2. Confocal microscopy of PTP20 and changes of its spatiotemporal distribution.** (A) Distribution of PTP20 in resting RBL cells as viualized using PTP20/35. (B) Distribution of PTP20 in RBL cells sensitized overnight with IgE and activated with TNP/BSA for 30 sec. Remarkable is a shift of PTP20 from the nuclear membrane to the cytoplasm. (C-D) Measurement of deassociation of PTP20 from the nuclear membrane after cell activation. 0.5 μm wide strip had been done across the randomly selected confocal microscopy cell image (C). Relative fluorescence of the strip was measured using AIDA software, and its intensity in the 0.4 μm long perinuclear area was recorded (D). (E-H) RBL cells were activated or not for the indicated time intervals with 5.14 dimerizing the FcεRI (E), labeled overnight with IgE and activated TNP/BSA (F), labeled overnight with biotinylated OX7 and activated for the indicated time intervals with streptavidine (G), or aincubated with TEC-21 mAb (H). The fixed and permeabilized cells were blocked with 1% BSA in PBS and than incubated with PTP20/35 followed by the incubation with FITC-labelled anti mouse IgM. Relative share of PTP20 present in the perinuclear space (0.4 μm) was calculated and

time-course of its changes is shown. Data shown are means ± SD from 4-8 independent photographs for each time-point.

**Fig. 3. PTP20-Csk and Csk-PAG association differs in BMMC and RBL cells.** The cells were sensitized with IgE and activated with TNP/BSA 500 ng/ml for the indicated time intervals, and solubilized with saponin/NP-40. PAG (A,D), Csk (B,E), and SHP-2 (C) were immunoprecipitated from RBL cells (A-C) or BMMC (D,E) and the precipitates were checked for the presence of tyrosine-phosphorylated proteins (PY-20), for the associated phosphatase activities (PTP a.), Csk, PTP20, or PAG respectively. Representative data from three to four experiments performed are shown.

**Fig. 4. Phosphatase activity of PTP20 is increased in activated RBL cells.** (A) PTP20 was precipitated using rabbit polyclonal serum raised against PTP20 from nonactivated RBL cells or from cells activated for 5 min with 5.14; 1 hod IgE and 5 min TNP/BSA; 5 min OX7; and 1 hod biotinylated OX7 and 5 min streptavidin. The samples were splitted into two parts, one was blotted for total PTP20, the another was used in the phosphatase in-gel assay to show the phosphatase activity changes based on covalent modifications of PTP20 during the cell activation. Only a weak increase of the PTP20 activity was observed after the cell activation. The phosphatase activity of a whole cell lysate (B) is shown as a control.

**Fig. 5. Distribution of PTP20 and Csk in sucrose density gradients differs in BMMC and RBL cells.** The RBL cells (A) and BMMC (B) were lysed, loaded to the sucrose density gradient and centrifuged. Individual fractions [1 (top) - 9

(bottom)] were collected and analyzed by immunoblotting for the presence of PTP20, Csk, Lyn, PAG, and STAT3. A typical experiment from three performed is shown. (C) Size of PTP20 complexes. Nonactivated cells and cells sensitized with IgE and activated for 10 min with TNP/BSA were lysed in 1% Triton X-100. Nuclei and other insoluble material was removed by centrifugation at 12 000 x g for 2 min at 4°C and 300 μl of the postnuclear supernatant was size fractionated on a Sepharose 4B minicolumn. The presence of PTP20 (left) and Lyn (right) complexes was detected by immunoblotting. Elution peaks of erythrocytes, IgM, and albumin were at fractions 2, 3, and 6, respectively.

**Table 1. Expression profile of nonreceptor PTPs in mouse BMMC and RBL cells.**

| PTP name/ other name | GeneBank acc. no. for primers, strain | 5'-primer* | 3'-primer* | Expression in BMMC** | Expression in RBL** |
|---|---|---|---|---|---|
| PTPN1 / PTP1B | NM_012637.2, rat | 669-689 | 1067-1084 | + | + |
| PTPN2 / TC-PTP | NM_008977.1, mouse | 918-941 | 1149-1172 | + | + |
| PTPN3 / PTPH1 | XM_001059701.1, rat | 1579-1597 | 2039-2058 | + | + |
| PTPN4 / PTP-MEG1 | NM_01993.1, mouse | 1246-1264 | 1502-1519 | + | + |
| PTPN5 / PTPSTEP | NM_019253, rat | 738-759 | 1530-1549 | - | - |
| PTPN6 / SHP-1, PTP-1C | RNU77038, rat | 981-1000 | 1933-1954 | + | + |
| PTPN7 / BPTP-4, HEPTP | NM_145683.1, rat | 509-528 | 1094-1113 | + | + |
| PTPN8 / LYP, PEP | NM_008979.1, mouse | 1120-1139 | 2174-2194 | - | - |
| PTPN9 / MEG2 / PTP-MEG2 | NM_019651.1, mouse | 1918-1936 | 2189-2207 | + | + |
| PTPN11 / SHP-2 / SH-PTP2 | NM_013088, rat | 18-44 | 817-840 | + | + |
| PTPN12 / PTP-PEST | NM_011203.2, mouse | 458-481 | 1242-1258 | + | + |
| PTPN13 / FAP-1 | D83966, mouse | 3530-3549 | 4420-4441 | + | + |
| PTPN14 / PTP36 | NM_008976.1, mouse | 1844-1860 | 2267-2289 | + | - |
| PTPN18 / BDP1 | NM_011206, mouse | 78-103 | 552-575 | - | - |
| PTPN21 / PTPRL10 | NM_011877.1, mouse | 525-545 | 1035-1054 | - | - |
| PTP4A1 / PRL-1 | NM_031579.1, rat | 449-469 | 1068-1087 | + | + |
| PTP4A2 / PRL-2 | BC060549.1, rat | 532-552 | 940-963 | + | - |
| PTP 4A3 / PRL-3 | NM_008975.2, mouse | 887-909 | 1267-1284 | - | - |

*Numbers correspond to nucleotides positioned in the sequences deposited in GeneBank with the accessin numbers indicated.

** Determined by RT-PCR

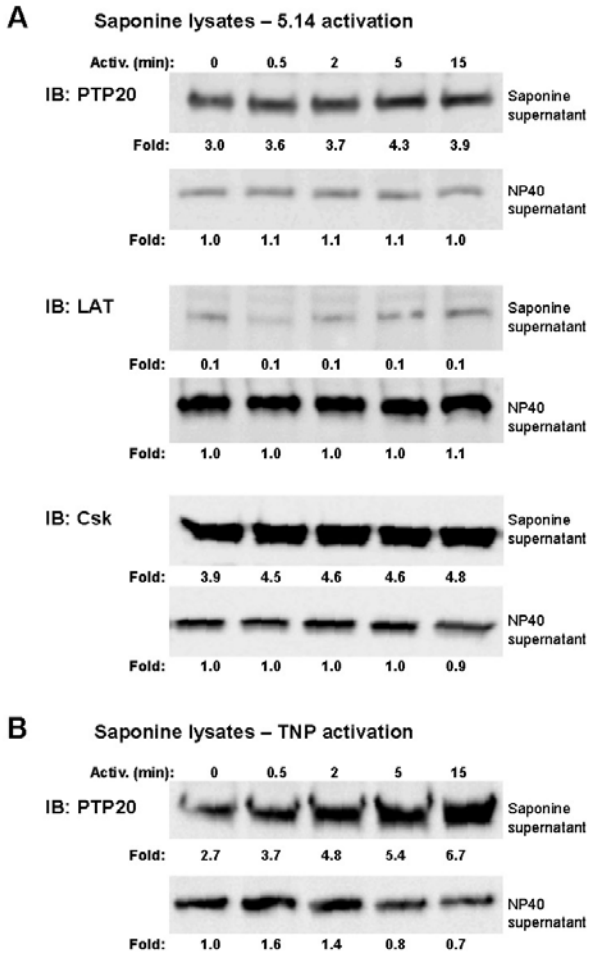
A
Saponine lysates – 5.14 activation
Activ. (min): 0 0.5 2 5 15
IB: PTP20
Saponine supernatant
Fold: 3.0 3.6 3.7 4.3 3.9
NP40 supernatant
Fold: 1.0 1.1 1.1 1.1 1.0
IB: LAT
Saponine supernatant
Fold: 0.1 0.1 0.1 0.1 0.1
NP40 supernatant
Fold: 1.0 1.0 1.0 1.0 1.1
IB: Csk
Saponine supernatant
Fold: 3.9 4.5 4.6 4.6 4.8
NP40 supernatant
Fold: 1.0 1.0 1.0 1.0 0.9
B
Saponine lysates – TNP activation
Activ. (min): 0 0.5 2 5 15
IB: PTP20
Saponine supernatant
Fold: 2.7 3.7 4.8 5.4 6.7
NP40 supernatant
Fold: 1.0 1.6 1.4 0.8 0.7

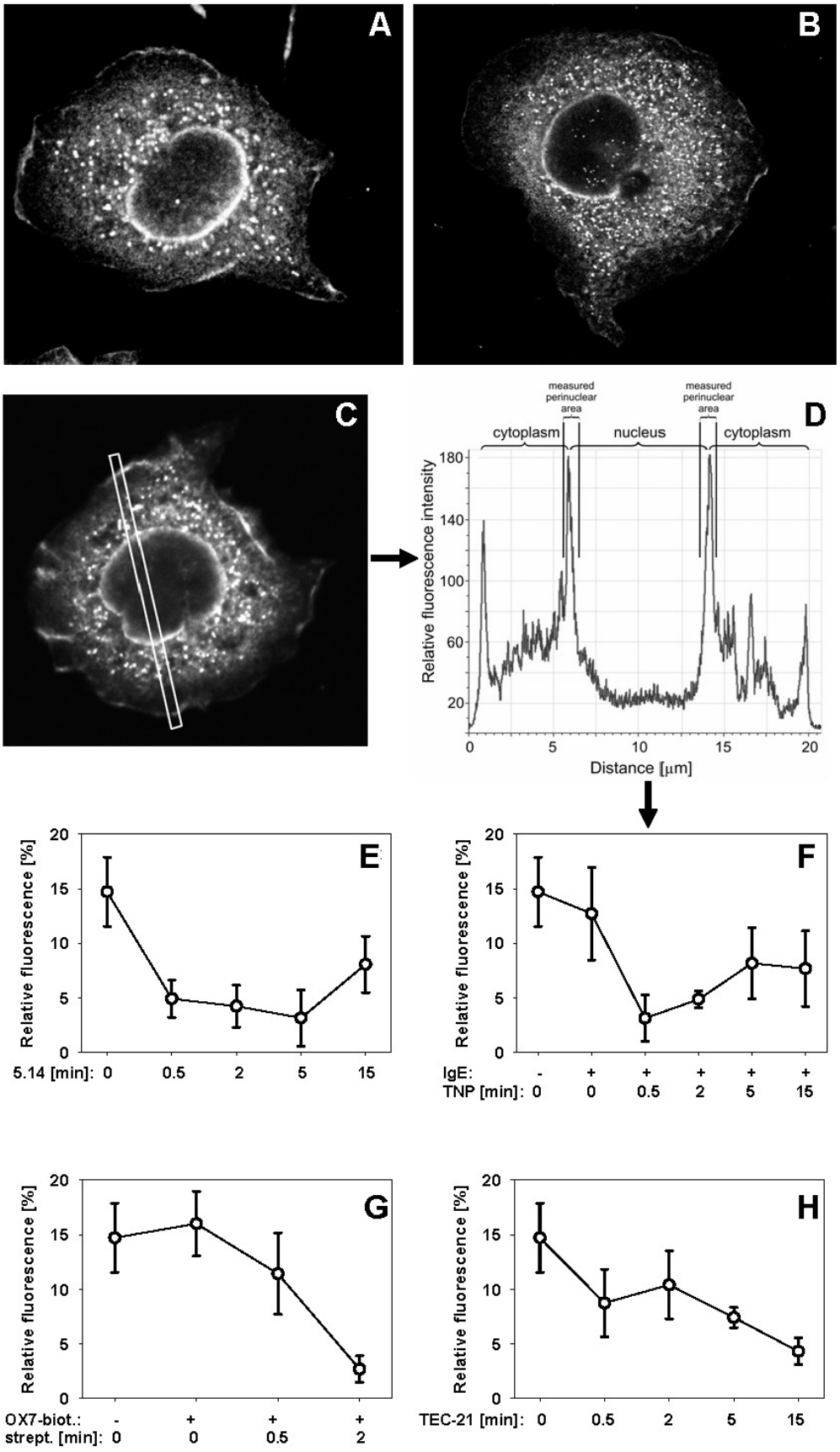
A
B
C
D
measured perinuclear area
measured perinuclear area
cytoplasm
nucleus
cytoplasm
Relative fluorescence intensity
180
140
100
60
20
0
5
10
15
20
Distance [µm]
E
Relative fluorescence [%]
20
15
10
5
0
5.14 [min]: 0 0.5 2 5 15
F
Relative fluorescence [%]
IgE: - + + + + +
TNP [min]: 0 0 0.5 2 5 15
G
Relative fluorescence [%]
OX7-biot.: - + + +
strept. [min]: 0 0 0.5 2
H
Relative fluorescence [%]
TEC-21 [min]: 0 0.5 2 5 15

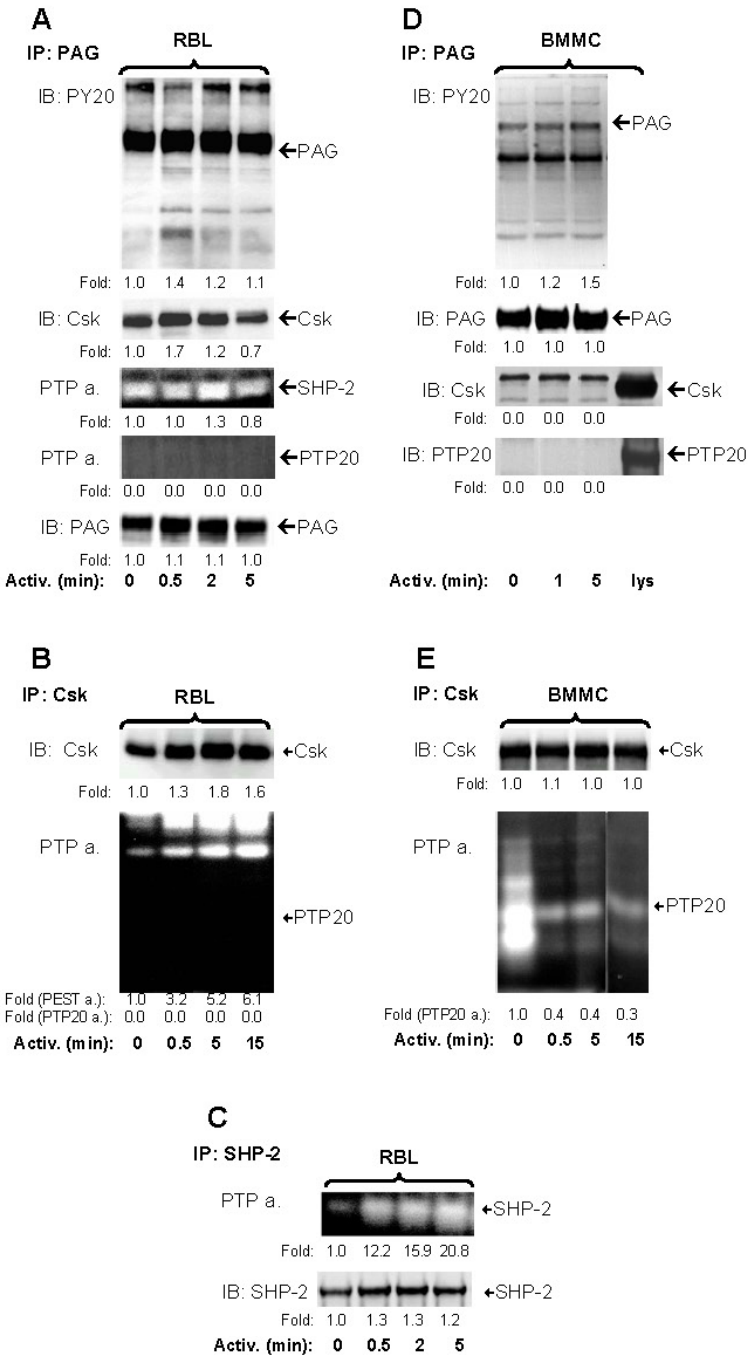
A
IP: PAG
RBL
IB: PY20
←PAG
Fold: 1.0 1.4 1.2 1.1
IB: Csk
←Csk
Fold: 1.0 1.7 1.2 0.7
PTP a.
←SHP-2
Fold: 1.0 1.0 1.3 0.8
PTP a.
←PTP20
Fold: 0.0 0.0 0.0 0.0
IB: PAG
←PAG
Fold: 1.0 1.1 1.1 1.0
Activ. (min): 0 0.5 2 5
D
IP: PAG
BMMC
IB: PY20
←PAG
Fold: 1.0 1.2 1.5
IB: PAG
←PAG
Fold: 1.0 1.0 1.0
IB: Csk
←Csk
Fold: 0.0 0.0 0.0
IB: PTP20
←PTP20
Fold: 0.0 0.0 0.0
Activ. (min): 0 1 5 lys
B
IP: Csk
RBL
IB: Csk
←Csk
Fold: 1.0 1.3 1.8 1.6
PTP a.
←PTP20
Fold (PEST a.): 1.0 3.2 5.2 6.1
Fold (PTP20 a.): 0.0 0.0 0.0 0.0
Activ. (min): 0 0.5 5 15
E
IP: Csk
BMMC
IB: Csk
←Csk
Fold: 1.0 1.1 1.0 1.0
PTP a.
←PTP20
Fold (PTP20 a.): 1.0 0.4 0.4 0.3
Activ. (min): 0 0.5 5 15
C
IP: SHP-2
RBL
PTP a.
←SHP-2
Fold: 1.0 12.2 15.9 20.8
IB: SHP-2
←SHP-2
Fold: 1.0 1.3 1.3 1.2
Activ. (min): 0 0.5 2 5

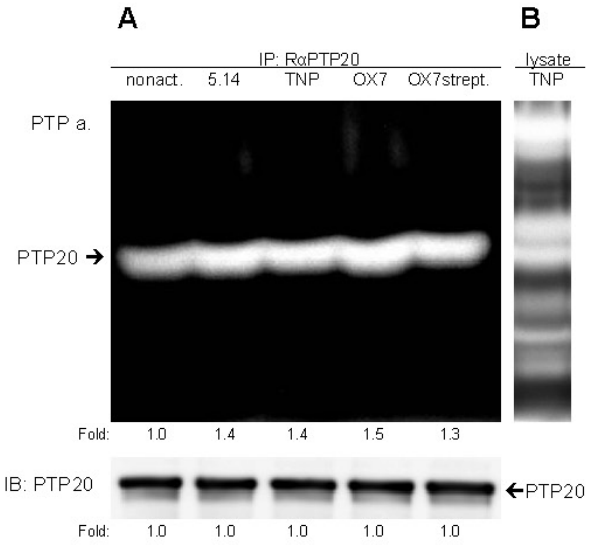
A
B
IP: RαPTP20
lysate
nonact.
5.14
TNP
OX7
OX7strept.
TNP
PTP a.
PTP20
Fold:
1.0
1.4
1.4
1.5
1.3
IB: PTP20
PTP20
Fold:
1.0
1.0
1.0
1.0
1.0

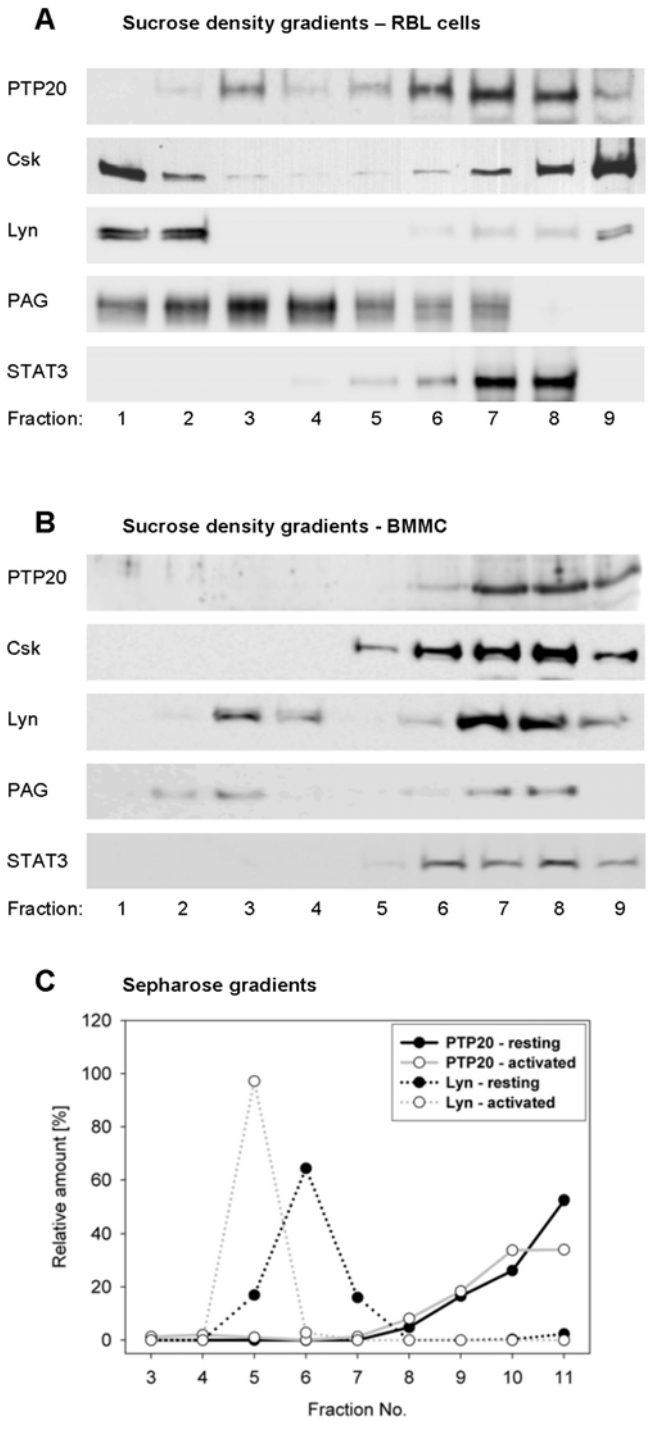
A
Sucrose density gradients – RBL cells
PTP20
Csk
Lyn
PAG
STAT3
Fraction: 1 2 3 4 5 6 7 8 9
B
Sucrose density gradients - BMMC
PTP20
Csk
Lyn
PAG
STAT3
Fraction: 1 2 3 4 5 6 7 8 9
C
Sepharose gradients
PTP20 - resting
PTP20 - activated
Lyn - resting
Lyn - activated
Relative amount [%]
120
100
80
60
40
20
0
3 4 5 6 7 8 9 10 11
Fraction No.

## 6.9

## PTP20/35 hybridoma cell line transfer protocols

## [in Czech]

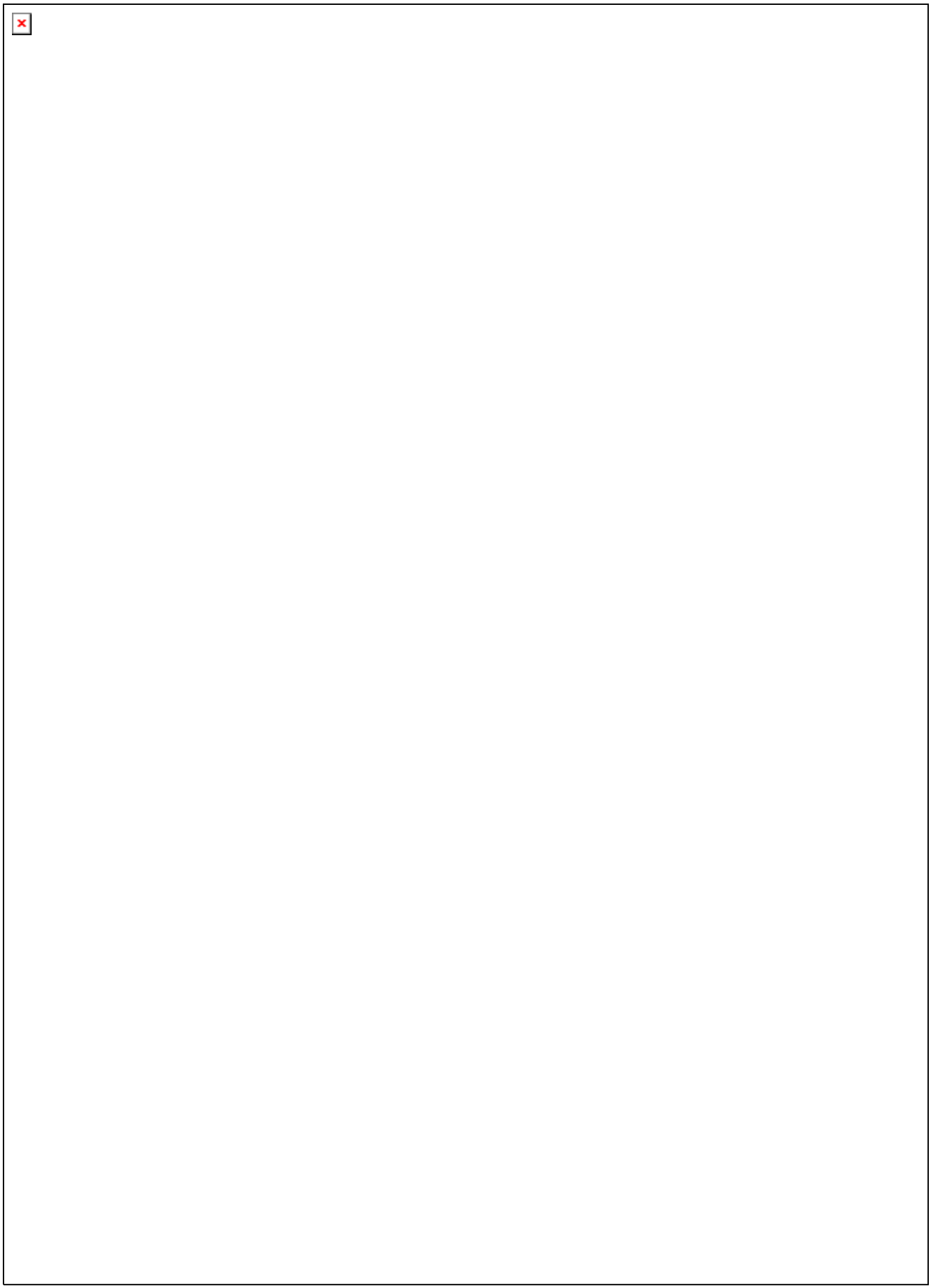

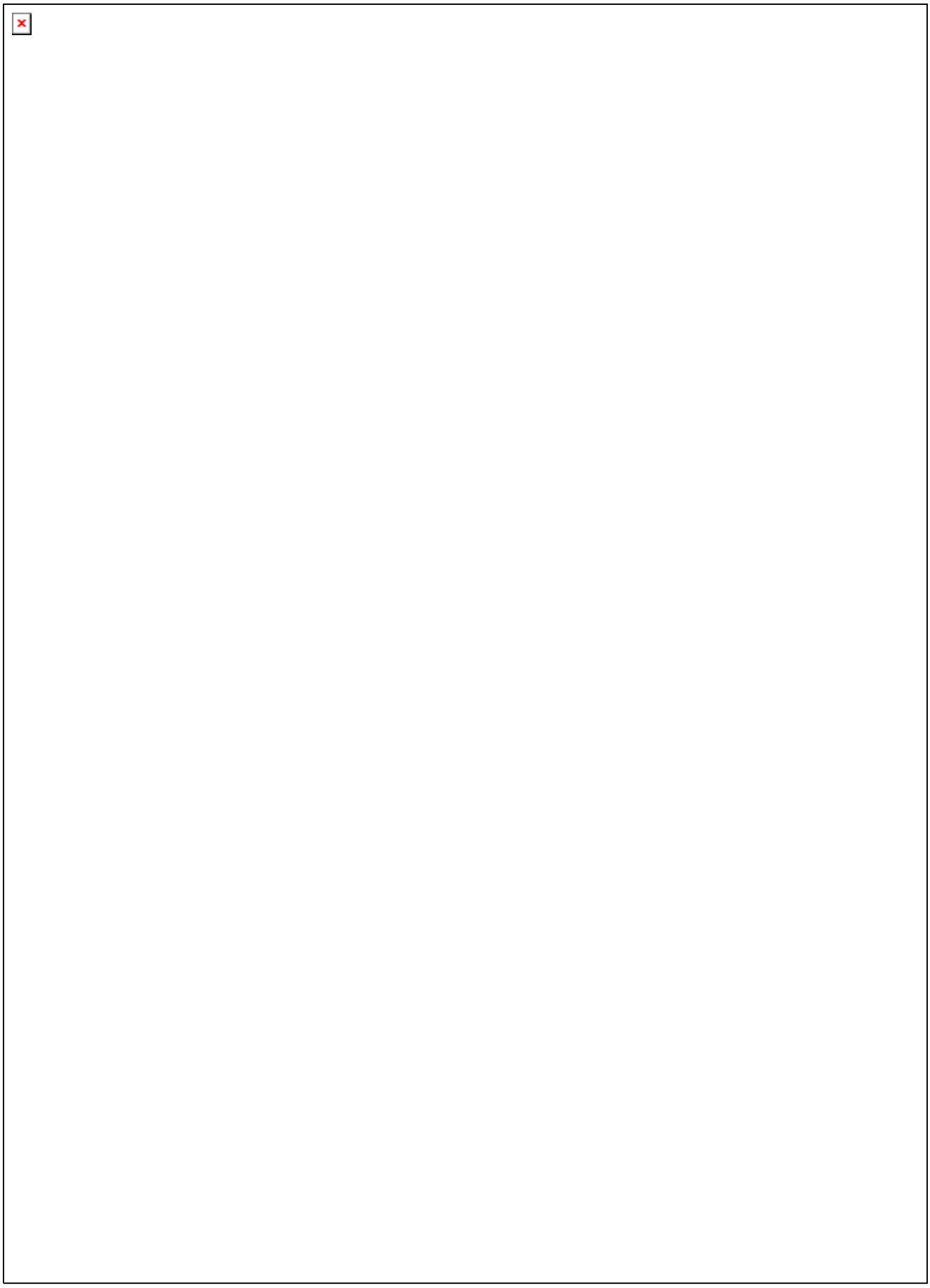

# 7 DISCUSSION

## 7.1 MAIN PARTICULAR OUTCOMES

The main scope of this thesis was to throw light on some of the important mechanisms of the cell signaling with the focus on mast cells, basophils, and hepatocytes. As my PhD studies resulted into eight manuscripts, each covering slightly different topic of the cell signaling, I will try here just to discuss the main outcomes related to the particular aims, as the detailed discussion of the results obtained is present in each of the papers attached.

The fist particular aim was to determine the role of actin in mast cell signaling *via* FcεRI and surface GPI-anchored proteins. We have shown that actin is polymerized not only following the FcεRI-crosslinking (Oka *et al.*, 2002;Torigoe *et al.*, 2004), but also following the dimerization of Thy-1.1 surface glycoprotein using the OX7 mAb (paper 1). Subsequent crosslinking of biotinylated OX7 resulted even into more rapid and extensive actin polymerization reaching its maximum one minute following the Thy-1.1 crosslinking. Unexpectedly, the Thy-1.1-induced actin polymerization was faster and stronger than those induced by FcεRI-crosslinking. This difference may reflect higher density of Thy-1.1 on the surface of RBL cells ($10^6$/cell) compared to the FcεRI ($3*10^5$/cell (Dráberová and Dráber, 1991)), or more likely the different molecular pathways involved in the signaling pathways triggered by Thy-1.1 and FcεRI. For instance FcεRI-driven actin polymerization requires activation of PKC, whereas actin polymerization driven by the adenosine receptor is PKC-independent, but G-protein-dependent (Hall *et al.*, 1997). Molecular background of Thy-1.1-induced actin polymerization remains unknown, but the time-course and extent of actin polymerization following Thy-1.1-crosslinking resembled those induced by the adenosine receptor activation (Apgar, 1994).

Inhibition of actin polymerization by latrunculin B or cytochalasin D resulted into dramatic changes of Thy-1.1-driven cell activation. Most prominent was the strongly enhanced secretory response following the Thy-1.1 aggregation (paper 1), phosphorylation of protein kinase Syk and adaptor proteins LAT and NTAL, and spatiotemporal distribution of PI3K, Gab2, and SHP-2. The effects of destabilization of actin filaments was similar to those observed in FcεRI-stimulated cells (Frigeri and Apgar, 1999;Holowka *et al.*, 2000). Although a connection of Thy-1.1 and FcεRI with actin was predicted long time ago (Seagrave and Oliver, 1990;Apgar, 1990), the mechanism is still not clear. It seems that direct interactions between certain membrane lipids and actin (Le Bihan *et al.*, 2005) may play a role as both Thy-1.1 and FcεRI reside in lipidic domains of specific properties.

The second particular aim was to analyze the role of adaptor NTAL in mast cell signaling *via* FcεRI and Thy-1. Although NTAL is known to be expressed in a variety of immune cells (Brdička *et al.*, 2002), genetic deletion in mice does not result in any notable phenotypic alteration except of mast

cells (paper 2; Zhu *et al.*, 2004;Wang *et al.*, 2005). NTAL$^{-/-}$ mast cells appear to develop normally both *in vitro* and *in vivo* as they epress normal levels of c-kit and FcεRI, their numbers do not differ from wild-type mice at least in the peritoneum, however their activation properties differ from the wild-type (paper 2). Interestingly mast cells and NK cells are the only cells, where both NTAL and LAT – sequentially highly similar adaptor proteins – are expressed together, thus NTAL and LAT may balance the mast cell activation by competing in recruitment of some mast cell signaling molecules and thus their mast cell expression level may be of a higher importance than in other immune cell types, where just one of these proteins is present.

*In vivo* challenge of the mice in an IgE-dependent anaphylaxis model revealed a subtle but increased mast cell degranulation as determined by detection of blood-circulating histamine (paper 2). This is the phenotype observed previously also in Lyn$^{-/-}$ and SHIP-1$^{-/-}$ mice (Huber *et al.*, 1998;Odom *et al.*, 2004). Compared to Lyn or SHIP-1$^{-/-}$ mast cells, NTAL$^{-/-}$ mast cells do not degranulate at suboptimal doses of antigen, whereas mast cells with deletion of the other two genes show enhanced degranulation at suboptimal doses of antigen (Huber *et al.*, 1998;Odom *et al.*, 2004).

When we tested our hypothesis that LAT and NTAL may compete for some of their interaction partners, we found that LAT

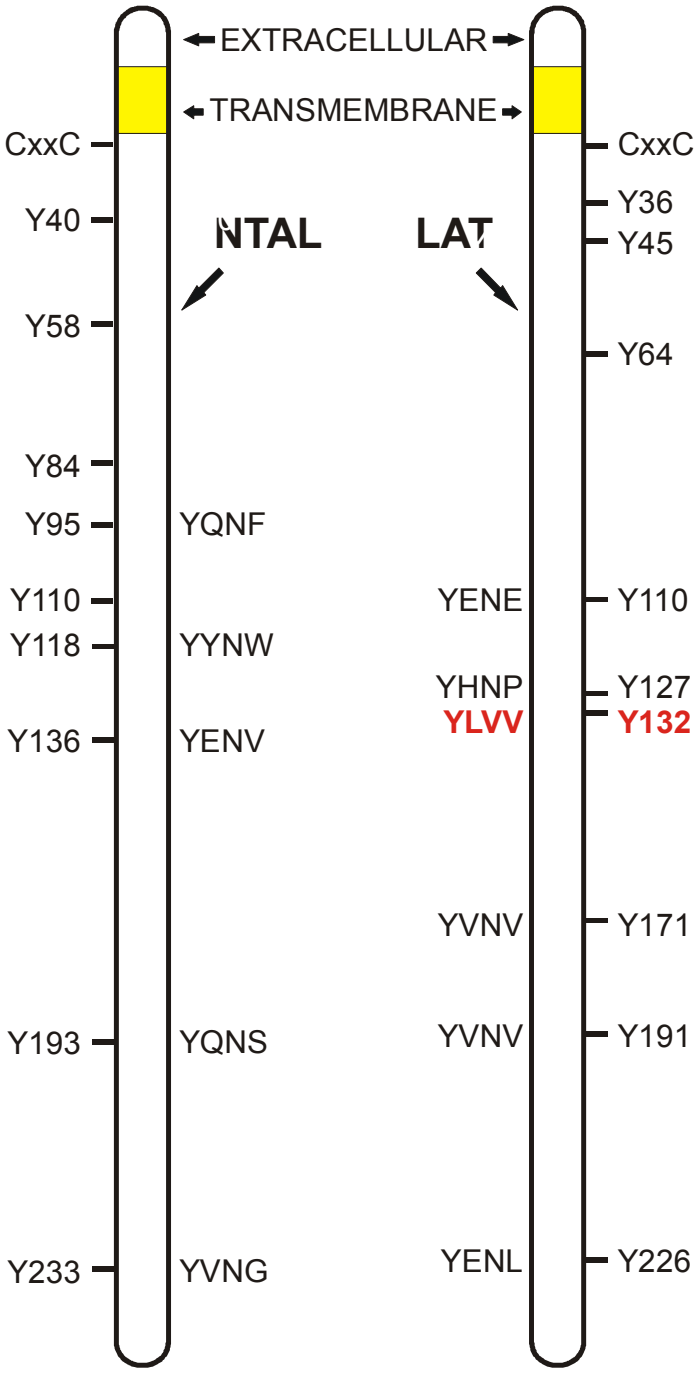


Figure 3. Human NTAL and LAT structural homology. Both adaptors contain a short extracellular part (extracellular) of approximately four aminoacids and a transmebrane domain (transmembrane, shown in yellow) of ~24 aminoacids. Both encode a conserved palmytoylation motif (CxxC) at the cytosolic transmembrane interface. Nine conserved tyrosine residues and their positions are shown. Some of them serve as putative binding sites for the Gads and Grb2 family adaptors (YxN). The motif YLVV (red) uniqe for LAT is known to be responsible for the binding of PLCγ; in mice LAT the PLCγ-binding site is at the position Y136.

phosphorylation is increased in the absence of NTAL (paper 2). In NTAL$^{-/-}$ cells, the molecules thought to be influenced directly by the NTAL deficiency, such as PI3K, ERK and SHP-2, all showed increased total activity. But interestingly, as the tyrosine phosphorylation of LAT was largely increased in in NTAL$^{-/-}$ cells, it can be hypothesized that the phosphorylation of LAT Y132/136 was increased as well. This tyrosine is known to bind PLCγ and regulating its activity in mast cells (Lin and Weiss, 2001;Saitoh *et al.*, 2003). The increased phosphorylation of LAT Y132/136 in NTAL$^{-/-}$ cells is known to result in the increased PLCγ activity, increased PI3 production and into the increased calcium flux, which is the key in mast-cell degranulation (Blank and Rivera, 2004;Rivera, 2005), thus upregulation of Y132/136 phosphorylation may partially explain the observed offects of NTAL deletion.

Both NTAL and LAT are known to be localized to DRMs (called also rafts) as detected by the sucrose gradient ultracentrifugation. Although some disputes exist regarding the portion of LAT and NTAL in DRM fractions (paper 2; Hořejší, 2003;Lindquist *et al.*, 2003;Zhu *et al.*, 2004) and regarding importance of raft localization (Zhang *et al.*, 1998b;Zhu *et al.*, 2005;Tanimura *et al.*, 2006), our study (paper 2) and the study of Zhu (Zhu *et al.*, 2004) showed that there is an increased content of LAT in raft fraction of cell lysates in NTAL$^{-/-}$ mast cells. But at the resolution level of electron microscopy, LAT and NTAL were found to be located into distinct membrane patches, which do not mix together, but can be located aside of each one after FcεRI-aggregation (paper 2). As both LAT and NTAL showed the unexpected distinct localization and spatiotemporal behaviour, we focused on them in detail in two other papers discussed below.

When we focused on NTAL and LAT in mast cell signaling *via* Thy-1, we found that Thy-1 aggregates colocalized with both these two transmembrane adaptor proteins (paper 4), which had been shown previously to inhabit different membrane microdomains (paper 2). Interestingly, extensive Thy-1 aggregation led to closer proximity of LAT and NTAL clusters. Thy-1 aggregation led to tyrosine phosphorylation of these two adaptors. A schematic model of the distribution of Thy-1 isoforms, NTAL and LAT in nonactivated and Thy-1-activated cells is shown in paper 4, figure 10. Although pretreatment with latrunculin did not affect association of several signaling proteins (Lyn, LAT, NTAL and Thy-1) with DRM, it enhanced tyrosine phosphorylation of LAT, NTAL and even Syk, which is not considered to be associated with lipid rafts. It should be noted, however, that Syk could be recruited to lipid rafts through its binding to lipid raft-residing molecules such as Lyn (Amoui *et al.*, 1997) or aggregated FcεRI (Field *et al.*, 1997;Dráberová *et al.*, 2004). Here we reported the first evidence that Thy-1 can affect signaling pathways using both NTAL and LAT adaptors. It indicates that aggregated GPI-anchored proteins can attract different membrane proteins in different clusters and thus can trigger different signaling pathways.

In our last NTAL-related paper, we focused on the analysis of adaptor NTAL in signaling *via* FcεRI in RBL cells (paper 7). We have shown that NTAL regulates FcεRI-mediated signaling at multiple steps and by different mechanisms. At early stages NTAL interferes with tyrosine phosphorylation of several substrates and formation of signaling assemblies, whereas at later stages it regulates the activity of store-operated calcium channels through a distinct mechanism independent of enhanced NTAL tyrosine phosphorylation.

Decreased tyrosine phosphorylation of FcεRI subunits in NTAL overexpressing cells suggested that the activity of Lyn kinase is inhibited. However, immunocomplex kinase assays showed Lyn kinase activity in NTAL overexpressing cells is undiminished, implying that NTAL interferes with the accessibility of Lyn to FcεRI. This possibility is strengthened by data indicating that the amount of Lyn coprecipitated with FcεRI was higher in activated RBL cells than in NTAL overexpressing cells. Because Lyn, like NTAL, seems to be localized in lipid rafts (Dráberová and Dráber, 1993;Brdička *et al.*, 2002), it is possible that direct or indirect interactions of Lyn with NTAL preclude the interaction between Lyn and FcεRI subunits. Although immunoprecipitation and immunocomplex kinase assays failed to show NTAL-Lyn interactions (Dráberová unpubl.), it is possible that procedures used to isolate NTAL immunocomplexes destroyed these interactions.

We also proposed a possible regulatory role of NTAL at different phases of FcεRI-mediated $Ca^{2+}$ signaling (paper 7, figure 9). At early stages of activation NTAL serves as a substrate for protein tyrosine kinases and thus could interfere with phosphorylation of FcεRI and LAT by a competitive mechanism. Furthermore, phosphorylated NTAL binds Grb2 and other signaling molecules, which could modulate the activity of various enzymes, including PI3K and PLCγ. Enhanced activity of PLCγ leads to increased production of IP3 and consequently to elevated levels of cytoplasmic $Ca^{2+}$. At later stages of activation, NTAL could affect the function of SOC channels, reflecting its direct or indirect interactions with channel-forming proteins and/or their regulators such as Orai1 and/or Stim1 (Liou *et al.*, 2005;Roos *et al.*, 2005;Zhang *et al.*, 2006;Cai, 2007;Jousset *et al.*, 2007;Lorin-Nebel *et al.*, 2007;Mignen *et al.*, 2007). This function of NTAL is not dependent on its enhanced tyrosine phosphorylation.

The third particular aim was to describe a role of reactive oxygen and nitrogen species in the regulation of mast cell PTPs. We focused on the major sources and targets of reactive oxide and nitrogen species in mast cells and basophils. In our review (paper 3), we discussed the direct and indirect regulations of class I and II Cys-based protein tyrosine phosphatases (LMW-PTP, PTEN, PTP-PEST, SHP-2, PTP1B, PTPα, PTPε, DEP-1, TC45, SHP-1, HePTP and LAR). The enhanced tyrosine phosphorylation of numerous substrates in $H_2O_2$ pretreated cells was described two decades ago (Hayes and Lockwood, 1987). But the physiological relevance of this phosphorylation was unclear until recently when reversible inactivation of PTP1B by $H_2O_2$ was demonstrated (Lee *et al.*,

1998). Modulation of enzyme activity by disulfide bond formation seems to be a universal mechanism of protein redox regulation in PTPs (Barrett *et al.*, 1999;Chiarugi *et al.*, 2001;Van der Wijk *et al.*, 2003;Li and Whorton, 2003;Cho *et al.*, 2004;Van der Wijk *et al.*, 2004;Barford, 2004;Tonks, 2005;Salmeen and Barford, 2005;Shelton *et al.*, 2005;Seth and Rudolph, 2006;Weibrecht *et al.*, 2007;Yang *et al.*, 2007). The oxidation products of reactive cysteines in PTPs are Cys-SOH, glutathiolylated Cys, a disulfide bond with the neighboring Cys, and most recently found sulfenyl-amide intermediate. The finding that activated mast cells are capable of producing ROS and RNS (paper 3, figures 1 & 2) suggests that these cells may undergo ROS- and RNS-mediated regulation of PTPs involved in FcεRI-mediated signaling. In this connection, it should be noted that NO gas was detected in exhaled breath of asthmatics (Kharitonov *et al.*, 1994), and that NO generated by NOS in lungs could exert combined beneficial and harmful effects in asthma development (Coleman, 2002). The combined data highlight the potential role of redox-regulation in allergy, asthma and inflammatory diseases and could lead to further research on generation of new causal treatments based on targeting of reactive oxide and nitrogen species or their redox-regulated targets involved in signal transduction pathways.

First diagnostic tests for ROS, RNS and their targets already appeared (Heffler *et al.*, 2006) suggesting usage of measurement of exhaled nitric oxide as a diagnostic marker for the airway inflammation in patients with suspected diagnosis of asthma. As rhinitis and asthma are manifestated similarly, nitric oxide detection can be used as a tool for discrimination between allergic rhinitis, chronic rhinosinusitis (both associated with the asthma diagnosis, high content of exhaled nitric oxide), and nonallergic rhinitic (rarely associated with the asthma diagnosis, low content of exhaled nitric oxide) (Rolla *et al.*, 2007). Interestingly, exhaled nitric oxide measurements can be used even for the prediction of asthma relapse in asymptomatic asthmatic children in whom inhaled corticosteroids are discontinued (Pijnenburg *et al.*, 2005).

As ROS and RNS were found to be implicated in the chronic airway inflammation related to the asthma and chronic obstructive pulmonary disease (Barnes, 1990;Repine *et al.*, 1997), it`s no surprise that they cause also contraction of tracheal smooth muscle cells with an augmentation of $Ca^{2+}$ in a ROS-concentration-dependent manner (Kojima *et al.*, 2007). Both the contractile force and calcium concentration increase following the ROS-treatment mimicked the 1μM methacholine treatment. In turn, verapamil (inhibitor of voltage-operated $Ca^{2+}$ channels), or SKF-96365 (1-{β-[3-(4-methoxyphenyl)propoxy]-4-methoxyphenethyl}-1*H*-imidazole hydrochloride, a non-selective inhibitor of $Ca^{2+}$ channels) inhibited the ROS-induced contractions partially (verapamil) or completely (SKF-96365). RhoA is probably responsible for the changes in cell shape as the contractions are inhibited also by the Rho-kinase inhibitor Y-27632 ((R)-(+)-*trans*-*N*-(4-Pyridyl)-4-(1-aminoethyl)-cyclohexanecarboxamide) (Kojima *et al.*, 2007).

The combined data show the unexpectedly high potential of ROS, RNS, and their targets for the farmacological treatment. The major obstruction that ROS and RNS can diffuse through plasma membranes of surrounding cells may be circumvented by targeting of the treatment by cell- and organelle-specific tags.

The fourth particular aim was to analyze the spatiotemporal distribution of surface glycoprotein Thy-1 at different levels of resolution. In this study (paper 4) we used RBL cells and their transfectants expressing both endogenous Thy-1.1 and exogenous Thy-1.2 genes and analyzed topography of the Thy-1 isoforms and Thy-1-induced signaling events. Light microscopy showed that both Thy-1 isoforms were in the plasma membrane distributed randomly and independently. Electron microscopy on isolated membrane sheets and fluorescence resonance energy transfer analysis indicated cross-talk between Thy-1.1 isoforms and between Thy-1.1 and FcεRI. This cross-talk was dependent on actin filaments, which might be explained by direct interactions of actin with certain membrane lipids (Le Bihan *et al.*, 2005) surrounding GPI-proteins-containing islets and by observations that whole rafts – containing both transmembrane and GPI-anchored molecules in a cholesterol-enriched environment – are attached to the actin cytoskeleton as observed using transmission electron microscopy of plasma membrane sheets (Lillemeier *et al.*, 2006). Interestingly, B.Wilson`s group reported recently that FcεRI-bearing domains contain <50% of fully saturated fatty acids, inconsistent with the recruitment of aggregated receptors or GPI-anchored proteins to liquid ordered domains (Surviladze *et al.*, 2007). Moreover they reported that FcεRI domains contained two times more sphingomyelin and a high ratio of cholesterol to total fatty acid content compared with Thy 1-enriched domains. But it seems that the spatial separation of molecules doesn`t necessarily mean that they will not communicate with the third molecule as Drbal *et al.* reported that in naive T-cells, the TCR triggering induced the immobilization of CD45 and CD48 at different positions within the T-cell interface. Moreover the second GPI protein, CD59, did not co-immobilize indicating lipid raft heterogeneity in living T lymphocytes (Drbal *et al.*, 2007). The system presented by Drbal *et al.* resemble that reported by us (paper 4) when Thy-1.1 associates with both, NTAL and LAT, and creates bridges between spatiotemporally separated clusters of these two adaptors. Analysis of the role of these two transmembrane adaptors in the Thy-1.1-driven signaling was a subject of the aim 2.

Although Thy-1 is the most abundant molecule at the surface of some immune cells (Zucchini *et al.*, 2001), function of Thy-1 in immune cells remains still enigmatic. Thy-$1^{-/-}$ thymocytes exhibit impaired maturation of $CD4^+/CD8^+$ cells to their single-positive stage, probably due to inappropriate negative selection (Hueber *et al.*, 1997) resulting in the reduced *in vivo* immune response including contact hypersensitivity, irritant dermatitis, and delayed-type hypersensitivity. On the molecular level, decreased protein tyrosine phosphorylation and reduced $Ca^{2+}$ flux was recorded after TCR/CD3 triggering of T-cells (Beissert *et al.*, 1998). Recently, various functions of Thy-1 were reported –

namely in cell-cell and cell-matrix interactions in axon regeneration, apoptosis, adhesion, migration, cancer, and fibrosis (Rege and Hagood, 2006a). From the viewpoint of mast-cell research, the proposed interactions between Src kinases and Thy-1 (Rege and Hagood, 2006a) are of a great importance. Thy-1 was reported to interact with Fyn and Lyn (Thomas and Samelson, 1992;NarisawaSaito *et al.*, 1996), but as the GPI anchor of Thy-1 does not span the plasma membrane, some connection mechanism is needed. First, Thy-1 might activate Src-family kinases through direct interactions of the GPI anchor of Thy-1 with palmitoylated cysteines of Src-family kinases (Rege and Hagood, 2006a). Second, Thy-1 may signal to Src-family kinases throught an intermediate transmembrane adaptor protein. In support of the second hypothesis, Thy-1 was previously reported to coprecipitate with an 85-90 kDa transmembrane phosphoprotein containing a binding site for SH2-domain-containing proteins (Durrheim *et al.*, 2001), which is probably PAG (Heneberg, unpubl.). Additionally, in this study, we have shown that Thy-1 co-localize with another two transmembrane adaptors, LAT and NTAL at the level of electron microscopy (paper 4, figure 8), and even it causes their phosphorylation (paper 4, figure 9).

The fifth particular aim was to analyze a topography of STAT3 complexes in the signaling of freshly isolated hepatocytes and HepG2 cells. Previous studies showed that removal of cholesterol by MβCD inhibits IL-6-induced tyrosine phosphorylation of STAT3. This was taken as an important evidence that lipid rafts are involved in IL-6 signaling (Sehgal *et al.*, 2002;Shah *et al.*, 2002). Moreover caveolin was thought to be responsible for the proper STAT3 signaling (Sehgal *et al.*, 2002;Shah *et al.*, 2002). However, in paper 5, we found that tyrosine phosphorylation of STAT3 is not dependent on intact lipid rafts and caveolin. Rather, it seems to be dependent on preassociated transducer complexes, which are sensitive to nonionic detergents. These complexes are involved in regulating equilibrium between kinases and phosphatases.

Further we extended our study performed on HepG2 cells to the isolated hepatocytes as tumor cells could exhibit changes in composition of glycosphingolipids and thus change the properties of plasma membrane microdomains (Hakomori *et al.*, 1983;Hiraiwa *et al.*, 1990). The most significant changes associated with malignant transformation are changes in composition of glycosphingolipids, reflecting aberrant glycosylation. This could be caused by a defect in single or multiple glycosyltransferases and is often followed by accumulation of precursor lipids. Alternatively, tumor cells could exhibit glycosphingolipid biosynthesis pathways which are minor or absent in non-transformed cells, resulting in formation of so-called “neoglycosphingolipids”. In HepG2 cells, the typical tumor-associated markers are sulfated and highly acidic glycosphingolipids, which are almost undetectable in normal liver tissue (Hiraiwa *et al.*, 1990). We have shown for the first time that in nonactivated as well as IL-6-, PV- or IL-6+PV-activated freshly isolated hepatocytes, almost all STAT3 is localized in high density fraction as well as in HepG2 cells and that only a small part of STAT3 (<2%) is found in

flotation fractions. Furthermore, *in vitro* kinase assays with hepatocytes confirmed the previous results obtained with HepG2 cells that STAT3 signaling assemblies are sensitive to nonionic detergents which preserve DRMs. Thus, the conclusions drawn in this study from HepG2 cells can be extended to normal hepatocytes. The topography of signaling molecules and the interplay between kinases and phosphatases in IL-6-mediated STAT3 triggering have to be critically reevaluated, as it seems to be the major pathway used by drugs such as rosuvastatin (Mayer *et al.*, 2007).

The sixth particular aim was to verify that our new method for isolation of plasma membrane sheets from nonadherent cells doesn`t lead to the unintentional cell activation (paper 6). Quarter-century before, Sanan and Anderson (1991) established a method for isolation of plasma membrane sheets from cells growing as adherent monolayer on the glass surface. As such cells are rare among non-transformed and non-activated leukocytes, we focused first to establish a new method for isolation of plasma membrane sheets from nonadherent cells (paper 6). Some authors employed cell immobilization using immunoligands or binding of cells to the poly-L-lysine (Schade and Levine, 2002;Lillemeier *et al.*, 2006), but these steps were both long-lasting and partially activating cell signaling pathways. Here we developed a new, very rapid method for the isolation of plasma membrane sheets from nonadherent cells. This method requires only ~1 min for settling the cells to ultraclean glass coverslips, and it is independent of binding of the cells to the poly-L-lysine. This method doesn`t induce any significant cell degranulation or phosphorylation of the cellular proteins (paper 6, figure 2), it even doesn`t require any preincubation of the cells at low temperatures. The method also doesn`t require active cytoskeleton-driven adsorption, thus it can be used in the presence of actin polymerization inhibitors (paper 6). Although the method is restricted to a fixed speciment, high-resolution electron microscopy combined with the immunogold labeling is a powerful technique used in a number of plasma membrane organization studies of us (papers 2, 4 & 7) and others (Wilson *et al.*, 2002;Prior *et al.*, 2003;Wilson *et al.*, 2004;Lillemeier *et al.*, 2006). Extension of the method to rapid and simple isolation of plasma membrane sheets from nonadherent cells contributes to its wider applicability and thus to the better understanding of signaling events in the immune cells.

The seventh particular aim was to screen for the nonreceptor protein tyrosine phosphatases in mast cells and basophils and to show the involvement of phosphatase PTP20 in the mast cell signaling (paper 8). Despite the progress within last years, mRNA for only seven nonreceptor PTPs was known from mast cells and basophils (Heneberg and Dráber, 2002a), which did not suffice the needs for explanation of changes in protein tyrosine phosphorylation in mast cells. Using RT-PCR, we detected mRNA for 11 nonreceptor PTPs in RBL and BMMC cells. Among the molecules new for mast cells were PTPN2, PTPN4, PTPN13, PTP4A1, PTP4A2, and PTP20. We identified new rat mRNAs of several potentially important phosphatase molecules – PTPN4 known to participate on Src/Fyn

signaling (Möller *et al.*, 1994;Edwards *et al.*, 2001), PTPN13 known to play role in apoptosis, oxidative stress, and cell migration (Nedachi and Conti, 2004;Wang *et al.*, 2004;Ying *et al.*, 2006;Ivanov *et al.*, 2006;Dromard *et al.*, 2007), and PTP-MEG2, reported from RBLs pursuant to antibody-based studies (Huynh *et al.*, 2004), but isolation of a clone AF520784 was the first sequential confirmation of its presence in RBL cells.

Out of the number of newly identified phosphatases in mast cells and basophils we selected PTP20 as it seems to be important for the immunoreceptor signaling beeing found previously to be associated with T-cell submembrane PTKs (Wang *et al.*, 2001a). It was reported to be expressed in brain, colon, in primitive haematopoietic cells and in several tumor-derived cell lines (Kim *et al.*, 1996;Cong *et al.*, 2000). As it was known to interact with Csk kinase (Wang *et al.*, 2001a), and with actin through PSTPIP-family adaptors (Wu *et al.*, 1998), we selected this molecule as a potential candidate molecule important for mast cell signaling. We found that PTP20 activity is slightly increased following FcεRI- or Thy-1-mediated activation. But, surprisingly, we coroborated the interaction of PTP20 with Csk only in BMMC, not in RBL cells. In Csk immunoprecipitates from RBL cells, PTP20 was replaced by another PEST-type phosphatase, PTP-PEST, and PTP20 wasn`t present even in large macromolecular aggregates nor in detergent-resistant membrane fractions. We expected that PTP20 could be present in PAG-Csk complexes in mast cells, but finally we found that these complexes common for RBL and many other cells (Brdička *et al.*, 2000;Ohtake *et al.*, 2002a) are not present in BMMC. As PTP20 was recently described as a possible tumor supressor (Gensler *et al.*, 2004;Gandhi *et al.*, 2005;Guimaraes *et al.*, 2006), it is possible that dissimilar properties of PTP20 in RBL cells, which are of the tumorigenic origin, compared to BMMC cultivated from freshly isolated bone marrows may reflect its tumor-suppresor activity.

To be able to detect specific activities of nonreceptor PTPs *in vitro*, I implemented the method of phosphatase in-gel assay. This method was developed in mid 90`s by Burridge and Nelson (1995) and can be applied to for detection of phosphatase activities of all the nonreceptor PTPs. The advantage of this method is that the researcher is able to detect exact molecular weight of the respective proteins with phosphatase activities and is able to distinguish between several PTPs in one sample, as the method involves sodium dodecyl sulfate polyacrylamide gel electrophoresis fractionation step. The ability to distinguish between different PTPs in one sample is a great advantage making the phosphatase in-gel assay highly usable in detection of phosphatase activities of co-precipitating molecules in immunoprecipitates of various signaling proteins. As phosphatases were recently found to be reversibly deactivated by oxidation of their active residues (paper 3; Meng *et al.*, 2002;Ross *et al.*, 2007;Weibrecht *et al.*, 2007), and thus regulated not only by reversible phosphorylation, but also by reversible oxidation, the phosphatase in-gel assay was currently improved. Iodoacetic acid is used now to alkylate selectively the thiolate anion of the active Cys in a

reduced form, whereas the oxidized Cys is resistant to alkylation. The standard phosphatase in-gel assay is then used and allows to discriminate between samples treated and untreated with the iodoacetic acid, thus showing changes in phosphatase activities caused by reversible oxidation of PTPs (Markova *et al.*, 2005;Meng *et al.*, 2005).

## 7.2 POSSIBLE PHARMACOTHERAPEUTICAL APPLICATIONS OF THE THESIS RESULTS

Understanding of cell submembrane signaling properties is the key premise to be able to treat and manage a vast number of diseases coupled with abnormalities in the membrane and submembrane signaling molecules. ***Though my thesis is focused mostly on the basic science, we achieved several application outcomes and elucidated number of cell signaling mechanisms utilizable in the search for new drugs against many widely widespread syndromes***.

Among these was the most frequent monogenic disease with dominant inheritance, **Noonan syndrome**, which occurs at an incidence of about 1:1,000 of life births (Nora *et al.*, 1974). Noonan syndrome – a disease with cardiac symptomatology - is caused by mutations in genes coding for the phosphatase SHP-2 and factor SOS1 (Araki *et al.*, 2004;Roberts *et al.*, 2007). Elucidation of the mechanism of SHP-2 involvement in the signalosomes of proteins Gab2 and Grb2 were among the particular aims of papers 1 and 2. For this purpose, I introduced a method of phosphatase in-gel assay (Burridge and Nelson, 1995) – it was the first use of this method in the Central and Eastern Europe.

I participated on the analysis of essential functions of the cellular **cytoskeleton in the signaling of mast cells** and basophils through the FcεRI (responsible for allergic reactions) and some GPI-anchored proteins (responsible i.a. for the cell communication with the extracellular parasites (Baorto *et al.*, 1997)). We found that actin cytoskeleton forms some form of a „fence“ hampering the unwanted contacts of individual molecules during the mast cell signaling (papers 1, 4 & 7), as reported before from some other cell types (Kusumi *et al.*, 1999;Boggs and Wang, 2004;Morone *et al.*, 2006). It is important to note, that inhibition of actin polymerization using latrunculin B mimicked the FcεRI- or Thy-1-driven activation (paper 1 & 4). As we reported that actin depolymerization led to the enhanced FRET between FcεRI and Thy-1 (paper 4) and as FcεRI is known to interact with the actin microfilaments itself (Frigeri and Apgar, 1999), we hypothesized that actin is the main regulator responsible for the physical separation of membrane molecules. This hypothesis was supported also by findings that actin-driven rearrangements of the cytoskeleton are responsible for the localization of GPI-anchored proteins in immunological synapses (Loertscher and Lavery, 2002). Interestingly, Thy-1 (a GPI-anchored protein of our interest) was previously reported to regulate cytoskeletal organization and migration by modulating the activity of RhoGAP and RhoGTPase (Barker *et al.*, 2004).

An important part of the thesis was the analysis of function of transmembrane adaptor proteins. Most of these molecules were described during the last decade and it is clear that they play very important role in the immune cell signaling (Ubersax and Ferrell, 2007;Engelke *et al.*, 2007). I focused mostly on the analysis of the role of transmembrane adaptor proteins NTAL and LAT, where we described characteristics of the NTAL$^{-/-}$ mice (paper 2), some spatiotemporal properties of both these adaptors (paper 4) and characteristics of RBL cells with enhanced or decreased NTAL expression (paper 7). As NTAL was originally cloned as one of genes deleted in the **Williams syndrome**, an autosomal dominant disorder appearing with the frequency 1:10,000 of life births (Grimm and Wesselhoeft, 1980), and as we and others shown its involvement in $Ca^{2+}$ signaling, cell adhesion, and in regulation of some other mast cell signaling cascades, NTAL seems to be an important pharmacological target. Another transmembrane adaptor, PAG, is known to be involved in the infection of cells by *Theileria parva*, an obligate intracellular protozoan parasite which is the causative agent of Corridor disease, Zimbabwean theileriosis, and above all **East Coast fever**, an acute, leukemia-like disease of cattle. The intralymphocytic stage of the parasite induces blastogenesis and clonal expansion of quiescent bovid lymphocytes accompanied by the increased PAG expression (Baumgartner *et al.*, 2003). Studies of the PAG interactions with its potential partners Csk and PTP20 were among the aims of the paper 8, and the research still continues more in detail at the department.

Another recently emerging topic in the mast cell research is the regulation of their physiological functions by the reactive oxide species. In contrary to previous views, it is thought that they are important not only for mast cell proliferation and apoptosis, but also for proper signaling through the FcεRI or c-kit (Swindle and Metcalfe, 2007). In our review (paper 3) we focused on the influence of reactive oxygen and nitrogen species on the regulation of PTPs. As nitric oxide was reported to be in exhaled breath of asthmatics (Kharitonov *et al.*, 1994) and as presence of exhaled nitric oxide was even used as a diagnostic test for **asthma** in rhinitic patients with asthmatic symptoms (Heffler *et al.*, 2006), the therapeutic potential of novel drugs regulating the production of reactive oxygen and nitrogen species is tremendous.

The last major topic included in this thesis was the detailed analysis of changes in spatiotemporal distribution of STAT3 in isolated hepatocytes and in the tissue cell line HepG2 activated by LI-6 cytokine. STAT3 is the key protein in the maintenance of glucose homeostasis. As STAT3 behaves as a latent transcription factor in resting cells, it need to be activated by IL-5, IL-6, IL-11, epidermal growth factor, leukemia inhibitory factor, oncostatin M, or ciliary neurotrophic factor (Lutticken *et al.*, 1994). The demand for some activation stimulus suggest its high utilizability in the **diabetes mellitus** farmacotherapy.

# 8 CONCLUSIONS

1 Thy-1 aggregation caused a rapid increase in the level of filamentous actin. Actin polymerization following Thy-1 aggregation was faster and more extensive than that observed following FcεRI-aggregation.

Inhibition of actin polymerization by latrunculin B or cytochalasin D resulted into dramatic increase of degranulation and calcium response in Thy-1-activated RBL cells.

Inhibition of actin polymerization by latrunculin B or cytochalasin D alone induced a weak increase in tyrosine phosphorylation of cellular proteins including phosphorylation of the β subunit of the FcεRI, but it didn`t shift the distribution of FcεRI on the sucrose density gradient in both resting and Thy-1-stimulated cells.

2. By comparing FcεRI-mediated signaling events in NTAL- and LAT-deficient BMMC, we found that antigen-mediated degranulation responses were unexpectedly increased in NTAL-deficient mast cells. The earliest event affected was enhanced tyrosine phosphorylation of LAT in antigen-activated cells. This was accompanied by enhanced tyrosine phosphorylation and enzymatic activity of PLCγ1 and PLCγ2 resulting in elevated levels of IP3 and free intracellular $Ca^{2+}$. NTAL-deficient BMMCs also exhibited an enhanced activity of PI3K and SHP-2. Although both LAT and NTAL are considered to be localized in membrane rafts, immunogold electron microscopy on isolated membrane sheets demonstrated their independent clustering. The combined data show that NTAL is functionally and topographically different from LAT.

We reported the first evidence that Thy-1 can affect signaling pathways using both NTAL and LAT adaptors. Thy-1 aggregates colocalized with both transmembrane adaptor proteins, NTAL and LAT, which had been shown to inhabit different membrane microdomains. Thy-1 aggregation led to tyrosine phosphorylation of both these adaptors. The combined data indicate that aggregated GPI-anchored proteins can attract different membrane proteins in different clusters and thus can trigger different signaling pathways.

We also analyzed properties of RBL cells with enhanced or reduced NTAL expression. Overexpression of NTAL led to changes in cell morphology, enhanced formation of actin filaments and inhibition of the FcεRI-induced tyrosine phosphorylation of the FcεRI subunits, Syk kinase and LAT and all downstream activation events, including calcium and secretory responses. In contrast, reduced expression of NTAL had little effect on early FcεRI-induced signaling events but inhibited calcium mobilization and secretory response. Calcium response was also repressed in Ag-activated cells defective in Grb2, a major target of phosphorylated

NTAL. Unexpectedly, in cells stimulated with thapsigargin, an inhibitor of the endoplasmic reticulum $Ca^{2+}$ ATPase, the amount of cellular NTAL directly correlated with the uptake of extracellular calcium even though no enhanced tyrosine phosphorylation of NTAL was observed.

We concluded that NTAL regulates FcεRI-mediated signaling at multiple steps and by different mechanisms. At early stages NTAL interferes with tyrosine phosphorylation of several substrates and formation of signaling assemblies, whereas at later stages it regulates the activity of store-operated calcium channels through a distinct mechanism independent of enhanced NTAL tyrosine phosphorylation.

3. We described a role of reactive oxygen and nitrogen species in the regulation of class I and II Cys-based protein tyrosine phosphatases together with the major sources and targets of reactive oxide and nitrogen species in mast cells and basophils. Redox-regulated protein tyrosine phosphatases are thought to be important targets in the development of new ways of therapeutic intervention in allergies and inflammatory diseases.

4. Using RBL cells and their transfectants expressing both endogenous Thy-1.1 and exogenous Thy-1.2 genes we analyzed topography of the Thy-1 isoforms and Thy-1-induced signaling events. Light microscopy showed that both Thy-1 isoforms were distributed randomly and independently in the plasma membrane. Electron microscopy on isolated membrane sheets and FRET analysis indicated cross-talk between Thy-1 isoforms and between Thy-1 and FcεRI. This cross-talk was dependent on actin filaments.

5. Pretreatment of HepG2 hepatoma cells with MβCD, which removes cholesterol and destroys lipid rafts, inhibited tyrosine phosphorylation of STAT3 in IL-6-activated, but not PV-activated cells. Furthermore, when the cells were lysed under conditions preserving lipid rafts, no IL-6- or PV-induced phosphorylation of STAT3 was observed. Although most of the STAT3 was found in large MβCD-resistant assemblies in both non-activated and IL-6-activated cells, its association with lipid rafts was weak or undetectable. The extent of IL-6-induced tyrosine phosphorylation of STAT3 was comparable in cells expressing low or high levels of caveolin. Similar STAT3 transducer complexes were observed in freshly isolated rat hepatocytes. The combined data suggest that STAT3 tyrosine phosphorylation occurs in preformed transducer complexes that can be activated in the absence of intact lipid rafts or caveolin.

6. Rapid, simple and versatile method for isolation of PM sheets from nonadherent cells was developed and used for examination of the topography of FcεRI, LAT and NTAL in murine BMMC. The data were compared with those obtained with widely used but tumor-derived RBL

cells and they demonstrated unexpected properties of FcεRI signaling assemblies in BMMC and emphasised the importance of studies of PM sheets isolated from non-tumor cells.

7. Using RT-PCR, we detected mRNA for 11 nonreceptor PTPs in RBL and BMMC cells. Among the molecules new for mast cells were PTPN2, PTPN4, PTPN13, PTP4A1, PTP4A2, and PTP20. We identified new rat mRNAs of several potentially important phosphatase molecules – PTPN4, PTPN13, and PTP-MEG2. Out of them we focused on PTP20 using newly developed monoclonal antibody against PTP20. We found that large pool of PTP20 interacts with a mast cell nuclear membrane, and deassociates from it in a time-dependent manner following the aggregation of FcεRI or surface glycoproteins Thy-1.1 and TEC-21. Another pool of PTP20 was present in perinuclear cytoplasm and the smallest part was associated with the plasma membrane. We found that PTP20 was associated with Csk and deassociates from it following the FcεRI aggregation. Interestingly, we did not find any PTP20 phosphatase activity in immunoprecipitates of PAG from RBL. In RBL cells, PAG complexes contained Csk and another phosphatase, SHP-2; Csk itself was found to interact with PTP-PEST, but not with PTP20. Association of SHP-2 and Csk with PAG was dependent of the FcεRI activation and on the expression of another adaptor NTAL. While in mouse BMMC, PAG did not associated with Csk, nor with PTP20. Interestingly, PTP-PEST was replaced by PTP20 in BMMC Csk complexes. PTP20-Csk interaction is not necessary for proper cell signaling and may be replaced by other PEST domain-bearing phosphatases.

   As an application output, I developed a set of mono- and polyclonal antibodies against nonreceptor PTPs. Monoclonal antibody PTP20/35 directed against phosphatase PTP20 was transferred to the spin-off company EXBIO Praha, a.s. for futher commercial utilization.

# 9 REFERENCES


Acuto O. & Cantrell D. (2000) T cell activation and the cytoskeleton. *Annual Review of Immunology* **18,** 165-184.

Aguado E., Richelme S., Nunez-Cruz S., Miazek A., Mura A.M., Richelme M., Guo X.J., Sainty D., He H.T., Malissen B., & Malissen M. (2002) Induction of T helper type 2 immunity by a point mutation in the LAT adaptor. *Science* **296,** 2036-2040.

Ali K., Bilancio A., Thomas M., Pearce W., Gilfillan A.M., Tkaczyk C., Kuehn N., Gray A., Giddings J., Peskett E., Fox R., Bruce I., Walker C., Sawyer C., Okkenhaug K., Finan P., & Vanhaesebroeck B. (2004) Essential role for the p110δ phosphoinositide 3-kinase in the allergic response. *Nature* **431,** 1007-1011.

Alonso A., Sasin J., Bottini N., Friedberg I., Friedberg I., Osterman A., Godzik A., Hunter T., Dixon J., & Mustelin T. (2004) Protein tyrosine phosphatases in the human genome. *Cell* **117,** 699-711.

Amoui M., Dráberová L., Tolar P., & Dráber P. (1997) Direct interaction of Syk and Lyn protein tyrosine kinases in rat basophilic leukemia cells activated via type I Fcε receptors. *European Journal of Immunology* **27,** 321-328.

Apgar J.R. (1990) Antigen-induced cross-linking of the IgE receptor leads to an association with the detergent-insoluble membrane skeleton of rat basophilic leukemia (RBL-2H3) cells. *Journal of Immunology* **145,** 3814-3822.

Apgar J.R. (1994) Polymerization of actin in RBL-2H3 cells can be triggered through either the IgE receptor or the adenosine receptor but different signaling pathways are used. *Molecular Biology of the Cell* **5,** 313-322.

Araki T., Mohi M.G., Ismat F.A., Bronson R.T., Williams I.R., Kutok J.L., Yang W.T., Pao L.I., Gilliland D.G., Epstein J.A., & Neel B.G. (2004) Mouse model of Noonan syndrome reveals cell type- and gene dosage-dependent effects of Ptpn11 mutation. *Nature Medicine* **10,** 849-857.

Ayscough K.R., Stryker J., Pokala N., Sanders M., Crews P., & Drubin D.G. (1997) High rates of actin filament turnover in budding yeast and roles for actin in establishment and maintenance of cell polarity revealed using the actin inhibitor latrunculin-A. *Journal of Cell Biology* **137,** 399-416.

Baorto D.M., Gao Z.M., Malaviya R., Dustin M.L., vanderMerwe A., Lublin D.M., & Abraham S.N. (1997) Survival of FimH-expressing enterobacteria in macrophages relies on glycolipid traffic. *Nature* **389,** 636-639.

Barford D. (2004) The role of cysteine residues as redox-sensitive regulatory switches. *Current Opinion in Structural Biology* **14,** 679-686.

Barker T.H., Grenett H.E., MacEwen M.W., Tilden G.S., Fuller G.M., Settleman J., Woods A., Murphy-Ullrich J., & Hagood J.S. (2004) Thy-1 regulates fibroblast focal adhesions, cytoskeletal organization and migration through modulation of p190 RhoGAP and Rho GTPase activity. *Experimental Cell Research* **295,** 488-496.

Barnes P.J. (1990) Reactive Oxygen Species and Airway Inflammation. *Free Radical Biology and Medicine* **9,** 235-243.

Barrett W.C., DeGnore J.P., Konig S., Fales H.M., Keng Y.F., Zhang Z.Y., Yim M.B., & Chock P.B. (1999) Regulation of PTP1B via glutathionylation of the active site cysteine 215. *Biochemistry* **38,** 6699-6705.

Baumgartner M., Angelisová P., Setterblad N., Mooney N., Werling D., Hořejší V., & Langsley G. (2003) Constitutive exclusion of Csk from Hck-positive membrane microdomains permits Src kinase-dependent proliferation of *Theileria*-transformed B lymphocytes. *Blood* **101,** 1874-1881.

Baumruker T. & Prieschl E.E. (2000) The role of sphingosine kinase in the signaling initiated at the high-affinity receptor for IgE (FcεRI) in mast cells. *International Archives of Allergy and Immunology* **122,** 85-90.

Beissert S., He H.T., Hueber A.O., Lellouch A.C., Metze D., Mehling A., Luger T.A., Schwarz T., & Grabbe S. (1998) Impaired cutaneous immune responses in Thy-1-deficient mice. *Journal of Immunology* **161,** 5296-5302.

Besmer P., Murphy J.E., George P.C., Qiu F., Bergold P.J., Lederman L., Snyder H.W., Brodeur D., Zuckerman E.E., & Hardy W.D. (1986) A New Acute Transforming Feline Retrovirus and Relationship of Its Oncogene V-Kit with the Protein-Kinase Gene Family. *Nature* **320,** 415-421.

Bischoff S.C. (2007) Role of mast cells in allergic and non-allergic immune responses: comparison of human and murine data. *Nature Reviews Immunology* **7,** 93-104.

Blank U. & Rivera J. (2004) The ins and outs of IgE-dependent mast-cell exocytosis. *Trends in Immunology* **25,** 266-273.

Boggs J.M. & Wang H.M. (2004) Co-clustering of galactosylceramide and membrane proteins in oligodendrocyte membranes on interaction with polyvalent carbohydrate and prevention by an intact cytoskeleton. *Journal of Neuroscience Research* **76,** 342-355.

Brdička T., Imrich M., Angelisová P., Brdičková N., Horváth O., Špička J., Hilgert I., Lusková P., Dráber P., Novák P., Engels N., Wienands J., Simeoni L., Osterreicher J., Aguado E., Malissen M., Schraven B., & Hořejší V. (2002) Non-T cell activation linker (NTAL): A transmembrane adaptor protein involved in immunoreceptor signaling. *Journal of Experimental Medicine* **196,** 1617-1626.

Brdička T., Pavlištová D., Leo A., Bruyns E., Kořínek V., Angelisová P., Scherer J., Shevchenko A., Shevchenko A., Hilgert I., Černý J., Drbal K., Kuramitsu Y., Kornacker B., Hořejší V., & Schraven B. (2000) Phosphoprotein associated with glycosphingolipid-enriched microdomains (PAG), a novel ubiquitously expressed transmembrane adaptor protein, binds the protein tyrosine kinase Csk and is involved in regulation of T cell activation. *Journal of Experimental Medicine* **191,** 1591-1604.

Brdičková N., Brdička T., Anděra L., Špička J., Angelisová P., Milgram S.L., & Hořejší V. (2001) Interaction between two adapter proteins, PAG and EBP50: a possible link between membrane rafts and actin cytoskeleton. *Febs Letters* **507,** 133-136.

Brdičková N., Brdička T., Angelisová P., Horváth O., Špička J., Hilgert I., Pačes J., Simeoni L., Kliche S., Merten C., Schraven B., & Hořejší V. (2003) LIME: A new membrane raft-associated adaptor protein involved in CD4 and CD8 coreceptor signaling. *Journal of Experimental Medicine* **198,** 1453-1462.

Brown D.A. (2006) Lipid rafts, detergent-resistant membranes, and raft targeting signals. *Physiology* **21,** 430-439.

Bruyns E., Kirchgessner H., Meuer S., & Schraven B. (1998) Biochemical analysis of the CD45-p56$^{lck}$ complex in Jurkat T cells lacking expression of lymphocyte phosphatase-associated phosphoprotein. *International Immunology* **10,** 185-194.

Bunnell S.C., Kapoor V., Trible R.P., Zhang W.G., & Samelson L.E. (2001) Dynamic actin polymerization drives T cell receptor-induced spreading: A role for the signal transduction adaptor LAT. *Immunity* **14,** 315-329.

Burridge K. & Nelson A. (1995) An In-Gel Assay for Protein-Tyrosine-Phosphatase Activity - Detection of Widespread Distribution in Cells and Tissues. *Analytical Biochemistry* **232,** 56-64.

Cai X.J. (2007) Molecular evolution and structural analysis of the $Ca^{2+}$ release-activated $Ca^{2+}$ channel subunit, Orai. *Journal of Molecular Biology* **368,** 1284-1291.

Chakraborty A., Dyer K.F., Cascio M., Mietzner T.A., & Tweardy D.J. (1999) Identification of a novel Stat3 recruitment and activation motif within the granulocyte colony-stimulating factor receptor. *Blood* **93,** 15-24.

Chazal N. & Gerlier D. (2003) Virus entry, assembly, budding, and membrane rafts. *Microbiology and Molecular Biology Reviews* **67,** 226-237.

Cheng P.C., Brown B.K., Song W.X., & Pierce S.K. (2001) Translocation of the B cell antigen receptor into lipid rafts reveals a novel step in signaling. *Journal of Immunology* **166,** 3693-3701.

Chiarugi P., Fiaschi T., Taddei M.L., Talini D., Giannoni E., Raugei G., & Ramponi G. (2001) Two vicinal cysteines confer a peculiar redox regulation to low molecular weight protein tyrosine phosphatase in response to platelet-derived growth factor receptor stimulation. *Journal of Biological Chemistry* **276,** 33478-33487.

Cho S.H., Lee C.H., Ahn Y., Kim H., Kim H., Ahn C.Y., Yang K.S., & Lee S.R. (2004) Redox regulation of PTEN and protein tyrosine phosphatases in $H_2O_2$-mediated cell signaling. *Febs Letters* **560,** 7-13.

Coleman J.W. (2002) Nitric oxide: a regulator of mast cell activation and mast cell-mediated inflammation. *Clinical and Experimental Immunology* **129,** 4-10.

Coleman J.W., Holliday M.R., Kimber I., Zsebo K.M., & Galli S.J. (1993) Regulation of mouse peritoneal mast-cell secretory function by stem-cell factor, IL-3 or IL-4. *Journal of Immunology* **150,** 556-562.

Columbo M., Horowitz E.M., Botana L.M., MacGlashan D.W., Bochner B.S., Gillis S., Zsebo K.M., Galli S.J., & Lichtenstein L.M. (1992) The human recombinant c-kit receptor ligand, Rhscf, induces mediator release from human cutaneous mast-cells and enhances IgE-dependent mediator release from both skin mast-cells and peripheral-blood basophils. *Journal of Immunology* **149,** 599-608.

Cong F., Spencer S., Cote J.F., Wu Y., Tremblay M.L., Lasky L.A., & Goff S.P. (2000) Cytoskeletal protein PSTPIP1 directs the PEST-type protein tyrosine phosphatase to the c-Abl kinase to mediate Abl dephosphorylation. *Molecular Cell* **6,** 1413-1423.

Contri A., Brunati A.M., Trentin L., Cabrelle A., Miorin M., Cesaro L., Pinna L.A., Zambello R., Semenzato G., & Donella-Deana A. (2005) Chronic lymphocytic leukemia B cells contain anomalous Lyn tyrosine kinase, a putative contribution to defective apoptosis. *Journal of Clinical Investigation* **115,** 369-378.

Cooper J.A. (1987) Effects of Cytochalasin and Phalloidin on Actin. *Journal of Cell Biology* **105,** 1473-1478.

Cruse G., Kaur D., Yang W., Duffy S.M., Brightling C.E., & Bradding P. (2005) Activation of human lung mast cells by monomeric immunoglobulin E. *European Respiratory Journal* **25,** 858-863.

Davidson D., Schraven B., & Veillette A. (2007) PAG-associated FynT regulates calcium signaling and promotes anergy in T lymphocytes. *Molecular and Cellular Biology* **27,** 1960-1973.

Denu J.M., Stuckey J.A., Saper M.A., & Dixon J.E. (1996) Form and function in protein dephosphorylation. *Cell* **87,** 361-364.

Dráberová L. & Dráber P. (1991) Functional expression of the endogenous Thy-1 gene and the transfected murine Thy-1.2 gene in rat basophilic leukemia cells. *European Journal of Immunology* **21,** 1583-1590.

Dráberová L. & Dráber P. (1993) Thy-1 glycoprotein and Src-like protein-tyrosine kinase p53/p56$^{Lyn}$ are associated in large detergent-resistant complexes in rat basophilic leukemia cells. *Proceedings of the National Academy of Sciences of the United States of America* **90,** 3611-3615.

Dráberová L., Lebduška P., Hálová I., Tolar P., Štokrová J., Tolarová H., Korb J., & Dráber P. (2004) Signaling assemblies formed in mast cells activated via Fcε receptor I dimers. *Eur.J.Immunol.* **34,** 2209-2219.

Drbal K., Moertelmaier M., Holzhauser C., Muhammad A., Fuertbauer E., Howorka S., Hinterberger M., Stockinger H., & Schutz G.J. (2007) Single-molecule microscopy reveals heterogeneous dynamics of lipid raft components upon TCR engagement. *International Immunology* **19,** 675-684.

Dromard M., Bompard G., Glondu-Lassis M., Puech C., Chalbos D., & Freiss G. (2007) The putative tumor suppressor gene PTPN13/PTPL1 induces apoptosis through insulin receptor substrate-1 dephosphorylation. *Cancer Research* **67,** 6806-6813.

Durrheim G.A., Garnett D., Dennehy K.M., & Beyers A.D. (2001) Thy-1 associated pp85-90 is a potential docking site for SH2 domain-containing signal transduction molecules. *Cell Biology International* **25,** 33-42.

Edwards K., Davis T., Marcey D., Kurihara J., & Yamamoto D. (2001) Comparative analysis of the Band 4.1/ezrin-related protein tyrosine phosphatase Pez from two Drosophila species: implications for structure and function. *Gene* **275,** 195-205.

Engelke M., Engels N., Dittmann K., Stork B., & Wienands J. (2007) $Ca^{2+}$ signaling in antigen receptor-activated B lymphocytes. *Immunological Reviews* **218,** 235-246.

Field K.A., Holowka D., & Baird B. (1997) Compartmentalized activation of the high affinity immunoglobulin E receptor within membrane domains. *Journal of Biological Chemistry* **272,** 4276-4280.

Field K.A., Holowka D., & Baird B. (1999) Structural aspects of the association of FcεRI with detergent-resistant membranes. *Journal of Biological Chemistry* **274,** 1753-1758.

Frigeri L. & Apgar J.R. (1999) The role of actin microfilaments in the down-regulation of the degranulation response in RBL-2H3 mast cells. *Journal of Immunology* **162,** 2243-2250.

Galli S.J., Nakae S., & Tsai M. (2005) Mast cells in the development of adaptive immune responses. *Nature Immunology* **6,** 135-142.

Gandhi T.K.B., Chandran S., Peri S., Saravana R., Amanchy R., Prasad T.S.K., & Pandey A. (2005) A Bioinformatics Analysis of Protein Tyrosine Phosphatases in Humans. *DNA Research* **12,** 79-89.

Gensler M., Buschbeck M., & Ullrich A. (2004) Negative regulation of HER2 signaling by the PEST-type protein-tyrosine phosphatase BDP1. *Journal of Biological Chemistry* **279,** 12110-12116.

Gilfillan A.M. & Tkaczyk C. (2006) Integrated signalling pathways for mast-cell activation. *Nature Reviews Immunology* **6,** 218-230.

Gounni A.S. (2006) The high-affinity IgE receptor (FcεRI): a critical regulator of airway smooth muscle cells? *American Journal of Physiology-Lung Cellular and Molecular Physiology* **291,** L312-L321.

Grimm T. & Wesselhoeft H. (1980) The Genetic-Aspects of Williams-Beuren Syndrome and the Isolated Form of the Supravalvular Aortic-Stenosis Investigation of 128 Families. *Zeitschrift fur Kardiologie* **69,** 168-172.

Gu H.H., Saito K., Klaman L.D., Shen J.Q., Fleming T., Wang Y.P., Pratt J.C., Lin G.S., Lim B., Kinet J.P., & Neel B.G. (2001) Essential role for Gab2 in the allergic response. *Nature* **412,** 186-190.

Guimaraes G.S., Latini F.R.M., Camacho C.P., Maciel R.M.B., Dias-Neto E., & Cerutti J.M. (2006) Identification of candidates for tumor-specific alternative splicing in the thyroid. *Genes Chromosomes & Cancer* **45,** 540-553.

Gupta N. & DeFranco A.L. (2007) Lipid rafts and B cell signaling. *Seminars in Cell & Developmental Biology* **in press.,** doi:10.1016/j.semcdb.2007.07.009.

Haan S., Hemmann U., Hassiepen U., Schaper F., Schneider-Mergener J., Wollmer A., Heinrich P.C., & Grotzinger J. (1999) Characterization and binding specificity of the monomeric STAT3-SH2 domain. *Journal of Biological Chemistry* **274,** 1342-1348.

Hakomori S., Kannagi R., Nudelman E., & Levery S. (1983) Oncodevelopmental Carbohydrate Determinants Defined by Monoclonal-Antibodies. *Hybridoma* **2,** 117.

Hall A.L., Wilson B.S., Pfeiffer J.R., Oliver J.M., & Sklar L.A. (1997) Relationship of ligand-receptor dynamics to actin polymerization in RBL-2H3 cells transfected with the human formyl peptide receptor. *Journal of Leukocyte Biology* **62,** 535-546.

Hálová I., Dráberová L., & Dráber P. (2002) A novel lipid raft-associated glycoprotein, TEC-21, activates rat basophilic leukemia cells independently of the type 1 Fcε receptor. *International Immunology* **14,** 213-223.

Hayes G.R. & Lockwood D.H. (1987) Role of Insulin-Receptor Phosphorylation in the Insulinomimetic Effects of Hydrogen-Peroxide. *Proceedings of the National Academy of Sciences of the United States of America* **84,** 8115-8119.

Heffler E., Guida G., Marsico P., Bergia R., Bommarito L., Ferrero N., Nebiolo F., De Stefani A., Usai A., Bucca C., & Rolla G. (2006) Exhaled nitric oxide as a diagnostic test for asthma in rhinitic patients with asthmatic symptoms. *Respiratory Medicine* **100,** 1981-1987.

Heinrich P.C., Behrmann I., Haan S., Hermanns H.M., Muller-Newen G., & Schaper F. (2003) Principles of interleukin (IL)-6-type cytokine signalling and its regulation. *Biochemical Journal* **374,** 1-20.

Heinrich P.C., Behrmann I., Muller-Newen G., Schaper F., & Graeve L. (1998) Interleukin-6-type cytokine signalling through the gp130/Jak/STAT pathway. *Biochemical Journal* **334,** 297-314.

Heneberg P. & Dráber P. (2002a) Nonreceptor protein tyrosine and lipid Phosphatases in type I Fcε receptor-mediated activation of mast cells and basophils. *International Archives of Allergy and Immunology* **128,** 253-263.

Heneberg P. & Dráber P. (2002b) Nonreceptor protein tyrosine and lipid Phosphatases in type I Fcε receptor-mediated activation of mast cells and basophils. *International Archives of Allergy and Immunology* **128,** 253-263.

Heneberg P. & Dráber P. (2002c) Nonreceptor protein tyrosine and lipid Phosphatases in type I Fcε receptor-mediated activation of mast cells and basophils. *International Archives of Allergy and Immunology* **128,** 253-263.

Heneberg P. & Dráber P. (2002d) Nonreceptor protein tyrosine and lipid Phosphatases in type I Fcε receptor-mediated activation of mast cells and basophils. *International Archives of Allergy and Immunology* **128,** 253-263.

Hiraiwa N., Fukuda Y., Imura H., Tadanoaritomi K., Nagai K., Ishizuka I., & Kannagi R. (1990) Accumulation of highly acidic sulfated glycosphingolipids in human hepatocellular carcinoma defined by a series of monoclonal antibodies. *Cancer Research* **50,** 2917-2928.

Holowka D., Sheets E.D., & Baird B. (2000) Interactions between FcεRI and lipid raft components are regulated by the actin cytoskeleton. *Journal of Cell Science* **113,** 1009-1019.

Holtick U., Vockerodt M., Pinkert D., Schoof N., Sturzenhofecker B., Kussebi N., Lauber K., Wesselborg S., Loffler D., Horn F., Trumper L., & Kube D. (2005) STAT3 is essential for Hodgkin lymphoma cell proliferation and is a target of tyrphostin AG17 which confers sensitization for apoptosis. *Leukemia* **19,** 936-944.

Hořejší V. (2003) The roles of membrane microdomains (rafts) in T cell activation. *Immunological Reviews* **191,** 148-164.

Hořejší V. (2004) Transmembrane adaptor proteins in membrane microdomains: important regulators of immunoreceptor signaling. *Immunology Letters* **92,** 43-49.

Huber M., Helgason C.D., Damen J.E., Liu L., Humphries R.K., & Krystal G. (1998) The src homology 2-containing inositol phosphatase (SHIP) is the gatekeeper of mast cell degranulation. *Proceedings of the National Academy of Sciences of the United States of America* **95,** 11330-11335.

Hueber A.O., Bernard A.M., Langlet el Battari C., Marguet D., Massol P., Foa C., Brun N., Garcia S., Stewart C., Pierres M., & He H.T. (1997) Thymocytes in Thy-1$^{-/-}$ mice show augmented TCR signaling and impaired differentiation. *Current Biology* **7,** 705-708.

Hundley T.R., Gilfillan A.M., Tkaczyk C., Andrasi T.B., Metcalfe D.D., & Beaven M.A. (2004) Kit and FcεRI mediate unique and convergent signals for release of inflammatory mediators from human mast cells. *Blood* **104,** 2410-2417.

Hutchcroft D.E., Geahlen R.L., Deanin G.G., & Oliver J.M. (1992) FcεRI-mediated tyrosine phosphorylation and activation of the 72-kDa protein tyrosine kinase, PTK72, in RBL-2H3 rat tumor mast cells. *Proceedings of the National Academy of Sciences of the United States of America* **89,** 9107-9111.

Huynh H., Bottini N., Williams S., Cherepanov V., Musumeci L., Saito K., Bruckner S., Vachon E., Wang X.D., Kruger J., Chow C.W., Pellecchia M., Monosov E., Greer P.A., Trimble W., Downey G.P., & Mustelin T. (2004) Control of vesicle fusion by a tyrosine phosphatase. *Nature Cell Biology* **6,** 831-839.

Ishizuka T., Chayama K., Takeda K., Hamelmann E., Terada N., Keller G.M., Johnson G.L., & Gelfand E.W. (1999) Mitogen-activated protein kinase activation through Fcε receptor I and stem cell factor receptor is differentially regulated by phosphatidylinositol 3-kinase and calcineurin in mouse bone marrow-derived mast cells. *Journal of Immunology* **162,** 2087-2094.

Ishizuka T., Kawasome H., Terada N., Takeda K., Gerwins P., Keller G.M., Johnson G.L., & Gelfand E.W. (1998) Stem cell factor augments FcεRI-mediated TNF-alpha production and stimulates MAP kinases via a different pathway in MC/9 mast cells. *Journal of Immunology* **161,** 3624-3630.

Ivanov V.N., Ronai Z., & Hei T.K. (2006) Opposite roles of FAP-1 and dynamin in the regulation of Fas (CD95) translocation to the cell surface and susceptibility to fas ligand-mediated apoptosis. *Journal of Biological Chemistry* **281,** 1840-1852.

Iwaki S., Jensen B.M., & Giffillan A.M. (2007) NTAL/LAB/LAT2. *International Journal of Biochemistry & Cell Biology* **39,** 868-873.

Janssen E., Zhu M.H., Craven B., & Zhang W. (2004) Linker for activation of B cells: A functional equivalent of a mutant linker for activation of T cells deficient in phospholipase C-γ1 binding. *Journal of Immunology* **172,** 6810-6819.

Jing S.Q. & Trowbridge I.S. (1990) Nonacylated Human Transferrin Receptors Are Rapidly Internalized and Mediate Iron Uptake. *Journal of Biological Chemistry* **265,** 11555-11559.

Jousset H., Frieden M., & Demaurex N. (2007) STIM1 knockdown reveals that store-operated $Ca^{2+}$ channels located close to sarco/endoplasmic $Ca^{2+}$ ATPases (SERCA) pumps silently refill the endoplasmic reticulum. *Journal of Biological Chemistry* **282,** 11456-11464.

Kalesnikoff J., Huber M., Lam V., Damen J.E., Zhang J., Siraganian R.P., & Krystal G. (2001) Monomeric IgE stimulates signaling pathways in mast cells that lead to cytokine production and cell survival. *Immunity* **14,** 801-811.

Kawakami T. & Galli S.J. (2002) Regulation of mast-cell and basophil function and survival by IgE. *Nature Reviews Immunology* **2,** 773-786.

Kharitonov S.A., Yates D., Robbins R.A., Logansinclair R., Shinebourne E.A., & Barnes P.J. (1994) Increased Nitric-Oxide in Exhaled Air of Asthmatic-Patients. *Lancet* **343,** 133-135.

Kim Y.W., Wang H.Y., Sures I., Lammers R., Martell K.J., & Ullrich A. (1996) Characterization of the PEST family protein tyrosine phosphatase BDP1. *Oncogene* **13,** 2275-2279.

Kishimoto T. (2005a) IL-6 - From laboratory to bedside. *Clinical Reviews in Allergy & Immunology* **28,** 177-185.

Kishimoto T. (2005b) Interleukin-6: From basic science to medicine - 40 years in immunology. *Annual Review of Immunology* **23,** 1-21.

Kleuss C. & Krause E. (2003) $G\alpha_s$ is palmitoylated at the N-terminal glycine. *Embo Journal* **22,** 826-832.

Kojima K., Kume H., Ito S., Oguma T., Shiraki A., Kondo M., Ito Y., & Shimokata K. (2007) Direct effects of hydrogen peroxide on airway smooth muscle tone: Roles of $Ca^{2+}$ influx and Rho-kinase. *European Journal of Pharmacology* **556,** 151-156.

Kraft S. & Kinet J.P. (2007) New developments in FcεRI regulation, function and inhibition. *Nature Reviews Immunology* **7,** 365-378.

Kurita A., Takizawa T., Takayama T., Totsukawa K., Katsubara S., Shibahara H., Orgebin-Crist M.C., Sendo F., Shinkai Y., & Araki Y. (2001) Identification, cloning, and initial characterization of a novel mouse testicular germ cell-specific antigen. *Biology of Reproduction* **64,** 935-945.

Kusumi A., Nakada C., Ritchie K., Murase K., Suzuki K., Murakoshi H., Kasai R.S., Kondo J., & Fujiwara T. (2005) Paradigm shift of the plasma membrane concept from the two-dimensional continuum fluid to the partitioned fluid: High-speed single-molecule tracking of membrane molecules. *Annual Review of Biophysics and Biomolecular Structure* **34,** 351-378.

Kusumi A., Suzuki K., & Koyasako K. (1999) Mobility and cytoskeletal interactions of cell adhesion receptors. *Current Opinion in Cell Biology* **11,** 582-590.

Lackmann M., Harpur A.G., Oates A.C., Mann R.J., Gabriel A., Meutermans W., Alewood P.F., Kerr I.M., Stark G.R., & Wilks A.F. (1998) Biomolecular interaction analysis of IFNγ-induced signaling events in whole-cell lysates: prevalence of latent STAT1 in high-molecular weight complexes. *Growth Factors* **16,** 39-51.

Laemmli U.K. (1970) Cleavage of structural proteins during the assembly of the head of bacteriophage T4. *Nature* **227,** 680-685.

Lafont F. & van der Goot F.G. (2005) Oiling the key hole. *Molecular Microbiology* **56,** 575-577.

Le Bihan T., Pelletier D., Tancrede P., Heppell B., Chauvet J.P., & Gicquaud C.R. (2005) Effect of the polar headgroup of phospholipids on their interaction with actin. *Journal of Colloid and Interface Science* **288,** 88-96.

Lee S.R., Kwon K.S., Kim S.R., & Rhee S.G. (1998) Reversible inactivation of protein-tyrosine phosphatase 1B in A431 cells stimulated with epidermal growth factor. *Journal of Biological Chemistry* **273,** 15366-15372.

Lencer W.I. & Saslowsky D. (2005) Raft trafficking of $AB_5$ subunit bacterial toxins. *Biochimica et Biophysica Acta-Molecular Cell Research* **1746,** 314-321.

Li S. & Whorton A.R. (2003) Regulation of protein tyrosine phosphatase 1B in intact cells by S-nitrosothiols. *Archives of Biochemistry and Biophysics* **410,** 269-279.

Li X., Oghi K.A., Zhang J., Krones A., Bush K.T., Glass C.K., Nigam S.K., Aggarwal A.K., Maas R., Rose D.W., & Rosenfeld M.G. (2003) Eya protein phosphatase activity regulates Six1-Dach-Eya transcriptional effects in mammalian organogenesis. *Nature* **426,** 247-254.

Lillemeier B.F., Pfeiffer J.R., Surviladze Z., Wilson B.S., & Davis M.M. (2006) Plasma membrane-associated proteins are clustered into islands attached to the cytoskeleton. *Proceedings of the National Academy of Sciences of the United States of America* **103,** 18992-18997.

Lin J. & Weiss A. (2001) Identification of the minimal tyrosine residues required for linked for activation of T cell function. *Journal of Biological Chemistry* **276,** 29588-29595.

Lindquist J.A., Simeoni L., & Schraven B. (2003) Transmembrane adapters: attractants for cytoplasmic effectors. *Immunological Reviews* **191,** 165-182.

Liou J., Kim M.L., Heo W.D., Jones J.T., Myers J.W., Ferrell J.E., & Meyer T. (2005) STIM is a $Ca^{2+}$ sensor essential for $Ca^{2+}$-store-depletion-triggered $Ca^{2+}$ influx. *Current Biology* **15,** 1235-1241.

Loertscher R. & Lavery P. (2002) The role of glycosyl phosphatidyl inositol (GPI)-anchored cell surface proteins in T-cell activation. *Transplant Immunology* **9,** 93-96.

Lorin-Nebel C., Xing J., Yan X.H., & Strange K. (2007) CRAC channel activity in C-elegans is mediated by Orai1 and STIM1 homologues and is essential for ovulation and fertility. *Journal of Physiology-London* **580,** 67-85.

Lu L.F., Lind E.F., Gondek D.C., Bennett K.A., Gleeson M.W., Pino-Lagos K., Scott Z.A., Coyle A.J., Reed J.L., Van Snick J., Strom T.B., Zheng X.X., & Noelle R.J. (2006) Mast cells are essential intermediaries in regulatory T-cell tolerance. *Nature* **442,** 997-1002.

Lutticken C., Wegenka U.M., Yuan J.P., Buschmann J., Schindler C., Ziemiecki A., Harpur A.G., Wilks A.F., Yasukawa K., Taga T., Kishimoto T., Barbieri G., Pellegrini S., Sendtner M., Heinrich P.C., & Horn F. (1994) Association of Transcription Factor Aprf and Protein-Kinase Jak1 with the Interleukin-6 Signal Transducer Gp130. *Science* **263,** 89-92.

Maksumova L., Le H.T., Muratkhodjaev F., Davidson D., Veillette A., & Pallen C.J. (2005) Protein tyrosine phosphatase $\alpha$ regulates Fyn activity and Cbp/PAG phosphorylation in thymocyte lipid rafts. *Journal of Immunology* **175,** 7947-7956.

Malbec O., Malissen M., Isnardi I., Lesourne R., Mura A.M., Fridman W.H., Malissen B., & Daeron M. (2004) Linker for activation of T cells integrates positive and negative signaling in mast cells. *Journal of Immunology* **173,** 5086-5094.

Mao S.Y. & Metzger H. (1997) Characterization of protein-tyrosine phosphatases that dephosphorylate the high affinity IgE receptor. *Journal of Biological Chemistry* **272,** 14067-14073.

Marie-Cardine A., Kirchgessner H., Bruyns E., Shevchenko A., Mann M., Autschbach F., Ratnofsky S., Meuer S., & Schraven B. (1999) SHP2-interacting transmembrane adaptor protein (SIT), a novel disulfide-linked dimer regulating human T cell activation. *Journal of Experimental Medicine* **189,** 1181-1194.

Markova B., Gulati P., Herlich P.A., & Böhmer F.D. (2005) Investigation of protein-tyrosine phosphatases by in-gel assays. *Methods* **35,** 22-27.

Marshall J.S. (2004) Mast-cell responses to pathogens. *Nature Reviews Immunology* **4,** 787-799.

Mayer C., Gruber H.J., Landl E.M., Pailer S., Scharnagl H., Truschnig-Wilders M., & Marz W. (2007) Rosuvastatin reduces interieukin-6-induced expression of C-reactive protein in hurnan hepatocytes in

a STAT3- and C/EBP-dependent fashion. *International Journal of Clinical Pharmacology and Therapeutics* **45,** 319-327.

Meier-Abt F., Faulstich H., & Hagenbuch B. (2004) Identification of phalloidin uptake systems of rat and human liver. *Biochimica et Biophysica Acta-Biomembranes* **1664,** 64-69.

Melkonian K.A., Ostermeyer A.G., Chen J.Z., Roth M.G., & Brown D.A. (1999) Role of lipid modifications in targeting proteins to detergent-resistant membrane rafts - Many raft proteins are acylated, while few are prenylated. *Journal of Biological Chemistry* **274,** 3910-3917.

Meng T.C., Fukada T., & Tonks N.K. (2002) Reversible oxidation and inactivation of protein tyrosine phosphatases in vivo. *Molecular Cell* **9,** 387-399.

Meng T.C., Hsu S.F., & Tonks N.K. (2005) Development of a modified in-gel assay to identify protein tyrosine phosphatases that are oxidized and inactivated *in vivo*. *Methods* **35,** 28-36.

Mignen O., Thompson J.L., & Shuttleworth T.J. (2007) STIM1 regulates $Ca^{2+}$ entry via arachidonate-regulated $Ca^{2+}$-selective (ARC) channels without store depletion or translocation to the plasma membrane. *Journal of Physiology-London* **579,** 703-715.

Moffett S., Brown D.A., & Linder M.E. (2000) Lipid-dependent targeting of G proteins into rafts. *Journal of Biological Chemistry* **275,** 2191-2198.

Möller N.P.H., Möller K.B., Lammers R., Kharitonenkov A., Sures I., & Ullrich A. (1994) Src kinase associates with a member of a distinct subfamily of protein-tyrosine phosphatases containing an ezrin-like domain. *Proceedings of the National Academy of Sciences of the United States of America* **91,** 7477-7481.

Montixi C., Langlet C., Bernard A.M., Thimonier J., Dubois C., Wurbel M.A., Chauvin J.P., Pierres M., & He H.T. (1998) Engagement of T cell receptor triggers its recruitment to low-density detergent-insoluble membrane domains. *Embo Journal* **17,** 5334-5348.

Morone N., Fujiwara T., Murase K., Kasai R.S., Ike H., Yuasa S., Usukura J., & Kusumi A. (2006) Three-dimensional reconstruction of the membrane skeleton at the plasma membrane interface by electron tomography. *Journal of Cell Biology* **174,** 851-862.

Mutch C.M., Sanyal R., Unruh T.L., Grigoriou L., Zhu M.H., Zhang W.G., & Deans J.P. (2007) Activation-induced endocytosis of the raft-associated transmembrane adaptor protein LAB/NTAL in B lymphocytes: evidence for a role in internalization of the B cell receptor. *International Immunology* **19,** 19-30.

NarisawaSaito M., Yamanashi Y., Morioka T., Oite T., & Shimizu F. (1996) Thy-1 molecule associates with protein tyrosine kinase(s) in rat mesangial cells. *Clinical and Experimental Immunology* **106,** 86-90.

Ndubuisi M.I., Guo G.G., Fried V.A., Etlinger J.D., & Sehgal P.B. (1999) Cellular physiology of STAT3: Where's the cytoplasmic monomer? *Journal of Biological Chemistry* **274,** 25499-25509.

Nedachi T. & Conti M. (2004) Potential role of protein tyrosine phosphatase nonreceptor type 13 in the control of oocyte meiotic maturation. *Development* **131,** 4987-4998.

Nora J.J., Nora A.H., Sinha A.K., Spangler R.D., & Lubs H.A. (1974) Ullrich-Noonan Syndrome - (Turner-Phenotype). *American Journal of Diseases of Children* **127,** 48-55.

Nosjean O. (1998) No prokaryotic GPI anchoring. *Nature Biotechnology* **16,** 799.

O'Rourke L. & Shepherd P.R. (2002) Biphasic regulation of extracellular-signal-regulated protein kinase by leptin in macrophages: role in regulating STAT3 $Ser^{727}$ phosphorylation and DNA binding. *Biochemical Journal* **364,** 875-879.

Odom S., Gomez G., Kovarova M., Furumoto Y., Ryan J.J., Wright H.V., Gonzalez-Espinosa C., Hibbs M.L., Harder K.W., & Rivera J. (2004) Negative regulation of immunoglobulin E-dependent allergic responses by Lyn kinase. *Journal of Experimental Medicine* **199,** 1491-1502.

Ohtake H., Ichikawa N., Okada M., & Yamashita T. (2002a) Cutting edge: Transmembrane phosphoprotein Csk-binding protein/phosphoprotein associated with glycosphingolipid-enriched microdomains as a negative feedback regulator of mast cell signaling through the FcεRI. *Journal of Immunology* **168,** 2087-2090.

Ohtake H., Ichikawa N., Okada M., & Yamashita T. (2002b) Cutting edge: Transmembrane phosphoprotein Csk-binding protein/phosphoprotein associated with glycosphingolipid-enriched microdomains as a negative feedback regulator of mast cell signaling through the FcεRI. *Journal of Immunology* **168,** 2087-2090.

Ohtake H., Ichikawa N., Okada M., & Yamashita T. (2002c) Cutting edge: Transmembrane phosphoprotein Csk-binding protein/phosphoprotein associated with glycosphingolipid-enriched microdomains as a negative feedback regulator of mast cell signaling through the FcεRI. *Journal of Immunology* **168,** 2087-2090.

Oka T., Sato K., Hori M., Ozaki H., & Karaki H. (2002) FcεRI cross-linking-induced actin assembly mediates calcium signalling in RBL-2H3 mast cells. *British Journal of Pharmacology* **136,** 837-846.

Paolini R., Jouvin M.H., & Kinet J.P. (1991) Phosphorylation and dephosphorylation of the high-affinity receptor for immunoglobulin-E immediately after receptor engagement and disengagement. *Nature* **353,** 855-858.

Parravicini V., Gadina M., Kovářová M., Odom S., Gonzalez-Espinosa C., Furumoto Y., Saitoh S., Samelson L.E., O'Shea J.J., & Rivera J. (2002) Fyn kinase initiates complementary signals required for IgE-dependent mast cell degranulation. *Nature Immunology* **3,** 741-748.

Pelkmans L. (2005) Secrets of caveolae- and lipid raft-mediated endocytosis revealed by mammalian viruses. *Biochimica et Biophysica Acta-Molecular Cell Research* **1746,** 295-304.

Pijnenburg M.W., Hofhuis W., Hop W.C., & de Jongste J.C. (2005) Exhaled nitric oxide predicts asthma relapse in children with clinical asthma remission. *Thorax* **60,** 215-218.

Pivniouk V.I., Snapper S.B., Kettner A., Alenius H., Laouini D., Falet H., Hartwig J., Alt F.W., & Geha R.S. (2003) Impaired signaling via the high-affinity IgE receptor in Wiskott-Aldrich syndrome protein-deficient mast cells. *International Immunology* **15,** 1431-1440.

Plowman S.J., Muncke C., Parton R.G., & Hancock J.F. (2005) H-ras, K-ras, and inner plasma membrane raft proteins operate in nanoclusters with differential dependence on the actin cytoskeleton. *Proceedings of the National Academy of Sciences of the United States of America* **102,** 15500-15505.

Prior I.A., Muncke C., Parton R.G., & Hancock J.F. (2003) Direct visualization of Ras proteins in spatially distinct cell surface microdomains. *Journal of Cell Biology* **160,** 165-170.

Rayapureddi J.P., Kattamuri C., Steinmetz B.D., Frankfort B.J., Ostrin E.J., Mardon G., & Hegde R.S. (2003) Eyes absent represents a class of protein tyrosine phosphatases. *Nature* **426,** 295-298.

Rege T.A. & Hagood J.S. (2006a) Thy-1 as a regulator of cell-cell and cell-matrix interactions in axon regeneration, apoptosis, adhesion, migration, cancer, and fibrosis. *Faseb Journal* **20,** 1045-1054.

Rege T.A. & Hagood J.S. (2006b) Thy-1, a versatile modulator of signaling affecting cellular adhesion, proliferation, survival, and cytokine/growth factor responses. *Biochimica et Biophysica Acta - Molecular Cell Research* **1763,** 991-999.

Repine J.E., Bast A., Lankhorst I., Debacker W., Dekhuijzen R., Demedts M., vanHerwaarden C., van Klaveren R., Lammers J.W., Larsson S., Lundback B., Petruzelli S., Postma D., Riise G., Vermeire P., Wouters E., Yernault J.C., & van Zandwijk N. (1997) Oxidative stress in chronic obstructive pulmonary disease. *American Journal of Respiratory and Critical Care Medicine* **156,** 341-357.

Rivera J. (2005) NTAL/LAB and LAT: a balancing act in mast-cell activation and function. *Trends in Immunology* **26,** 119-122.

Roberts A.E., Araki T., Swanson K.D., Montgomery K.T., Schiripo T.A., Joshi V.A., Li L., Yassin Y., Tamburino A.M., Neel B.G., & Kucherlapati R.S. (2007) Germline gain-of-function mutations in SOS1 cause Noonan syndrome. *Nature Genetics* **39,** 70-74.

Rohlich P. (1975) Membrane-Associated Actin-Filaments in Cortical Cytoplasma of Rat Mast-Cell. *Experimental Cell Research* **93,** 293-298.

Rolla G., Guida G., Heffler E., Badiu I., Bommarito L., De Stefani A., Usai A., Cosseddu D., Nebiolo F., & Bucca C. (2007) Diagnostic classification of persistent rhinitis and its relationship to exhaled nitric oxide and asthma - A clinical study of a consecutive series of patients. *Chest* **131,** 1345-1352.

Roos J., di Gregorio P.J., Yeromin A.V., Ohlsen K., Lioudyno M., Zhang S.Y., Safrina O., Kozak J.A., Wagner S.L., Cahalan M.D., Velicelebi G., & Stauderman K.A. (2005) STIM1, an essential and conserved component of store-operated $Ca^{2+}$ channel function. *Journal of Cell Biology* **169,** 435-445.

Ross S.H., Lindsay Y., Safrany S.T., Lorenzo O., Villa F., Toth R., Clague M.J., Downes C.P., & Leslie N.R. (2007) Differential redox regulation within the PTP superfamily. *Cellular Signalling* **19,** 1521-1530.

Saalbach A., Wetzig T., Haustein U.F., & Anderegg U. (1999) Detection of human soluble Thy-1 in serum by ELISA. Fibroblasts and activated endothelial cells are a possible source of soluble Thy-1 in serum. *Cell & Tissue Research* **298,** 307-315.

Saitoh S., Arudchandran R., Manetz T.S., Zhang W.G., Sommers C.L., Love P.E., Rivera J., & Samelson L.E. (2000) LAT is essential for Fc epsilon RI-mediated mast cell activation. *Immunity* **12,** 525-535.

Saitoh S., Odom S., Gomez G., Sommers C.L., Young H.A., Rivera J., & Samelson L.E. (2003) The four distal tyrosines are required for LAT-dependent signaling in FcεRI-mediated mast cell activation. *Journal of Experimental Medicine* **198,** 831-843.

Salmeen A. & Barford D. (2005) Functions and mechanisms of redox regulation of cysteine-based phosphatases. *Antioxidants & Redox Signaling* **7,** 560-577.

Sanan D.A. & Anderson R.G.W. (1991) Simultaneous visualization of LDL receptor distribution and clathrin lattices on membranes torn from the upper surface of cultured cells. *Journal of Histochemistry & Cytochemistry* **39,** 1017-1024.

Schade A.E. & Levine A.D. (2002) Lipid raft heterogeneity in human peripheral blood T lymphoblasts: A mechanism for regulating the initiation of TCR signal transduction. *Journal of Immunology* **168,** 2233-2239.

Seagrave J. & Oliver J.M. (1990) Antigen-dependent transition of IgE to a detergent-insoluble form is associated with reduced IgE receptor-dependent secretion from RBL-2H3 mast cells. *Journal of Cellular Physiology* **144,** 128-136.

Sehgal P.B. (2000) STAT-signalling through the cytoplasmic compartment - Consideration of a new paradigm. *Cellular Signalling* **12,** 525-535.

Sehgal P.B., Guo G.G., Shah M., Kumar V., & Patel K. (2002) Cytokine signaling - STATs in plasma membrane rafts. *Journal of Biological Chemistry* **277,** 12067-12074.

Seth D. & Rudolph J. (2006) Redox regulation of MAP kinase phosphatase 3. *Biochemistry* **45,** 8476-8487.

Shah M., Patel K., Fried V.A., & Sehgal P.B. (2002) Interactions of STAT3 with caveolin-1 and heat shock protein 90 in plasma membrane raft and cytosolic complexes - Preservation of cytokine signaling during fever. *Journal of Biological Chemistry* **277,** 45662-45669.

Shelton M.D., Chock P.B., & Mieyal J.J. (2005) Glutaredoxin: Role in reversible protein S-glutathionylation and regulation of redox signal transduction and protein translocation. *Antioxidants & Redox Signaling* **7,** 348-366.

Shi X.Q., Zhang H., Paddon H., Lee G., Cao X.M., & Pelech S. (2006) Phosphorylation of STAT3 Serine-727 by cyclin-dependent kinase 1 is critical for nocodazole-induced mitotic arrest. *Biochemistry* **45,** 5857-5867.

Singer S.J. & Nicolson G.L. (1972) The fluid mosaic model of the structure of cell membranes. *Science* **175,** 720-731.

Smith P.D. & Crompton M.R. (1998) Expression of v-src in mammary epithelial cells induces transcription via STAT3. *Biochemical Journal* **331,** 381-385.

Sohn H.W., Tolar P., Jin T., & Pierce S.K. (2006) Fluorescence resonance energy transfer in living cells reveals dynamic membrane changes in the initiation of B cell signaling. *Proceedings of the National Academy of Sciences of the United States of America* **103,** 8143-8148.

Sommers C.L., Park C.S., Lee J., Feng C.G., Fuller C.L., Grinberg A., Hildebrand J.A., Lacana E., Menon R.K., Shores E.W., Samelson L.E., & Love P.E. (2002) A LAT mutation that inhibits T cell development yet induces lymphoproliferation. *Science* **296,** 2040-2043.

Spector I., Braet F., Schochet N.R., & Bubb M.R. (1999) New anti-actin drugs in the study of the organization and function of the actin cytoskeleton. *Microscopy Research and Technique* **47,** 18-37.

Sprangers M., Feldhahn N., Herzog S., Hansmann M.L., Reppel M., Hescheler J., Jumaa H., Siebert R., & Muschen M. (2006) The Src family kinase Lyn redirects B cell receptor signaling in human SLP65-deficient B cell lymphoma cells. *Oncogene* **25,** 5056-5062.

Surviladze Z., Dráberová L., Kovářová M., Boubelík M., & Dráber P. (2001) Differential sensitivity to acute cholesterol lowering of activation mediated via the high-affinity IgE receptor and Thy-1 glycoprotein. *European Journal of Immunology* **31,** 1-10.

Surviladze Z., Dráberová L., Kubínová L., & Dráber P. (1998) Functional heterogeneity of Thy-1 membrane microdomains in rat basophilic leukemia cells. *European Journal of Immunology* **28,** 1847-1858.

Surviladze Z., Harrison K.A., Murphy R.C., & Wilson B.S. (2007) FcεRI and Thy-1 domains have unique protein and lipid compositions. *Journal of Lipid Research* **48,** 1325-1335.

Swindle E.J. & Metcalfe D.D. (2007) The role of reactive oxygen species and nitric oxide in mast cell-dependent inflammatory processes. *Immunological Reviews* **217,** 186-205.

Taniguchi T. (1995) Cytokine Signaling Through Nonreceptor Protein-Tyrosine Kinases. *Science* **268,** 251-255.

Tanimura N., Saitoh S., Kawano S., Kosugi A., & Miyake K. (2006) Palmitoylation of LAT contributes to its subcellular localization and stability. *Biochemical and Biophysical Research Communications* **341,** 1177-1183.

Tasaka K., Akagi M., & Miyoshi K. (1986) Distribution of Actin-Filaments in Rat Mast-Cells and Its Role in Histamine-Release. *Agents and Actions* **18,** 49-52.

Taylor A.M., Galli S.J., & Coleman J.W. (1995) Stem-Cell Factor, the Kit-Ligand, Induces Direct Degranulation of Rat Peritoneal Mast-Cells In-Vitro and In-Vivo - Dependence of the In-Vitro Effect on Period of Culture and Comparisons of Stem-Cell Factor with Other Mast Cell-Activating Agents. *Immunology* **86,** 427-433.

Thomas P.M. & Samelson L.E. (1992) The Glycophosphatidylinositol-Anchored Thy-1 Molecule Interacts with the $p60^{Fyn}$ Protein Tyrosine Kinase in T-Cells. *Journal of Biological Chemistry* **267,** 12317-12322.

Tkaczyk C., Hořejší V., Iwaki S., Dráber P., Samelson L.E., Satterthwaite A.B., Nahm D.H., Metcalfe D.D., & Gilfillan A.M. (2004) NTAL phosphorylation is a pivotal link between the signaling cascades leading to human mast cell degranulation following kit activation and FcεRI aggregation. *Blood* **104,** 207-214.

Tolar P., Dráberová L., & Dráber P. (1997) Protein tyrosine kinase Syk is involved in Thy-1 signaling in rat basophilic leukemia cells. *European Journal of Immunology* **27,** 3389-3397.

Tonks N.K. (2005) Redox redux: Revisiting PTPs and the control of cell signaling. *Cell* **121,** 667-670.

Tootle T.L., Silver S.J., Davies E.L., Newman V., Latek R.R., Mills I.A., Selengut J.D., Parlikar B.E.W., & Rebay I. (2003) The transcription factor Eyes absent is a protein tyrosine phosphatase. *Nature* **426,** 299-302.

Torigoe C., Song J.M., Barisas B.G., & Metzger H. (2004) The influence of actin microfilaments on signaling by the receptor with high-affinity for IgE. *Molecular Immunology* **41,** 817-829.

Ubersax J.A. & Ferrell J.E. (2007) Mechanisms of specificity in protein phosphorylation. *Nature Reviews Molecular Cell Biology* **8,** 530-541.

van der Wijk T., Blanchetot C., Overvoorde J., & den Hertog J. (2003) Redox-regulated rotational coupling of receptor protein-tyrosine phosphatase alpha dimers. *Journal of Biological Chemistry* **278,** 13968-13974.

van der Wijk T., Overvoorde J., & den Hertog J. (2004) $H_2O_2$ induced intermolecular disulfide bond formation between receptor protein-tyrosine phosphatases. *J Biol Chem.* **279,** 44355-44361.

Volná P., Lebduška P., Dráberová L., Šímová Š., Heneberg P., Boubelík M., Bugajev V., Malissen B., Wilson B.S., Hořejší V., Malissen M., & Dráber P. (2004) Negative regulation of mast cell signaling and function by the adaptor LAB/NTAL. *Journal of Experimental Medicine* **200,** 1001-1013.

Wang B., Lemay S., Tsai S., & Veillette A. (2001a) SH2 domain-mediated interaction of inhibitory protein tyrosine kinase Csk with protein tyrosine phosphatase-HSCF. *Molecular and Cellular Biology* **21,** 1077-1088.

Wang T.Y., Leventis R., & Silvius J.R. (2001b) Partitioning of lipidated peptide sequences into liquid-ordered lipid domains in model and biological membranes. *Biochemistry* **40,** 13031-13040.

Wang Y., Horváth O., Hamm-Baarke A., Richelme M., Gregoire C., Guinamard R., Hořejší V., Angelisová P., Špička J., Schraven B., Malissen B., & Malissen M. (2005) Single and combined deletions of the NTAL/LAB and LAT adaptors minimally affect B-cell development and function. *Molecular and Cellular Biology* **25,** 4455-4465.

Wang Z.H., Shen D., Parsons D.W., Bardelli A., Sager J., Szabo S., Ptak J., Silliman N., Peters B.A., van der Heijden M.S., Parmigiani G., Yan H., Wang T.L., Riggins G., Powell S.M., Willson J.K.V., Markowitz S., Kinzler K.W., Vogelstein B., & Velculescu V.E. (2004) Mutational analysis of the tyrosine phosphatome in colorectal cancers. *Science* **304,** 1164-1166.

Weber J.R., Orstavik S., Torgersen K.M., Danbolt N.C., Berg S.F., Ryan J.C., Taskén K., Imboden J.B., & Vaage J.T. (1998) Molecular cloning of the cDNA encoding pp36, a tyrosine-phosphorylated adaptor protein selectively expressed by T cells and natural killer cells. *Journal of Experimental Medicine* **187,** 1157-1161.

Weibrecht I., Böhmer S.A., Dagnell M., Kappert K., Östman A., & Böhmer F.D. (2007) Oxidation sensitivity of the catalytic cysteine of the protein-tyrosine phosphatases SHP-1 and SHP-2. *Free Radical Biology and Medicine* **43,** 100-110.

Wilson B.S., Pfeiffer J.R., & Oliver J.M. (2002) FcεRI signaling observed from the inside of the mast cell membrane. *Molecular Immunology* **38,** 1259-1268.

Wilson B.S., Steinberg S.L., Liederman K., Pfeiffer J.R., Surviladze Z., Zhang J., Samelson J.E., Yang L.H., Kotula P.G., & Oliver J.M. (2004) Markers for detergent-resistant lipid rafts occupy distinct and dynamic domains in native membranes. *Molecular Biology of the Cell* **15,** 2580-2592.

Wolf A.A., Jobling M.G., Wimer-Mackin S., Ferguson-Maltzman M., Madara J.L., Holmes R.K., & Lencer W.I. (1998) Ganglioside structure dictates signal transduction by cholera toxin and association with caveolae-like membrane domains in polarized epithelia. *Journal of Cell Biology* **141,** 917-927.

Wu Y., Dowbenko D., & Lasky L.K. (1998) PSTPIP 2, a second tyrosine phosphorylated, cytoskeletal-associated protein that binds a PEST-type protein-tyrosine phosphatase. *Journal of Biological Chemistry* **273,** 30487-30496.

Xavier R., Brennan T., Li Q.Q., McCormack C., & Seed B. (1998) Membrane compartmentation is required for efficient T cell activation. *Immunity* **8,** 723-732.

Yamasaki S., Ishikawa E., Sakuma M., Kanagawa O., Cheng A.M., Malissen B., & Saito T. (2007) LAT and NTAL mediate immunoglobulin E-induced sustained extracellular signal-regulated kinase activation critical for mast cell survival. *Molecular and Cellular Biology* **27,** 4406-4415.

Yang J., Groen A., Lemeer S., Jans A., Slijper M., Roe S.M., den Hertog J., & Barford D. (2007) Reversible oxidation of the membrane distal domain of receptor PTP alpha is mediated by a cyclic sulfenamide. *Biochemistry* **46,** 709-719.

Yeung Y.G., Wang Y., Einstein D.B., Lee P.S.W., & Stanley E.R. (1998) Colony-stimulating factor-1 stimulates the formation of multimeric cytosolic complexes of signaling proteins and cytoskeletal components in macrophages. *Journal of Biological Chemistry* **273,** 17128-17137.

Ying J., Li H., Cui Y., Wong A.H.Y., Langford C., & Tao Q. (2006) Epigenetic disruption of two proapoptotic genes MAPK10/JNK3 and PTPN13/FAP-1 in multiple lymphomas and carcinomas through hypermethylation of a common bidirectional promoter. *Leukemia* **20,** 1173-1175.

Zacharias D.A., Violin J.D., Newton A.C., & Tsien R.Y. (2002) Partitioning of lipid-modified monomeric GFPs into membrane microdomains of live cells. *Science* **296,** 913-916.

Zhang S.L., Yeromin A.V., Zhang X.H.F., Yu Y., Safrina O., Penna A., Roos J., Stauderman K.A., & Cahalan M.D. (2006) Genome-wide RNAi screen of $Ca^{2+}$ influx identifies genes that regulate $Ca^{2+}$ release-activated $Ca^{2+}$ channel activity. *Proceedings of the National Academy of Sciences of the United States of America* **103,** 9357-9362.

Zhang S.Q., Yang W.T., Kontaridis M.I., Bivona T.G., Wen G.Y., Araki T., Luo J.C., Thompson J.A., Schraven B.L., Philips M.R., & Neel B.G. (2004) SHP2 regulates Src family kinase activity and Ras/Erk activation by controlling Csk recruitment. *Molecular Cell* **13,** 341-355.

Zhang W.G., Sloan-Lancaster J., Kitchen J., Trible R.P., & Samelson L.E. (1998a) LAT: The ZAP-70 tyrosine kinase substrate that links T cell receptor to cellular activation. *Cell* **92,** 83-92.

Zhang W.G., Trible R.P., & Samelson L.E. (1998b) LAT palmitoylation: Its essential role in membrane microdomain targeting and tyrosine phosphorylation during T cell activation. *Immunity* **9,** 239-246.

Zhang W.G., Trible R.P., Zhu M.H., Liu S.K., McGlade J., & Samelson L.E. (2000) Association of Grb2, Gads, and phospholipase C$\gamma$1 with phosphorylated LAT tyrosine residues - Effect of LAT tyrosine mutations on T cell antigen receptor-mediated signaling. *Journal of Biological Chemistry* **275,** 23355-23361.

Zhu M.H., Janssen E., Leung K., & Zhang W.G. (2002) Molecular cloning of a novel gene encoding a membrane-associated adaptor protein (LAX) in lymphocyte signaling. *Journal of Biological Chemistry* **277,** 46151-46158.

Zhu M.H., Liu Y., Koonpaew S., Granillo O., & Zhang W.G. (2004) Positive and negative regulation of Fc$\varepsilon$RI-mediated signaling by the adaptor protein LAB/NTAL. *Journal of Experimental Medicine* **200,** 991-1000.

Zhu M.H., Shen S.D., Liu Y., Granillo O., & Zhang W.G. (2005) Cutting edge: Localization of linker for activation of T cells to lipid rafts is not essential in T cell activation and development. *Journal of Immunology* **174,** 31-35.

Zucchini A., Del Zotto G., Brando B., & Canonico B. (2001) CD90. *Journal of Biological Regulators and Homeostatic Agents* **15,** 82-85.

# 10 ABBREVIATIONS

| | |
|---|---|
| Brij 96 | polyoxyetheylene (10) oleyl ether |
| BMMC | bome marrow mast cells |
| Btk | Bruton's tyrosine kinase |
| Cbp | Csk-binding protein |
| Cbl | Casitas B cell lymphoma |
| CD | cluster of differentiation |
| Cdc25 | cell division cycle 25C |
| Csk | c-Src tyrosine kinase |
| DAP-10 | DNAX-activating protein of 10 kDa |
| DAP-12 | DNAX activation protein of 12 kDa |
| DEP-1 | high cell density–enhanced PTP 1 |
| DNA | deoxyribonucleic acid |
| DRM | detergent-resistant membranes |
| EBP50 | ezrin-radixin-moesin binding phosphoprotein 50 |
| ECL | enhanced chemiluminiscence |
| EDTA | ethylenediaminetetraacetic acid |
| ERK | extracellular signal-regulated kinase |
| EST | expressed sequence tag |
| F-actin | filamentous actin |
| FcεRI | high-affinity receptor for IgE, type I |
| FERM | band 4.1, ezrin, radixin, moesin |
| FITC | fluorescein isothiocyanate |
| FRET | fluorescence resonance energy transfer |
| Gab | Grb2-associated binding protein |
| G-actin | globular actin |
| Gads | Grb2-related adaptor downstream of Shc |
| GFP | green fluorescent protein |
| GM1 | monosialotetrahexosylganglioside |
| gp | glycoprotein |
| GPI | glycosylphosphatidylinositol |
| Grap | Grb2-related adaptor protein |
| Grb2 | growth factor receptor-bound protein 2 |
| GTP | guanosine-tri-phosphate |
| HePTP | haematopoietic protein tyrosine phosphatase |

| | |
|---|---|
| IgE | immunoglobulin E |
| IgG | immunoglobulin G |
| IL | interleukin |
| ITAM | immunoreceptor tyrosine-based activation motif |
| JAK | Janus kinase |
| LAB | linker for activation of B cells |
| LAR | leucocyte common antigen-related phosphatase |
| LAT | linker for activation of T cells 2 |
| LAX | linker for activation of X cells |
| Lck | Leukocyte specific kinase |
| LTIIb | *E. coli* heat-labile toxin type II |
| LIME | Lck-interacting membrane protein |
| LMW-PTP | low molecular weight protein tyrosine phosphatase |
| mAb | monoclonal antibody |
| MβCD | methyl-β-cyklodextrin |
| MAPK | mitogen-activated protein kinase |
| MEK | mitogen-activated protein kinase/ERK kinase |
| NK | natural killer |
| NOS | nitric oxide synthase |
| NP40 | Nonidet P-40 |
| NTAL | non-T cell activation linker |
| PAG | phosphoprotein associated with GEMs |
| PCMC | peritoneal cell-derived mast cells |
| PDZ | postsynaptic density 95/Discs Large/Zonula Occludens 1 domain |
| PI3K | phosphoinositide 3-kinase |
| PIP3 | phosphatidylinositol-3,4,5-triphosphate |
| PKC | protein kinase C |
| PLCγ | phospholipase C γ |
| PMA | phorbol 12-myristate 13-acetate |
| PRL | phosphatase of regenerating liver |
| PSTPIP | proline-serine-threonine phosphatase interacting protein |
| PTEN | phosphatase and tensin homologue deleted on chromosome ten |
| PTK | protein tyrosine kinase |
| PTP | protein tyrosine phosphatase |
| PTP-MEG | megakaryocyte protein tyrosine phosphatase |
| PTPN | nonreceptor protein tyrosine phosphatase |
| PTP-PEST | (Pro-Glu-Ser-Thr) domain containing protein tyrosine phosphatase |

| | |
|---|---|
| Rac | Ras-related C3 botulinum toxin substrate |
| RACE | rapid amplification of complementary DNA ends |
| Ras | rat sarcoma |
| RBL | rat basophilic leukemia |
| Rho | Ras-homologous |
| RhoGAP | RhoGTPase-activating protein |
| SCF | stem cell factor |
| SEC14 | domain in homologues of a S. cerevisiae phosphatidylinositol transfer protein |
| SH2 | Src-homology domain 2 |
| SHIP | Src homology 2 domain–containing 5-inositol phosphatase |
| SHP | src homology 2 domain-containing tyrosine phosphatase |
| siRNA | small interfering ribonucleic acid |
| SIT | SHP2 interacting transmembrane adaptor protein |
| SLP-76 | SH2 domain containing leukocyte protein of 76kDa |
| SOC | store-operated calcium |
| SOS | son of sevenless |
| STAT | signal transducer and activator of transcription |
| Stim1 | stromal interaction molecule 1 |
| Syk | Splenic tyrosine kinase |
| TC45 | 45 kDa variant of the T cell protein tyrosine phosphatase |
| TCR | T cell receptor |
| TH2 | T helper type 2 |
| TEC | teratocarcinoma |
| TEX101 | TES101-reactive protein |
| TRIM | T cell receptor-interacting molecule |
| TRITC | tetramethylrhodamine isothiocyanate |
| Tyk2 | tyrosine kinase 2 |
| uPAR | urokinase plasminogen activator receptor |
| VH1 | variola H1 |
| ZAP70 | zeta-chain associated protein kinase 70kDa |

aminoacids are abbreviated in both one- or three-letter form depending on the context